Chapter 4

DECAY

Conveners: E. Eichten, C. Patrignani, A. Vairo

Authors: D. Z. Besson, E. Braaten, A. Deandrea, E. Eichten, T. Ferguson, F. A. Harris, V. V. Kiselev, P. Kroll, Y.- P. Kuang, A. Leibovich, S. L. Olsen, C. Patrignani, A. Vairo

1 INTRODUCTION[1]

The study of decay observables has witnessed in the last years a remarkable progress. New experimental measurements, mainly coming from Belle, BES, CLEO and E835 have improved existing data on inclusive (Section 3 and 4), electromagnetic (Section 3) and several exclusive (Section 5) decay channels as well as on several electromagnetic (Section 6) and hadronic (Section 7) transition amplitudes. In some cases the new data have not only led to a reduction of the uncertainties but also to significant shifts in the central values. Also the error analysis of several correlated measurements has evolved and improved our determination of quarkonium branching fractions (Section 2). New data have also led to the discovery of new states. These have been mainly discussed in Chapter 3.

From a theoretical point of view several heavy quarkonium decay observables may be studied nowadays in the framework of effective field theories of QCD. These have been introduced in Chapters 1 and 3. In some cases, like inclusive and electromagnetic decay widths, factorization of high and low energy contributions has been achieved rigorously. In some others, where more degrees of freedom, apart from the heavy-quarkonium state, are entangled and the problem becomes quite complicated, models are still used to some extent and factorization formulas, if there are, are on a less solid ground. There is room there for new theoretical developments. High energy contributions can be calculated in perturbation theory. Low energy matrix elements, which may include, among others, heavy quarkonium wave functions, colour-octet matrix elements, correlators, overlap integrals in radiative transitions, multipole gluon emission factors, can be determined either by suitable fitting of the data or on the lattice or by means of potential models. They typically set the precision of the theoretical determinations.

In each of the following sections we will have a first part where the theoretical framework is reviewed and the basic formalism set up and a second part that summarizes the phenomenological applications and presents the experimental status. In the last section of the chapter, Section 8, we will discuss decay modes of the B_c. There are no data available yet (apart from the lifetime), but B_c will be copiously produced at future hadron colliders. This system, differently from bottomonium and charmonium, decays only weakly. Therefore, it opens in quarkonium physics a window to some of the electroweak parameters of the Standard Model.

The outline of the chapter is the following. We will start in Section 2 by making some general remarks on the determination of quarkonium branching ratios from experiments. In Section 3 we will discuss inclusive and electromagnetic decay widths, in Section 4 Υ inclusive radiative decays, in Section 5 exclusive decays, in Section 6 radiative and in Section 7 hadronic transitions. Finally, Section 8 will be devoted to the decays of the B_c.

[1] Author: A. Vairo

2 BRANCHING RATIO MEASUREMENTS[2]

The measurement of branching ratios (or partial widths) $\mathcal{B}$ is deceptively simple: the total number of events observed in a given final state $N^{\rm obs}_{Q\bar{Q}\to f}$ is proportional to the total number of events produced $N^{\rm prod}_{Q\bar{Q}}$ for that particular resonance:

$$N^{\rm obs}_{Q\bar{Q}\to \rm f} = \rm eff \times N^{\rm prod}_{Q\bar{Q}} \times \mathcal{B}(Q\bar{Q}\to \rm f), \tag{4.1}$$

$N^{\rm prod}_{Q\bar{Q}}$ in turn needs to be measured by counting some specific events. In most cases, depending on the process under study and the analysis strategy, $N^{\rm prod}_{Q\bar{Q}}$ is calculated from the number of events observed in a given "reference" final state $N^{\rm obs}_{Q\bar{Q}\to \rm Ref}$:

$$N^{\rm prod}_{Q\bar{Q}} = \frac{N^{\rm obs}_{Q\bar{Q}\to \rm Ref}}{\rm eff'\ \mathcal{B}_{Ref}}.$$

The reported value of $\mathcal{B}(Q\bar{Q}\to \rm f)$ will therefore use $\mathcal{B}_{\rm Ref}$ as reported by some previous experiment:

$$\mathcal{B}(Q\bar{Q}\to \rm f) = \frac{N^{\rm obs}_{Q\bar{Q}\to \rm f}}{N^{\rm obs}_{Q\bar{Q}\to \rm Ref}}\ \frac{\rm eff'}{\rm eff}\ \mathcal{B}_{\rm Ref}. \tag{4.2}$$

As discussed in [1], there are a number of potentially dangerous consequences in this procedure. First of all different experiments might use the same reference mode, so their values of $\mathcal{B}$ are not independent. Even worse, the $\mathcal{B}(Q\bar{Q}\to \rm f)$ reported in Eq. (4.2) will also be (hiddenly) correlated to the normalization Ref$'$ chosen by the previous experiment(s) where $\mathcal{B}_{\rm Ref}$ had been measured, and ultimately may depend on some other branching ratio $\mathcal{B}'_{\rm Ref'}$. Such hidden correlations are hard to identify and can have pernicious consequences on the evaluation of $\mathcal{B}'$ based on independent measurements from different experiments.

For precision determination of branching ratios or partial widths, it is important to know the normalization used in each measurement and to quote explicitly the quantity that is indeed directly measured by each experiment

$$\frac{\mathcal{B}(Q\bar{Q}\to \rm f)}{\mathcal{B}_{\rm Ref}} = \frac{N^{\rm obs}_{Q\bar{Q}\to \rm f}}{N^{\rm obs}_{Q\bar{Q}\to \rm Ref}}\frac{\rm eff'}{\rm eff}, \tag{4.3}$$

i.e., the ratio or product of branching ratios (even of different particles), which is most directly related to the event yield. Many experiments could also provide measurements of ratios of branching ratios

$$R_{\mathcal{B}}(f/f') = \frac{\mathcal{B}(Q\bar{Q}\to \rm f)}{\mathcal{B}(Q\bar{Q}\to \rm f')}, \tag{4.4}$$

which do not depend on the normalization, and where usually also a number of other systematics cancel.

With the increased statistical precision that is to be expected in the next few years, it will become increasingly important for an appropriate branching ratio and partial width evaluation that individual measurements are reported according to Eq. (4.3) and whenever possible also as in Eq. (4.4). In order to perform the best estimate based on a set of measurements from different experiments, it might also become important to take into account the systematic errors that are common to all measurements performed by the same experiment. An appropriate choice of a set of independent measurements of (4.3) and (4.4) from each experiment is likely the best option for a global fit to quarkonium branching ratios. A comparison of $R_{\mathcal{B}}(f/f')$ that could be directly measured by virtually all experiments, could also

[2] Author: C. Patrignani

help understand possible systematic effects, which are going to be the limiting factor on branching ratio determinations.

Here, we briefly outline the experimental techniques and analysis strategies adopted to determine these branching ratios with emphasis on the corresponding possible normalization choices, as a necessary ingredient to understand possible mutual dependencies and constraints.

2.1 Branching ratios measured in e^+e^- formation experiments

e^+e^- formation experiments are undoubtedly the most important tool to investigate charmonium and bottomonium branching ratios by a variety of techniques. In these experiments the n^3S_1 quarkonium states can be directly formed and the $\mathcal{B}(n^3S_1 \to \mathrm{f})$ are determined either normalizing to a specific decay mode, i.e., providing a direct measurement of $\dfrac{\mathcal{B}(n^3S_1 \to \mathrm{f})}{\mathcal{B}(n^3S_1 \to \mathrm{Norm})}$, or measuring the number of n^3S_1 by performing a scan of the resonance.

The usual choice for the normalization channel is the inclusive hadronic decay mode, which is close to 100% for all resonances, i.e., it provides to a good approximation an absolute normalization. However, it requires subtraction of the non resonant hadronic cross-section whose yield (at the given running condition) must be calculated taking into account the interference with the resonance. When the total number of events is determined by a scan of the resonance (which also provides measurements of Γ_{tot}, $\mathcal{B}_{\ell\ell}$ and $\mathcal{B}_{\mathrm{hadr}}$), there is in principle a possible correlation of the branching ratio to the values for these quantities that is likely small if the scan has many points, but should not be overlooked. As stressed in Chapter 2, Section 8.5, interference with the continuum for any specific final state might introduce sizeable corrections. A measurement of the ratio $R_{\mathcal{B}}(f/\mathrm{Norm})$ across the formation energy of the resonance is needed to understand the interference and its impact on branching ratios.

All other states are studied in hadronic or radiative decays, and the number of events produced for each state must be determined using the appropriate n^3S_1 branching ratio:

$$N^{\mathrm{prod}}_{n'^3P_J} = N^{\mathrm{prod}}_{n^3S_1} \times \mathcal{B}(n^3S_1 \to \gamma\, n'^3P_J), \tag{4.5}$$

$$N^{\mathrm{prod}}_{n'^1S_0} = N^{\mathrm{prod}}_{n^3S_1} \times \mathcal{B}(n^3S_1 \to \gamma\, n'^1S_0). \tag{4.6}$$

Thus, for ${}^3P_J$ and ${}^1S_0$ states these experiments can only directly measure the ratios $R_{\mathcal{B}}(f/f')$ and the following combinations of branching ratios:

$$\frac{\mathcal{B}(n^3S_1 \to \gamma\, n'^3P_J)}{\mathcal{B}(n^3S_1 \to \mathrm{Norm})}\,\mathcal{B}(n^3P_J \to \mathrm{f}), \tag{4.7}$$

$$\frac{\mathcal{B}(n^3S_1 \to \gamma\, n'^1S_0)}{\mathcal{B}(n^3S_1 \to \mathrm{Norm})}\,\mathcal{B}(n'^1S_0 \to \mathrm{f}). \tag{4.8}$$

On the other hand, since the $\mathcal{B}(\psi(2S) \to J/\psi\pi^+\pi^-)$ is reasonably large, and the events can be easily selected by just reconstructing the $\pi^+\pi^-$ recoiling against the J/ψ, absolute measurements of J/ψ branching ratios have been obtained based on "tagged" J/ψ samples:

$$\mathcal{B}(J/\psi \to \mathrm{f}) = \frac{eff_{\pi^+\pi^- X}}{eff_{\pi^+\pi^-\,\mathrm{f}}}\,\frac{N^{\mathrm{obs}}(\psi' \to (\pi^+\pi^-)_{\mathrm{recoil}}\mathrm{f})}{N^{\mathrm{obs}}(\psi' \to (\pi^+\pi^-)_{\mathrm{recoil}}\, X)}. \tag{4.9}$$

From the experimental point of view this is a particularly clean measurement, since the efficiency ratio can be determined with high precision. With the increased CLEO III samples, it would be interesting to fully exploit the possibility of using "tagged" $\Upsilon(2S)$ and $\Upsilon(3S)$ samples to perform absolute $\Upsilon(1S)$ and $\Upsilon(2S)$ branching ratios determinations.

Radiative decay branching ratios (e.g., direct $1^{--} \to \gamma\, X$ and $1^{--} \to \gamma\, X \to \gamma\gamma X'$) have also been directly measured.

In all cases, photon candidates that are likely to originate from π^0 are not considered (π^0 veto), and the efficiency correction relies on Monte Carlo, and ultimately on the event generator used to model the particle multiplicities, and the angular and momentum distributions.

Despite efforts to tune JETSET [2] fragmentation parameters to reproduce specific classes of inclusive events (e.g., hadronic events in the continuum [3] below $D\bar{D}$ threshold or J/ψ, $\psi(2S)$ decays [4]), there are simply not enough experimentally measured χ_c, χ_b, η_c, η_b decays to light hadrons ($l.h.$) to compare these models with. That could eventually become a limiting systematic to these measurements.

2.2 Branching ratios and partial widths measured in $p\bar{p}$ formation experiments

In these experiments [5] a scan of the resonance allows direct measurements of mass, total width and $\mathcal{B}(p\bar{p})\mathcal{B}_{\rm f}$ for all charmonium resonances.[3] For resonances whose natural width is comparable or smaller than the beam width ($\mathcal{O}(700\,\mathrm{MeV})$ for E760 and E835), the product $\mathcal{B}(p\bar{p})\mathcal{B}_{\rm f}$ is highly correlated to the total width, and the quantity $\Gamma(p\bar{p})\mathcal{B}_{\rm f}$ is more precisely determined. By detecting the resonance formation in more than one final state, the ratio of branching ratios $R_{\mathcal{B}}(f/f')$ can be determined independently from the total width and $\mathcal{B}(p\bar{p})$, in general with small systematic errors since the final state is fully reconstructed, and the angular distribution only depends on a limited number of decay and formation amplitudes. Interference effects with the continuum could affect the measurement of $\mathcal{B}(p\bar{p})\mathcal{B}_{\rm f}$ and $R_{\mathcal{B}}(f/f')$, but as in e^+e^- experiments, their relevance could be estimated by a measurement of $R_{\mathcal{B}}(f/f')$ across the formation energy of the resonance. Unfortunately, only a few highly characteristic final states of charmonium (e^+e^-, $J/\psi\,X$, $\gamma\gamma$) can be detected by these experiments, because of the large hadronic non-resonant cross-section.

Recently, a pioneering study of $p\bar{p}\to\pi^0\pi^0$ [6] and $\eta\eta$ differential cross-sections at the χ_{c0} formation energy has shown that also selected exclusive two-body hadronic decays can be successfully measured. The interference with the continuum could be successfully exploited by the next generation of $p\bar{p}$ annihilation experiments to extend the knowledge of χ_c and η_c branching ratios to baryons or light hadrons.

2.3 Branching ratios and partial widths measured in two-photon reactions

The number of events observed for a specific final state is proportional to $\Gamma_{\gamma\gamma}\mathcal{B}_{\rm f}\times\mathcal{L}_{\gamma\gamma}$, where the effective two-photon luminosity function $\mathcal{L}_{\gamma\gamma}$ (see Chapter 2, Section 8.4) is calculated by all experiments using the same formalism (even if not all using the same generator). The only directly measurable quantity is

$$\Gamma_{\gamma\gamma}\mathcal{B}_{\rm f}, \tag{4.10}$$

or (if more than one final state is detected) $R_{\mathcal{B}}(f/f')$. The theoretical uncertainties in $\mathcal{L}_{\gamma\gamma}$ are largely common to all experiments and that should be taken into account for future high statistics measurements. It might be worth mentioning here that the values reported in the past by different experiments for the $\Gamma_{\gamma\gamma}$, derived from their measurement of (4.10), are not independent and they are not always easily comparable since some of them are obtained by a weighted average of many decay modes, which are individually poorly known.

2.4 Branching ratios and partial widths measured by radiative return (ISR)

Because of initial state radiation (ISR, also referred to as hard photon emission or radiative return), e^+e^- colliders are effectively at the same time (asymmetric) colliders for all $\sqrt{s}$ energies below nominal collision energy. The effective luminosity (and therefore event yields) can be sizeable [7] and can be determined quite accurately by counting $\mu\mu\gamma$ events, for which precise expressions (and event generators

[3] The $p\bar{p}$ branching ratios of bottomonium states are likely 3 orders of magnitudes smaller than for charmonium, and only when a measurement will be available, it will be possible to judge on the feasibility of such experiments.

based on them) are commonly available. The major advantage of this technique is that $e^+e^-\to X$ can be measured simultaneously and under uniform detector conditions over a broad range of $\sqrt{s}$. And they "come for free" at any of the e^+e^- factories, which are expected to collect large data samples.

The main interest is the measurement of R, but for any exclusive final state those experiments could obtain a direct measurement of $\Gamma_{e^+e^-}\mathcal{B}_{\rm f}$ for any resonance whose mass is lower than the collision energy, and, again by detecting more than one final state, $R_{\mathcal{B}}(f/f')$. To date only BES [8] and BaBar [9] have used this technique to measure $\Gamma(\psi'\to e^+e^-)\mathcal{B}(\psi'\to J/\psi\pi\pi)$ and $\Gamma(J/\psi\to e^+e^-)\mathcal{B}(J/\psi\to\mu^+\mu^-)$ respectively. Measurements of $\Gamma_{e^+e^-}\mathcal{B}_{l^+l^-}$ would provide important constraints on both the total width and $\Gamma_{e^+e^-}$ for all 1^{--} states, providing at the same time an important cross check for possible systematic errors.

2.5 Branching ratios measured in B decays

Asymmetric B factories focused originally on exclusive B decays to final states involving a $c\bar{c}$ as the cleanest modes to study CP violation.

With the impressive amount of data collected so far (more than 500 fb^{-1} as of summer 2004 adding Belle and BaBar) and $\mathcal{B}(B\to c\bar{c}\,X)$ of order 10^{-3}, both experiments are collecting larger and larger samples of exclusive B decays to charmonia, and they are obviously interested in reconstructing them into as many different final states as possible. The same is true for D0 and CDF, since the preliminary reconstruction of highly characteristic exclusive charmonium (and bottomonium) final states is needed for other analyses.

For charmonium the quantity directly measured by these experiments is

$$\mathcal{B}(B\to c\bar{c}\,X)\times\mathcal{B}(c\bar{c}\to{\rm f}), \tag{4.11}$$

and again from the number of fully reconstructed events into different final states these experiments can directly measure $R_{\mathcal{B}}(f/f')$ for a variety of final states and for virtually all quarkonium states. Even if the precision might not always compete with other techniques, the wide range of possible $R_{\mathcal{B}}(f/f')$ measurements, with likely different sources of systematic errors, would certainly be important in evaluating quarkonium branching ratios, in particular for those states (χ_Q and η_Q) whose branching ratios are largely unknown.

2.6 Indirect determinations as a tool to investigate systematic effects

The possibilities offered by the mutual constraints posed by measurements of different products or ratios of branching ratios have so far been only partially exploited.

The first advantage is that branching ratios measured by different techniques have different sources of systematic errors, and the comparison can provide insight on how to nail them down. The current best estimate for $\mathcal{B}(\chi_{c2}\to\gamma J/\psi)$ [10] is largely determined by measurements of $\Gamma(\chi_{c2}\to p\bar{p})\mathcal{B}(\chi_{c2}\to\gamma J/\psi)$, $\Gamma(\chi_{c2}\to\gamma\gamma)\mathcal{B}(\chi_{c2}\to\gamma J/\psi)$ and $\mathcal{B}(\chi_{c2}\to\gamma\gamma)/\mathcal{B}(\chi_{c2}\to\gamma J/\psi)$, to the point that these measurements indirectly constrain the estimate of $\mathcal{B}(\psi'\to\gamma\chi_{c2})$ to a value significantly lower than the world average of direct measurements, since the product $\mathcal{B}(\psi'\to\gamma\chi_{c2})\mathcal{B}(\chi_{c2}\to\gamma J/\psi)$ has been measured with high precision.[4]

The other advantage is that measurements of different product and ratios of branching ratios pose constraints on their values: for χ_{c0} at present the partial widths $\Gamma_{\gamma\gamma}$ and $\Gamma_{\gamma J/\psi}$ are known to $\approx$10% [10], even if none of the many measurements more or less directly related to these quantities (Γ, $\Gamma_{\gamma\gamma}\mathcal{B}_{4\pi}$, $\Gamma_{\gamma\gamma}/\Gamma_{\gamma J/\psi}$, $\Gamma_{\gamma J/\psi}\mathcal{B}_{p\bar{p}}$, $\mathcal{B}(\psi'\to\gamma\chi_{c0})$, $\mathcal{B}(\psi'\to\gamma\chi_{c0})\mathcal{B}_{p\bar{p}}$, $\mathcal{B}(\psi'\to\gamma\chi_{c0})\mathcal{B}_{\gamma J/\psi}$ and others) is individually known much better than that.

[4] New more precise measurements of $\mathcal{B}(\psi'\to\gamma\chi_{c2})$ might in turn provide constraints for $\mathcal{B}(\psi'\to\gamma\chi_{c2})\mathcal{B}(\chi_{c2}\to\gamma J/\psi)$

The proposed next generation of $p\bar{p}$ experiments with extended PID ability could provide invaluable information by measuring $p\bar{p}\to p\bar{p}$ differential cross-section at the η_c (and possibly at the χ_{c0}). This would provide a direct measurement of $\mathcal{B}(c\bar{c}\to p\bar{p})$, indirectly constraining the radiative J/ψ (and ψ') M1 transitions from the well measured $\mathcal{B}(J/\psi\to\gamma\eta_c\to\gamma p\bar{p})$. Since at present the ≈30% uncertainty in $\mathcal{B}(J/\psi\to\gamma\eta_c)$ is the major source of uncertainty in all η_c branching ratios, this will also directly affect all η_c branching ratios.

With the increased statistics available at B factories it might soon become possible to determine at least some of the $\mathcal{B}(B\to c\bar{c}\,l.h.)$ branching ratios without explicitly reconstructing the charmonium. In this case, simultaneous measurements of the same B decay mode in exclusive final states $\mathcal{B}(B\to c\bar{c}\,l.h.)\mathcal{B}(c\bar{c}\to\mathrm{f})$ would allow B factories to directly measure $\mathcal{B}(c\bar{c}\to\mathrm{f})$ from Eq. (4.11). Considering that the photon in $\psi(2S)\to\gamma\eta_c(2S)$ is very soft and that this inclusive radiative transition will likely be difficult to measure for both CLEO-c and BES III, this might well be the best way of determining the $\eta_c(2S)$ branching ratios, and indirectly determining the partial width for the M1 $\psi(2S)\to\gamma\eta_c(2S)$ transition itself.

3 ELECTROMAGNETIC AND INCLUSIVE DECAYS INTO LIGHT PARTICLES[5]

3.1 Theoretical framework

The main dynamical mechanism of heavy-quarkonium decay into light particles is quark–antiquark annihilation. Since this happens at a scale $2m$ (m is the heavy quark mass), which is perturbative, the heavy quarks annihilate into the minimal number of gluons allowed by colour conservation and charge conjugation. The gluons subsequently create light quark–antiquark pairs that form the final state hadrons: $Q\bar{Q}\to ng^*\to m(q\overline{q})$. Values of n are given for various quarkonia in Table 4.1; for comparison the minimal number of photons into which a $Q\bar{Q}$ pair can annihilate is also listed. Experimentally this fact is reflected by the narrow width of the heavy quarkonia decays into hadronic channels in a mass region where strong decays typically have widths of hundreds of MeV. As an example let us consider the J/ψ decay into light hadrons. Following [11], this process is regarded as the decay into three real gluons. The calculation of this width leads to the result

$$\Gamma(J/\psi\to l.h.) \;=\; \frac{10}{81}\,\frac{\pi^2-9}{\pi e_c^2}\,\frac{\alpha_{\rm s}^3}{\alpha_{\rm em}^2}\,\Gamma(J/\psi\to e^+e^-) = 205\ \mathrm{keV}\,\left(\frac{\alpha_{\rm s}}{0.3}\right)^3 . \qquad (4.12)$$

Although this value is somewhat larger than the experimental one it explains the narrowness of the hadronic decays of the quarkonia. Corrections like relativistic, $\alpha_{\rm s}$ or colour-octet ones, may lead to a better agreement with experiment. A systematic way to include these corrections is provided by nonrelativistic effective field theories of QCD.

In an effective field theory language[6], at scales lower than m heavy-quarkonium annihilation is resolved as a contact interaction. This is described at the Lagrangian level by four-fermion operators whose matching coefficients develop an imaginary part. Consequently, the annihilation width of a heavy quarkonium state $|H\rangle$ into light particles may be written as

$$\Gamma(H\to light\ particles) = 2\,\mathrm{Im}\,\langle H|\mathcal{L}_{\psi\chi}|H\rangle, \qquad (4.13)$$

where $\mathcal{L}_{\psi\chi}$ is given by Eq. (1.8) of Chapter 1 up to four-fermion operators of dimension 6. The low-energy dynamics is encoded in the matrix elements of the four-fermion operators evaluated on the heavy-quarkonium state. If one assumes that only heavy-quarkonium states with quark-antiquark in a colour-singlet configuration can exist, then only colour-singlet four-fermion operators contribute and the matrix elements reduce to heavy-quarkonium wave functions (or derivatives of them) calculated at the origin.

[5] Authors: T. Ferguson, C. Patrignani, A. Vairo

[6] We refer to Chapter 1 for a basic introduction to effective field theories and NRQCD.

Table 4.1: Quantum numbers of quarkonium states and the minimal number of virtual gluons and photons into which they can annihilate. The subscript d refers to a gluonic colour-singlet state that is totally symmetric under permutations of the gluons.

	$^{2S+1}L_J$	$I^G(J^{PC})$	gluons	photons
η_c, η_b	$^1S_0$	$0^+(0^{-+})$	2g	2γ
J/ψ, $\Upsilon(1S)$	$^3S_1$	$0^-(1^{--})$	$(3g)_d$	γ
h_c, h_b	$^1P_1$	$0^-(1^{+-})$	$(3g)_d$	3γ
χ_{c0}, χ_{b0}	$^3P_0$	$0^+(0^{++})$	2g	2γ
χ_{c1}, χ_{b1}	$^3P_1$	$0^+(1^{++})$	2g	2γ
χ_{c2}, χ_{b2}	$^3P_2$	$0^+(2^{++})$	2g	2γ

This assumption is known as the "colour-singlet model". Explicit calculations show that at higher order the colour-singlet matching coefficients develop infrared divergences (for P waves this happens at NLO [12]). In the colour-singlet model, these do not cancel in the expression of the decay widths. It has been the first success of NRQCD [13, 14] to show that the Fock space of a heavy-quarkonium state may contain a small component of quark–antiquark in a colour-octet configuration, bound with some gluonic degrees of freedom (the component is small because operators coupling transverse gluons with quarks are suppressed by powers of $v \ll 1$, v being the heavy-quark velocity in the centre-of-mass frame), that due to this component, matrix elements of colour-octet four-fermion operators contribute and that exactly these contributions absorb the infrared divergences of the colour-singlet matching coefficients in the decay widths, giving rise to finite results [14, 15]. NRQCD is now the standard framework to study heavy-quarkonium inclusive decays.

The NRQCD factorization formulas are obtained by separating contributions coming from degrees of freedom of energy m from those coming from degrees of freedom of lower energy. In the case of heavy-quarkonium decay widths, they have been rigorously proved [14]. High-energy contributions are encoded into the imaginary parts of the four-fermion matching coefficients, $f, g_{1,8,ee,\gamma\gamma,\ldots}(^{2S+1}L_J)$ and are ordered in powers of α_s (coefficients labeled with ee, $\gamma\gamma$, ... refer to pure electromagnetic decays into e^+e^-, $\gamma\gamma$, ...). Low-energy contributions are encoded into the matrix elements of the four-fermion operators on the heavy-quarkonium states $|H\rangle$ ($\langle\ldots\rangle_H \equiv \langle H|\ldots|H\rangle$). These are, in general, nonperturbative objects, which can scale as powers of $\Lambda_{\rm QCD}$, mv, mv^2, ... (i.e., of the low-energy dynamical scales of NRQCD). Therefore, matrix elements of higher dimensionality are suppressed by powers of v or $\Lambda_{\rm QCD}/m$. Including up to four-fermion operators of dimension 8, the NRQCD factorization formulas for inclusive decay widths of heavy quarkonia into light hadrons, which follow from Eq. (4.13), read [14, 15]:

$$\begin{aligned}\Gamma(V_Q(nS) \to l.h.) = \frac{2}{m^2}\Bigg(& \mathrm{Im}\, f_1(^3S_1)\, \langle O_1(^3S_1)\rangle_{V_Q(nS)} \\ & + \mathrm{Im}\, f_8(^3S_1)\, \langle O_8(^3S_1)\rangle_{V_Q(nS)} + \mathrm{Im}\, f_8(^1S_0)\, \langle O_8(^1S_0)\rangle_{V_Q(nS)} \\ & + \mathrm{Im}\, g_1(^3S_1)\, \frac{\langle \mathcal{P}_1(^3S_1)\rangle_{V_Q(nS)}}{m^2} + \mathrm{Im}\, f_8(^3P_0)\, \frac{\langle O_8(^3P_0)\rangle_{V_Q(nS)}}{m^2} \\ & + \mathrm{Im}\, f_8(^3P_1)\, \frac{\langle O_8(^3P_1)\rangle_{V_Q(nS)}}{m^2} + \mathrm{Im}\, f_8(^3P_2)\, \frac{\langle O_8(^3P_2)\rangle_{V_Q(nS)}}{m^2}\Bigg), \end{aligned} \quad (4.14)$$

$$\Gamma(P_Q(nS) \to l.h.) = \frac{2}{m^2}\Bigg(\mathrm{Im}\, f_1(^1S_0)\, \langle O_1(^1S_0)\rangle_{P_Q(nS)} + \mathrm{Im}\, f_8(^1S_0)\, \langle O_8(^1S_0)\rangle_{P_Q(nS)} + \mathrm{Im}\, f_8(^3S_1)\, \langle O_8(^3S_1)\rangle_{P_Q(nS)} + \mathrm{Im}\, g_1(^1S_0)\, \frac{\langle \mathcal{P}_1(^1S_0)\rangle_{P_Q(nS)}}{m^2} + \mathrm{Im}\, f_8(^1P_1)\, \frac{\langle O_8(^1P_1)\rangle_{P_Q(nS)}}{m^2}\Bigg), \quad (4.15)$$

$$\Gamma(\chi_Q(nJS) \to l.h.) = \frac{2}{m^2}\Bigg(\mathrm{Im}\, f_1(^{2S+1}P_J)\, \frac{\langle O_1(^{2S+1}P_J)\rangle_{\chi_Q(nJS)}}{m^2} + \mathrm{Im}\, f_8(^{2S+1}S_S)\, \langle O_8(^1S_0)\rangle_{\chi_Q(nJS)}\Bigg). \quad (4.16)$$

At the same order the electromagnetic decay widths are given by:

$$\Gamma(V_Q(nS) \to e^+e^-) = \frac{2}{m^2}\Bigg(\mathrm{Im}\, f_{ee}(^3S_1)\, \langle O_{\rm EM}(^3S_1)\rangle_{V_Q(nS)} + \mathrm{Im}\, g_{ee}(^3S_1)\, \frac{\langle \mathcal{P}_{\rm EM}(^3S_1)\rangle_{V_Q(nS)}}{m^2}\Bigg), \quad (4.17)$$

$$\Gamma(P_Q(nS) \to \gamma\gamma) = \frac{2}{m^2}\Bigg(\mathrm{Im}\, f_{\gamma\gamma}(^1S_0)\, \langle O_{\rm EM}(^1S_0)\rangle_{P_Q(nS)} + \mathrm{Im}\, g_{\gamma\gamma}(^1S_0)\, \frac{\langle \mathcal{P}_{\rm EM}(^1S_0)\rangle_{P_Q(nS)}}{m^2}\Bigg), \quad (4.18)$$

$$\Gamma(\chi_Q(nJ1) \to \gamma\gamma) = 2\,\mathrm{Im}\, f_{\gamma\gamma}(^3P_J)\, \frac{\langle O_{\rm EM}(^3P_J)\rangle_{\chi_Q(nJ1)}}{m^4}, \quad J = 0, 2\,. \quad (4.19)$$

The symbols V_Q and P_Q indicate respectively the vector and pseudoscalar S-wave heavy quarkonium and the symbol χ_Q the generic P-wave quarkonium (the states $\chi_Q(n10)$ and $\chi_Q(nJ1)$ are usually called $h_Q((n-1)P)$ and $\chi_{QJ}((n-1)P)$, respectively).

The operators $O, \mathcal{P}_{1,8,\rm EM}(^{2S+1}L_J)$ are the dimension 6 and 8 four-fermion operators of the NRQCD Lagrangian. They are classified by their transformation properties under colour as singlets (1) and octets (8), and under spin (S), orbital (L) and total angular momentum (J). The operators with the subscript EM are the colour-singlet operators projected on the QCD vacuum. The explicit expressions of the operators can be found in [14] (or listed in Appendix A of [16]). The dimension 6 operators are also given in Eq. (1.8) of Chapter 1.

In general different power countings are possible at the level of NRQCD, due to the fact that different scales (mv, $\Lambda_{\rm QCD}$, mv^2, $\sqrt{m\Lambda_{\rm QCD}}$, ...) are still dynamically entangled [17, 18]. Likely different power countings will apply to different physical systems. Therefore, the relative importance of the different matrix elements that appear in Eqs. (4.14)–(4.19) may change in going from lower to higher quarkonium states and from bottomonium to charmonium. Whatever the power counting is, the pseudoscalar and vector state decay widths are dominated by the colour-singlet matrix elements, which contribute at order mv^3. The hadronic P-state decay widths have two contributions (the colour-singlet and colour-octet matrix elements), which contribute at the same order mv^5, if we assume that a fraction v of the P-state wave function projects onto the colour-octet operator.

Since NRQCD is an expansion in two small parameters ($\alpha_{\rm s}$ and v), progress comes typically from (1) improving the perturbative series of the matching coefficients either by fixed order calculations or by resumming large contributions (large logs or large contributions associated to renormalon singularities);

(2) improving the knowledge of the NRQCD matrix elements either by direct evaluation, which may be obtained by fitting the experimental data, by lattice calculations, and by models, or by exploiting the hierarchy of scales still entangled in NRQCD and constructing EFTs of lower energy.

3.1.1 The perturbative expansion

The imaginary parts of the four-fermion matching coefficients have been calculated over the last twenty years to different levels of precision. Up to order α_s^3 the imaginary parts of $f_8(^1S_0)$, $f_1(^3P_1)$, and $f_8(^3P_J)$ can be found in [19], the imaginary parts of $f_8(^3S_1)$, $f_8(^1P_1)$ in [20] and the imaginary part of $f_1(^1S_0)$ in [19,21]. Two different determinations of $f_1(^3P_0)$ and $f_1(^3P_2)$ exist at NLO in [19] and [22]. The imaginary part of $f_1(^3S_1)$ has been calculated (numerically) up to order α_s^4 in [23]. The imaginary part of $g_1(^3S_1)$ at order α_s^3 can be found in [24], the imaginary part of $g_1(^1S_0)$ at order α_s^2 in [14]. Where the electromagnetic coefficients are concerned, the imaginary part of $f_{ee}(^3S_1)$ has been calculated up to order $\alpha^2\alpha_s^2$ in [25,26], the imaginary parts of $f_{\gamma\gamma}(^1S_0)$ and $f_{\gamma\gamma}(^3P_{0,2})$ up to order $\alpha^2\alpha_s$ can be found in [19,27] and $g_{ee}(^3S_1)$ and $g_{\gamma\gamma}(^1S_0)$ up to order α^2 in [14]. A complete list of the above matching coefficients at our present level of knowledge can be found in Appendix A of [28]. The LL running for the imaginary parts of the matching coefficients of the four-fermion NRQCD operators of dimension 6 and 8 have been obtained in [16] and can be read there in Appendix C. The tree-level matching of dimension 9 and 10 S-wave operators can be found in [29]. The tree-level matching of dimension 9 and 10 electromagnetic P-wave operators can be found in [30].

The convergence of the perturbative series of the four-fermion matching coefficients is often poor. While the large two-loop contribution of $\mathrm{Im}\, f_{ee}(^3S_1)$ seems to be related, at least in the bottomonium case, to the factorization scale and, therefore, may be put presumably under control via renormalization group improvement techniques [26,31], large corrections appearing in other S-wave decay channels have been ascribed to renormalon-type contributions [32]. There is no such study so far for P-wave decays.

3.1.2 The relativistic expansion

The NRQCD matrix elements may be fitted to the experimental decay data [33–35] or calculated on the lattice [36, 37]. The matrix elements of colour-singlet operators can be linked at leading order to the Schrödinger wave functions at the origin [14][7] and, hence, may be evaluated by means of potential models [38] or potentials calculated on the lattice [39]. In [34] by fitting to the charmonium P-wave decay data it was obtained that $\langle O_1(^1P_1)\rangle_{h_c(1P)} \approx 8.1 \times 10^{-2}$ GeV^5 and $\langle O_8(^1S_0)\rangle_{h_c(1P)} \approx 5.3 \times 10^{-3}$ GeV^3 in the $\overline{\mathrm{MS}}$ scheme and at the factorization scale of 1.5 Gev. In the quenched lattice simulation of [37] it was obtained that $\langle O_1(^1S_0)\rangle_{\eta_c(1S)} \approx 0.33$ GeV^3, $\langle O_1(^1P_1)\rangle_{h_c(1P)} \approx 8.0 \times 10^{-2}$ GeV^5 and $\langle O_8(^1S_0)\rangle_{h_c(1P)} \approx 4.7 \times 10^{-3}$ GeV^3 in the $\overline{\mathrm{MS}}$ scheme and at the factorization scale of 1.3 Gev. In the lattice simulation of [36] and in the three light-quark flavours extrapolation limit it was obtained that $\langle O_1(^1S_0)\rangle_{\eta_b(1S)} \approx 4.1$ GeV^3, $\langle O_1(^1P_1)\rangle_{h_b(1P)} \approx 3.3$ GeV^5 and $\langle O_8(^1S_0)\rangle_{h_b(1P)} \approx 5.9 \times 10^{-3}$ GeV^3 in the $\overline{\mathrm{MS}}$ scheme and at the factorization scale of 4.3 GeV.

It has been discussed in [30] and [29], that higher-order operators, not included in the formulas (4.14)–(4.19), even if parametrically suppressed, may turn out to give sizable contributions to the decay widths. This may be the case, in particular, for charmonium, where $v^2 \sim 0.3$, so that relativistic corrections are large, and for P-wave decays where the above formulas provide, indeed, only the leading-order contribution in the velocity expansion. In fact it was pointed out in [30] (see also [40]) that if no special cancellations among the matrix elements occur, then the order v^2 relativistic corrections to the electromagnetic decays $\chi_{c0}\to\gamma\gamma$ and $\chi_{c2}\to\gamma\gamma$ may be as large as the leading terms.

In [24, 34] it was also noted that the numerical relevance of higher-order matrix elements may be enhanced by their multiplying matching coefficients. This is, indeed, the case for the decay width of S-wave vector states, where the matching coefficients multiplying the colour-octet matrix elements (with

[7] This statement acquires a precise meaning only in the context of pNRQCD, see Section 3.1.3.

the only exception of $\mathrm{Im}f_8(^3P_1)$) are enhanced by α_s with respect to the coefficient $\mathrm{Im}f_1(^3S_1)$ of the leading colour-singlet matrix element.

In the bottomonium system, 14 S- and P-wave states lie below the open flavour threshold ($\Upsilon(nS)$ and $\eta_b(nS)$ with $n = 1, 2, 3$; $h_b(nP)$ and $\chi_{bJ}(nP)$ with $n = 1, 2$ and $J = 0, 1, 2$) and in the charmonium system 8 ($\psi(nS)$ and $\eta_c(nS)$ with $n = 1, 2$; $h_c(1P)$ and $\chi_{cJ}(1P)$ with $J = 0, 1, 2$). For these states Eqs. (4.14)–(4.19) describe the decay widths into light hadrons and into photons or e^+e^- in terms of 46 NRQCD matrix elements (40 for the S-wave decays and 6 for the P-wave decays), assuming the most conservative power counting. More matrix elements are needed if higher-order operators are included.

3.1.3 pNRQCD

The number of nonperturbative parameters may be reduced by integrating out from NRQCD degrees of freedom with energy lower than m, since each degree of freedom that is integrated out leads to a new factorization. Eventually, one ends up with pNRQCD [41, 42], where only degrees of freedom of energy mv^2 are left dynamical. In the context of pNRQCD, the NRQCD four-fermion matrix elements can be written either as convolutions of Coulomb amplitudes with non-local correlators (in the dynamical situation $mv^2 \gtrsim \Lambda_{\mathrm{QCD}}$) or as products of wave functions at the origin by non-local correlators (in the dynamical situation $mv^2 \ll \Lambda_{\mathrm{QCD}}$).

The first situation may be the relevant one at least for the bottomonium ground state [42–44]. In the limiting case $mv^2 \gg \Lambda_{\mathrm{QCD}}$, the correlators reduce to local condensates and explicit formulas have been worked out in [45, 46]. Concerning the perturbative calculation of the electromagnetic decay widths, the NLL renormalization group improved expression can be found in [47] and has been used in a phenomenological analysis in [48]. The perturbative wave functions at the origin at NNLO order can be found in [49]. Recently, a full NNLL analysis has been carried out in [31]; the authors predict $\Gamma(\eta_b \to \gamma\gamma)/\Gamma(\Upsilon(1S) \to e^+e^-) = 0.502 \pm 0.068 \pm 0.014$, where the first error is an estimate of the theoretical uncertainty and the second reflects the uncertainty in α_s. We also mention that there exists a determination of $\Gamma(\Upsilon(2S) \to e^+e^-) \,/\, \Gamma(\Upsilon(1S) \to e^+e^-)$ in lattice NRQCD with 2+1 flavours of dynamical quarks [50]. The calculated ratio is still far from the experimental result, although the unquenching has considerably reduced the discrepancy.

The last situation is expected to be the relevant one for most of the existing excited heavy-quarkonium states (with the possible exception of the lowest bottomonium states) and has been studied in [16, 51, 52]. However, a general consensus on the above assignments of heavy-quarkonium states to dynamical regions has not been reached yet (see also Chapter 3).

At leading order in the v and Λ_{QCD}/m expansion, the colour-singlet matrix elements can be expressed in terms of the wave functions at the origin only [14, 16]:

$$\begin{aligned}\langle O_1(^3S_1)\rangle_{V_Q(nS)} &= \langle O_1(^1S_0)\rangle_{P_Q(nS)} = \langle O_{\mathrm{EM}}(^3S_1)\rangle_{V_Q(nS)} \\ &= \langle O_{\mathrm{EM}}(^1S_0)\rangle_{P_Q(nS)} = C_A \frac{|R^{(0)}_{n0}(0)|^2}{2\pi}, \end{aligned} \tag{4.20}$$

$$\langle O_1(^{2S+1}P_J)\rangle_{\chi_Q(nJS)} = \langle O_{\mathrm{EM}}(^{2S+1}P_J)\rangle_{\chi_Q(nJS)} = \frac{3}{2}\frac{C_A}{\pi}|R^{(0)\prime}_{n1}(0)|^2, \tag{4.21}$$

where $R^{(0)}_{n\ell}$ is the zeroth-order radial part of the heavy-quarkonium wave function, obtained from the pNRQCD Hamiltonian [18, 53] and $C_A = N_c = 3$.

In the situation $mv^2 \ll \Lambda_{\mathrm{QCD}}$ there are no dynamical gluons at energies of order mv^2. Under the conditions that: (a) all higher gluonic excitations between the two heavy quarks develop a mass gap of order Λ_{QCD}, (b) threshold effects are small, and (c) contributions coming from virtual pairs of quark–antiquark with three-momentum of order $\sqrt{m\Lambda_{\mathrm{QCD}}}$ are subleading,[8] the NRQCD colour-octet matrix

[8] Condition (b) may be problematic for the $\psi(2S)$, whose mass is very close to the $D\bar{D}$ production threshold.

elements relevant for Eqs. (4.14)–(4.19) can be written at leading order in the v and $\Lambda_{\rm QCD}/m$ expansion as [16, 51]:

$$\langle O_8(^3S_1)\rangle_{V_Q(nS)} = \langle O_8(^1S_0)\rangle_{P_Q(nS)} = C_A \frac{|R^{(0)}_{n0}(0)|^2}{2\pi}\left(-\frac{2(C_A/2-C_F)\mathcal{E}_3^{(2)}}{3m^2}\right), \tag{4.22}$$

$$\langle O_8(^1S_0)\rangle_{V_Q(nS)} = \frac{\langle O_8(^3S_1)\rangle_{P_Q(nS)}}{3} = C_A \frac{|R^{(0)}_{n0}(0)|^2}{2\pi}\left(-\frac{(C_A/2-C_F)c_F^2\mathcal{B}_1}{3m^2}\right), \tag{4.23}$$

$$\frac{\langle O_8(^3P_J)\rangle_{V_Q(nS)}}{2J+1} = \frac{\langle O_8(^1P_1)\rangle_{P_Q(nS)}}{9} = C_A \frac{|R^{(0)}_{n0}(0)|^2}{2\pi}\left(-\frac{(C_A/2-C_F)\mathcal{E}_1}{9}\right), \tag{4.24}$$

$$\langle O_8(^1S_0)\rangle_{\chi_Q(nJS)} = \frac{T_F}{3}\frac{|R^{(0)\prime}_{n1}(0)|^2}{\pi m^2}\mathcal{E}_3, \tag{4.25}$$

where c_F stands for the chromomagnetic matching coefficient, which is known at NLL [54], $C_F = (N_c^2-1)/(2N_c) = 4/3$ and $T_F = 1/2$. Therefore, at the considered order, the colour-octet matrix elements factorize into the product of the heavy-quarkonium wave function with some chromoelectric and chromomagnetic correlator (Wilson lines connecting the fields are not explicitly shown, but understood):

$$\mathcal{E}_n = \frac{1}{N_c}\int_0^\infty dt\, t^n \langle {\rm Tr}(g\mathbf{E}(t)\cdot g\mathbf{E}(0))\rangle, \qquad \mathcal{B}_n = \frac{1}{N_c}\int_0^\infty dt\, t^n \langle {\rm Tr}(g\mathbf{B}(t)\cdot g\mathbf{B}(0))\rangle, \tag{4.26}$$

$$\mathcal{E}_3^{(2)} = \frac{1}{4N_c}\int_0^\infty dt_1\int_0^{t_1} dt_2\int_0^{t_2} dt_3\,(t_2-t_3)^3\Big\{\langle {\rm Tr}(\{g\mathbf{E}(t_1)\cdot, g\mathbf{E}(t_2)\}\,\{g\mathbf{E}(t_3)\cdot, g\mathbf{E}(0)\})\rangle_c - \frac{4}{N_c}\langle {\rm Tr}(g\mathbf{E}(t_1)\cdot g\mathbf{E}(t_2))\,{\rm Tr}(g\mathbf{E}(t_3)\cdot g\mathbf{E}(0))\rangle_c\Big\}, \tag{4.27}$$

where

$$\langle {\rm Tr}\,(g\mathbf{E}(t_1)\cdot g\mathbf{E}(t_2)\; g\mathbf{E}(t_3)\cdot g\mathbf{E}(0))\rangle_c = \langle {\rm Tr}\,(g\mathbf{E}(t_1)\cdot g\mathbf{E}(t_2)\; g\mathbf{E}(t_3)\cdot g\mathbf{E}(0))\rangle - \frac{1}{N_c}\langle {\rm Tr}(g\mathbf{E}(t_1)\cdot g\mathbf{E}(t_2))\rangle\langle {\rm Tr}(g\mathbf{E}(t_3)\cdot g\mathbf{E}(0))\rangle. \tag{4.28}$$

These correlators are universal in the sense that they do not depend on the heavy-quarkonium state and, hence, may be calculated once and for all, either by means of lattice simulations [55], or specific models of the QCD vacuum [56], or extracted from some set of experimental data [51].

Finally, at leading order the matrix elements of the $\mathcal{P}_1$ operators can be written as:

$$\langle \mathcal{P}_1(^3S_1)\rangle_{V_Q(nS)} = \langle \mathcal{P}_1(^1S_0)\rangle_{P_Q(nS)} = \langle \mathcal{P}_{\rm EM}(^3S_1)\rangle_{V_Q(nS)} = \langle \mathcal{P}_{\rm EM}(^1S_0)\rangle_{P_Q(nS)} = C_A\frac{|R^{(0)}_{n0}(0)|^2}{2\pi}\left(mE^{(0)}_{n0}-\mathcal{E}_1\right), \tag{4.29}$$

where $E^{(0)}_{n0} \simeq M - 2m \sim mv^2$ is the leading-order binding energy. Equation (4.29) reduces to the formula obtained in [24] if the heavy-quarkonium state satisfies also the condition $mv \gg \Lambda_{\rm QCD}$.

The leading corrections to the above formulas come from quark–antiquark pairs of three momentum of order $\sqrt{m\Lambda_{\rm QCD}}$. The existence of this degree of freedom in the heavy-quarkonium system has been pointed out in [52], where the leading correction to Eq. (4.20) has been calculated.

The pNRQCD factorization formulas reduce, when applicable, the number of nonperturbative parameters needed to describe heavy-quarkonium decay widths [16]. In particular, using charmonium data to extract $\mathcal{E}_3$, in Ref. [51] it was found $\mathcal{E}_3(1{\rm GeV}) = 5.3^{+3.5}_{-2.2}$, where the errors account for the experimental uncertainties only. This value has been used to predict P-wave bottomonium inclusive decay widths in [51, 57]. We will come back to this in Section 3.2.4.

3.2 Experimental status

This section is a snapshot of the current status of various experimental results on the electromagnetic and inclusive hadronic decays of heavy-quarkonium states. The results come from the CLEO experiment at CESR, the BES experiment at BEPC and E835 at Fermilab.

3.2.1 Υ widths

Crucial parameters for any heavy-quarkonium state are its total width and its hadronic and three leptonic partial widths. For the three Υ bound states, since their total widths, $\Gamma_{\rm tot}$, are much less than the energy spread of the CESR machine ($\approx$ 4 MeV) where they are studied, the procedure is to scan over each resonance measuring the hadronic and $\mu^+\mu^-$ rates. Then we use:

$$\int \sigma_{\rm had}\, dE_{\rm cm} \;\propto\; \left(\frac{\Gamma_{ee}\,\Gamma_{\rm had}}{\Gamma_{\rm tot}}\right) \quad \text{and} \quad \mathcal{B}_{\mu\mu} \;=\; \frac{\Gamma_{\mu\mu}}{\Gamma_{\rm tot}}. \tag{4.30}$$

Assuming lepton universality, we have: $\Gamma_{\rm tot} \;=\; \Gamma_{\rm had} \;+\; 3\;\Gamma_{\ell\ell}$. This allows us to solve for the total width and the partial widths into electrons and hadrons:

$$\Gamma_{ee} \;=\; \frac{(\Gamma_{ee}\Gamma_{\rm had}/\Gamma_{\rm tot})}{1 \;-\; 3\;\mathcal{B}_{\mu\mu}}, \qquad \Gamma_{\rm tot} = \frac{\Gamma_{ee}}{\mathcal{B}_{\mu\mu}}, \qquad \Gamma_{\rm had} \;=\; \Gamma_{\rm tot}(1-3\mathcal{B}_{\mu\mu})\,. \tag{4.31}$$

Once the total width is known, the partial width into $\tau^+\tau^-$ can then be determined from its respective branching ratio. The current experimental status from the 2004 PDG [10] is shown in Table 4.2.

Table 4.2: Present PDG values [10] for the parameters of the Υ states.

Resonance	$\Gamma_{\rm tot}$ (keV)(% error)	Γ_{ee} (keV)(% error)	$\mathcal{B}_{\mu\mu}$(%)(% error)	$\mathcal{B}_{\tau\tau}$(%)(% error)
Υ(1S)	53.0 $\pm$ 1.5 (2.8%)	1.314 $\pm$ 0.029 (2.2%)	2.48 $\pm$ 0.06 (2.4%)	2.67 $\pm$ 0.15 (5.6%)
Υ(2S)	43 $\pm$ 6 (14%)	0.576 $\pm$ 0.024 (4.2%)	1.31 $\pm$ 0.21 (16%)	1.7 $\pm$ 1.6 (94%)
Υ(3S)	26.3 $\pm$ 3.4 (13%)	–	1.81 $\pm$ 0.17 (9.4%)	–

The PDG does not use the 1984 CLEO measurement of $\Gamma_{ee}(3S) \;=\; 0.42 \;\pm\; 0.05$ keV because new radiative corrections have now been accepted which were not used in that analysis, thus invalidating the measurement. From the large percentage errors on many of the quantities in the table, it is obvious that there is much room for improvement. To this end, the CLEO III detector devoted a large amount of running at each of the three Υ resonances, as shown in Table 4.3.

Table 4.3: Summary of the CLEO III running at the three Υ bound states.

Resonance	$\int$ L dt (fb^{-1})	Number of Decays (M)	Factor Increase Over CLEO!II
Υ(1S)	1.2	29	15
Υ(2S)	0.9	6.0	12
Υ(3S)	1.5	6.5	14

All the results from this running have not yet been finalized, but new measurements of the muonic branching ratios for the 3 bound Υ states have been published [58]. These new measurements are shown in Table 4.4, along with the corresponding new values for the total widths. The new $\Upsilon(2S)$ and $\Upsilon(3S)$

Table 4.4: New CLEO measurements [58] of the muonic branching ratios for the 3 Υ states, along with their statistical and systematic errors and the corresponding new values for the total widths.

Resonance	$\mathcal{B}_{\mu\mu}$(%)(% error)	$\Gamma_{\rm tot}$ (keV)(% error)
Υ(1S)	2.49 $\pm$ 0.02 $\pm$ 0.07 (2.8%)	52.8 $\pm$ 1.8 (3.4%)
Υ(2S)	2.03 $\pm$ 0.03 $\pm$ 0.08 (4.0%)	29.0 $\pm$ 1.6 (5.5%)
Υ(3S)	2.39 $\pm$ 0.07 $\pm$ 0.10 (5.1%)	20.3 $\pm$ 2.1 (10.3%)

muonic branching ratio measurements are substantially higher than previous results, giving correspondingly smaller total widths for these resonances.

From the number of detected hadronic and leptonic events and a knowledge of the CLEO detector performance, estimates of the final statistical and systematic errors for the other resonance parameters can be made. These are shown in Table 4.5. Thus, once the analyses are complete, there will be a tremendous improvement in our knowledge of the basic parameters of the Υ bound-state resonances.

Table 4.5: Expected fractional errors for various quantities from the eventual CLEO III measurements.

Parameter	Statistical Error	Systematic Error	Total Error
$\Gamma_{ee}\Gamma_{\rm had}/\Gamma_{\rm tot}$	1%	2.5%	3%
Γ_{ee}	2%	2%	3%
$\mathcal{B}_{\tau\tau}$	2%	3%	4%
$\Gamma_{\rm tot}$	2%	3%	4%

3.2.2 J/ψ and $\psi(2S)$ widths

In the last two years the knowledge of both J/ψ and $\psi(2S)$ parameters has improved. In 2002, the BES collaboration reported results [59] from a new scan of the $\psi(2S)$ resonance, corresponding to an integrated luminosity of 1.15 pb^{-1} and 114k $\psi(2S)$ hadronic decays. In 2004 BaBar has presented the first measurement of $\Gamma_{ee}\mathcal{B}_{\mu\mu}$ [9] from ISR production of J/ψ in 88.4 fb^{-1} taken at the $\Upsilon(4S)$ resonance. Table4.6 lists the values of the widths and leptonic branching ratios for J/ψ and $\psi(2S)$ from PDG [10].

Table 4.6: Present PDG values [10] for the parameters of the J/ψ and $\psi(2S)$ states.

Resonance	$\Gamma_{\rm tot}$ (keV)(% error)	Γ_{ee} (keV)(% error)	$\mathcal{B}_{\mu\mu}$(%)(% error)	$\mathcal{B}_{\tau\tau}$(%)(% error)
J/ψ	91.0 $\pm$ 3.2 (3.5%)	5.40 $\pm$ 0.15$\pm$0.07 (3.1%)	5.88 $\pm$ 0.10 (1.7%)	—
ψ(2S)	281 $\pm$ 17 (6%)	2.12 $\pm$ 0.12 (9%)	0.73 $\pm$ 0.08 (11%)	0.28$\pm$ 0.07 (25%)

3.2.3 Two-photon partial widths measurements

Experimental determinations of two-photon partial widths of quarkonia depend on measurements of products and ratios of branching ratios performed by more than one experiment, and the best estimate

is obtained from a global fit to directly measured quantities as it is done by the PDG [10]. When more measurements are available, subsets of measurements may allow a direct extraction of the value for $\Gamma_{\gamma\gamma}$, in general with a larger error than a global fit. But this can be useful both as a cross check for the global fit and to identify which measurements could yield improvements.

The simplest case is the χ_{c2}, where direct measurements of three independent quantities allows one to extract $\Gamma_{\gamma\gamma}$ and $\Gamma_{J/\psi\gamma}$:

$$\Gamma = 2.00 \pm 0.18\,\mathrm{MeV}, \tag{4.32}$$

$$\Gamma_{\gamma\gamma}\mathcal{B}_{J/\psi\gamma} = 121 \pm 13\,\mathrm{eV}\ , \tag{4.33}$$

and

$$\frac{\mathcal{B}_{\gamma\gamma}}{\mathcal{B}_{J/\psi\gamma}} = (1.02 \pm 0.15)\cdot 10^{-3}, \tag{4.34}$$

where experimental values are world averages [10] except in Eq. (4.34) where we averaged the E835 result with the ratio of $\mathcal{B}_{p\bar{p}}\mathcal{B}_{\gamma\gamma}$ and $\mathcal{B}_{p\bar{p}}\mathcal{B}_{J/\psi\gamma}$ measured by E760 [61, 62]. The product of Eq. (4.32), Eq. (4.33), and Eq. (4.34), yields $\Gamma_{\gamma\gamma} = 0.50 \pm 0.05$ keV, while taking Eq. (4.33) multiplied by Eq. (4.32) and divided by Eq. (4.34), we would obtain $\Gamma_{J/\psi\gamma} = 490 \pm 50\,\mathrm{keV}$, or $\mathcal{B}_{J/\psi\gamma} = 0.244 \pm 0.024$. The global fit to all measurements [10] (including all other measurements related to $\mathcal{B}_{J/\psi\gamma}$) improves on $\Gamma_{J/\psi\gamma} = 430 \pm 40\,\mathrm{keV}$ and $\mathcal{B}_{J/\psi\gamma} = 0.202 \pm 0.017$, but has almost no effect on $\Gamma_{\gamma\gamma} = 0.52 \pm 0.05$ keV, indicating that the measurements considered above are the only ones relevant to $\Gamma_{\gamma\gamma}$.

The case for χ_{c0} is similar to that of the χ_{c2}, even if apparently more complicated. The world average of total width measurements is [10]

$$\Gamma = 10.2 \pm 0.9\,\mathrm{MeV}. \tag{4.35}$$

There is a measurement of

$$\Gamma_{\gamma\gamma}\mathcal{B}_{2\pi^+2\pi^-} = 75 \pm 13 \pm 8\ \mathrm{eV}\ \ [63], \tag{4.36}$$

and measurements (from a single experiment) of $\mathcal{B}_{p\bar{p}}\mathcal{B}_{\gamma\gamma}$ [64] and $\mathcal{B}_{p\bar{p}}\mathcal{B}_{\pi^0\pi^0}$ [6], from which we can calculate (assuming isospin symmetry) the ratio

$$\frac{\mathcal{B}_{\gamma\gamma}}{\mathcal{B}_{\pi\pi}} = 0.043 \pm 0.011\ . \tag{4.37}$$

Even if $\mathcal{B}_{\pi\pi}$ and $\mathcal{B}_{2\pi^+2\pi^-}$ are not directly measured, their ratio can be determined from quantities measured by a single experiment (in this case BES [65–67]):

$$\frac{\mathcal{B}_{\pi\pi}}{\mathcal{B}_{2\pi^+2\pi^-}} = 0.47 \pm 0.10\,. \tag{4.38}$$

This means that we can extract $\Gamma_{\gamma\gamma} = 3.9 \pm 0.8$ keV from the product of the four quantities in Eqs. (4.35), (4.36), (4.37), and (4.38). Notice that including MARK II measurements in the evaluation of Eq. (4.38) would give $\Gamma_{\gamma\gamma} = 3.1 \pm 0.8$. The global fit (which does not include the new measurement of $\mathcal{B}_{p\bar{p}}\mathcal{B}_{\gamma\gamma}$ [64]) yields a significantly more precise value $\Gamma_{\gamma\gamma} = 2.6 \pm 0.5$ keV, indicating that in this case there are other measurements that are relevant, such as $\mathcal{B}(\psi(2S)\to\gamma\chi_{c0}\to 3\gamma)$.

The case for $\eta_c(1S)$ and $\eta_c(2S)$ is different. To date these states have been observed in two-photon reactions with direct measurement of

$$\eta_c(1S): \quad \Gamma_{\gamma\gamma}\mathcal{B}_{K\bar{K}\pi} = 0.48 \pm 0.06\ \mathrm{keV}\,, \tag{4.39}$$

$$\eta_c(2S): \quad \Gamma_{\gamma\gamma}\mathcal{B}_{K\bar{K}\pi} = 73 \pm 23\ \mathrm{eV}\ \ [68]\,. \tag{4.40}$$

The $\eta_c(1S)$ has also been observed in $\bar{p}p$ annihilations with direct measurement of

$$\mathcal{B}_{\gamma\gamma}\mathcal{B}_{p\bar{p}} = (0.26 \pm 0.05) \times 10^{-6}. \tag{4.41}$$

In this case there are no measurements of the ratio of branching ratios between the $\gamma\gamma$ and any other decay mode, so it is necessary to use the values of $\mathcal{B}_{K\bar{K}\pi}$ or $\mathcal{B}_{p\bar{p}}$ that (for $\eta_c(1S)$ only) are determined by

$$\mathcal{B}_X = \frac{\mathcal{B}(J/\psi \to \gamma\eta_c \to \gamma\, X)}{\mathcal{B}(J/\psi \to \gamma\eta_c)}, \tag{4.42}$$

with precision limited by the $\approx 30\%$ uncertainty in $\mathcal{B}(J/\psi \to \gamma\eta_c)$ that is to date a common systematic to all two-photon partial widths of $\eta_c(1S)$. Since no measurement is yet available for the $\eta_c(2S)$ branching ratio to $K\bar{K}\pi$, its $\Gamma_{\gamma\gamma}$ cannot be determined.

The most obvious strategy to increase the precision on $\Gamma_{\gamma\gamma}$ is to improve the measurements for quantities used in its determination. But based on the case of χ_{c2} discussed above, a major improvement could be obtained by measuring the pair of quantities $\Gamma_{\gamma\gamma}\mathcal{B}_X$ and $\mathcal{B}_{\gamma\gamma}/\mathcal{B}_X$ for more than one final state X. B factories can reasonably measure to $< 10\%$ precision $\Gamma_{\gamma\gamma}\mathcal{B}_X$ for more than one final state. It is also reasonable that total widths will be more precisely measured in $p\bar{p}$ experiments, thus the question is whether it is possible to measure to better than 10% the ratios $\mathcal{B}_{\gamma\gamma}/\mathcal{B}_X$. How well can BES and CLEO measure $\psi(2S)$ or J/ψ to 3γ? How well can $\bar{p}p \to \gamma\gamma$ be measured and what are the channels that could be measured in these experiments simultaneously to $\bar{p}p \to \gamma\gamma$? With a magnetic detector, $p\bar{p} \to \phi\phi$ is the obvious choice, but interference with two-body non-resonant reactions may offer other opportunities (e.g., $p\bar{p} \to p\bar{p}$). The goal of $< 5\%$ precision on two-photon widths is not unreasonable.

3.2.4 χ_b widths

Since the $\chi_b(2P_J)$ states are not produced directly in e^+e^- annihilations, their hadronic widths cannot be measured using the same technique as for the S states. However, we can use the fact that the partial width for their photonic E1 transitions to the $\Upsilon(2S)$ state are proportional to a common matrix element squared times a phase space factor of E_γ^3 (see Secs. 6.1.3 and 6.2.2, $E_\gamma = k$). Thus, from measuring the individual photon energies and branching ratios for the decays $\chi_b(2P_J) \to \Upsilon(2S) + \gamma$, along with the branching ratios for $\chi_b(2P_J) \to \Upsilon(1S) + \gamma$, we can measure the ratio of the $\chi_b(2P_J)$ hadronic partial widths, $\Gamma(\mathrm{had})$. We first use:

$$\mathcal{B}(2S) \;=\; \frac{\Gamma(2S)}{\Gamma(1S) \;+\; \Gamma(2S) \;+\; \Gamma(\mathrm{had})}, \tag{4.43}$$

where $\mathcal{B}(2S) \;=\; \mathcal{B}(\chi_b(2P_J) \;\to\; \Upsilon(2S) + \gamma)$ and $\mathcal{B}(1S) \;=\; \mathcal{B}(\chi_b(2P_J) \;\to\; \Upsilon(1S) + \gamma)$ are the two E1 branching ratios, and $\Gamma(2S)$ and $\Gamma(1S)$ are the corresponding partial widths. Then, since $\Gamma(2S)/\Gamma(1S) = \mathcal{B}(2S)/\mathcal{B}(1S)$, we can solve for the hadronic partial width, obtaining:

$$\Gamma(\mathrm{had}) \;=\; \Gamma(2S)\left[\frac{1 - \mathcal{B}(1S)}{\mathcal{B}(2S)} \;-\; 1\right]. \tag{4.44}$$

Making the assumption mentioned above that the partial widths for E1 transitions of different J states to the same Υ state should be proportional to a common matrix element squared times E_γ^3, we obtain an expression for the ratio of hadronic partial widths for two different $\chi_b(2P_J)$ states. For example, for J = 0 and J = 2, we get:

$$\frac{\Gamma_{\mathrm{had}}(2P_0)}{\Gamma_{\mathrm{had}}(2P_2)} \;=\; \left(\frac{E_\gamma(2P_0 \to 2S + \gamma)}{E_\gamma(2P_2 \to 2S + \gamma)}\right)^3 \;\left(\frac{\frac{1-\mathcal{B}(1S)_0}{\mathcal{B}(2S)_0} - 1}{\frac{1-\mathcal{B}(1S)_2}{\mathcal{B}(2S)_2} - 1}\right), \tag{4.45}$$

where $\mathcal{B}(2S)_0 = \mathcal{B}(\chi_b(2P_0) \to \Upsilon(2S) + \gamma)$, etc. Using this technique and the E1 branching ratios given in Section 6.2.2, CLEO III finds the ratio of the J = 0 to the J = 2 hadronic widths to be:

$$\frac{\Gamma_{\mathrm{had}}(2P_0)}{\Gamma_{\mathrm{had}}(2P_2)} \;=\; 6.1 \;\pm\; 2.8. \tag{4.46}$$

For the J = 1 and J = 2 states, CLEO III measures:

$$\frac{\Gamma_{\rm had}(2P_1)}{\Gamma_{\rm had}(2P_2)} \;=\; 0.25 \;\pm\; 0.09. \tag{4.47}$$

Since the J = 1 state cannot annihilate into two massless gluons, to first order its hadronic width is expected to be suppressed by one order of $\alpha_{\rm s}$ compared to the J = 2 state. The measurement confirms this suppression.

As discussed in Section 3.1, at leading order in the heavy-quark velocity expansion, the above ratios depend on a colour-octet matrix element. One can consider the combination

$$\frac{\Gamma_{\rm had}(2P_0) - \Gamma_{\rm had}(2P_1)}{\Gamma_{\rm had}(2P_2) - \Gamma_{\rm had}(2P_1)}, \tag{4.48}$$

which is completely determined by perturbative QCD [15]. Using (4.46) and (4.47), this ratio is measured by CLEO III to be:

$$\frac{\Gamma_{\rm had}(2P_0) - \Gamma_{\rm had}(2P_1)}{\Gamma_{\rm had}(2P_2) - \Gamma_{\rm had}(2P_1)} \;=\; 7.8 \;\pm\; 3.8. \tag{4.49}$$

LO QCD predicts 15/4 = 3.75 for this ratio, and NLO QCD about 7, which is quite consistent with (4.49). However, the combination (4.48) distinguishes between bottomonium and charmonium only at NNLO, while the ratios (4.46) and (4.47) do so at NLO. A direct determination of these ratios has been done in the framework of pNRQCD, as discussed in Section 3.1.3, using the factorization formula (4.25) and fixing the nonperturbative constant to the value found from charmonium data. The result at NLO is $\Gamma_{\rm had}(2{\rm P}_0)/\Gamma_{\rm had}(2{\rm P}_2) \;\simeq\; 4.0$, consistent with (4.46), and $\Gamma_{\rm had}(2{\rm P}_1)/\Gamma_{\rm had}(2{\rm P}_2) \;\simeq\; 0.50$, which is somewhat larger than (4.47) [51,57].

CLEO cannot resolve the individual photon lines for the similar decays from the $\Upsilon(3S)$ to the $\chi_b(1P_J)$ states (see Sec. 6.2.2). However, we can use the quite old $\chi_b(1P_J) \to \Upsilon(1S) + \gamma$ branching ratios from the PDG [10] for $J = 1$ and 2 (the $J = 0$ branching ratio is very small, given the large hadronic width of that state). In this case, the ratio of the hadronic widths for the two states can be found from:

$$\frac{\Gamma_{\rm had}(1P_1)}{\Gamma_{\rm had}(1P_2)} \;=\; \left(\frac{E_\gamma(1P_1 \to 1S + \gamma)}{E_\gamma(1P_2 \to 1S + \gamma)}\right)^3 \left(\frac{\frac{1}{\mathcal{B}(1S)_1} - 1}{\frac{1}{\mathcal{B}(1S)_2} - 1}\right). \tag{4.50}$$

This leads to the result:

$$\frac{\Gamma_{\rm had}(1P_1)}{\Gamma_{\rm had}(1P_2)} \;=\; 0.46 \;\pm\; 0.20, \tag{4.51}$$

showing again the suppression of the $J = 1$ state's hadronic width compared to the $J = 2$, albeit with larger errors in this case.

3.2.5 χ_c widths

The χ_c states are also not directly produced in e^+e^- annihilations. However, in this case an extremely powerful alternative method has been used to measure their masses and total widths. In an experimental technique first pioneered by experiment R704 at CERN, and continued by experiments E760 and E835 at the Fermilab Antiproton Accumulator, a stochastically cooled $\overline{p}$ beam collides with a hydrogen gas jet target. In the subsequent $p\overline{p}$ annihilations, all J^{PC} states can be formed via 2 or 3 gluons. Thus, the P-wave charmonium states are directly accessible. By scanning the proton beam energy over each resonance, the mass and total width of each P state can be measured with extremely high accuracy.

As mentioned in Section 3.2.3, these experiments have also measured products or ratios of branching ratios that help constrain the radiative and $\gamma\gamma$ widths of those states. Table 4.7 shows the current best estimates of the χ_c widths, using data from PDG [10]. E835 is finalizing the analysis of the scans of the χ_{c1} and χ_{c2} resonances [69], with an anticipated precision of $\approx 7\%$ on χ_{c1} and χ_{c2} total widths.

Table 4.7: Widths of χ_c states from PDG [10].

Resonance	$\Gamma_{\rm tot}$ (MeV)(% error)	$\Gamma(\gamma J/\psi)$ (keV)(% error)	$\Gamma(\gamma\gamma)(\%)$(% error)
χ_{c0}	10.1 ± 0.8 (8%)	119 ± 16 (13%)	2.6 ± 0.5 (19%)
χ_{c1}	0.91 ± 0.13 (14%)	290 ± 50 (17%)	—
χ_{c2}	2.11 ± 0.16 (8%)	430 ± 40 (9%)	0.52 ± 0.05 (10%)

In order to show the impact of the new measurements of the χ_c widths, in Table 4.8 we compare the PDG 2000 [70] with the PDG 2004 [10] determinations of different ratios of hadronic and electromagnetic widths (similar ratios have been considered in the previous section for the χ_b case). There have been sizable shifts in some central values and considerable reductions in the errors. In particular, the error on the ratio of the electromagnetic χ_{c0} and χ_{c2} widths has been reduced by about a factor 10, while in all other ratios the errors have been reduced by a factor 2 or 3. The considered ratios of hadronic and electromagnetic widths do not depend at leading order in the velocity expansion (see Eqs. (4.16) and (4.19)) on any nonperturbative parameter. Therefore, they can be calculated in perturbation theory. The last two columns of Table 4.8 show the result of a leading and next-to-leading order calculation respectively. Despite the fact that the convergence is not always very good and that, therefore, the NLO calculation should be taken with some care (see also Section 3.1.1), all data now clearly prefer (and are consistent with) NLO results.

3.2.6 $\Upsilon(1S) \to \gamma$ + X and $\Upsilon(1S) \to$ X

There has been much theoretical interest lately in trying to predict the direct photon energy distribution for Υ(1S) $\to \gamma$ + X inclusive decays [71]. See the following section. The last reported measurement was from the CLEO II experiment in 1997 [72], based on 1.4 million Υ(1S) decays. Besides the photon energy spectrum, they measured the ratio:

$$\frac{\Gamma(\gamma gg)}{\Gamma(ggg)} \;=\; (2.75 \;\pm\; 0.04 \;\pm\; 0.15)\,\%\,, \tag{4.52}$$

which allowed a fairly accurate determination of $\Lambda_{\overline{\rm MS}}$ and $\alpha_{\rm s}$. Given the small statistical errors in these measurements, it is doubtful that the CLEO III experiment will repeat them using their 29 million Υ(1S) decays. Rather, the emphasis will be on detailed studies of exclusive γ + X decays of the Υ(1S), especially the search for possible glueball candidates.

For measurements of the inclusive production of various hadronic particle types from the Υ(1S), one must go back to a 1985 paper by the CLEO I experiment [73], based on only 50k Υ(1S) decays. They measured the average multiplicities and momentum distributions of π, K, ρ, K^*, ϕ, p, Λ and Ξ in Υ(1S) decays and compared them to those from the nearby continuum. The only addition to these results was a 2003 CLEO II measurement [74] of the inclusive η' production from the Υ(1S), based on 1.9 million decays and motivated by the large observed $B \to \eta' + X$ branching ratio.

4 INCLUSIVE RADIATIVE DECAYS[9]

The radiative inclusive decay of heavy quarkonium has been investigated for about a quarter century. Here we will study $\Upsilon \to X\gamma$ decays in particular. The direct radiative decay is calculated by using the operator product expansion, where the operators are the same nonperturbative matrix elements that appear in the inclusive decay to hadrons (see Section 3.1). Thus we obtain an expansion in the velocity, v,

[9] Author: A. Leibovich

Table 4.8: Comparison of ratios of χ_{cJ} partial widths. The experimental values PDG 2004 are obtained from the world averages of [10], with the assumption $\Gamma(\chi_{c0}\to l.h.) \approx \Gamma(\chi_{c0}) = 10.1 \pm 0.8$ MeV, $\Gamma(\chi_{c1}\to l.h.) \approx \Gamma(\chi_{c1})\,[1-\mathcal{B}(\chi_{c1}\to\gamma J/\psi)]$ =0.62±0.10 MeV, $\Gamma(\chi_{c2}\to l.h.) \approx \Gamma(\chi_{c2})\,[1-\mathcal{B}(\chi_{c2}\to\gamma J/\psi)]$ =1.68±0.15 MeV. Similarly the experimental values PDG 2000 have been obtained from [70]. The chosen ratios do not depend at leading order in the velocity expansion on octet or singlet matrix elements. The LO and NLO columns refer to a leading and next-to-leading order calculation done at the renormalization scale $2m_c$ with the following choice of parameters: $m_c = 1.5$ Gev and $\alpha_s(2m_c) = 0.245$.

Ratio	PDG 2004	PDG 2000	LO	NLO
$\frac{\Gamma(\chi_{c0}\to\gamma\gamma)}{\Gamma(\chi_{c2}\to\gamma\gamma)}$	5.1±1.1	13±10	3.75	≈ 5.43
$\frac{\Gamma(\chi_{c2}\to l.h.)-\Gamma(\chi_{c1}\to l.h.)}{\Gamma(\chi_{c0}\to\gamma\gamma)}$	410±100	270±200	≈ 347	≈ 383
$\frac{\Gamma(\chi_{c0}\to l.h.)-\Gamma(\chi_{c1}\to l.h.)}{\Gamma(\chi_{c0}\to\gamma\gamma)}$	3600±700	3500±2500	≈ 1300	≈ 2781
$\frac{\Gamma(\chi_{c0}\to l.h.)-\Gamma(\chi_{c2}\to l.h.)}{\Gamma(\chi_{c2}\to l.h.)-\Gamma(\chi_{c1}\to l.h.)}$	7.9±1.5	12.1±3.2	2.75	≈ 6.63
$\frac{\Gamma(\chi_{c0}\to l.h.)-\Gamma(\chi_{c1}\to l.h.)}{\Gamma(\chi_{c2}\to l.h.)-\Gamma(\chi_{c1}\to l.h.)}$	8.9±1.1	13.1±3.3	3.75	≈ 7.63

of the heavy quarks. The rate is written as

$$\frac{1}{\Gamma_0}\frac{d\Gamma^{\rm dir}}{dz} = \sum_n C_n(M,z)\langle\Upsilon|O_n|\Upsilon\rangle, \tag{4.53}$$

where $M = 2m_b$, $z = 2E_\gamma/M$, the $C_n(z,M)$ are short distance Wilson coefficients, calculable in perturbation theory, and the NRQCD matrix elements scale with a certain power in v. The lowest order contribution is the colour-singlet $^3S_1$ operator, where the quark–antiquark pair annihilate into a photon and two gluons. Therefore, in the $v\to 0$ limit, we obtain the colour-singlet model calculation of Ref. [75]. At higher order in the velocity expansion, there are direct contributions from the colour-octet matrix elements [76]. The decay through a colour-octet matrix element can occur at one lower order in α_s, with the $b\bar{b}$ decaying to a photon and a single gluon.

However, this calculation is only valid in the intermediate range of photon energies ($0.3 \lesssim z \lesssim 0.7$). For low photon energies, $z \lesssim 0.3$, the major photon production mechanism is fragmentation [76, 77]. At large photon energies, $z \gtrsim 0.7$, the perturbative [76] and nonperturbative expansions [78] both break down.

4.1 Photon fragmentation

The inclusive photon spectrum can be written as a sum of a direct and a fragmentation contribution [77],

$$\frac{d\Gamma}{dz} = \frac{d\Gamma^{\rm dir}}{dz} + \frac{d\Gamma^{\rm frag}}{dz}, \tag{4.54}$$

where in the direct term the photon is produced in the hard scattering, and in the fragmentation term the photon fragments from a parton produced in the initial hard scattering. The fragmentation contribution has been well studied in Ref. [76].

Catani and Hautmann pointed out the importance of fragmentation for the photon spectrum in quarkonium decays [77]. The fragmentation rate can be written as

$$\frac{d\Gamma^{\rm frag}}{dz} = \sum_{a=q,\bar{q},g} \int_z^1 \frac{dx}{x} \frac{d\Gamma_a}{dx} D_{a\gamma}\left(\frac{z}{x}, M\right), \tag{4.55}$$

where the rate to produce parton a, $d\Gamma_a/dx$, is convoluted with the probability that the parton fragments to a photon, $D_{a\gamma}$, with energy fraction z/x. The rate to produce parton a can again be expanded in powers of v [76], with the leading term being the colour-singlet rate for an Υ to decay to three gluons,

$$\frac{d\Gamma^{\rm frag}_{\rm LO}}{dz} = \int_z^1 \frac{dx}{x} \frac{d\Gamma_{ggg}}{dx} D_{g\gamma}\left(\frac{z}{x}, M\right). \tag{4.56}$$

At higher orders in v, there are three colour-octet fragmentation contributions, where the photon can fragment off either a quark or a gluon.

The partonic rates must be convoluted with the fragmentation functions, $D_{a\gamma}(z, M)$. The M-dependence of the fragmentation functions can be predicted using perturbative QCD via Altarelli–Parisi evolution equations. However, the solution depends on nonperturbative fragmentation function at some input scale Λ, which must be measured from experiment. This has been done by the ALEPH collaboration for the $D_{q\gamma}$ fragmentation function [79], but the $D_{g\gamma}$ fragmentation function is unknown, so at this point it must be modeled.

4.2 Resumming the large z contribution

The colour-octet contributions to the rate are the first subleading terms in the operator product expansion. Diagrammatically, these contributions occur for the quark–antiquark pair annihilating into a photon back-to-back with a gluon. Thus the ${}^1S_0$ and ${}^3P_0$ colour-octet contributions begin as a delta function of $(1-z)$ [76]. If we look at the integrated rate near the endpoint, the colour-octet contributions are as important as the "leading" colour-singlet piece, in the region $1 - v^2 \lesssim z \leq 1$. Perturbative corrections to the colour-octet contributions have large kinematic logarithms, which destroy the perturbative expansion. The $\alpha_{\rm s}$ correction to the leading colour-singlet rate was calculated numerically in Ref. [80]. It leads to small corrections over most of phase space; however, in the endpoint region the corrections are of order the leading contribution. Thus both higher orders in v and in $\alpha_{\rm s}$ are not suppressed in the endpoint region. Both the nonperturbative and perturbative series break down.

This breakdown at large z is due to NRQCD not including collinear degrees of freedom. In the endpoint region, the outgoing gluons are moving back-to-back to the photon, with large energy and small invariant mass (i.e., a collinear jet). The correct effective field theory is a combination of NRQCD for the heavy degrees of freedom and the soft-collinear effective theory (SCET) [81,82] for the light degrees of freedom.

SCET is an effective field theory describing collinear fields interacting with soft degrees of freedom. It is thus the appropriate effective field theory to use when there are energetic particles moving with small invariant mass, such as $\Upsilon \to X\gamma$ in the endpoint region. We therefore use NRQCD to describe the

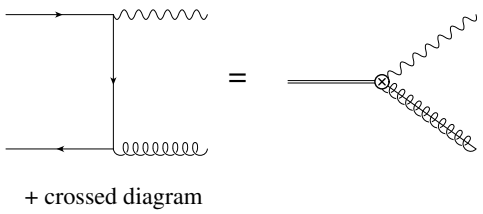

Fig. 4.1: Matching QCD onto NRQCD and SCET. The double lines represents the Υ, while the spring with the line through it represent a collinear gluon.

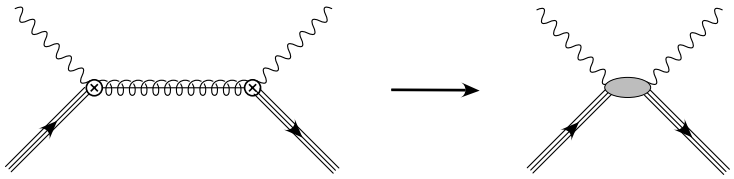

Fig. 4.2: The leading OPE: tree level matching of the time ordered product in the collinear-soft theory to a nonlocal operator in the soft theory.

quarkonium, and SCET to describe the jet of collinear particles. The invariant mass of the jet of particles is $p^2 \sim M_\Upsilon^2(1-z)$, which is small as $z \to 1$. In SCET there are three mass scales: the hard scale, which for this process is $\mu_h \sim M_\Upsilon$, the collinear scale, which is $\mu_c \sim M_\Upsilon\sqrt{1-z}$, and the ultrasoft scale, $\mu_u \sim M_\Upsilon(1-z)$. These scales are widely separated in the endpoint region. SCET allows us to separate the physics coming from the disparate scales.

To calculate, the QCD process is matched onto operators in SCET and NRQCD. For example, the matching for the colour-octet channel is pictured in Fig. 4.1. Then to resum the kinematic logarithms, we use the renormalization group equations in SCET, by evolving from μ_h to μ_u. So we first renormalize the operators in SCET, and calculate the anomalous dimensions in the usual way. Then by running the SCET operators to the ultrasoft scale, the logarithms of $1-z$ are summed.

The colour-singlet process does not run below the collinear scale. This is because the ultrasoft gluons cannot couple to the colour-singlet jet or the incoming colour-singlet quarkonium. This fact was first pointed out by Hautmann [83]. However, there are still logarithms that are generated between the hard and collinear scales [71, 84]. For the colour-octet processes [85], at the collinear scale μ_c we integrate out collinear modes. Since there are collinear particles in the final state, we first perform an OPE for the inclusive Υ radiative decay rate in the endpoint region, and match onto the large energy effective theory [86]. The result is a nonlocal OPE in which the two currents are separated along a light-like direction. Diagrammatically this is illustrated in Fig. 4.2. This is run to the ultrasoft scale, at which point we are left with a nonperturbative shape function, which describes the movement of the heavy quark–antiquark pair within the meson. This function is precisely what was shown to occur in Ref. [78]. Unfortunately, this nonperturbative function is unknown, and must be modeled.

Before we proceed we need the NRQCD matrix elements. We can extract the colour-singlet matrix elements from the Υ leptonic width. The colour-octet matrix elements are more difficult to determine. NRQCD predicts that the colour-octet matrix elements scale as v^4 compared to the singlet matrix elements. In Ref. [19] it was argued that an extra factor of $1/2N_c$ should be included. By looking at the shape of the resummed colour-octet rates, it appears that these channels would give a contribution an order of magnitude too large compared with the data in the endpoint region if they were even as small as $v^4/2N_c$ times the colour-singlet, as shown in Fig. 4.3, so we will set them to zero. This eliminates two

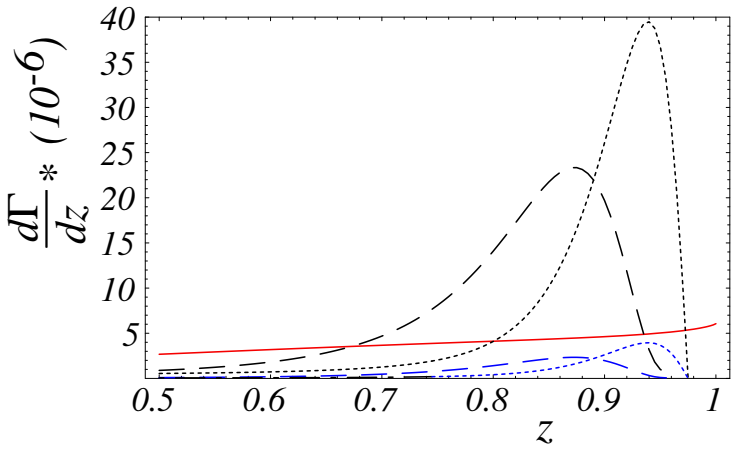

Fig. 4.3: The differential decay spectra in the region $0.5 < z$. The dashed curves are the fully resummed colour-octet result convoluted with a model for the shape function for two choices of the colour-octet matrix elements. The larger curves have the colour-octet matrix elements suppressed by $v^4/10$, while the lower curves have $v^4/100$. In addition we have interpolated the fully resummed result with the next-to-leading order result in the region away from the endpoint. The dotted curves are the next-to-leading result convoluted with the structure function for two choices of the matrix elements. The solid curve is the tree-level colour-singlet contribution.

of the three possible colour-octet matrix elements, leaving the ${}^3S_1$. It also eliminates the dependence at this order on the unknown shape functions and the largest dependence on the unknown fragmentation function, $D_{g\gamma}$. We set the colour-octet ${}^3S_1$ matrix element to be v^4 suppressed compared to the colour-singlet matrix element extracted from the leptonic width, where we use $v^2 = 0.08$. This colour colour-octet matrix element does not give a large contribution in the large z region, but is important at low z, due to the fragmentation function $D_{q\gamma}$.

The CLEO collaboration measured the number of photons in inclusive $\Upsilon(1S)$ radiative decays [72]. The data does not remove the efficiency or energy resolution and is the number of photons in the fiducial region, $|\cos\theta| < 0.7$. In order to compare our theoretical prediction to the data, we integrate over the barrel region and convolute with the efficiency that was modeled in the CLEO paper. We do not do a bin-to-bin smearing of our prediction.

In Fig. 4.4 we compare the prediction to the data. The error bars on the data are statistical only. The dashed line is the direct tree-level plus fragmentation result, while the solid curve includes the resummation of the kinematic logarithms. For these two curves we use the α_s extracted from these data, $\alpha_s(M_\Upsilon) = 0.163$, which corresponds to $\alpha_s(M_Z) = 0.110$ [72]. The shape of the resummed result is much closer to the data than the tree-level curve, though it is not a perfect fit. We also show the resummed plus fragmentation result, using the PDG value of $\alpha_s(M_Z)$, including theoretical uncertainties, denoted by the shaded region. To obtain the darker band, we first varied the choice of m_b between $4.7\ \mathrm{GeV} < m_b < 4.9\ \mathrm{GeV}$ and the value of α_s within the errors given in the PDG, $\alpha_s(M_Z) = 0.1172(20)$ [87]. We also varied the collinear scale, μ_c from $M\sqrt{(1-z)/2} < \mu_c < M\sqrt{2(1-z)}$. Finally, the lighter band also includes the variation, within the errors, of the parameters for the quark to photon fragmentation function extracted by ALEPH [79]. The low z prediction is dominated by the quark to photon fragmentation coming from the colour-octet ${}^3S_1$ channel. We did not assign any error to the colour-octet ${}^3S_1$ matrix elements. Since it is unknown, there is a very large uncertainty in the lower part of the prediction that we decided not to show. Recently, colour-octet ${}^1S_0$ and ${}^3P_0$ contributions, calculated in the weak-coupling regime, have been included in the analysis [88]. They appear to improve the agreement with the data in the end-point region. Also recently operator mixing between the gluon jet, considered here, and the quark–antiquark jet has been considered in [89].

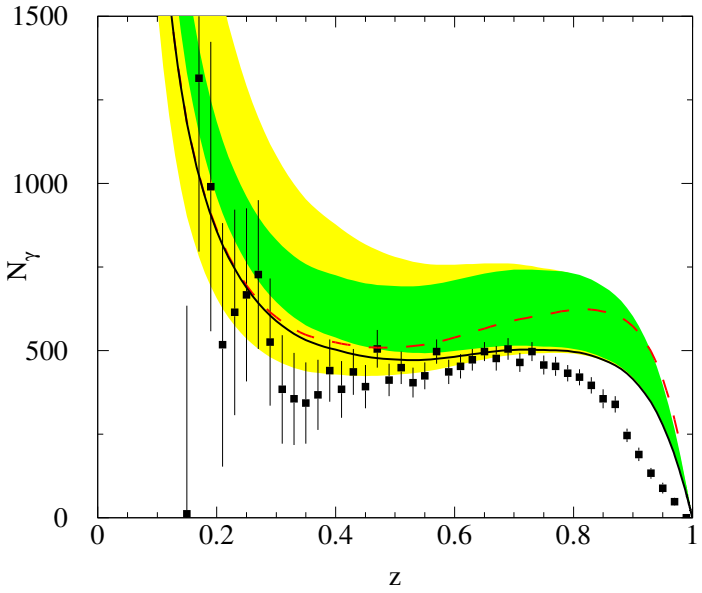

Fig. 4.4: The inclusive photon spectrum, compared with data [72]. The theory predictions are described in the text. The plot is from Ref. [71].

5 EXCLUSIVE DECAYS[10]

Exclusive charmonium decays have been investigated within QCD by many authors, e.g., [90–93]. As already argued at the beginning of Section 3.1 the dominant dynamical mechanism is $c\bar{c}$ annihilation into the minimal number of gluons allowed by symmetries and subsequent creation of light quark–antiquark pairs forming the final state hadrons.

In hard exclusive reactions higher Fock-state contributions are usually suppressed by inverse powers of the hard scale, Q, appearing in the process ($Q \sim m_c$ for exclusive charmonium decays), as compared to the valence Fock-state contributions. Hence, higher Fock-state contributions are expected to be negligible in most cases. It has turned out, however, that higher Fock states of the charmonium play an important role in understanding the production (see Chapter 5) and the inclusive decays of charmonium (see Section 3.1). As shown in [14] the long-distance matrix elements can there be organized into a hierarchy according to their scaling with v, the typical velocity of the c quark in the charmonium. The velocity expansion can also be applied to exclusive charmonium decays [94]. The Fock expansions of the charmonium states start (in the power counting of [14]) as

$$\begin{aligned}
|J/\psi\rangle &= \underbrace{|c\bar{c}_1(^3S_1)\rangle}_{\mathcal{O}(1)} + \underbrace{|c\bar{c}_8(^3P_J)\,g\rangle}_{\mathcal{O}(v)} + \underbrace{|c\bar{c}_8(^3S_1)\,gg\rangle}_{\mathcal{O}(v^2)} + \ldots, \\
|\,\eta_c\,\rangle &= \underbrace{|c\bar{c}_1(^1S_0)\rangle}_{\mathcal{O}(1)} + \underbrace{|c\bar{c}_8(^1P_1)\,g\rangle}_{\mathcal{O}(v)} + \underbrace{|c\bar{c}_8(^1S_0)\,gg\rangle}_{\mathcal{O}(v^2)} + \ldots, \\
|\,\chi_{cJ}\rangle &= \underbrace{|c\bar{c}_1(^3P_J)\rangle}_{\mathcal{O}(1)} + \underbrace{|c\bar{c}_8(^3S_1)\,g\rangle}_{\mathcal{O}(v)} + \ldots,
\end{aligned} \tag{4.57}$$

where the subscripts at the $c\bar{c}$ pair specify whether it is in a colour-singlet (1) or colour-octet (8) state; $\mathcal{O}(1)$, $\mathcal{O}(v)$ and $\mathcal{O}(v^2)$ are the orders to which the corresponding Fock states contribute, once evaluated

[10] Author: P. Kroll (with contributions from C. Patrignani)

in a matrix element. The amplitude for a two-body decay of a charmonium state satisfies a factorization formula, which separates the scale m_c from the lower momentum scales. The decay amplitude is then expressed as a convolution of a partonic subprocess amplitude that involves the scale m_c, the charmonium wave function for the initial state that involves scales of order $m_c\,v$ and lower, and a factor that takes into account the light hadron wave functions for the final state. This factor involves only the scale $\Lambda_{\rm QCD}$. In the formal limit of $m_c{\to}\infty$ the dominant terms in the factorization formula involve the minimal number of partons in the hard scattering, which is given by the valence quarks of the hadrons participating in the considered process. Terms involving additional partons in the initial state are suppressed by powers of v while terms involving additional partons in the final state are suppressed by powers of $\Lambda_{\rm QCD}/m_c$. Moreover, in this limit of an asymptotically large charm quark mass, the valence quarks of a light hadron move collinear with it, their transverse quark momenta can be neglected. In this situation the soft parton–hadron transition is described by a leading-twist distribution amplitude, $\Phi(x,\mu_F)$, for finding valence quarks in the hadron, each carrying some fraction x_i of the hadron's momentum and for which the quark helicities sum up to the hadronic one. The distribution amplitudes, which represent light-cone wave functions integrated over transverse momenta up to a factorization scale μ_F of order m_c [91, 92], are the only nonperturbative input required in the calculation of decay amplitudes along these lines. The convolution formula in such a leading-twist calculation of a charmonium decay into a pair of hadrons h_1, h_2 reads

$$M \;=\; \int [dx]_N [dy]_N [d^3k]_{N'}\, \Phi_1(x,\mu_F)\, \Phi_2(y,\mu_F)\, T_H(x,y,m_c,\mu_F)\, \Psi_c(k)\,, \tag{4.58}$$

where $x(y)$ represents the set of independent momentum fractions for an N-particle Fock state of a light hadron and Ψ_c is the charmonium wave function for an N'-particle Fock state. k denotes the set of momenta of the particles in that Fock state. Soft and hard physics is separated at the factorization scale μ_F.

The relative strength of various contributions to specific decay processes can be easily estimated. Typical lowest-order Feynman graphs are shown in Fig. 4.5. A P-wave $c\bar{c}$ pair requires a power of the c-quark's relative momentum $\mathbf{k}$ ($k \sim m_c v$) from the hard scattering amplitude, which is to be combined with a $\mathbf{k}$ from the P-wave charmonium spin wave function in a k^2. In contrast to $\mathbf{k}$ itself, a term proportional to k^2 does not lead to a vanishing contribution after the $\mathbf{k}$ integration. Since, for dimensional reasons, $\mathbf{k}$ is to be replaced by $\mathbf{k}/m_c$ the subprocess amplitude involving a P-wave $c\bar{c}$ pair, is of order v. Combining this fact with the Fock-state expansion (4.57), one finds for the amplitude of χ_{cJ} decays into, say, a pairs of pseudoscalar mesons (P) the behaviour

$$M(\chi_{cJ}{\to}PP) \;=\; a_1\,\alpha_{\rm s}^2 v + a_8\,\alpha_{\rm s}^2\big(v\sqrt{\alpha_{\rm s}}\big) + \mathcal{O}(v^2)\,, \tag{4.59}$$

where the a_i are process-typical constants. For the reaction $J/\psi{\to}B\overline{B}$ (B stands for baryon), on the other hand, one has

$$M(J/\psi{\to}B\overline{B}) \;=\; \tilde{a}_1\,\alpha_{\rm s}^3 + \tilde{a}_8\,\alpha_{\rm s}^3 v\big(v\sqrt{\alpha_{\rm s}}\big) + \tilde{b}_8\,\alpha_{\rm s}^3\; v^2\alpha_{\rm s} + \mathcal{O}(v^3)\,. \tag{4.60}$$

Or, for the η_c decaying for instance into a scalar (S) and a pseudoscalar meson

$$\mathcal{M}(\eta_c{\to}SP) \;=\; \hat{a}_1\,\alpha_{\rm s}^2 + \hat{a}_8\,\alpha_{\rm s}^2 v\big(v\sqrt{\alpha_{\rm s}}\big) + \hat{b}_8\,\alpha_{\rm s}^2 (v\sqrt{\alpha_{\rm s}})^2 + \mathcal{O}(v^3)\,. \tag{4.61}$$

Thus, one sees that in the case of the χ_{cJ} the colour-octet contributions $\propto a_8$ are not suppressed by powers of either v or $1/m_c$ as compared to the contributions from the valence Fock states [94]. For charmonium decays $\sqrt{\alpha_{\rm s}}$ is large and does not suppress the colour-octet contribution considerably. Hence, the colour-octet contribution, i.e., the next higher Fock state of the charmonium state, has to be included for a consistent analysis of P-wave charmonium decays. The situation is different for J/ψ decays into baryon–antibaryon pairs or $\eta_c{\to}SP$: higher Fock state contributions first start at $\mathcal{O}(v^2)$. Moreover, there

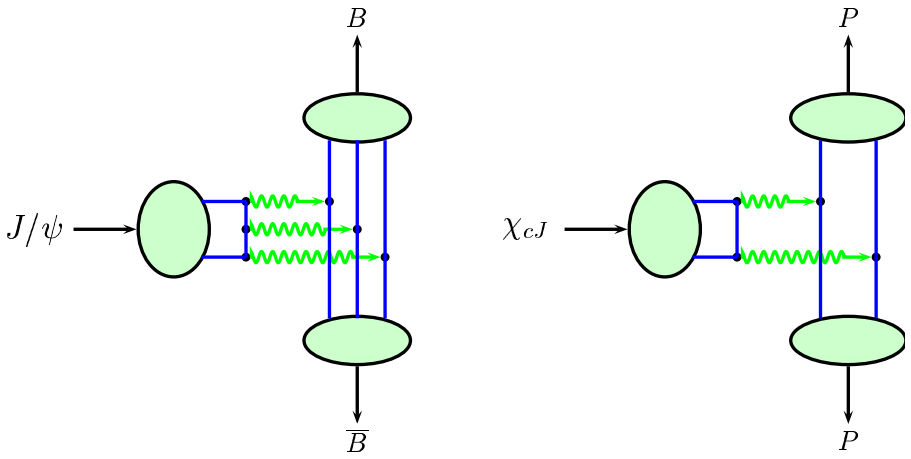

Fig. 4.5: Typical lowest-order Feynman graphs for J/ψ decays into a baryon-antibaryon pair (left) and χ_{cJ} decays into a pair of pseudoscalar mesons (right). The wavy lines represent gluons.

is no obvious enhancement of the corresponding subprocess amplitudes, they appear with at least the same power of α_s as the valence Fock state contributions. Thus, despite of the fact that m_c is not very large and v not small ($v^2 \simeq 0.3$), it seems reasonable to expect small higher Fock-state contributions to the baryonic decays of the J/ψ.

The leading-twist formation of the light hadrons in the final state has implications for their helicity configurations. As a consequence of the vector nature of QCD (and QED) time-like virtual gluons (or photons) create light, (almost) massless quarks and antiquarks in opposite helicity states, see Fig. 4.6. To leading-twist accuracy such partons form the valence quarks of the light hadrons and transfer their helicities to them (see Fig. 4.6). Hence, the total hadronic helicity is zero

$$\lambda_1 + \lambda_2 \;=\; 0\,. \tag{4.62}$$

The conservation of hadronic helicities is a dynamical consequence of QCD (and QED) which holds to leading-twist order. The violation of helicity conservation in a decay process signals the presence of higher-twist, higher Fock state and/or soft, non-factorizable contributions. Such processes (e.g., $J/\psi \to \rho\pi$, $\eta_c \to \rho\rho$) have indeed been observed experimentally with often sizeable branching ratios. For the two-meson channels involving pseudoscalar (P) and vector mesons (V) they are characterized by

$$(-1)^{J_c}\, P_c \neq (-1)^{J_1+J_2}\, P_1 P_2\,, \tag{4.63}$$

where J_i and P_i are the spin and parity of the meson i. The amplitudes for processes of this kind are proportional to the Levi-Civita tensor, ε, which is to be contracted in all possible ways with the available Lorentz vectors, namely the two independent light hadron momenta, p_1 and p_2, and the polarization vectors (or tensors) of the light vector mesons and the charmonium state. As an example let us consider the process $J/\psi \to VP$, for which the amplitude reads

$$\mathcal{M}_{\lambda_V,\lambda_{J/\psi}}(J/\psi \to VP) \;=\; \frac{A}{M_{J/\psi}^2}\,\varepsilon(p_1, p_2, \epsilon^*(\lambda_V), \epsilon(\lambda_{J/\psi}))\,, \tag{4.64}$$

where A is a constant. Now, in the rest frame of the decaying meson, the polarization vector of a helicity zero vector meson can be expressed by a linear combination of the two final state momenta. The number of independent Lorentz vectors is, therefore, insufficient to contract the Levi-Civita tensor with the consequence of a vanishing amplitude for processes involving longitudinally polarized vector mesons.

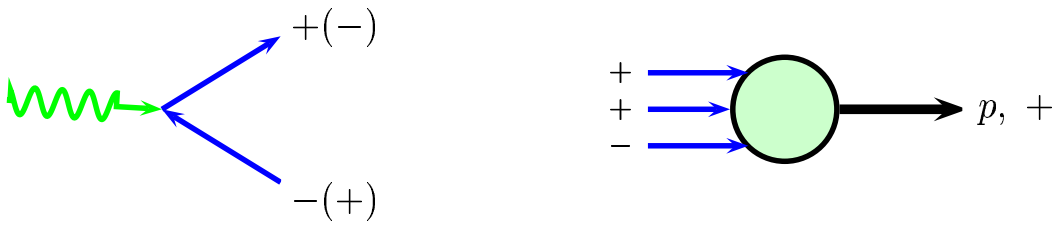

Fig. 4.6: Helicity configurations in the creation of a light $q\overline{q}$ pair (left) and for a leading-twist parton–proton transition (right).

Thus, hadronic helicity conservation (4.62) is violated in $J/\psi \to VP$ decays. By the same argument longitudinally polarized vector mesons are forbidden in the decay $\eta_c \to VV$. Since angular momentum conservation requires the same helicity for both vector mesons, hadronic helicity is not conserved in the case of transversally polarized vector mesons, too. With similar arguments the processes $\chi_{c1}, h_c \to VV$ and $\chi_{c2} \to VP$ are also forbidden to leading twist order. We note that hadronic helicity conservation does also not hold in η_c and χ_{c0} decays into baryon–antibaryon pairs where, in the charmonium rest frame, angular momentum conservation requires $\lambda_B = \lambda_{\overline{B}}$. A systematic investigation of higher-twist contributions to these processes is still lacking despite some attempts of estimating them, for a review see [95]. Recent progress in classifying higher-twist distribution amplitudes and understanding their properties [96, 97] now permits such analyses. The most important question to be answered is whether or not factorization holds for these decays to higher-twist order. It goes without saying that besides higher-twist effects, the leading-twist forbidden channels might be under control of other dynamical mechanisms such as higher Fock state contributions or soft power corrections. In Section 5.1 a variety of such mechanisms will be discussed.

Next, let us consider G-parity and isospin. G-parity or isospin-violating decays are not strictly forbidden since they can proceed through electromagnetic $c\bar{c}$ annihilation and may receive contributions from the isospin-violating part of QCD. The latter contributions, being related to the $u - d$ quark mass difference, seem to be small [92]. G-parity or isospin-violating decays of C-even charmonia (e.g., $\eta_c, \chi_{c1}, \chi_{c2} \to PV$ for non-strange final state mesons) have not been observed experimentally as yet [10]. Proceeding on the assumption that these decays are dominantly mediated by $c\bar{c} \to 2\gamma^* \to PV$, this is understandable. They are suppressed by a factor $(\alpha_{\rm em}/\alpha_{\rm s})^4$ as compared to the G-parity and isospin allowed decays of the C-even charmonia and their decay widths are therefore extremely small. Channels involving strange mesons (e.g., KK^*), are also expected to be strongly suppressed by virtue of U-spin invariance. For J/ψ decays the situation is different. Many G-parity violating (e.g., $\pi^+\pi^-$) or isospin-violating (e.g., $\omega\pi^0$) decays have been observed, the experimental branching ratios being of the order of 10^{-4}–10^{-3} [10]. As compared to G-parity and isospin allowed J/ψ decays they are typically suppressed by factors of about 10^{-2}–10^{-1} in accord with what is expected for an electromagnetic decay mechanism, see Fig. 4.7. An overview over the allowed and forbidden charmonium decays into pseudoscalar and vector mesons is given in Table 4.9.

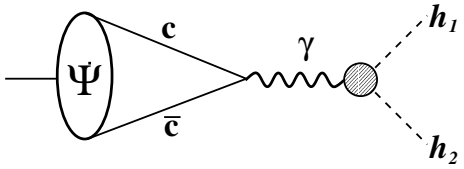

Fig. 4.7: Electromagnetic $\psi(nS)$ decays into pairs of hadrons. The shaded blob indicates a time-like electromagnetic transition form factor.

Table 4.9: Charmonium decays into PP, PV and VV meson pairs. The symbols 0, ϵ, $\surd$ denote channels forbidden by angular momentum and parity conservation, forbidden to leading-twist accuracy, and allowed, respectively. The brackets indicate that these channels violate either G-parity or isospin invariance for non-strange mesons.

	PP	PV	VV
η_c	0	$(\surd)$	ϵ
J/ψ	$(\surd)$	ϵ	$(\surd)$
h_c	0	$\surd$	ϵ
χ_{c0}	$\surd$	0	$\surd$
χ_{c1}	0	$(\surd)$	ϵ
χ_{c2}	$\surd$	(ϵ)	$\surd$

All what we have discussed so far holds for exclusive bottomonium decays as well. The situation is even better in this case. Due to the larger mass of the b quark, corrections to the leading-twist QCD results for bottomonium decays are probably reasonably small. Thus, the data on branching ratios can be expected to exhibit the pattern of leading-twist predictions. Exclusive quarkonium decays constitute an interesting laboratory for investigating corrections to the leading-twist lowest-order approach from various sources such as power and higher-twist corrections as well as higher Fock-state contributions. A systematic study of such is still lacking.

5.1 Decays of J/ψ and $\psi(2S)$ into two mesons[11]

The most dramatic unsolved problem in quarkonium physics is probably the ρ–π puzzle. In analyzing the 2-body decays of the J/ψ and $\psi(2S)$ into two light hadrons h_1 and h_2, it is convenient to consider the following quantity:

$$\kappa[h_1h_2] = \frac{\mathcal{B}(\psi(2S)\to h_1h_2)}{\mathcal{B}(J/\psi\to h_1h_2)}\,\frac{\mathcal{B}(J/\psi\to e^+e^-)}{\mathcal{B}(\psi(2S)\to e^+e^-)}\,\frac{\varrho[J/\psi h_1h_2]}{\varrho[\psi(2S)h_1h_2]}, \tag{4.65}$$

where

$$\varrho[Hh_1h_2] = \sqrt{1-2(M_{h_1}^2+M_{h_2}^2)/M_H^2+(M_{h_1}^2-M_{h_2}^2)^2/M_H^4}\,. \tag{4.66}$$

is a phase space factor that depends on the masses of the hadrons H, h_1, and h_2. As will be explained shortly, very simple theoretical considerations lead to the expectation that this quantity should be close to 1 for all light hadrons h_1 and h_2:

$$\kappa[h_1h_2] = 1. \tag{4.67}$$

This prediction was once referred to as the 12% rule because the experimental value of the ratio of the electronic branching fractions of the $\psi(2S)$ and J/ψ was at one time near 12%. That experimental value is now $15 \pm 2\%$. The last factor in (4.65) is a phase space factor that is close to 1 for hadrons whose masses are much smaller than that of the J/ψ. Thus the prediction (4.67) implies that the ratio of the branching fractions of the $\psi(2S)$ and J/ψ into h_1h_2 should be near 15%. All the baryon–antibaryon decay modes that have been measured are compatible with the prediction (4.67), see Sec. 5.2. Some two-meson decay modes are compatible with this prediction, but there are others for which it is badly violated. The most severe violation that has been observed is in the $\rho\pi$ decay mode. The first hint of this problem was seen by the Mark II collaboration in 1983 [98]. The decay $J/\psi\to\rho\pi$, with a branching fraction of about 1.3%, is the largest 2-body hadronic decay mode of the J/ψ. In contrast, the partial

[11] Author: E. Braaten

width for $\psi(2S)\to\rho\pi$ is so small that this decay was not observed until very recently by the CLEO and BES collaborations [99,100]. The branching fraction is measured to be 0.46 ± 0.09, and the ratio defined in (4.65) is $\kappa[\rho\pi]=0.028\pm0.006$. The dramatic discrepancy between this result and the prediction in Eq. (4.67) is the $\rho-\pi$ puzzle.

We proceed to explain the assumptions underlying the prediction (4.67). Because there is a nonzero amplitude for the J/ψ to be a pure $c\bar{c}$ state, the matrix element for its decay into two light hadrons h_1 and h_2 can be expressed in the form

$$\mathcal{M}(J/\psi\to h_1h_2)=\int\frac{d^3p}{(2\pi)^3}\psi_{J/\psi}(\mathbf{p})\mathcal{A}(c(\mathbf{p})\bar{c}(-\mathbf{p})\to h_1h_2), \tag{4.68}$$

where $\psi_{J/\psi}(\mathbf{p})$ is the momentum-space wave function for the pure $c\bar{c}$ component of the J/ψ. This can be regarded as an exact formula that defines the amplitude $\mathcal{A}(c\bar{c}\to h_1h_2)$. It relies on the fact that wave functions satisfy integral equations, so even if there are other components of the J/ψ wave function besides $c\bar{c}$, the iteration of the integral equation will eventually produce a pure $c\bar{c}$ state. The annihilation of the $c\bar{c}$ pair produces an intermediate state consisting of partons with momenta of order m_c, which is much larger than either the momentum scale $p\sim m_cv$ for the $c\bar{c}$ wave function of the J/ψ or the scale $\Lambda_{\rm QCD}$ associated with the wave functions of the light hadrons h_1 and h_2. If the factored expression in (4.68) also corresponds to a separation of small momenta associated with the wave function of J/ψ from small momenta associated with the wave functions of h_1 and h_2, then the amplitude $\mathcal{A}$ in (4.68) should be insensitive to the value of $\mathbf{p}$. It can be approximated by its value at $\mathbf{p}=0$ up to corrections suppressed by powers of v and $\Lambda_{\rm QCD}/m_c$:

$$\mathcal{A}(c(\mathbf{p})\bar{c}(-\mathbf{p})\to h_1h_2)\approx\mathcal{A}(c(\mathbf{0})\bar{c}(\mathbf{0})\to h_1h_2). \tag{4.69}$$

With this approximation, the matrix element (4.68) reduces to

$$\mathcal{M}(J/\psi\to h_1h_2)\approx\psi_{J/\psi}(\mathbf{r}=0)\mathcal{A}(c(\mathbf{0})\bar{c}(\mathbf{0})\to h_1h_2), \tag{4.70}$$

where $\psi_{J/\psi}(\mathbf{r})$ is the coordinate-space wave function for the pure $c\bar{c}$ component of J/ψ. The decay rate then has the factored form

$$\Gamma(J/\psi\to h_1h_2)\approx\left|\psi_{J/\psi}(\mathbf{r}=0)\right|^2\left|\mathcal{A}(c(\mathbf{0})\bar{c}(\mathbf{0})\to h_1h_2)\right|^2\frac{\varrho[J/\psi h_1h_2]}{16\pi M_{J/\psi}}. \tag{4.71}$$

The corresponding expression for the decay $\psi(2S)\to h_1h_2$ differs only in the mass and the wave function factor. These factored expressions apply equally well to decays into e^+e^-. Taking the ratio of decay rates in (4.65), we obtain the prediction $\kappa[h_1h_2]=1$ for any light hadrons h_1 and h_2. Any significant deviation of $\kappa[h_1h_2]$ from 1 indicates a breakdown of the approximation (4.69).

An important reference point for the prediction (4.67) is provided by the (leading twist) asymptotic predictions of perturbative QCD [91, 92]. These predictions are most easily described using a ratio R defined by

$$R_{J/\psi}[h_1h_2]=\frac{\Gamma(J/\psi\to h_1h_2)}{\Gamma(J/\psi\to e^+e^-)}. \tag{4.72}$$

The asymptotic predictions for this ratio depend on the helicities λ_1 and λ_2 of the two hadrons h_1 and h_2. If the hadrons are mesons and the decay proceeds via the annihilation process $c\bar{c}\to ggg$, the prediction for the scaling behavior of the ratio is

$$R_{J/\psi}[h_1(\lambda_1)h_2(\lambda_2)]\sim\frac{\alpha_s^6(m_c)}{\alpha_{\rm em}^2}\left(\frac{\Lambda_{\rm QCD}}{m_c}\right)^{4+2|\lambda_1+\lambda_2|}. \tag{4.73}$$

If the decay proceeds via the annihilation process $c\bar{c}\to\gamma^*$, the prefactor $\alpha_{\rm s}^6/\alpha_{\rm em}^2$ is replaced by $\alpha_{\rm s}^2$. The scaling behavior (4.73) illustrates one of the basic qualitative features of the asymptotic QCD predictions: light hadron helicity conservation. The dominant decay modes are predicted to satisfy the helicity

selection rule (4.62). In the case of the decay $J/\psi \to \rho\pi$, the helicity of the pion is $\lambda_\pi = 0$ and the helicity of the ρ is constrained by Lorentz invariance to be $\lambda_\rho = \pm 1$. Thus this decay necessarily violates the helicity selection rule, and its rate is predicted to be suppressed by $\Lambda^2_{\rm QCD}/m_c^2$ relative to modes that are compatible with the helicity selection rule. But $\rho\pi$ is observed to be the largest 2-body decay mode of the J/ψ. This appears to be a clear violation of the asymptotic PQCD predictions. An understanding of the ρ–π puzzle may have important implications for the relevance of asymptotic PQCD to charmonium decays.

The dramatic failure of the prediction (4.67) in some channels indicates a breakdown of the approximation (4.69) for either the J/ψ decay or the $\psi(2S)$ decay or both. The contribution to the amplitude $\mathcal{A}$ from the annihilation of $c\bar{c}$ into 3 hard gluons or a virtual photon should be insensitive to the relative momentum $\mathbf{p}$ of the $c\bar{c}$ pair. The failure of the prediction (4.67) indicates that at least one other dynamical mechanism must be involved. The sensitivity of the amplitude to $\mathbf{p}$ could arise from a fluctuation of the charmonium state into some component of the wave function other than $c\bar{c}$. In a hadronic basis, this fluctuation can be expressed in terms of mixing of the charmonium state with other hadrons. In a parton basis, it can be expressed in terms of $c\bar{c}$ annihilation from a higher Fock state that includes soft gluons.

Many explanations for the $\rho\pi$ puzzle have been proposed. The small upper bound on $\kappa[\rho\pi]$ can be explained either by an enhancement of the rate for $J/\psi \to \rho\pi$ or by a suppression of the rate for $\psi(2S) \to \rho\pi$. The enhancement of $J/\psi \to \rho\pi$ relative to $\psi(2S) \to \rho\pi$ could occur through mixing of J/ψ with another narrow state that has a much larger branching fraction into $\rho\pi$. One such possibility is

1. mixing of J/ψ with a narrow glueball [101, 102].

Direct searches have failed to reveal any evidence for such a glueball. The suppression of $\psi(2S) \to \rho\pi$ relative to $J/\psi \to \rho\pi$ could be explained if the decay is dominated by a particular component of the wave function that is suppressed for $\psi(2S)$ relative to J/ψ. The possibilities include

2. suppression of the $c\bar{c}$ wave function at the origin for a component of $\psi(2S)$ in which the $c\bar{c}$ is in a colour-octet $^3S_1$ state [103],
3. suppression of the $\omega\phi$ component of $\psi(2S)$ [104].

The suppression of $\psi(2S) \to \rho\pi$ relative to $J/\psi \to \rho\pi$ could be explained if the amplitude is dominated by two components of the wave function that nearly cancel in the case of $\psi(2S)$ but not for J/ψ. The possibilities include

4. cancellation between $c\bar{c}$ and $D\bar{D}$ components of $\psi(2S)$ [105],
5. cancellation between $c\bar{c}$ and glueball components of $\psi(2S)$ [105],
6. cancellation between S-wave $c\bar{c}$ and D-wave $c\bar{c}$ components of $\psi(2S)$ [106].

This last proposal leads to the very simple and unambiguous prediction that the D-wave charmonium state $\psi(3770)$ should have a branching fraction into $\rho\pi$ of about 4×10^{-4} [106]. A recently proposed explanation for the ρ–π puzzle is a

7. cancellation between the amplitudes for the resonant process $e^+e^- \to \psi(2S) \to \rho\pi$ and the direct process $e^+e^- \to \rho\pi$. See Sec. 2.8.5.

This proposal predicts that the observed suppression of $\psi(2S) \to \rho\pi$ relative to $J/\psi \to \rho\pi$ is specific to e^+e^- annihilation and should not occur for other charmonium production processes, such as B-meson decay.

It is reasonable to expect that a definitive solution to the ρ–π puzzle should also explain the deviations of $\kappa[h_1h_2]$ from the prediction 1 for other hadrons h_1 and h_2. The existing measurements of the branching fractions into two mesons for J/ψ and $\psi(2S)$ are shown in Table 4.10. While many of the values of $\kappa[h_1h_2]$ are compatible with 1, there are modes other than $\rho\pi$ for which κ is significantly smaller than 1, such as ρa_2, and and there are modes for which κ is significantly greater than 1, such as $K^0_S K^0_L$.

Table 4.10: Comparison of J/ψ and ψ' branching ratios to VP, PP, PA, VS, VV and VT mesons. Unless specified data are from PDG [10]. Where specified we have included in the averages recent data on $\psi(2S)$ decays from BES [100, 107–109] and CLEO [99], the latter derived from reported ratios of branching ratios using values in PDG [10].

Decay mode h_1h_2	$\mathcal{B}(J/\psi \to h_1h_2)$ ($\times 10^4$)	$\mathcal{B}(\psi' \to h_1h_2)$ ($\times 10^4$)	$\kappa[h_1h_2]$ (Eq. 4.65)
$\varrho\pi$	127 ± 9	0.46 ± 0.09 [99] [100]	0.028 ± 0.006
$\omega\pi^0$	4.2 ± 0.6	0.22 ± 0.09 [99] [109]	0.40 ± 0.17
$\varrho\eta$	1.93 ± 0.23	0.23 ± 0.12 [99] [109]	0.9 ± 0.5
$\omega\eta$	15.8 ± 1.6	< 0.11 [108]	< 0.06
$\phi\eta$	6.5 ± 0.7	0.35 ± 0.11 [99] [108]	0.40 ± 0.13
$\varrho\eta'(958)$	1.05 ± 0.18	$0.19^{0.16}_{-0.11} \pm 0.03$ [109]	2.5 ± 0.9
$\omega\eta'(958)$	1.67 ± 0.25	< 0.81 [108]	< 4.3
$\phi\eta'(958)$	3.3 ± 0.4	$0.33 \pm 0.13 \pm 0.07$ [108]	0.71 ± 0.33
$K^*(892)^\mp K^\pm$	50 ± 4	0.26 ± 0.11 [99] [107]	0.039 ± 0.017
$\bar{K}^*(892)^0 K^0$+c.c.	42 ± 4	1.55 ± 0.25 [99] [107]	0.28 ± 0.05
$\pi^+\pi^-$	1.47 ± 0.23	0.8 ± 0.5	4.3 ± 2.7
K^+K^-	2.37 ± 0.31	1.0 ± 0.7	3.2 ± 2.3
$K^0_S K^0_L$	1.46 ± 0.26	0.52 ± 0.07	2.7 ± 0.6
$\pi^\pm b_1(1235)^\mp$	30 ± 5	3.9 ± 1.6 (incl. [99])	1.0 ± 0.4
$\pi^0 b_1(1235)^0$	23 ± 6	$4.0^{+0.9}_{-0.8} \pm 0.6$ [99]	1.3 ± 0.5
$K^\pm K_1(1270)^\mp$	< 30	10.0 ± 2.8	> 1.7
$K^\pm K_1(1400)^\mp$	38 ± 14	< 3.1	< 0.8
$\omega f_0(980) \to \omega\pi\pi$	1.1 ± 0.4		
$\phi f_0(980) \to \phi\pi\pi$	2.5 ± 0.7	0.60 ± 0.22	1.7 ± 0.8
$\omega f_0(1710) \to \omega K\bar{K}$	4.8 ± 1.1		
$\phi f_0(1710) \to \phi K\bar{K}$	3.6 ± 0.6		
$\omega f_1(1420)$	6.8 ± 2.4		
$\phi f_1(1285)$	2.6 ± 0.5		
$\omega f_2(1270)$	43 ± 6	2.1 ± 0.6 [111]	0.34 ± 0.11
$\varrho a_2(1320)$	109 ± 22	2.6 ± 0.9 [111]	0.17 ± 0.07
$K^*(892)^0 \bar{K}^*_2(1430)^0$ + c.c.	67 ± 26	1.9 ± 0.5 [111]	0.19 ± 0.09
$\phi f'_2(1525)$	12.3 ± 2.1	0.44 ± 0.16 [111]	0.22 ± 0.09

One clue to the mechanism is how $\kappa[h_1h_2]$ depends on the J^{PC} quantum numbers for hadrons h_1h_2 with the same flavour quantum numbers as $\rho\pi$. As can be seen in Table 4.10, there also seems to be suppression in the vector-tensor (VT) channel ρa_2, but there seems to be no significant suppression in the axial vector-pseudoscalar (AP) channel $b_1\pi$ or in the pseudoscalar-pseudoscalar (PP) channel $\pi^+\pi^-$. The absence of any suppression in the channel $\pi^+\pi^-$ is to be expected, because it proceeds predominantly through $c\bar{c}$ annihilation into a single photon, and therefore the approximation (4.70) should hold.

Another clue to the suppression mechanism is the pattern of $\kappa[h_1h_2]$ for different radial excitations of mesons with the same J^{PC} quantum numbers. An example is the AP decay modes $K^\pm K_1^\mp$ for different K_1 resonances. The mode $K^\pm K_1(1400)^\mp$ has been observed in J/ψ decays but not in $\psi(2S)$ decays. The mode $K^\pm K_1(1270)^\mp$ has been observed in $\psi(2S)$ decays but not in J/ψ decays. The lower bound on κ for $K^\pm K_1(1270)^\mp$ is significantly greater than the upper bound on κ for $K^\pm K_1(1400)^\mp$. This demonstrates that whether κ is suppressed or enhanced relative to the prediction (4.67) is not determined solely by the J^{PC} quantum numbers of the mesons.

The suppression pattern in a given channel as a function of the flavour quantum numbers should also provide important clues to the suppression mechanism. The channel for which the most measurements are available is the VP channel. The decay amplitude for $J/\psi \to VP$ can be resolved into 3 terms with distinct flavour structures:

- a flavour-connected amplitude g with quark structure $(q_i\bar{q}_j)(q_j\bar{q}_i)$,
- a flavour-disconnected amplitude h with quark structure $(q_i\bar{q}_i)(q_j\bar{q}_j)$,
- an electromagnetic amplitude e with quark structure $Q_{ik}(q_i\bar{q}_j)(q_j\bar{q}_k)$ where Q is the light quark charge matrix.

For example, the amplitude for $J/\psi \to \rho\pi$ is proportional to $g + e$. A quantitative analysis should also take into account SU(3) symmetry breaking from the strange quark mass and $\mathrm{U_A}(1)$ symmetry breaking from the triangle anomaly. In the case of J/ψ, there are enough precise measurements of VP decays to completely determine the flavour decomposition of the amplitude [112, 113]. The conclusion is that $|e|$ and $|h|$ are comparable in magnitude and about an order of magnitude smaller than $|g|$.

The analogous flavour decomposition for $\psi(2S) \to VP$ expresses the decay amplitudes as a linear combination of amplitudes g', h', and e' with distinct flavour structures. The same reasoning that led to the prediction $\kappa[h_1h_2] = 0$ implies that these amplitudes g', h' and e' should differ from the corresponding amplitudes g_1, h_1 and e for J/ψ by the factor

$$\left(\frac{M_{\psi(2S)}\Gamma(\psi(2S)\to e^+e^-)}{M_{J/\psi}\Gamma(J/\psi\to e^+e^-)}\right)^{1/2} \approx 0.70. \tag{4.74}$$

However, the measurement $\kappa[\rho\pi] \approx 0.028$ implies $|g' + e'| \approx 0.12|g + e|$. Since $|g| \gg |e|$, this requires $|g'|$ to be suppressed relative to $0.70|g|$. A mechanism for such a suppression was proposed in Ref. [103]. If g' was so strongly suppressed that it was small compared to $|e'|$, it would make the rate for $\psi(2S) \to \rho\pi$ comparable to electromagnetic processes such as $\psi(2S) \to \omega\pi^0$. The stronger suppression of $\psi(2S) \to \rho\pi$ that is observed requires that g' and e' be comparable in magnitude and to have phases such that there is a further cancellation in the sum $g' + e'$.

The CLEO collaboration has recently presented the first evidence for two-body decays of the $\Upsilon(1S)$ [114]. They observed signals with a statistical significance of greater than 5σ for decays into $\phi f_2'(1525)$ and $\bar{K}K_1(1400)$. The decay of $\Upsilon(1S)$ into $\bar{K}K_1(1270)$ is observed to be suppressed relative to $\bar{K}K_1(1400)$, which is the same pattern observed in J/ψ decays. The CLEO collaboration also set upper limits on other decay modes, the strongest of which is $\mathcal{B}(\Upsilon(1S)\to\rho\pi) < 4 \times 10^{-6}$.

5.2 Decays of J/ψ and $\psi(2S)$ into baryon–antibaryon

As we already discussed these decays seem to be dominated by hard physics where the charm and anticharm quark annihilate into gluons at short distances. In a leading-order calculation of decay widths

for the $B\overline{B}$ channels contributions from higher charmonium Fock states can be neglected since they only produce $\mathcal{O}(v^2)$ corrections, see Eq. (4.60); contributions from higher baryon Fock states are suppressed by powers of $1/m_c$. For consistency, the masses of the J/ψ and $\psi(2S)$ are to be replaced by $2m_c$ (except in phase space factors) since the energy for the binding of a $c\bar{c}$ pair in a charmonium state is an $\mathcal{O}(v^2)$ effect. The only soft physics information on the charmonium state needed in a calculation to lowest order in v is its decay constant. The corresponding electronic decay widths

$$\Gamma(J/\psi\to e^+e^-) \;=\; \frac{4\pi}{3}\,\frac{e_c^2\,\alpha_{\rm em}^2\,f_{J/\psi}^2}{M_{J/\psi}}\,, \tag{4.75}$$

provide their values: $f_{J/\psi} = 409\,\mathrm{MeV}$, $f_{\psi(2S)} = 282\,\mathrm{MeV}$. The other soft physics information required is the leading-twist baryon distribution amplitude. As can be shown [115] the proton is described by one independent distribution amplitude, $\Phi^{\,p}_{123}(x)$, to leading-twist accuracy. The set of subscripts $1,2,3$ refers to the quark configuration $u_+\,u_-\,d_+$ of a proton with positive helicity. The distribution amplitudes for other valence quark configurations in the proton are obtained by permutations of the subscripts. Since flavour SU(3) is a good symmetry, only mildly broken by quark mass effects, it is reasonable to assume that the other members of the lowest-lying baryon octet are also described by only one independent distribution amplitude, which, up to flavour symmetry breaking effects, is the same as the proton one.

To start with and for orientation, we present the leading-twist result for the width of the decays of transversely polarized J/ψs, as for instance are produced in e^+e^- annihilations, into proton–antiproton pairs. The width, evaluated from the asymptotic form of the baryon wave function $\Phi^{\,B}_{\rm AS} = 120\,x_1\,x_2\,x_3$, reads

$$\Gamma(J/\psi\to p\bar{p}) \;=\; \frac{5^6\,2^{10}}{3^5}\,\pi^5\,\alpha_{\rm s}(m_c)^6\,\frac{\varrho[J/\psi\,p\bar{p}]}{M_{J/\psi}}\,\left(\frac{f_{J/\psi}\,f_p^2}{{m_c}^4}\right)^2\,I_{\rm AS}^2\,, \tag{4.76}$$

where

$$I_{\rm AS} \;=\; 6\int [dx]_3\,[dy]_3\,\frac{x_1y_3}{[x_1(1-y_1)+(1-x_1)y_1][x_3(1-y_3)+(1-x_3)y_3]}\,. \tag{4.77}$$

The normalization parameter f_p represents the proton's light-cone wave function for zero spatial separation of the quarks. Strictly speaking, it is defined by [116]

$$\frac{f_p(\mu_F)}{8\sqrt{n_c!}}\,\Phi^{\,p}_{123}(x,\mu_F) \;=\; \int^{\mu_F}[d^2k_\perp]_3\Psi^{\,p}_{123}(x,k_\perp)\,, \tag{4.78}$$

with

$$\int [dx]_3\Phi^{\,p}_{123}(x,\mu_F) \;=\; 1\,. \tag{4.79}$$

Both the distribution amplitude and f_p are subject to evolution [116]. A typical value for f_p is $\simeq 6\times 10^{-3}\,\mathrm{GeV}^2$ [92, 117]. Evaluating the branching ratio from (4.76), (4.77), one obtains

$$\mathcal{B}(J/\psi\to p\bar{p}) \;=\; 1.5\times 10^{-3}\,\left(\frac{\alpha_{\rm s}}{0.4}\right)^3\,\left(\frac{1.5\,\mathrm{GeV}}{m_c}\right)^7\,\left(\frac{f_p}{6\times 10^{-3}\,\mathrm{GeV}^2}\right)^4\,, \tag{4.80}$$

which is in quite good agreement with experiment, see Table 4.11. The predictions for the branching ratio are more robust than that from the $J/\psi\to p\bar{p}$ decay widths since the total J/ψ width is dominated by the decays into light hadrons. Hence, according to (4.12) and (4.75), the branching ratios approximately scale as $1/m_c^7$ and $\alpha_{\rm s}^3$.

In previous calculations [92, 118] of the $J/\psi\to p\bar{p}$ decay width, distribution amplitudes have been employed that are strongly concentrated in the end-point regions where one of the momentum fractions is small. The use of such distribution amplitudes has been heavily criticized [119]. Due to their properties the bulk of the amplitude for the subprocess $c\bar{c}\to 3g^*\to 3(q\bar{q})$ is accumulated in the soft end-point regions where the use of perturbative QCD is inconsistent. Moreover, such distribution amplitudes lead

to extremely strong contributions to the decay amplitude and require compensation by small values of α_s, typically in the range of 0.2–0.3. Such values are unrealistically small with regard to the characteristic scales available in charmonium decays. For an average gluon virtuality of about $1\,\mathrm{GeV}^2$ one would expect α_s to be rather 0.4.

Recent theoretical [97, 120] and phenomenological [117] studies provide evidence that the proton distribution amplitude is close to the asymptotic form for baryons: the end-point concentrated forms seem to be obsolete. In a recent analysis of the J/ψ and $\psi(2S)$ decays into baryon–antibaryon pairs [121] use is made of the phenomenological proton distribution amplitude proposed in [117]

$$\Phi_{123}^{p}(x,\mu_0) \;=\; \Phi_{\mathrm{AS}}^{B}\,\frac{1}{2}\,(1+3x_1)\,, \tag{4.81}$$

which is valid at the factorization scale $\mu_0 = 1\,\mathrm{GeV}$. This distribution amplitude goes along with the normalization parameter $f_p(\mu_0) = 6.64 \times 10^{-3}\,\mathrm{GeV}^2$. In [121] the distribution amplitude (4.81) has been suitably generalized to the cases of hyperons and decuplet baryons by allowing for flavour symmetry breaking due to the effect of the strange quark mass. Instead of the collinear approximation as used in [92, 118] or in (4.76), the modified perturbative approach [122] is applied in [121]. In this approach quark transverse momenta are retained and Sudakov suppressions, comprising those gluonic radiative corrections not included in the evolution of the distribution amplitude, are taken into account. The advantage of the modified perturbative approach is the strong suppression of the soft end-point regions where perturbative QCD cannot be applied. If distribution amplitudes close to the asymptotic form are employed the difference between a calculation on the basis of the collinear approximation and one within the modified perturbative approach is, however, not substantial given that the $J/\psi \to B\overline{B}$ amplitude is anyhow not very sensitive to the end-point regions. This is in marked contrast to the case of the proton's electromagnetic form factor [123]. On the other hand, a disadvantage of the modified perturbative approach is that the full baryon light-cone wave function is needed and not just the distribution amplitude. In [121] the transverse momentum dependence of the baryon wave functions has been parameterized by a simple Gaussian

$$\propto \exp\left[-a_B^2\,\sum k_{\perp i}^2/x_i\right], \tag{4.82}$$

where a value of $0.75\,\mathrm{GeV}^{-1}$ has been adopted for the transverse size parameter a_B. For the decuplet baryons a somewhat larger value has been used ($0.85\,\mathrm{GeV}^{-1}$). Calculating the subprocess amplitude from the Feynman graphs shown in Fig. 4.5 and working out the convolution of subprocess amplitude and baryon wave functions, one obtains the widths Γ_{3g} for the J/ψ decays into $B\overline{B}$ pairs mediated by the hard annihilation process $c\bar{c} \to 3g^* \to 3(q\bar{q})$. The results are listed and compared to experimental data in Table 4.11. In addition to the three-gluon contribution there is also an isospin symmtetry violating electromagnetic one generated by the subprocess $c\bar{c} \to \gamma^* \to 3(q\bar{q})$, see Fig. 4.7. According to [121] this contribution is probably small, of the order of a few percent only. An important ingredient in this estimate of the size of the electromagnetic contribution is the agreement of the experimental widths for J/ψ decays into $n\bar{n}$ and $p\bar{p}$ within the errors [10]. The contributions from the $c\bar{c} \to g^*g^*\gamma^* \to 3(q\bar{q})$ to the baryon–antibaryon channels amount to less than 1% of the three-gluon contribution and can be neglected.

The widths for the corresponding decays of the $\psi(2S)$ are easily obtained within the perturbative approach by rescaling the J/ψ ones by the ratio of the electronic $\psi(2S)$ and J/ψ decay widths, the 15% rule, i.e., Eq. (4.65) with $\kappa[B\overline{B}] = 1$, holds strictly in the approach put forward in [121]. The results obtained that way are also quoted in Table 4.11. Good agreement between theory and experiment [10] is observed. Predictions of the absolute value of a decay width are subject to many uncertainties, see (4.76) while ratios of any two $B\overline{B}$ decay widths are robust since most of the uncertainties cancel to a large extent. It is to be emphasized that the $\psi(2S)$ and J/ψ decay widths do not scale as $(M_{J/\psi}/M_{\psi(2S)})^8 \simeq 1/4$ as suggested in [91] since the subprocess amplitude in a calculation to lowest order in the charm quark velocity (see (4.60)) has to be calculated with $2m_c$ and not with the bound state mass.

Table 4.11: Results for J/ψ and $\psi(2S)$ branching ratios for $B\overline{B}$ channels in units of 10^{-3} and 10^{-4}, respectively. The three-gluon contributions, taken from [121], are evaluated from $m_c = 1.5$ Gev, and the one-loop α_s with $\Lambda_{\rm QCD} = 210$ MeV. Unless specified data are taken from Ref. [10]. For the $J/\psi \to p\bar{p}$ we have included the recent BES measurement [124] in the average. The theoretical branching ratios are evaluated using $\Gamma(J/\psi) = 91.0 \pm 3.2\,\text{keV}$ [10].

channel	$p\bar{p}$	$\Sigma^0\overline{\Sigma}^0$	$\Lambda\overline{\Lambda}$	$\Xi^-\overline{\Xi}^+$	$\Delta^{++}\overline{\Delta}^{--}$	$\Sigma^{*-}\overline{\Sigma}^{*+}$
$\mathcal{B}_{3g}(J/\psi)$	1.91	1.24	1.29	0.69	0.72	0.45
$\mathcal{B}_{\rm exp}$ [10]	2.16 ± 0.08	1.27 ± 0.17	1.30 ± 0.12	0.90 ± 0.20	1.10 ± 0.29	1.03 ± 0.13
$\mathcal{B}_{3g}(\psi(2S))$	2.50	1.79	1.79	1.11	1.07	0.80
$\mathcal{B}_{\rm exp}$ [10]	2.07 ± 0.31	1.2 ± 0.6	1.81 ± 0.34	0.94 ± 0.31	1.28 ± 0.35	1.10 ± 0.40

Bottomonium decays into $B\overline{B}$ pairs can be calculated along the same lines. The hard scale is now provided by the b-quark mass. Hence, relativistic and higher-twist corrections are expected to be smaller than in the charmonium case. But, as it turns out, the predicted decay widths for the baryonic channels are very small. Approximately, i.e., ignoring the fact that the $k_\perp$-dependent suppression of the three-gluon contribution is perhaps a bit different in the two cases, one finds the following rescaling formula

$$\begin{aligned}\Gamma(\Upsilon \to B\overline{B}) &= \frac{\varrho[\Upsilon B\overline{B}]}{\varrho[J/\psi B\overline{B}]}\,\frac{\Gamma(\Upsilon \to e^+e^-)}{\Gamma(J/\psi \to e^+e^-)} \\ &\times \left(\frac{e_c}{e_b}\right)^2 \left(\frac{\alpha_s(m_b)}{\alpha_s(m_c)}\right)^6 \left(\frac{m_b}{m_c}\right)^8 \Gamma(J/\psi \to B\overline{B})\,. \end{aligned} \tag{4.83}$$

Using $m_b = 4.5\,\text{GeV}$ one obtains, for instance, a value of $0.02\,\text{eV}$ for the $\Upsilon \to p\bar{p}$ decay width, which value corresponds to a branching ratio of 0.3×10^{-7} well below the present experimental upper bound [10].

It goes without saying that the hard contributions, Γ_{3g}, to the J/ψ and $\psi(2S)$ decays into $B\overline{B}$ pairs respect the helicity sum rule (4.62), i.e., the amplitude for the production of baryon and antibaryon in equal helicities states vanishes. Measurements of the angular distribution in $e^+e^- \to J/\psi,\ \psi(2S) \to B_8\overline{B}_8$

$$\frac{d\Gamma}{d\cos\vartheta} \propto 1 + \alpha_{B_8}\,\cos^2\vartheta\,, \tag{4.84}$$

where B_8 is any member of the lowest-lying baryon octet and ϑ the c.m.s. production angle, allow for a test of this prediction. In the formal limit of an infinitely heavy charm quark $\alpha_{B_8} = 1$ as a consequence of hadronic helicity conservation [91]. The available data [124–128], listed in Table 4.12, tell us that only a fraction of about 10% of the total number of $B_8\overline{B}_8$ pairs are produced with the same helicity of baryon and antibaryon. This observation is in fair agreement with hadronic helicity conservation. The production of $B_8\overline{B}_8$ pairs with equal helicities has been modeled as a constituent quark [129,130] and/or hadron mass effect [131], both the effects are part of the $\mathcal{O}(v^2)$ and higher-twist/power corrections. Also electromagnetic effects in α_B have been investigated. For results we refer to Table 4.12.

5.3 Hadronic two-body decays of the η_c

Such decays of the η_c have been observed in experiment only for the $B\overline{B}$ and VV channels, upper bounds exist for a few others like $a_0(980)\pi$. Decays into PP and PV have not been observed, they are either

Table 4.12: Experimental and theoretical results for the parameter α_{B_8} in $J/\psi, \psi(2S) \to B_8\overline{B}_8$ as defined in Eq. (4.84). Experimental values obtained averaging data from BES [124], DM2 [125], MARK II [126], E760 [127] and E835 [128].

$\alpha_{B_8}(J/\psi)$	$p\overline{p}$	$\Lambda\overline{\Lambda}$	$\Sigma^0\overline{\Sigma}^0$
Predicted: [131]	0.46	0.32	0.31
[129] (no e.m. corr)	0.69	0.51	0.43
[129] (incl. e.m. corr)	0.70		
Experiment: J/ψ	0.66 ± 0.05	0.65 ± 0.19	0.26 ± 0.30
$\psi(2S)$	0.68 ± 0.14		

strictly forbidden or strongly suppressed, see Table 4.9. As noted at the beginning of this section the $B\overline{B}$ and VV channels are forbidden to leading-twist accuracy since hadronic helicity conservation (4.62) is in conflict with angular momentum conservation for these processes. In contrast to the expectation from the leading-twist approximation the measured branching ratios are rather large (10^{-3}–10^{-2}). We repeat, it is worthwhile to explore the role of higher-twist baryon and vector meson wave functions in the decays of the η_c [96, 97].

In [104] a mixing approach for the explanation of these η_c decays has been advocated. As is well-known the $U_{\rm A}(1)$ anomaly leads to mixing among the pseudoscalar mesons $\eta - \eta' - \eta_c$ [132, 133]. This mixing can adequately be treated in the quark-flavour mixing scheme [134] where one starts from the quark-flavour basis and assumes that the basis states and their decay constants follow the same pattern of mixing with common mixing angles. This assumption is supported by an analysis of the $\gamma - \eta$ and $\gamma - \eta'$ transition form factors at large momentum transfer [135]. The quark-flavour basis states are defined by the flavour content of their valence Fock states

$$\eta_q \to (u\bar{u} + d\bar{d})/\sqrt{2}\,, \qquad \eta_s \to s\bar{s}\,, \qquad \eta_{c0} \to c\bar{c}\,. \tag{4.85}$$

The admixture of the light quarks to the η_c, which we need here in this work, is controlled by a mixing angle θ_c [134]

$$|\eta_c\rangle \;=\; |\eta_{c0}\rangle \;-\; \frac{\theta_c}{\sqrt{1+y^2/2}} \left[\, |\eta_q\rangle + \frac{y}{\sqrt{2}}\, |\eta_s\rangle \right] . \tag{4.86}$$

The ratio of the basis decay constants f_q and f_s is denoted by y

$$y \;=\; f_q/f_s\,. \tag{4.87}$$

According to [134], its value amounts to 0.81 while $\theta_c = -1^\circ \pm 0.1^\circ$. The light-quark admixture to the η_c (4.86) is somewhat smaller than estimates given in [132] but slightly larger than quoted in [136]. In combination with the strong vertex $q\overline{q} \to VV$ this small light-quark component of the η_c suffices to account for the VV decays. In the spirit of this dynamical mechanism (see Fig. 4.8) the invariant amplitude, A, for the $\eta_c \to VV$ decays can be parameterized as

$$A(\eta_c \to VV) \;=\; C_{VV}^{\rm mix}\; \sigma_{VV}\; F_{\rm mix}(s = M_{\eta_c}^2)\,. \tag{4.88}$$

It is related to the decay width by

$$\Gamma(\eta_c \to VV) \;=\; \frac{1}{32\pi S_{VV}}\, \frac{\varrho[\eta_c VV]^3}{M_{\eta_c}}\; |A(\eta_c \to VV)|^2\;. \tag{4.89}$$

Table 4.13: Mixing factors as well as experimental and theoretical ratios of decay widths for $\eta_c \to V^0 V^0$. The ratios are quoted with respect to the $\rho^0\rho^0$ channel ($C^{\rm mix}_{\rho^0\rho^0} = 1$). Experimental ratios are calculated taking into account the common systematics.

VV	$C^{\rm mix}_{VV}$	$R_{\rm th}$	$R_{\rm exp}$
$\omega\omega$	1	0.63	< 0.37 [137]
			< 0.75 [138]
$K^{*0}\overline{K}^{*0}$	$(1+y^2)/2$	0.61	0.47 ± 0.09 [138]
			0.55 ± 0.27 [137]
$\phi\phi$	y^2	0.13	0.93 ± 0.33 [137]
			0.35 ± 0.10 [138]
			0.30 ± 0.10 [139]
			0.21 ± 0.14 [140]

The statistical factor for the decay into a pair of identical particles is denoted by S_{VV}. The mixing factor $C^{\rm mix}_{VV}$ embodies the mixing of the η_c with the basis states η_q and η_s (4.86). These factors are quoted in Table 4.13. Flavour symmetry breaking effects in the transitions $\eta_i \to VV$ ($i = q, s$) are absorbed in the factor σ_{VV}. As a simple model for it one may take the square of the vector meson's decay constants as a representative of SU(3) violations in these transitions ($f_\rho = 216\,\mathrm{MeV}$, $f_\omega = 195\,\mathrm{MeV}$, $f_\phi = 237\,\mathrm{MeV}$, $f_{K^*} = 214\,\mathrm{MeV}$). In order to have a dimensionless quantity, f_V^2 is scaled by the squared vector meson mass

$$\sigma_{VV} \;=\; \left(\frac{f_V}{M_V}\right)^2 . \tag{4.90}$$

Ratios of decay widths are free of the unknown transition form factor $F_{\rm mix}$. With respect to the $\rho^0\rho^0$ channel one finds for the other uncharged vector mesons channels

$$\frac{\Gamma(\eta_c \to V^0V^0)}{\Gamma(\eta_c \to \rho^0\rho^0)} \;=\; \frac{2}{S_{V^0V^0}} \left(C^{\rm mix}_{V^0V^0}\right)^2 \left(\frac{\sigma_{V^0V^0}}{\sigma_{\rho^0\rho^0}}\right)^2 \left(\frac{\varrho[\eta_c V^0V^0]}{\varrho[\eta_c\rho^0\rho^0]}\right)^3 . \tag{4.91}$$

The theoretical and experimental results on the ratios are listed in Table 4.13. Reasonable agreement between theory and experiment can be seen although the errors are large. Assuming a monopole behaviour for the transition form factor $F_{\rm mix}$ and fitting its strength to the $\rho\rho$ data, one obtains a value that is in accord with the concept of mixing.

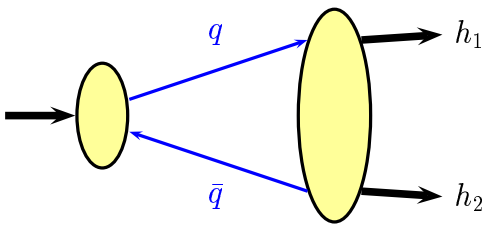

Fig. 4.8: The mixing mechanism for charmonium decays into light hadrons.

The mixing approach can also be applied to the η_c decays into baryon–antibaryon pairs. It seems that at least the $p\bar{p}$ channel for which the decay width has been measured, is also controlled by the mixing mechanism [104].

5.4 The decays of the χ_{cJ} and the role of the colour-octet contribution

The colour-singlet contribution to χ_{cJ} decays into pairs of pseudoscalar or vector mesons is well-known, it has been calculated several times [90, 92, 95]. The convolution of wave functions and hard subprocess amplitudes, which are to be calculated from Feynman graphs as shown in Fig. 4.5, leads to a decay width for the $\pi^+\pi^-$ channel as ($J = 0, 2$)

$$\begin{aligned}\Gamma(\chi_{cJ}\to\pi^+\pi^-) &= 2\,\frac{\pi^2}{3^5}\,\frac{\varrho[\chi_{cJ}\,\pi\pi]}{M_{\chi_{cJ}}}\,\frac{f_\pi^4}{m_c^7}\,|R'_{\chi_{cJ}}(0)|^2\,\alpha_{\rm s}^4(m_c)\\ &\times \left|a_J + b_J\,B_2^\pi(m_c) + c_J\,B_2^\pi(m_c)^2\right|^2\,, \end{aligned} \tag{4.92}$$

where the parameters a_J, b_J and c_J are analytically calculable real numbers in the leading-twist approximation; they represent the convolution of distribution amplitudes an subprocess amplitude. The parameter a_0, for instance, reads

$$a_0 \;=\; 27\pi^2/2 - 36\,. \tag{4.93}$$

The representation (4.92) also holds in the modified perturbative approach but the parameters are then complex valued. The constant $B_2^\pi(\mu_0)$ is the first coefficient of the expansion of the leading-twist pion distribution amplitude upon Gegenbauer polynomials $C_n^{3/2}$ [116]

$$\Phi_\pi \;=\; \Phi_{\rm AS}^M\left[1 + \sum_{n=2,4,\cdots} B_n^\pi(\mu_F)\,C_n^{3/2}(2x-1)\right]\,, \tag{4.94}$$

where $\Phi_{\rm AS}^M$ is the asymptotic form of a meson distribution amplitude

$$\Phi_{\rm AS}^M \;=\; 6x(1-x)\,, \tag{4.95}$$

and

$$B_n(\mu_F) \;=\; \left(\frac{\ln(\mu_F^2/\Lambda^2_{\rm QCD})}{\ln(\mu_0^2/\Lambda^2_{\rm QCD})}\right)^{\gamma_n}\,B_n(\mu_0)\,. \tag{4.96}$$

In Eq. (4.92) terms of order higher than 2 in the expansion are neglected and the factorization scale dependence of the Gegenbauer coefficient B_2 is controlled by $\gamma_2 = -50/81$. As the starting scale of the evolution, μ_0, a value of 1 GeV is taken. Finally, f_π (= 132 MeV) is the pion decay constant and $R'_{\chi_{cJ}}(0)$ (= 0.22 GeV$^{5/2}$ [33, 141]) denotes the derivative of the nonrelativistic radial $c\bar{c}$ wave functions at the origin (in coordinate space). As usual a normalization factor $f_\pi/(2\sqrt{6})$ is pulled out from the distribution amplitude.

The distribution amplitude of the pion is fairly well-known by now from analyses of the $\pi^0 - \gamma$ transition form factor. It is close to the asymptotic form of a meson distribution amplitude [142]. Deviations from that form are difficult to estimate since they strongly depend on details of the analysis such as whether or not NLO, higher-twist corrections or tranverse degrees of freedom are taken into account [142, 143]. But in any case the Gegenbauer coefficient B_2^π seems to be small in magnitude. Combining the results from different analyses of the $\pi^0 - \gamma$ transition form factor, one may conclude that $|B_2^\pi| \lesssim 0.1$ at $\mu_0 = 1$ GeV. Taking first $B_2^\pi = 0$ in (4.92), one evaluates from (4.92) the branching ratio

$$\mathcal{B}(\chi_{c0(2)}\to\pi^+\pi^-) \simeq 0.31\,(0.10)\times 10^{-3}\,\left(\frac{\alpha_{\rm s}}{0.4}\right)^2\,\left(\frac{1.5\,{\rm GeV}}{m_c}\right)^3\,. \tag{4.97}$$

The majority of the widths of the χ_{c0} and χ_{c2} come from decays into light hadrons. The contribution coming from the decay of a colour-singlet $c\bar{c}$ into real gluons is given by [33]

$$\Gamma(\chi_{cJ}\to l.h.) \;\propto\; |R'_{\chi_{cJ}}(0)|^2\,\frac{\alpha_{\rm s}^2}{{m_c}^4}\,. \tag{4.98}$$

Therefore, the branching ratios approximately scale as given in (4.97) and not as in (4.92). The $c\bar{c}$ wave function $R'_{\chi_{cJ}}(0)$ almost cancel in the ratio. Otherwise its well-known scaling properties [144] would have to be taken into account as well.

The variation of the branching ratio with the Gegenbauer coefficient B_2^π is displayed in Fig. 4.9. One can conclude that, stretching all parameters (B_2^π, α_s, m_c) to the extreme, the predictions for $\mathcal{B}(\chi_{c0(2)} \to \pi^+\pi^-)$ from the colour-singlet contribution to leading-twist accuracy stay a factor 3–6 below the data. Results of similar magnitude are found within the modified perturbative approach.

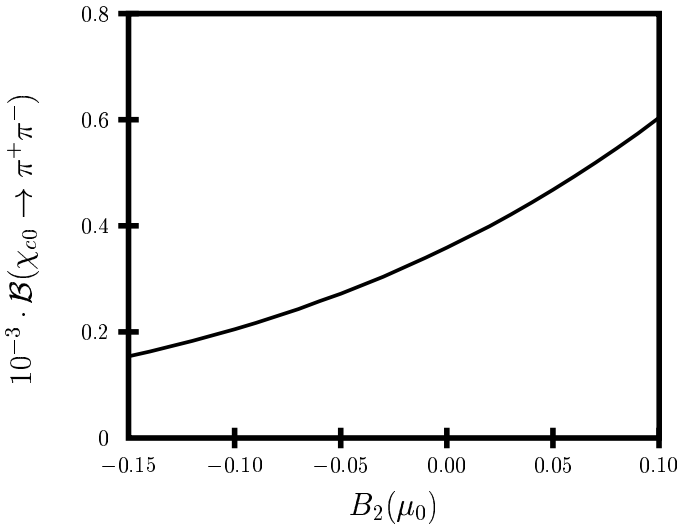

Fig. 4.9: Dependence of the leading-twist colour-singlet contribution to the $\chi_{c0} \to \pi^+\pi^-$ branching ratio on the expansion parameter B_2^π of the pion distribution amplitude at the scale $\mu_0 = 1\,\mathrm{GeV}$. The evolution of B_2^π is evaluated from $\Lambda_{\mathrm{QCD}} = 200\,\mathrm{MeV}$.

Thus, there is obviously room for the colour-octet contributions (see (4.59)), i.e., from the subprocess $c\bar{c}g \to 2(q\overline{q})$. A first attempt to include the colour-octet contribution has been undertaken in [94]. This calculation, performed within the modified perturbative approach [122], is based on a very rough model for the colour-octet χ_{cJ} wave function, the new ingredient of this calculation. Despite this the authors of Ref. [94] were able to show that the combined colour-singlet and -octet contributions are likely large enough to account for the data [10, 66], see Table 4.14. The calculation of the $\chi_{cJ} \to \pi^+\pi^-$ decay width can be generalized to other pseudoscalar meson channels with results of similar quality as for the $\pi\pi$ channels. For the $\eta'\eta'$ channel an additional two-gluon Fock component of the η' is to be taken into account whose leading-twist distribution amplitude has recently been extracted from a NLO analysis of the $\eta - \gamma$ and $\eta' - \gamma$ transition form factor [145, 146]. For the $\eta\eta$ channel the two-gluon contribution is probably negligible.

The colour-singlet contribution to the decays $\chi_{cJ} \to p\bar{p}$ ($J = 1, 2$) has been investigated by many authors [92, 95, 118, 150]. Employing the proton distribution amplitude (4.81) or a similar one, one again finds results that are clearly below experiment, which again signals the lack of the colour-octet contributions. An analysis of the $\chi_{c1(2)}$ decays into the octet and decuplet baryons along the same lines as for the pseudoscalar meson channels [94] has been carried through by Wong [147]. The branching ratios have been evaluated from the baryon wave functions (4.81), (4.82) and the same colour-octet χ_{cJ} wave function as in [94]. Some of the results obtained in [147] are shown and compared to experiment in Table 4.14. As can be seen from the table the results for the $p\bar{p}$ channels are in excellent agreement with experiment while the branching ratios for $\Lambda\overline{\Lambda}$ channels are much smaller than experiment [148] although the errors are large. A peculiar fact has to be noted: the experimental $\Lambda\overline{\Lambda}$ branching ratios are larger than the proton–antiproton ones although there is agreement within two standard deviations.

Table 4.14: Comparison of theoretical and experimental branching ratios for various χ_{cJ} decays into pairs of light hadrons. The theoretical values have been computed within the modified perturbative approach, colour-singlet and -octet contributions are taken into account ($B_2^\pi = B_2^\eta = B_1^K = 0$, $B_2^K = -0.1$, baryon wave functions (4.81), (4.82)). The branching ratios are quoted in units of 10^{-3} for the mesonic channels and 10^{-5} for the baryonic ones. Data taken from [10]. The values listed for $p\bar{p}$ branching rates do not include the most recent values $\left(27.4^{+4.2}_{-4.0} \pm 4.5\right) \cdot 10^{-5}$, $\left(5.7^{+1.7}_{-1.5} \pm 0.9\right) \cdot 10^{-5}$ and $\left(6.9^{+2.5}_{-2.2} \pm 1.1\right) \cdot 10^{-5}$ measured by BES [149] for $\chi_c 0$, χ_{c1} and χ_{c2} respectively.

process	theory	experiment
$\mathcal{B}(\chi_{c0} \to \pi^+ \pi^-)$	3.0 [94]	4.9 ± 0.6
$\mathcal{B}(\chi_{c2} \to \pi^+ \pi^-)$	1.8 [94]	1.77 ± 0.27
$\mathcal{B}(\chi_{c0} \to K^+ K^-)$	2.4 [94]	6.0 ± 0.9
$\mathcal{B}(\chi_{c2} \to K^+ K^-)$	1.4 [94]	0.94 ± 0.21
$\mathcal{B}(\chi_{c0} \to \eta\, \eta)$	2.0 [94]	2.1 ± 1.1
$\mathcal{B}(\chi_{c2} \to \eta\, \eta)$	1.3 [94]	< 1.5
$\mathcal{B}(\chi_{c0} \to p\, \bar{p})$	–	22.4 ± 2.7
$\mathcal{B}(\chi_{c1} \to p\, \bar{p})$	6.4 [147]	7.2 ± 1.3
$\mathcal{B}(\chi_{c2} \to p\, \bar{p})$	7.7 [147]	6.8 ± 0.7
$\mathcal{B}(\chi_{c0} \to \Lambda\, \overline{\Lambda})$	–	47 ± 16
$\mathcal{B}(\chi_{c1} \to \Lambda\, \overline{\Lambda})$	3.8 [147]	26 ± 12
$\mathcal{B}(\chi_{c2} \to \Lambda\, \overline{\Lambda})$	3.5 [147]	34 ± 17

The present analyses of the χ_{cJ} decays suffer from the rough treatment of the colour-octet charmonium wave function. As we mentioned before a reanalysis of the decays into the PP and $B\overline{B}$ channels as well as an extension to the VV ones is required. Our knowledge of the colour-octet wave function has been improved recently due to the intense analyses of inclusive processes involving charmonia, e.g., [151]. This new information may be used to ameliorate the analysis of the $\chi_{cJ} \to PP, B\overline{B}$ decays and, perhaps, to reach a satisfactory quantitative understanding of these processes. We finally want to remark that the colour-octet contribution does not only play an important role in the χ_{cJ} decays into PP and $B\overline{B}$ pairs but potentially also in their two-photon decays [30, 33, 152] (see also Section 3).

The leading-twist forbidden $\chi_{c0} \to B\overline{B}$ decays have sizeable experimental branching ratios, see Table 4.14. There is no reliable theoretical interpretation of these decays as yet. The only proposition [153] is the use of a diquark model, a variant of the leading-twist approach in which baryons are viewed as being composed of quarks and quasi-elementary diquarks. With vector diquarks as constituents one may overcome the helicity sum rule (4.62). The diquark model in its present form, however, contends with difficulties. Large momentum transfer data on the Pauli form factor of the proton as well as a helicity correlation parameter for Compton scattering off protons are in severe conflict with predictions from the diquark model.

5.5 Radiative decays of charmonia into light hadrons

First let us consider the process $J/\psi \to \gamma\pi^0$. The apparently leading contribution to it is generated by the subprocess $c\bar{c} \to \gamma\, g^* g^* \to \gamma q\bar{q}$, which, in principle, leads to a decay width of order α_s^4. However, due to the pion's flavour content $\propto u\bar{u} - d\bar{d}$ this contribution exactly cancels to zero in the limit of massless quarks. A VDM contribution $J/\psi \to \rho\pi$ followed by a $\rho - \gamma$ conversion [95] seems to dominate this

process. Indeed, an estimate of the VDM contribution leads to a branching ratio of 3.3×10^{-5}, which compares favorably with the experimental result of $(3.9 \pm 1.3) \times 10^{-5}$ [10]. Analogue estimates of the $\gamma\eta$ and $\gamma\eta'$ branching ratios lead to similar values, about 1×10^{-5}, which fall short of the experimental results by two orders of magnitude. The solution of this discrepancy is a gluonic contribution, which occurs as a consequence of the $\mathrm{U_A}(1)$ anomaly; it formally presents a power correction. According to Novikov et al. [154], the photon is emitted by the c quark with a subsequent annihilation of the $c\bar{c}$ pair into lighter quarks through the effect of the anomaly. The creation of the corresponding light quarks is controlled by the gluonic matrix element $\langle 0|\alpha_s G\widetilde{G}\,|\eta^{(\prime)}\rangle$ where G is the gluon field strength tensor and $\widetilde{G}$ its dual. Photon emission from the light quarks is negligible as can be seen from the smallness of the $\gamma\pi$ width. This mechanism leads to the following width for the radiative J/ψ decay into $\eta^{(\prime)}$ [154]

$$\Gamma(J/\psi\to\gamma\eta^{(\prime)}) \;=\; \frac{2^5}{5^2 3^8}\,\pi e_c^2\alpha_{\mathrm{em}}^3\,\varrho[J/\psi\gamma\eta^{(\prime)}]\,\left(\frac{M_{J/\psi}}{{m_c}^2}\right)^4\,\frac{|\langle\,0\,|\,\frac{\alpha_s}{4\pi}\,G\widetilde{G}\,|\,\eta^{(\prime)}\,\rangle|^2}{\Gamma(J/\psi\to e^+e^-)}\,. \tag{4.99}$$

In the quark-flavour mixing scheme the gluonic matrix element for the η is given by [155]

$$\langle\,0\,|\frac{\alpha_s}{4\pi}\,G\widetilde{G}|\,\eta\,\rangle \;=\; -\sin\theta_8\,\sqrt{2+y^2}\,f_q\,a^2\,. \tag{4.100}$$

For the η' matrix element $\sin\theta_8$ is to be replaced by $\cos\theta_8$. The angle θ_8 controls the mixing of the octet decay constants. In [134] the various mixing parameters have been determined; their values amount to:

$$\theta_8 \;=\; -21.2^\circ\,;\quad f_q \;=\; 1.07 f_\pi\,;\quad a^2 \;=\; 0.265\,\mathrm{GeV}^2\,;\quad \phi \;=\; 39.3^\circ\,. \tag{4.101}$$

The latter angle is the mixing angle in the quark-flavour basis. The parameter y has been defined in Eq. (4.87). Evaluating the decay width or rather the branching ratio from these parameter values, one obtains

$$\mathcal{B}(J/\psi\to\gamma\eta) \;=\; 3.7\times 10^{-4}\,\left(\frac{1.5\,\mathrm{GeV}}{m_c}\right)^7\,. \tag{4.102}$$

The comparison with the experimental value of $(8.6\pm0.8)\cdot10^{-4}$ [10] reveals that the order of magnitude is correctly predicted. As happens frequently in exclusive charmonium decays the charm-quark mass appears to a high power in the theoretical estimates of branching ratios with the consequence of large uncertainties in the predicted values. With regard to the fact that the total J/ψ decay width is dominated by the decays into light hadrons (4.12), the power of m_c in (4.102) is approximately seven. The mass of the J/ψ appears in (4.99) through a pole saturation of a QCD sum rule [154]; it should not be replaced by $2m_c$.

While the calculation of the individual decay widths is not easy, ratios of the η and η' widths can be reliably predicted from $\eta-\eta'$ mixing. Using the quark-flavour mixing scheme again, one finds from (4.99) and (4.100) the following ratios for radiative J/ψ decays [134]

$$\frac{\mathcal{B}(J/\psi\to\gamma\eta')}{\mathcal{B}(J/\psi\to\gamma\eta)} \;=\; \cot^2\theta_8\,\left(\frac{\varrho[J/\psi\gamma\eta']}{\varrho[J/\psi\gamma\eta]}\right)^3\,. \tag{4.103}$$

The extension to the η_c is also possible. With (4.86) one obtains

$$\frac{\mathcal{B}(J/\psi\to\gamma\eta')}{\mathcal{B}(J/\psi\to\gamma\eta_c)} \;=\; \theta_c^2\cos^2\theta_8\,\left(\frac{\varrho[J/\psi\gamma\eta']}{\varrho[J/\psi\gamma\eta_c]}\right)^3\,. \tag{4.104}$$

This approach leads to the following numerical results:

$$\begin{aligned}
\frac{\mathcal{B}(J/\psi\to\gamma\eta')}{\mathcal{B}(J/\psi\to\gamma\eta)} \;&=\; 5.39\,, \qquad \mathrm{Exp:}\;\; 5.0\;\pm 0.6\;\;[10]\;,\\
\frac{\mathcal{B}(J/\psi\to\gamma\eta')}{\mathcal{B}(J/\psi\to\gamma\eta_c)} \;&=\; 0.48\,, \qquad \mathrm{Exp:}\;\; 0.33\pm 0.1\;\;[10]\;.
\end{aligned} \tag{4.105}$$

Due to the large uncertainties in the angle θ_c the prediction for the second ratio has an error of about 20%.

It is tempting to extend the anomaly dominance to the case of the radiative Υ decays. One obtains

$$\frac{\mathcal{B}(\Upsilon\to\gamma\eta')}{\mathcal{B}(\Upsilon\to\gamma\eta)} \;=\; 6.51\,, \qquad \frac{\mathcal{B}(\Upsilon\to\gamma\eta')}{\mathcal{B}(\Upsilon\to\gamma\eta_c)} \;=\; 3.5\times 10^{-4}\,. \tag{4.106}$$

Comparison with experiment is not yet possible, only upper bounds exist for the individual branching ratios. Doubts have, however, been raised by Ma [156] on the validity of this approach for the Υ decays. Generalizing the result for the J/ψ case (4.99) appropriately, one finds a too large branching ratio, namely $\simeq 8.3\times 10^{-5}$, as compared to the experimental upper limit of $\leq 1.6\times 10^{-5}$ [10]. The estimate advocated for by Ma, is based on the assumption of scale independence of the gluonic matrix element. With regard to the well separated scales m_c and m_b this assumption is suspicious. Nonetheless, the investigation of the $\Upsilon\to\gamma\eta^{(\prime)}$ decays is to be addressed further. Of interest would also be an investigation of the radiative h_c decays into pseudoscalar mesons. It is likely that these decays are under control of the same dynamical mechanism as the corresponding J/ψ decays. Results analogue to (4.103), (4.104) would then hold. Instead of the decays into pseudoscalar mesons one may also explore radiative quarkonium decays into scalar mesons. As is well-known scalar mesons may have sizeable glue–glue Fock components [157], they may even be glueballs although they likely have sizeable admixtures of light quarks [158, 159]. It would be interesting to unravel the dynamics mediating these decays. For first attempts see for instance [159, 160].

The decays $J/\psi\to\rho\eta^{(\prime)}$ can be treated analogously to the radiative decays. Since in these processes G-parity is not conserved, they proceed through $c\bar{c}\to\gamma^*$. On account of the flavour content of the ρ meson, the $\gamma^*\to\rho\eta^{(\prime)}$ transition only probes the η_q component of the $\eta^{(\prime)}$ if OZI-suppressed contributions are neglected. Hence,

$$\frac{\mathcal{B}(J/\psi\to\rho\eta')}{\mathcal{B}(J/\psi\to\rho\eta)} \;=\; \tan^2\phi\,\left(\frac{\varrho[J/\psi\rho\eta']}{\varrho[J/\psi\rho\eta]}\right)^3\,, \tag{4.107}$$

the $\rho-\eta_q$ form factor cancels in the ratio. Equation (4.107) leads to 0.52 for the ratio of the decay widths while the experimental value is 0.54 ± 0.21 [10].

Finally, we want to mention the radiative J/ψ decay into a proton–antiproton pair. Recently, an enhancement near $2M_p$ in the invariant mass spectrum of $p\bar{p}$ pairs has been observed while $J/\psi\to\pi^0 p\bar{p}$ behaves regular near the $p\bar{p}$ threshold [161]. The combination of both the results hints at a peculiar behaviour of the $p\bar{p}$ pair in an isospin-zero state. The enhancement observed in $J/\psi\to\gamma p\bar{p}$ parallels similar anomalies near the $p\bar{p}$ threshold. They have been reported by Belle [162] for the decays $B^+\to K^+ p\bar{p}$ and $\overline{B}^0\to D^0 p\bar{p}$. An anomalous threshold behaviour is also seen in the proton's time-like form factor [163], in the charged pion spectrum from $\bar{p}d\to\pi^-\pi^0 p$ and $\pi^+\pi^- n$ reactions [164] and in the real part of the elastic proton–antiproton forward amplitude [165].

Frequently these anomalies have been associated with narrow $p\bar{p}$ bound states. Indeed, an analysis of the BES provides evidence for an S-wave bound state with a mass of $1859\,^{+3}_{-10}\,(\mathrm{stat})\,^{+5}_{-25}\,(\mathrm{syst})$ MeV and a total width less than 30 MeV [161]. A P-wave bound state instead of an S-wave one cannot be excluded from the BES data. This BES result is very close to findings from an analysis of $\bar{p}d$ reactions [166] (a bound state mass of $1870\,\mathrm{MeV}$ and a width of $10\,\mathrm{MeV}$) and from a proton–antiproton forward dispersion relation [167] (mass: $1852\,\mathrm{MeV}$, width: $35\,\mathrm{MeV}$). In the CERN WA56 experiment [168], on the other hand, a narrow peak (mass $2.02\,\mathrm{GeV}$) has been observed in the $p\bar{p}$ invariant mass spectrum of the reaction $\pi^- p\to p_f\pi^-[p\bar{p}]$ where p_f is a fast forward going proton. Puzzling is, however, the fact that this peak is not seen in $J/\psi\to\gamma p\bar{p}$ [161] while there is no indication of a threshold enhancement in the WA56 measurement. Several authors [169] have pointed out that the dynamics of the low-energy $p\bar{p}$ system such as pion exchange or the physics inherent in the effective range expansion, provides an important contribution to the threshold enhancement. An appealing mechanism has been suggested by Rosner [170]. He assumes that the partonic subprocess in the process $J/\psi\to\gamma p\bar{p}$ is $c\bar{c}\to\gamma gg$ followed

by a nonperturbative $gg \to (p\bar{p})_S$ transition where the subscript indicates a $p\bar{p}$ pair in a resonant S-state. Rosner further assumes that the corresponding B decays, for instance $B^+ \to K^+ p\bar{p}$, receives a substantial contribution associated with the subprocess $\bar{b} \to \bar{s}gg$ and the same nonperturbative $gg \to (p\bar{p})_S$ transition as for $J/\psi \to \gamma p\bar{p}$. Producing an η' through this mechanism instead of the proton–antiproton pair leads to similar contributions except that now a different gluonic matrix element occurs, see (4.99). In ratios of these processes most details cancel and, according to Rosner, one arrives at

$$\frac{\mathcal{B}(B^+ \to K^+ (p\bar{p})_S)|_{gg}}{\mathcal{B}(B^+ \to K^+ \eta')|_{gg}} = \frac{\varrho[B^+ K^+ (p\bar{p})_S]}{\varrho[B^+ K^+ \eta']} \left(\frac{\varrho[J/\psi\gamma\eta']}{\varrho[J/\psi\gamma(p\bar{p})_S]} \right)^3 \frac{\mathcal{B}(J/\psi \to \gamma(p\bar{p})_S)}{\mathcal{B}(J/\psi \to \gamma\eta')} \,. \tag{4.108}$$

The gg subscript at the B-meson matrix elements is meant as a hint that there might be other non-negligible contributions to the B decays than those from the subprocess $\bar{b} \to \bar{s}gg$. This mechanism relates the threshold enhancement in $B^+ \to K^+ p\bar{p}$ to that in $J/\psi \to \gamma p\bar{p}$. Using the experimental information on the latter process, Rosner found that this mechanism provides a substantial fraction of the first one. It is to be stressed that the ratio of $B^{+(0)}$ decays into $K^{+(0)}\eta'$ and $K^{+(0)}\eta$ are not in conflict with this interpretation.

6 ELECTROMAGNETIC TRANSITIONS[12]

For quarkonium states, $Q_1\bar{Q}_2$, above the ground state but below threshold for strong decay into a pair of heavy flavoured mesons, electromagnetic transitions are often significant decay modes. In fact, the first charmonium states not directly produced in e^+e^- collisions, the χ_c^J states, were discovered in photonic transitions of the ψ' resonance. Even today, such transitions continue to be used to observe new quarkonium states [171].

6.1 Theoretical framework

6.1.1 Effective Lagrangian

The theory of electromagnetic transitions between these quarkonium states is straightforward. Much of the terminology and techniques are familiar from the study of EM transitions in atomic and nuclear systems. The photon field $\mathbf{A}^\mu_{\rm em}$ couples to charged quarks through the electromagnetic current:

$$j_\mu \equiv \sum_{i=\rm u,d,s} j^i_\mu + \sum_{i=\rm c,b,t} j^i_\mu \,. \tag{4.109}$$

The heavy valence quarks (c, b, t) can be described by the usual effective action:

$$\mathcal{L}_{\rm NRQCD} = \psi^\dagger \left\{ iD_0 + \frac{\mathbf{D}^2}{2m} + c_F\, g \frac{\boldsymbol{\sigma}\cdot\mathbf{B}}{2m} + c_D\, g \frac{[\mathbf{D}\cdot, \mathbf{E}]}{8m^2} + ic_S\, g \frac{\boldsymbol{\sigma}\cdot[\mathbf{D}\times, \mathbf{E}]}{8m^2} + \ldots \right\} \psi \,, \tag{4.110}$$

where the $\mathbf{E}$ and $\mathbf{B}$ fields are the chromoelectric and chromomagnetic fields. Corrections to the leading NR behaviour are determined by the expansion in the quark and antiquark velocities. For photon momentum small compared to the heavy quark masses, the form of the EM interaction (in Coulomb gauge) is determined in the same way as the NRQCD action itself [13, 14, 42, 172], the leading order terms are:

$$\mathbf{j}\cdot\mathbf{A}_{\rm em} = e_Q \psi^\dagger \left\{ \frac{\{\mathbf{D}\cdot, \mathbf{A}_{\rm em}\}}{2m} + (1+\kappa_Q)\, \frac{\boldsymbol{\sigma}\cdot\mathbf{B}_{\rm em}}{2m} + \ldots \right\} \psi \,. \tag{4.111}$$

The first term of Eq. (4.111) produces electric and the second magnetic transitions. The coefficient κ_Q is a possible anomalous magnetic moment for the heavy quark. It is a perturbative quantity at the level

[12] Author: E. Eichten

of NRQCD, but may get nonperturbative contributions in going to lower energy effective field theories, once the scale $\Lambda_{\rm QCD}$ has been integrated out. Since we may assume that potential models are an attempt to mimic such theories, we will interpret in this last way the quantity κ_Q that appears there and will be used in the following.

For quarkonium systems, light quarks (u, d, s) only contribute to internal quark loops, described perturbatively at short distance and as virtual pairs of heavy flavour mesons at large distance. In the SU(3) limit the total contribution from light quarks vanishes since its EM current has no SU(3) singlet part. Hence, to leading order in SU(3) breaking these contributions can be ignored. We return to these corrections in Sec. 6.5.

6.1.2 Transition amplitudes

Within a $\bar{Q}_2 Q_1$ quarkonium system, the electromagnetic transition amplitude is determined by the matrix element of the EM current, $\langle f|j^\mu_{\rm em}|i\rangle$, between an initial quarkonium state, i, and a final state f. Including the emission of a photon of momentum k and polarization ϵ_γ, the general form of the transition amplitude is the sum of two terms

$$\mathcal{M}(i \to f) = [\mathbf{M}^{(1)}(i \to f) + \mathbf{M}^{(2)}(i \to f)] \cdot \epsilon_\gamma(k), \tag{4.112}$$

where in the term $\mathbf{M}^{(1)}$ the photon is emitted off the quark Q_1 with mass m_1 and charge e_1,

$$\mathbf{M}^{(1)}(i \to f) = \frac{e_1}{2m_1} \int d^3x \langle i|Q_1^\dagger(x)(\mathbf{D}, \exp(i\mathbf{x}\cdot\mathbf{k}) + (1+\kappa_{Q_1})\boldsymbol{\sigma} \times \mathbf{k} \exp(i\mathbf{x}\cdot\mathbf{k}))Q_1(x)|f\rangle, \tag{4.113}$$

and in the corresponding term $\mathbf{M}^{(2)}$ the photon is emitted off the antiquark $\bar{Q}_2$ with mass m_2 and charge $-e_2$.

Electromagnetic transition amplitudes can be computed from first principles in Lattice QCD [173]. Preliminary studies [174] have even included electromagnetic interactions directly into Lattice QCD simulations. However, these transitions for quarkonium systems have not yet been computed. Various relations between transitions also arise from QCD sum rules [175].

Although other calculational models, e.g., using the MIT bag model [176], have been explored, only potential model approaches provide the detailed predictions for the strength of individual transition amplitudes needed to compare with experiments. The remainder of this section will focus on the issues within potential model approaches.

Within nonrelativistic (NR) potential models, a quarkonium state is characterized by a radial quantum number, n, orbital angular momentum, l, total spin, s, and total angular momentum, J. In the NR limit the spin dependence decouples from the spatial dependence. The spatial wave function for a NR state, $\psi(x)$, can be expressed in terms of a radial wave function, $u_{nl}(r)$ and an orbital angular momentum dependence by:

$$\psi(x) = Y_{lm}(\theta, \phi)\frac{u_{nl}(r)}{r}. \tag{4.114}$$

The spatial dependence of EM transition amplitudes reduces to expectation values of various functions of quark position and momentum between the initial and final state wave functions. Expanding Eq. (4.113) in powers of photon momentum generates the electric and magnetic multipole moments. This is also an expansion in powers of velocity. The leading order transition amplitudes are electric dipole (E1) or magnetic dipole (M1).

6.1.3 Electric transitions

Electric transitions do not change quark spin. The lowest NR order transition is the electric dipole (E1) transition. These transitions have $\Delta l = \pm 1$ and $\Delta s = 0$. To compute the E1 transition amplitudes

$\exp(i\mathbf{x}\cdot\mathbf{k})$ can be replaced by 1 in electric transition term in Eq. (4.113). Separating out the overall centre of mass motion of the system, the quark momentum operator, $i\mathbf{D}/m_Q$, can be replaced by the commutator, $[h,\mathbf{x}]$, of the bound state Hamiltonian, h, with the quark position operator, $\mathbf{x}$. Finally, the Hamiltonian acting on the initial or final state is simply the mass of that state. To leading NR order, this is equal to the momentum of the final photon $k=(M_i^2-M_f^2)/(2M_i)$. The E1 radiative transition amplitude between initial state $(n^{2s+1}{}_J)$, i, and final state $(n'^{2s'+1}{}_{J'})$, f, is [177]:

$$\begin{aligned}\mathbf{M}^e(i\to f)_\mu &= \delta_{s,s'}(-1)^{s+J+J'+1+M'}k\sqrt{(2J+1)(2J'+1)(2l+1)(2l'+1)}\\ &\quad\begin{pmatrix} J' & 1 & J\\ -M' & \mu & M\end{pmatrix}\begin{pmatrix} l' & 1 & l\\ 0 & 0 & 0\end{pmatrix}\begin{Bmatrix} l & s_a & J\\ J' & 1 & l'\end{Bmatrix}\langle e_Q\rangle\,\mathcal{E}_{if},\end{aligned}\tag{4.115}$$

where $\langle e_Q\rangle=(e_1m_2-e_2m_1)/(m_1+m_2)$ and the overlap integral $\mathcal{E}_{if}$ is

$$\mathcal{E}_{if}=\int_0^\infty dr\,u_{n\ell}(r)ru_{n'\ell'}(r).\tag{4.116}$$

If the full photon momentum dependence in Eq. (4.113) is retained (even through this is formally a higher order relativistic corrections); the overlap integral $\mathcal{E}$ for $m_1=m_2$ and $e_1=-e_2=e_Q$ is given by

$$\mathcal{E}_{if}=\frac{3}{k}\int_0^\infty dr\,u_{n\ell}(r)u_{n'\ell'}(r)\left[\frac{kr}{2}j_0\left(\frac{kr}{2}\right)-j_1\left(\frac{kr}{2}\right)\right]+\mathcal{O}(k/m).\tag{4.117}$$

The spin averaged decay rate is given by

$$\Gamma(i\xrightarrow{\text{E1}}f+\gamma)=\frac{4\alpha e_Q^2}{3}(2J'+1)\mathrm{S}_{if}^{\mathrm{E}}k^3|\mathcal{E}_{if}|^2,\tag{4.118}$$

where the statistical factor $\mathrm{S}_{if}^{\mathrm{E}}=\mathrm{S}_{fi}^{\mathrm{E}}$ is

$$\mathrm{S}_{if}^{\mathrm{E}}=\max(\ell,\ell')\begin{Bmatrix} J & 1 & J'\\ \ell' & s & \ell\end{Bmatrix}^2.\tag{4.119}$$

6.1.4 Magnetic transitions

Magnetic transitions flip the quark spin. The M1 transitions have $\Delta l=0$ and the amplitude is given by:

$$\begin{aligned}\mathbf{M}^m(i\to f)_\mu &= \delta_{\ell,\ell'}(-1)^{l+J'+J+l+\mu+M'}3\sqrt{(2J+1)(2J'+1)(2s+1)(2s'+1)}\\ &\sum_{\nu,\sigma}k_\sigma\begin{pmatrix} 1 & 1 & 1\\ -\mu & \sigma & \nu\end{pmatrix}\begin{pmatrix} J' & J & 1\\ -M' & M & \nu\end{pmatrix}\begin{Bmatrix} s & l & J\\ J' & 1 & s'\end{Bmatrix}\begin{Bmatrix} 1 & 1/2 & 1/2\\ 1/2 & s & s'\end{Bmatrix}\\ &\left[\frac{e_1}{m_1}+(-1)^{s+s'}\frac{e_2}{m_2}\right]\mathcal{M}_{if}\,,\end{aligned}\tag{4.120}$$

where for equal mass quarks the overlap integral $\mathcal{M}$ is given by

$$\mathcal{M}_{if}=(1+\kappa_Q)\int_0^\infty dr\,u_{n\ell}(r)u'_{n'\ell}(r)\,j_0\left(\frac{kr}{2}\right)+\mathcal{O}(k/m)\,.\tag{4.121}$$

The spin-flip radiative transition rate between an initial state $(n^{2s+1}\ell_J)$, i, and a final state $(n'^{2s^\ell+1}S_{J'})$, f, is:

$$\Gamma(i\xrightarrow{\text{M1}}f+\gamma)=\frac{4\alpha e_Q^2}{3m_Q^2}(2J'+1)k^3\mathrm{S}_{if}^{\mathrm{M}}|\mathcal{M}_{if}|^2,\tag{4.122}$$

where the statistical factor $\mathrm{S}_{if}^{\mathrm{M}}=\mathrm{S}_{fi}^{\mathrm{M}}$ is

$$\mathrm{S}_{if}^{\mathrm{M}}=6(2s+1)(2s'+1)\begin{Bmatrix} J & 1 & J'\\ s' & \ell & s\end{Bmatrix}^2\begin{Bmatrix} 1 & \frac{1}{2} & \frac{1}{2}\\ \frac{1}{2} & s' & s\end{Bmatrix}^2.\tag{4.123}$$

For $l=0$ transitions, $S_{if}^{\mathrm{M}}=1$.

6.1.5 Relativistic corrections

The leading relativistic corrections for electric transitions have been considered by a number of authors [178–186]. A general form was derived by Grotch, Owen and Sebastian [184]. For example, for the equal mass quark–antiquark $\bar{c}c$ and $\bar{b}b$ systems the E1 transition amplitude is $\langle f|\mathbf{X}_0 + \mathbf{X}_1|i\rangle$,

$$\begin{aligned}
\mathbf{X}_0 &= e_Q \mathbf{r}, \\
\mathbf{X}_1 &= -i\frac{k e_Q}{2m_Q}\left(\frac{1}{10}\left(\{r^2, \mathbf{p}\} - \frac{1}{2}[\mathbf{r}, [\mathbf{r}\cdot, \mathbf{p}]]\right) - \frac{\kappa_Q}{2}(\mathbf{r}\times\mathbf{S})\right) ,
\end{aligned} \tag{4.124}$$

where κ_Q is the quark anomalous magnetic moment and $\mathbf{p}$ is the relative momentum. The decay rate then has the general form:

$$\Gamma^{\rm E1} = \Gamma^{\rm E1}_{\rm NR}(1 + R1 + R2 + R3), \tag{4.125}$$

where $R1$ are corrections due to the modification of the nonrelativistic wave functions, $R2$ originates from the relativistic modification of the transition operator and $R3$ are the finite size corrections (arising from the plane wave expansion for the emitted photon). For the $1^3P_J \to 1^3S_1$ E1 transition:

$$\begin{aligned}
R1 &= 2E_1^J + (E_1^J)^2, \\
R2 &= \frac{k\kappa_Q}{2m_Q}\left[\frac{J(J+1)}{2} - 2\right], \\
R3 &= -\frac{1}{10}(M_i - M_f)^2 E_2 + \frac{k}{8m_Q}E_3,
\end{aligned} \tag{4.126}$$

where

$$\begin{aligned}
E_1 &= \frac{\displaystyle\int_0^\infty dr\, r\, \left[u_{10}^{(0)}(r)u_{11}^{(1)J}(r) + u_{10}^{(1)}(r)u_{11}^{(0)}(r)\right]}{\mathcal{E}_{if}}, \\
E_2 &= \frac{\displaystyle\int_0^\infty dr\, r^3\, u_{10}^{(0)}(r)u_{11}^{(0)}(r)}{\mathcal{E}_{if}}, \\
E_3 &= \frac{\displaystyle\int_0^\infty dr\, r\, \left[u_{10}^{(0)}(r)\left(2r\frac{d}{dr}u_{11}^{(0)}(r) - u_{11}^{(0)}(r)\right) - \left(2r\frac{d}{dr}u_{10}^{(0)}(r) - u_{10}^{(0)}(r)\right)u_{11}^{(0)}(r)\right]}{\mathcal{E}_{if}},
\end{aligned} \tag{4.127}$$

and $u^{(1)}(r)$ is the first order relativistic correction to the NR (reduced) radial wave function, $u^{(0)}(r)$.

The corrections for M1 transitions are more complicated and depend explicitly on the structure of the nonrelativistic potential. Assuming that the potential can be decomposed into three terms $V(r) = V_p(r) + (1-\eta)V_v(r) + \eta V_s(r)$, i.e., a perturbative part $V_p(r)$ and a (nonperturbative) confining part, which is a linear combination of a Lorentz vector $V_v(r)$ and a scalar $V_s(r)$ term, the expression $|\mathcal{M}_{if}|^2$ in Eq. (4.121) is replaced by [183] $|I_1 + I_2 + I_3 + I_4|^2$, where for S wave transitions in $\bar{Q}Q$ systems:

$$\begin{aligned}
I_1 &= \int_0^\infty dr\, u_{n'0}^{(0)}(r)u_{n0}^{(0)}(r)\left[(1+\kappa_Q)j_0\left(\frac{kr}{2}\right) + \frac{k(1+2\kappa_Q)}{4m_Q}\right] , \\
I_2 &= \int_0^\infty dr\, u_{n'0}^{(0)}(r)u_{n0}^{(0)}(r)\left[-(1+\kappa_Q)\frac{\mathbf{p}^2}{2m_Q^2} - \frac{\mathbf{p}^2}{3m_Q^2}\right] , \\
I_3 &= \int_0^\infty dr\, u_{n'0}^{(0)}(r)u_{n0}^{(0)}(r)\left[\frac{\kappa_Q r}{6m_Q}\frac{\partial(V_p + (1-\eta)V_v)}{\partial r}\right] , \\
I_4 &= \int_0^\infty dr\, u_{n'0}^{(0)}(r)u_{n0}^{(0)}(r)\left[-\frac{\eta V_s}{m_Q}j_0\left(\frac{kr}{2}\right)\right] .
\end{aligned} \tag{4.128}$$

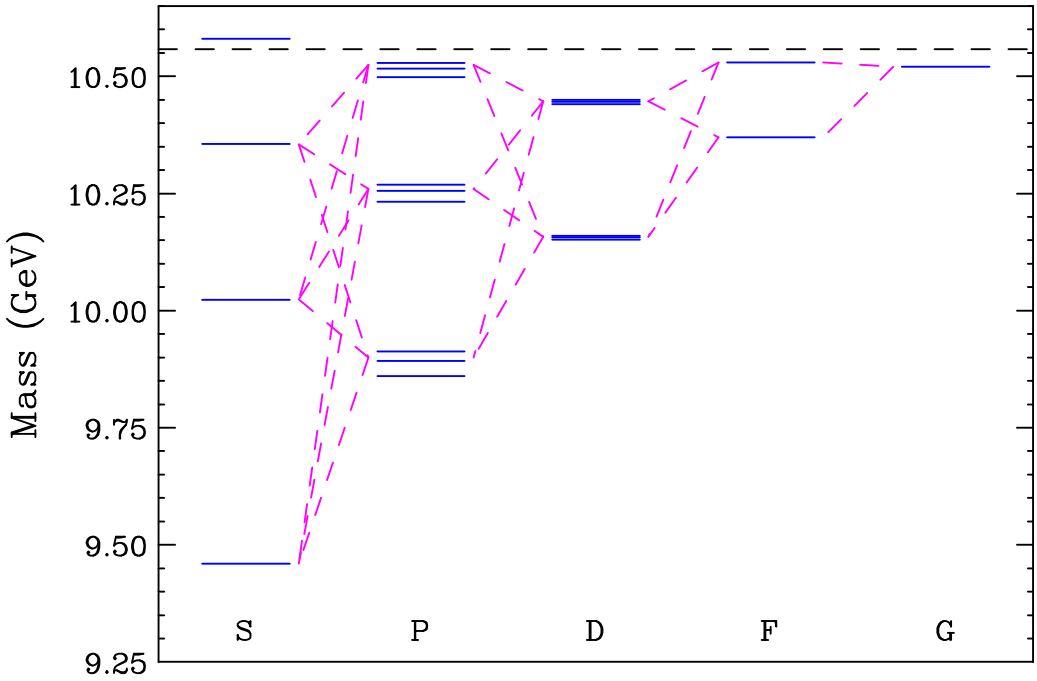

Fig. 4.10: E1 transitions in the narrow spin triplet $\bar{b}b$ states. For each S–P transition indicated there are three individual transitions (one for each P_J state); while for transitions involving any other pair of orbital angular momenta (P–D, D–F, F–G, ...) there are six individual transitions ($\Delta J = 0, \pm 1$).

Further details of these relativistic corrections can been found at the original papers of Feinberg and Sucher [178–180], Zambetakis and Byers [182] and Grotch and Sebastian [183, 184]. General treatments of relativistic corrections for all quarkonium states can be found in recent works [185, 186].

6.2 E1 transitions

Since the discovery of the J/ψ and ψ' resonances in November 1974, E1 transitions have played an important theoretical and experimental role in quarkonium physics. Initial theoretical papers on charmonium [187, 188] predicted the $1P$ states in the $\bar{c}c$ system and suggested that the triplet $1P$ states could be observed through the E1 transitions from the ψ' resonance. In fact, explicit calculations of the $2S \to 1P$ and $1P \to 1S$ E1 transition amplitudes $\mathcal{E}_{if}$ by the Cornell group [187] agree within 25% with present experimental values [189].

Today there is a wealth of theoretical predictions and experimental data on E1 transitions. Many E1 transitions have been observed in the $\bar{c}c$, $\bar{b}b$ and more are expected. For example, Fig. 4.10 shows the E1 transitions from narrow spin triplet states in the $\bar{b}b$ system. Transitions occur between two states differing in L by one and J by zero or one; thus for the $\bar{b}b$ system there are a total of 99 E1 transitions, 30 of which are theoretically accessible in e^+e^- collisions from the Υ(2S) and Υ(3S) resonances.

6.2.1 Model predictions

The theoretical models used to calculate the E1 transitions can be classified by the following two considerations: (1) What nonrelativistic potential was used? and (2) Which relativistic corrections (as shown in Eq. (4.125)) were included in the calculations?

An early choice for the potential was the Cornell model [177, 187, 190–192]. Here the exchange interaction was the time component of a vector with a Coulomb short range part $-K/r$ plus a linear r/a^2 long range confining part. The Coulomb part was modified to agree with perturbative QCD at short

Table 4.15: E1 transition rates for low-lying $\bar{c}c$ states. The measured masses are used for observed states. The mass values used for the $^3D_2$, $^1D_2$ and $^3D_3$ states are suggested by the coupled channel calculations of Ref. [207]. The E1 rates are shown for the (NR) model described in the text. The variation of results for $\mathcal{E}_{if}$ with inclusion of relativistic corrections is shown for two models of Ref. [186] with scalar confinement (RA) and a mixture of vector and scalar confining terms (RB).

Transition $i \xrightarrow{\mathrm{E1}} f$		k (MeV)	$\mathrm{S}_{if}^{\mathrm{E}}$	$\Gamma(i \to f)$(NR) (keV)	$\mathcal{E}_{if}$(NR) (GeV^{-1})	$\mathcal{E}_{if}$(RA) (GeV^{-1})	$\mathcal{E}_{if}$(RB) (GeV^{-1})
$1^3P_0(3.415)$	$1^3S_1(3.097)$	304	$\frac{1}{9}$	120	1.724	2.121	1.720
$1^3P_1(3.511)$	$1^3S_1(3.097)$	389	$\frac{1}{9}$	241	1.684	1.896	1.767
$1^1P_1(3.526)$	$1^1S_0(2.979)$	504	$\frac{1}{3}$	482	1.615	1.742	1.742
$1^3P_2(3.556)$	$1^3S_1(3.097)$	430	$\frac{1}{9}$	315	1.661	1.596	1.689
$2^3S_1(3.686)$	$1^3P_0(3.415)$	261	$\frac{1}{9}$	47.0	−2.350	−2.296	−1.775
$2^1S_0(3.638)$	$1^1P_1(3.526)$	110	$\frac{1}{3}$	35.1	−2.469	−2.126	−2.126
$2^3S_1(3.686)$	$1^3P_1(3.511)$	171	$\frac{1}{9}$	42.8	−2.432	−2.305	−1.782
$2^3S_1(3.686)$	$1^3P_2(3.556)$	127	$\frac{1}{9}$	30.1	−2.460	−2.362	−1.901
$1^3D_1(3.770)$	$1^3P_0(3.415)$	338	$\frac{2}{9}$	299	2.841	2.718	2.802
$1^3D_1(3.770)$	$1^3P_1(3.511)$	250	$\frac{1}{18}$	99.0	2.957	2.799	2.969
$1^3D_1(3.770)$	$1^3P_2(3.556)$	208	$\frac{1}{450}$	3.88	3.002	3.016	3.348
$1^3D_2(3.831)$	$1^3P_1(3.511)$	307	$\frac{1}{10}$	313	2.886	2.593	2.593
$1^3D_2(3.831)$	$1^3P_2(3.556)$	265	$\frac{1}{50}$	69.5	2.940	2.781	2.991
$1^1D_2(3.838)$	$1^1P_1(3.526)$	299	$\frac{2}{15}$	389	2.896	2.610	2.610
$1^3D_3(3.872)$	$1^3P_2(3.556)$	303	$\frac{2}{25}$	402	2.892	2.508	2.402

distance by Buchmüller and Tye [141, 193]. Other simple forms for the potential, logarithmic [144, 194] and power law [195, 196], were also proposed.

In the NRQCD limit the quark–antiquark interaction is spin independent, but including relativistic corrections introduces dependencies on the Lorentz structure of the potential. Of particular importance is the vector versus scalar nature of the long-range confining interaction. Many modern theoretical calculations assume a long range scalar confining potential [197] or a linear combination of the form $\eta V_S(r) + (1-\eta)V_V(r)$ [181, 186, 198]. Moxhay and Rosner [199] assumed an additional long range tensor force.

The second consideration is the extent of the inclusion of the relativistic corrections. Some calculations are essentially nonrelativistic. These calculations often include some finite size effects ($R3$ of Eq. (4.125)) by retaining the form for $\mathcal{E}_{if}$ given in Eq. (4.117) [177, 187, 190–192, 200]. Other models also include relativistic corrections to the wave functions ($R1$ of Eq. (4.125)) either perturbatively or nonperturbatively. The relativistic quark model of Godfrey and Isgur [201] is an example in this class. Gupta, Radford and Repko computed the relativistic corrections using only the gluon exchange interactions of QCD perturbation theory [202–204]. Many models include the full relativistic corrections [181, 184, 185, 199, 205, 206].

Differences in theoretical assumptions and experimental input for the various potential model calculations of E1 transitions make it difficult to draw sharp conclusions from the level of agreement of

Table 4.16: E1 transition rates for low-lying spin triplet $\bar{b}b$ states.

Transition $i \xrightarrow{\mathrm{E1}} f$		k (MeV)	$\mathrm{S}^{\mathrm{E}}_{if}$	$\Gamma(i \to f)$(NR) (keV)	$\mathcal{E}_{if}$(NR) (GeV^{-1})	$\mathcal{E}_{if}$(RA) (GeV^{-1})	$\mathcal{E}_{if}$(RB) (GeV^{-1})
$1^3P_0(9.860)$	$1^3S_1(9.460)$	392	$\frac{1}{9}$	22.2	1.013	1.205	1.178
$1^3P_1(9.893)$	$1^3S_1(9.460)$	423	$\frac{1}{9}$	27.8	1.010	1.175	1.163
$1^3P_2(9.913)$	$1^3S_1(9.460)$	442	$\frac{1}{9}$	31.6	1.007	1.124	1.137
$2^3S_1(10.023)$	$1^3P_2(9.913)$	110	$\frac{1}{9}$	2.04	−1.597	−1.800	−1.778
$2^3S_1(10.023)$	$1^3P_1(9.893)$	130	$\frac{1}{9}$	2.00	−1.595	−1.781	−1.759
$2^3S_1(10.023)$	$1^3P_0(9.860)$	162	$\frac{1}{9}$	1.29	−1.590	−1.803	−1.781
$1^3D_1(10.151)$	$1^3P_2(9.913)$	236	$\frac{1}{450}$	0.564	1.896	2.104	2.104
$1^3D_1(10.151)$	$1^3P_1(9.893)$	255	$\frac{1}{18}$	10.7	1.890	2.050	2.050
$1^3D_1(10.151)$	$1^3P_0(9.860)$	287	$\frac{2}{9}$	20.1	1.880	2.106	2.106
$1^3D_2(10.157)$	$1^3P_2(9.913)$	241	$\frac{1}{50}$	5.46	1.894	2.048	2.048
$1^3D_2(10.157)$	$1^3P_1(9.893)$	261	$\frac{1}{10}$	20.5	1.888	1.999	1.999
$1^3D_3(10.160)$	$1^3P_2(9.913)$	244	$\frac{2}{25}$	22.6	1.893	1.979	1.979
$2^3P_0(10.232)$	$1^3D_1(10.151)$	81	$\frac{2}{9}$	1.13	−1.723	−1.740	−1.740
$2^3P_0(10.232)$	$2^3S_1(10.023)$	207	$\frac{1}{9}$	9.17	1.697	1.872	1.855
$2^3P_0(10.232)$	$1^3S_1(9.460)$	743	$\frac{1}{9}$	10.9	0.272	0.214	0.239
$2^3P_1(10.255)$	$1^3D_2(10.157)$	98	$\frac{1}{10}$	1.49	−1.720	−1.751	−1.751
$2^3P_1(10.255)$	$1^3D_1(10.151)$	104	$\frac{1}{18}$	0.593	−1.718	−1.721	−1.721
$2^3P_1(10.255)$	$2^3S_1(10.023)$	229	$\frac{1}{9}$	12.4	1.688	1.837	1.831
$2^3P_1(10.255)$	$1^3S_1(9.460)$	764	$\frac{1}{9}$	12.0	0.274	0.228	0.216
$2^3P_2(10.268)$	$1^3D_3(10.160)$	108	$\frac{2}{25}$	2.25	−1.717	−1.763	−1.763
$2^3P_2(10.268)$	$1^3D_2(10.157)$	111	$\frac{1}{50}$	0.434	−1.717	−1.737	−1.737
$2^3P_2(10.268)$	$1^3D_1(10.151)$	117	$\frac{1}{450}$	0.034	−1.715	−1.766	−1.766
$2^3P_2(10.268)$	$2^3S_1(10.023)$	242	$\frac{1}{9}$	14.5	1.682	1.792	1.797
$2^3P_2(10.268)$	$1^3S_1(9.460)$	776	$\frac{1}{9}$	12.7	0.274	0.207	0.218
$3^3S_1(10.355)$	$2^3P_2(10.268)$	86	$\frac{1}{9}$	2.40	−2.493	−2.663	−2.644
$3^3S_1(10.355)$	$2^3P_1(10.255)$	100	$\frac{1}{9}$	2.20	−2.489	−2.607	−2.586
$3^3S_1(10.355)$	$2^3P_0(10.232)$	122	$\frac{1}{9}$	1.35	−2.479	−2.608	−2.582
$3^3S_1(10.355)$	$1^3P_2(9.913)$	433	$\frac{1}{9}$	0.015	0.016	0.063	0.045
$3^3S_1(10.355)$	$1^3P_1(9.893)$	452	$\frac{1}{9}$	0.008	0.011	0.063	0.045
$3^3S_1(10.355)$	$1^3P_0(9.860)$	483	$\frac{1}{9}$	0.001	0.004	0.063	0.045

Table 4.17: E1 transition rates for low-lying spin singlet $\bar{b}b$ states.

Transition $i \xrightarrow{\mathrm{E1}} f$		k (MeV)	$\mathrm{S}_{if}^{\mathrm{E}}$	$\Gamma(i \to f)$(NR) (keV)	$\mathcal{E}_{if}$(NR) (GeV^{-1})	$\mathcal{E}_{if}$(RA) (GeV^{-1})	$\mathcal{E}_{if}$(RB) (GeV^{-1})
$1^1P_1(9.900)$	$1^1S_0(9.400)$	487	$\frac{1}{3}$	41.8	1.001	1.149	1.149
$2^1S_0(9.990)$	$1^1P_1(9.900)$	90	$\frac{1}{3}$	1.99	-1.600	-1.743	-1.743
$1^1D_2(10.157)$	$1^1P_1(9.900)$	254	$\frac{2}{15}$	25.3	1.891	2.002	2.002
$2^1P_1(10.260)$	$2^1S_0(9.990)$	266	$\frac{1}{3}$	19.0	1.671	1.817	1.817
$2^1P_1(10.260)$	$1^1D_2(10.157)$	102	$\frac{2}{15}$	2.29	-1.719	-1.782	-1.782
$3^1S_0(10.328)$	$2^1P_1(10.260)$	68	$\frac{1}{3}$	2.10	-2.498	-2.571	-2.571
$3^1S_0(10.328)$	$1^1P_1(9.900)$	419	$\frac{1}{3}$	0.007	0.010	0.064	0.064

a particular model and experimental data. However, it is known that there is usually very little model variation in the NR predictions (lowest order) if the models are fit to the same states [200]. The only exceptions are transitions where the overlap integral $\mathcal{E}_{if}$ exhibits large dynamical cancellations. Therefore, to compare the variations in results due to the inclusion of relativistic corrections from a common base, three models for E1 radiative transitions are presented, which are fit with the same input masses. First a reference Cornell model [191] (NR), with parameters (a and K) adjusted to fit the COG positions of the 1S, 1P and 2S states in each of the $\bar{c}c$ and $\bar{b}b$ systems [208]. Here E1 transitions are computed with $\mathcal{E}_{if}$ given in Eq. (4.117), i.e., with only finite size relativistic corrections included. Second, a recent model by Ebert, Faustov and Galkin [186] with full relativistic corrections in two cases: (RA) $\eta = 1$ (scalar confinement) and (RB) $\eta = -1$ (a fitted mixture of scalar and vector confinement).

The results for $\mathcal{E}_{if}$ are shown for the $\bar{c}c$ narrow states in Table 4.15. The size of the relativistic corrections to $\mathcal{E}_{if}$ shown in Table 4.15 vary as much as $\pm 25\%$. This variation is perfectly consistent with naive expectations for v^2/c^2 corrections. McClary and Byers [181] first emphasized that because of the node in the radial wave function of the $2S$ state the overlap $\mathcal{E}_{\mathrm{2S,1P}}$ is particularly sensitive to relativistic corrections in the $\bar{c}c$ system. The significant leptonic width for the $\Psi(3770)$ resonance implies that there is a sizeable S-D mixing between the 2^3S_1 and 1^3D_1 states. This mixing arises both from the usual relativistic correction terms and coupling to strong decay channels and will affect the $\Psi(3686) \to 1^3P_J$ and $\Psi(3770) \to 1^3P_J$ E1 transitions rates (See Section 6.2.3). For the $1D$ states there may be additional large effects on rates associated with this coupling to nearby strong decay channels. (See Section 6.5.)

Results for narrow $\bar{b}b$ states accessible from the Υ(3S) or Υ(2S) resonances are shown for spin-triplets in Table 4.16 and for the spin-singlets in Table 4.17. The typical size of the relativistic corrections for $\mathcal{E}_{if}$ are approximately half as large as in the corresponding $\bar{c}c$ transition. This is again as expected, since $\langle v^2/c^2 \rangle$ is smaller in the $\bar{b}b$ system. There is a notable exception for the overlap $\mathcal{E}_{\mathrm{3S,1P}}$. In the NR limit this overlap is less than 5% of any other S–P overlap. This dynamical accident makes these transition rates very sensitive to the details of wave functions and relativistic corrections, which are *not* well under control theoretically.

Finally, for completeness, radiative transitions involving $\bar{b}b$ states not accessible from the $3S$ states are shown in Table 4.18. Only the NR rates are shown. One observes large dynamical cancellations for the overlap $\mathcal{E}_{\mathrm{3P,1D}}$ and to a lesser extent in the overlaps $\mathcal{E}_{\mathrm{3P,1S}}$, $\mathcal{E}_{\mathrm{2D,1P}}$ and $\mathcal{E}_{\mathrm{3P,2S}}$.

Table 4.18: E1 transition rates for the remaining spin triplet $\bar{b}b$ states. For each (n' and ℓ') only the final state J' with the largest rate is shown. The transition rates for spin-singlet $\bar{b}b$ states differ from the corresponding spin triplet rates by the ratio of statistical factors $\mathrm{S}^{\mathrm{E}}(s=0)/\mathrm{S}^{\mathrm{E}}(s=1)$: 3, 2/3, 9/8 and 16/15 for S–P, P–D, D–F and F–G transitions respectively.

Transition $i \xrightarrow{\mathrm{E1}} f$		k (MeV)	$\mathrm{S}^{\mathrm{E}}_{if}$	$\mathcal{E}_{if}$ (GeV^{-1})	$\Gamma(i \to f)$ (keV)
$1^3F_2(10.370)$	$1^3D_1(10.151)$	217	$\frac{3}{25}$	2.681	28.5
$1^3F_3(10.370)$	$1^3D_2(10.157)$	211	$\frac{8}{105}$	2.684	27.8
$1^3F_4(10.370)$	$1^3D_3(10.160)$	208	$\frac{3}{49}$	2.686	30.0
$2^3D_1(10.441)$	$1^3F_2(10.370)$	71	$\frac{3}{25}$	−1.904	0.833
$2^3D_1(10.441)$	$2^3P_0(10.232)$	207	$\frac{2}{9}$	2.487	13.1
$2^3D_1(10.441)$	$1^3P_0(9.860)$	565	$\frac{2}{9}$	0.288	3.60
$2^3D_2(10.446)$	$1^3F_3(10.370)$	76	$\frac{8}{105}$	−1.903	0.907
$2^3D_3(10.450)$	$1^3F_4(10.370)$	80	$\frac{3}{49}$	−1.902	1.09
$2^3D_3(10.450)$	$2^3P_2(10.268)$	180	$\frac{2}{25}$	2.506	15.8
$2^3D_3(10.450)$	$1^3P_2(9.913)$	524	$\frac{2}{25}$	0.278	4.80
$3^3P_0(10.498)$	$2^3D_1(10.441)$	57	$\frac{2}{9}$	−2.584	0.884
$3^3P_0(10.498)$	$3^3S_1(10.355)$	142	$\frac{1}{9}$	2.308	5.47
$3^3P_0(10.498)$	$1^3D_1(10.151)$	341	$\frac{2}{9}$	−0.047	0.063
$3^3P_0(10.498)$	$2^3S_1(10.023)$	464	$\frac{1}{9}$	0.351	4.44
$3^3P_0(10.498)$	$1^3S_1(9.460)$	986	$\frac{1}{9}$	0.137	6.46
$3^3P_1(10.516)$	$2^3D_2(10.446)$	70	$\frac{1}{10}$	−2.579	1.22
$3^3P_1(10.516)$	$3^3S_1(10.355)$	160	$\frac{1}{9}$	2.295	7.71
$3^3P_1(10.516)$	$1^3D_2(10.157)$	353	$\frac{1}{10}$	−0.050	0.060
$3^3P_1(10.516)$	$2^3S_1(10.023)$	481	$\frac{1}{9}$	0.355	5.06
$3^3P_1(10.516)$	$1^3S_1(9.460)$	1003	$\frac{1}{9}$	0.137	6.86
$1^3G_3(10.520)$	$1^3F_2(10.498)$	22	$\frac{4}{49}$	3.812	0.068
$1^3G_4(10.520)$	$1^3F_3(10.498)$	22	$\frac{5}{84}$	3.812	0.069
$1^3G_5(10.520)$	$1^3F_4(10.498)$	22	$\frac{4}{81}$	3.812	0.074
$3^3P_2(10.529)$	$2^3D_3(10.450)$	79	$\frac{2}{25}$	−2.576	1.96
$3^3P_2(10.529)$	$3^3S_1(10.355)$	172	$\frac{1}{9}$	2.284	9.63
$3^3P_2(10.529)$	$1^3D_3(10.160)$	363	$\frac{2}{25}$	−0.053	0.082
$3^3P_2(10.529)$	$2^3S_1(10.023)$	494	$\frac{1}{9}$	0.358	5.54
$3^3P_2(10.529)$	$1^3S_1(9.460)$	1014	$\frac{1}{9}$	0.138	7.16
$2^3F_2(10.530)$	$2^3D_1(10.441)$	89	$\frac{3}{25}$	3.337	3.02
$2^3F_3(10.530)$	$2^3D_2(10.446)$	84	$\frac{8}{105}$	3.340	2.69
$2^3F_4(10.530)$	$2^3D_3(10.450)$	80	$\frac{3}{49}$	3.342	2.62
$2^3F_2(10.530)$	$1^3G_3(10.520)$	10	$\frac{4}{49}$	−2.262	0.003
$2^3F_3(10.530)$	$1^3G_4(10.520)$	10	$\frac{5}{84}$	−2.262	0.003
$2^3F_4(10.530)$	$1^3G_5(10.520)$	10	$\frac{4}{81}$	−2.262	0.003

6.2.2 *Comparison with experiment: S and P states* [13]

There is now extensive data on electromagnetic transitions among heavy quarkonium states. Figure 4.11 shows the inclusive photon spectra from the $\bar{c}c$ and $\bar{b}b$ $2^3\mathrm{S}_1$ decays measured with the CLEO detector [209]. This section provides a snapshot of the current status of various S–P transitions. New data come mainly from the CLEO experiment at CESR.

In the NR limit the overlap $\mathcal{E}_{\mathrm{nS,n'P_J}} = |\langle n'P_J|r|nS\rangle|$ is independent of J. Experimentally, it is useful to define averages over J by

$$\begin{aligned}\mathcal{E}_{\mathrm{nS,n'P}}(\mathrm{avg}) &= \sqrt{\frac{\mathcal{B}(nS\to\gamma n'P_J)\,\Gamma_{\mathrm{tot}}(nS)}{D\,\sum_J(2J+1)E_\gamma(nS\to n'P_J)^3}} \\ \mathcal{E}_{\mathrm{nP,n'S}}(\mathrm{avg}) &= \sqrt{\frac{\mathcal{B}(nP_J\to\gamma n'S)\,\Gamma_{\mathrm{tot}}(nP_J)}{D\,\sum_J E_\gamma(nP_J\to n'S)^3}}\end{aligned} \tag{4.129}$$

where $D = 4/3\,\alpha\,{e_b}^2\mathrm{S}^{\mathrm{E}}_{^3P_J,^3S_1}$. These quantities reduce to the usual overlaps in the NR limit. In order to see the relativistic corrections (which vary with J) it is also useful to define ratios, $\mathcal{E}_{\mathrm{nS,n'P_J}}/\mathcal{E}_{\mathrm{nS,n'P}}(\mathrm{avg})$. Given the total width of the initial state these overlaps can be determined directly from experimental branching ratios. The experimental results for the $\bar{c}c$ and $\bar{b}b$ states are shown in Table 4.19. These results are extracted from the world average results for $\mathcal{B}(\chi_c(1P_J)\to\gamma J/\psi)$ and $\mathcal{B}(\psi(2S)\to\gamma\chi_c(1P_J))$. Also shown are recent results from CLEO-c for $\mathcal{B}(\psi(2S)\to\gamma\chi_c(1P_J))$ transitions [210]. Results for $\mathcal{B}(\Upsilon(3S)\to\gamma\chi_b(2P_J))$ and $\mathcal{B}(\Upsilon(2S)\to\gamma\chi_b(1P_J)$ are taken from Ref. [10]. The E1 transitions show clear evidence of J dependence and, hence, relativisitic corrections in S state transitions. The largest relativistic effects are in the 2^3S_1 to 1^3P_J $\bar{c}c$ transitions.

With their large Υ(3S) data sample and excellent CsI electromagnetic calorimeter, the CLEO III experiment has been able to measure the E1 photon transitions from the Υ(3S) to the $\chi_b(2\mathrm{P}_J)$ states, and the subsequent photon decays of those states to the Υ(2S) and Υ(1S). They identify exclusive $\gamma\gamma\ell^+\ell^-$ events, which are consistent with photon transitions through the $\chi_b(2\mathrm{P}_J)$ states to the Υ(2S) or Υ(1S), followed by the leptonic decay of the Υ. This provides a very clean signal with little background. Tables 4.20 and 4.21 give a summary of their preliminary results [211] on the product branching ratios, along with comparisons with the previous CLEO II [212] and CUSB [213] measurements. Then, by using the world average values for the $\Upsilon(3\mathrm{S}) \to \chi_b(2\mathrm{P}_J) + \gamma$ and Υ leptonic branching ratios, the $\chi_b(2\mathrm{P}_J) \to \Upsilon + \gamma$ branching ratios can be obtained.

For the similar transitions through the $\chi_b(1\mathrm{P}_J)$ states: $\Upsilon(3\mathrm{S}) \to \gamma\chi_b(1\mathrm{P}_J)$, $\chi_b(1\mathrm{P}_J) \to \gamma\Upsilon(1\mathrm{S})$, the photon lines for the different J states cannot be resolved, due to the finite crystal energy resolution. The J = 0 branching ratio is expected to be small, given the large hadronic width of this state. So CLEO III gives a combined product branching ratio, summed over the J = 1 and J = 2 states. The results are shown in Table 4.22.

We can extract the $|\mathcal{E}_{1\mathrm{P,3S}}|$ matrix element from the photon transitions via the $\chi_b(1P)$ states:

$$\mathcal{E}_{1\mathrm{P,3S}}(\mathrm{avg}) = \sqrt{\frac{\mathcal{B}(3S\to\gamma 1P, 1P\to\gamma 1S)\,\Gamma_{\mathrm{tot}}(3S)}{D\,\sum_J(2J+1)E_\gamma(1P_J\to 1S)^3\mathcal{B}(1P_J\to\gamma 1S)}}. \tag{4.130}$$

This formula assumes that the matrix element is spin independent. Taking $\mathcal{B}(3S\to\gamma 1P, 1P\to\gamma 1S)$ from Table 4.22 and the world average values for the other quantities from PDG04 [10], we obtain:

$$\mathcal{E}_{1\mathrm{P,3S}}(\mathrm{avg}) = (0.050 \pm 0.006)\,\mathrm{GeV}^{-1}\,.$$

The error here includes the statistical and systematic uncertainties on all quantities added in quadrature. The averaging is only over $J = 1$ and $J = 2$.

[13] Authors: E. Eichten, T. Ferguson

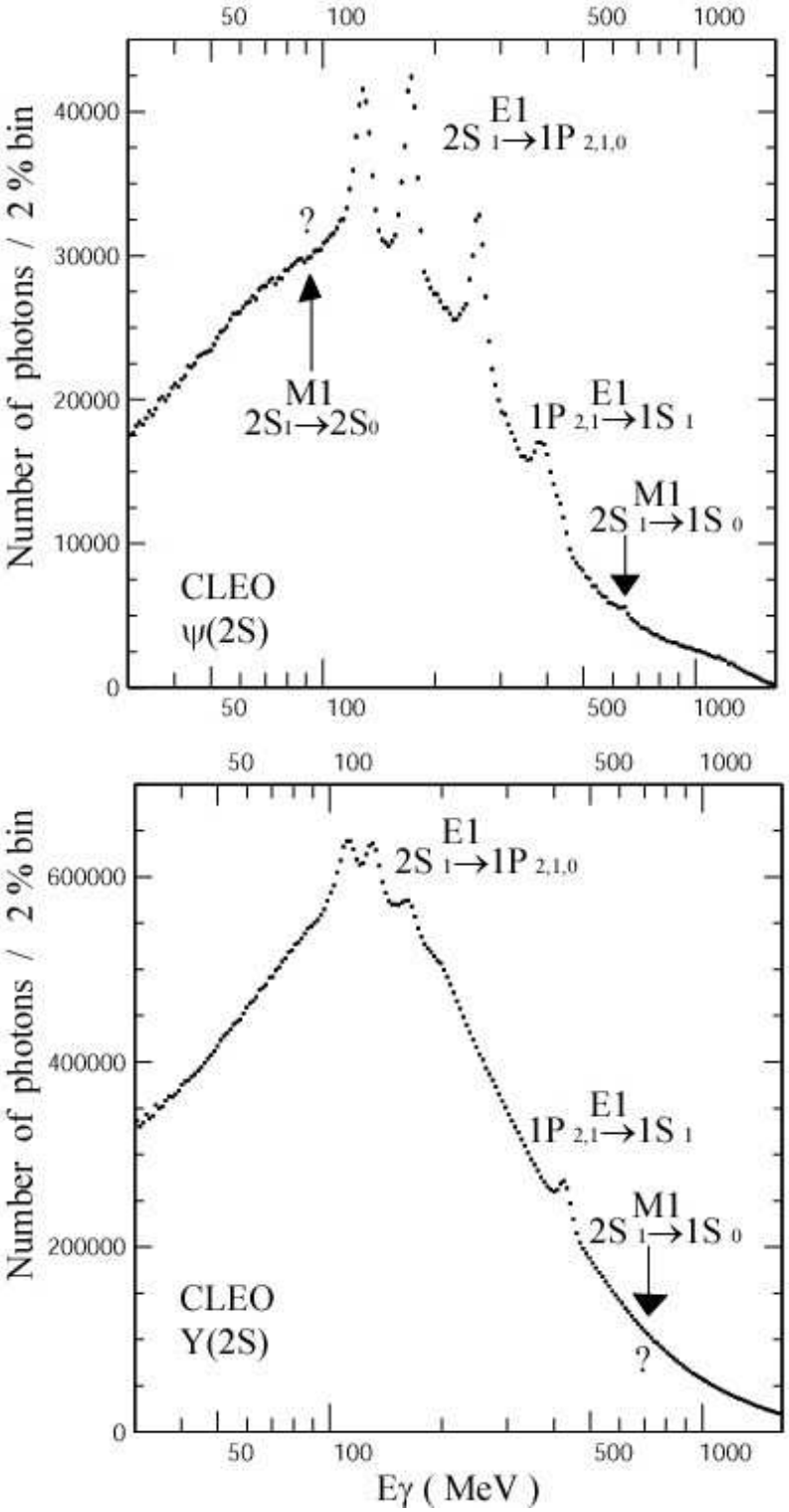

Fig. 4.11: Inclusive photon spectrum from 2^3S_1 decays in the $\bar{c}c$ (top) and $\bar{b}b$ (bottom) systems measured with the CLEO detector. The data correspond to about 1.5M $\psi(2S)$ and 9M Υ(2S) decays. From Skwarnicki [209].

Table 4.19: Measured E1 overlap integrals for S–P transitions. Transition rates use branching ratios and total widths from PDG04 world averages [10] except for second set of values for the $\bar{c}c$ transition $2^3S_1 \to 1^3P_J$, which uses branching ratios from recent results of CLEO-c [210].

Transition $i \xrightarrow{\text{E1}} f$	$\lvert\mathcal{E}_{\text{avg}}\rvert$ (GeV^{-1})	$\mathcal{E}_J/\mathcal{E}_{\text{avg}}$ $J=0$	$J=1$	$J=2$
$\bar{c}c$				
$1^3P_J \quad 1^3S_1$	1.87 ± 0.07	0.92 ± 0.05	0.99 ± 0.06	1.04 ± 0.03
$2^3S_1 \quad 1^3P_J$	1.78 ± 0.07	0.94 ± 0.04	1.01 ± 0.05	1.07 ± 0.05
	1.94 ± 0.07	0.90 ± 0.02	0.97 ± 0.03	1.19 ± 0.04
$\bar{b}b$				
$3^3S_1 \quad 2^3P_J$	2.75 ± 0.21	0.92 ± 0.06	1.06 ± 0.05	1.02 ± 0.06
$2^3S_1 \quad 1^3P_J$	1.94 ± 0.18	0.92 ± 0.06	1.09 ± 0.05	0.98 ± 0.06

Table 4.20: CLEO III preliminary results [211] for $\Upsilon(3S) \to \gamma\ \chi_b(2P_J) \to \gamma\gamma\ \Upsilon(2S) \to \gamma\gamma\ell^+\ell^-$, along with comparisons with CLEO II [212] and CUSB [213].

Parameter (units)	Ref.	J = 2	J = 1	J = 0
$\mathcal{B}(\gamma\gamma\ell^+\ell^-)$ (10^{-4})	[211]	$2.73 \pm 0.15 \pm 0.24$	$5.84 \pm 0.17 \pm 0.41$	$0.17 \pm 0.06 \pm 0.02$
	[212]	$2.49 \pm 0.47 \pm 0.31$	$5.11 \pm 0.60 \pm 0.63$	< 0.60
	[213]	$2.74 \pm 0.33 \pm 0.18$	$3.30 \pm 0.33 \pm 0.19$	$0.40 \pm 0.17 \pm 0.03$
$\mathcal{B}(\Upsilon(3S) \to \gamma\gamma\Upsilon(2S))$ (%)	[211]	$2.20 \pm 0.12 \pm 0.31$	$4.69 \pm 0.14 \pm 0.62$	$0.14 \pm 0.05 \pm 0.02$
$\mathcal{B}(\chi_b(2P_J) \to \gamma\Upsilon(2S))$ (%)	[211]	$19.3 \pm 1.1 \pm 3.1$	$41.5 \pm 1.2 \pm 5.9$	$2.59 \pm 0.92 \pm 0.51$

Table 4.21: CLEO III preliminary results [211] for $\Upsilon(3S) \to \gamma\ \chi_b(2P_J) \to \gamma\gamma\ \Upsilon(1S) \to \gamma\gamma\ell^+\ell^-$, along with comparisons with CLEO II [212] and CUSB [213].

Parameter (units)	Ref.	J = 2	J = 1	J = 0
$\mathcal{B}(\gamma\gamma\ell^+\ell^-)$ (10^{-4})	[211]	$1.93 \pm 0.12 \pm 0.17$	$3.19 \pm 0.13 \pm 0.18$	< 0.16
	[212]	$2.51 \pm 0.47 \pm 0.32$	$3.24 \pm 0.56 \pm 0.41$	< 0.32
	[213]	$1.98 \pm 0.28 \pm 0.12$	$2.34 \pm 0.28 \pm 0.14$	$0.13 \pm 0.10 \pm 0.03$
$\mathcal{B}(\Upsilon(3S) \to \gamma\gamma\Upsilon(1S))$ (%)	[211]	$0.79 \pm 0.05 \pm 0.07$	$1.31 \pm 0.05 \pm 0.08$	< 0.08
$\mathcal{B}(\chi_b(2P_J) \to \gamma\Upsilon(1S))$ (%)	[211]	$7.0 \pm 0.4 \pm 0.8$	$11.6 \pm 0.4 \pm 0.9$	< 1.44

Table 4.22: CLEO III preliminary results [211] for $\Upsilon(3S) \to \gamma\ \chi_b(1P_J) \to \gamma\gamma\ \Upsilon(1S) \to \gamma\gamma\ell^+\ell^-$, along with comparisons with the CUSB experiment [213]. The values are summed over the J = 1 and J = 2 transitions.

Parameter	Ref.	J = 1 and 2 Combined
$\mathcal{B}(\gamma\gamma\ell^+\ell^-)$ (10^{-4})	[211]	$0.520 \pm 0.054 \pm 0.052$
$\mathcal{B}(\Upsilon(3S) \to \gamma\gamma\Upsilon(1S))$ (%)	[211]	$0.241 \pm 0.022 \pm 0.021$
	[213]	$0.12 \pm 0.04 \pm 0.01$

Table 4.23: Comparison of average E1 matrix elements and their ratios predicted by different potential models with measurements from $\bar{b}b$ data. "NR" denotes nonrelativistic calculations and "rel" refers to models with relativistic corrections. The first set of model entries are the reference models considered here. The second set is a selection of other models taken from Ref. [211].

	$\lvert\mathcal{E}_{3S,2P}\rvert$		$\lvert\mathcal{E}_{2S,1P}\rvert$		$\lvert\mathcal{E}_{3S,1P}\rvert$		$\frac{\lvert\mathcal{E}_{2P,1S}\rvert}{\lvert\mathcal{E}_{2P,2S}\rvert}$	
	GeV^{-1}		GeV^{-1}		GeV^{-1}			
DATA	2.7 ± 0.2		1.9 ± 0.2		0.050 ± 0.006		0.096 ± 0.005	
	World Average				CLEO III [211]			
Model	NR	rel	NR	rel	NR	rel	NR	rel
NR	2.5		1.6		0.014		0.16	
RA		2.6		1.8		0.063		0.12
RB		2.6		1.8		0.045		0.12
Kwong, Rosner [200]	2.7		1.6		0.023		0.13	
Fulcher [214]	2.6		1.6		0.023		0.13	
Büchmuller et al. [141, 193]	2.7		1.6		0.010		0.12	
Moxhay, Rosner [199]	2.7	2.7	1.6	1.6	0.024	0.044	0.13	0.15
Gupta et al. [204]	2.6		1.6		0.040		0.11	
Gupta et al. [202, 203]	2.6		1.6		0.010		0.12	
Fulcher [215]	2.6		1.6		0.018		0.11	
Danghighian et al. [206]	2.8	2.5	1.7	1.3	0.024	0.037	0.13	0.10
McClary, Byers [181]	2.6	2.5	1.7	1.6			0.15	0.13
Eichten et al. [191]	2.6		1.7		0.110		0.15	
Grotch et al. [184]	2.7	2.5	1.7	1.5	0.011	0.061	0.13	0.19

Results for the values of $\mathcal{E}$(avg) in the $\bar{b}b$ P system are compared to various potential model predictions in Table 4.23. We also include results for $\mathcal{E}_{3S,2P}$ and $\mathcal{E}_{2S,1P}$ from Table 4.19 extracted from the world average results for $\mathcal{B}(\Upsilon(3S)\to\gamma\chi_b(2P_J))$ and $\mathcal{B}(\Upsilon(2S)\to\gamma\chi_b(1P_J)$ [10]. While most of the potential models have no trouble reproducing the large matrix elements, $\mathcal{E}_{3S,2P}$, $\mathcal{E}_{2S,1P}$, which show also little model dependence, only a few models predict $\mathcal{E}_{3S,1P}$ in agreement with measurements. Clearly, the latter transition is highly sensitive to the underlying description of $\bar{b}b$ states as discussed above.

The branching ratios given in the Tables 4.20–4.22 can also be used to measure the ratios of various E1 matrix elements, which can then be compared to different potential model predictions. First, the ratio of the matrix elements for the decay of the same $\chi_b(2P_J)$ state to different Υ states can be found using:

$$\frac{\mathcal{E}_{2P_J,1S}}{\mathcal{E}_{2P_J,2S}} = \sqrt{\frac{\mathcal{B}(3S \to \gamma 2P_J, 2P_J \to \gamma 1S)}{\mathcal{B}(3S \to \gamma 2P_J, 2P_J \to \gamma 2S)} \left(\frac{E_\gamma(2P_J \to 2S)}{E_\gamma(2P_J \to 1S)}\right)^3} \tag{4.131}$$

With this method, the following values are obtained:

$$\frac{\mathcal{E}_{2P_2,1S}}{\mathcal{E}_{2P_2,2S}} = 0.105 \pm 0.004 \pm 0.006, \qquad \frac{\mathcal{E}_{2P_1,1S}}{\mathcal{E}_{2P_1,2S}} = 0.087 \pm 0.002 \pm 0.005, \tag{4.132}$$

$$\frac{\mathcal{E}_{2P_2,1S}}{\mathcal{E}_{2P_2,2S}} \Big/ \frac{\mathcal{E}_{2P_1,1S}}{\mathcal{E}_{2P_1,2S}} = 1.21 \pm 0.06, \qquad \frac{\mathcal{E}_{2P_{1,2},1S}}{\mathcal{E}_{2P_{1,2},2S}} = 0.096 \pm 0.002 \pm 0.005. \tag{4.133}$$

To compare to potential model predictions, the last number above is an average over the J = 1 and J = 2 values. In the nonrelativistic limit, the E1 matrix elements should not depend on J. Since the values

for the J = 1 and J = 2 matrix elements differ by 3.5 standard deviations, there appears to be evidence for relativistic effects in the $\bar{b}b$ system in both the S and P states transitions. Again these results are compared to various potential model predictions in Table 4.23. Predictions for the ratio $|\mathcal{E}_{2P,1S}|/|\mathcal{E}_{2P,2S}|$ are very model dependent, but somewhat higher than the experimental values.

Overall, the comparison of the measured matrix elements and the predictions of various potential models shows that the recent theoretical calculations that incorporate relativistic effects are better at reproducing the data [209, 211].

6.2.3 D states

In the $\bar{c}c$ system, the 1^3D_1 and 1^3D_3 states are above $D\bar{D}$ threshold and have open flavour strong decays. The $J = 2$ states 1^3D_2 and 1^1D_2 are below (or at) the $D^*\bar{D} + D\bar{D}^*$ threshold and are expected to be narrow. In all cases, the coupling to real and virtual strong decay channels is likely to significantly alter the potential model radiative transition rates shown in Table 4.15. (We will discuss this further in Section 6.5 below.) One effect of these couplings is that the $\psi(3770)$ state will not be a pure 1^3D_1 state but will have a sizeable mixing component with the 2^3S_1 state:

$$\psi(3770) = \cos(\phi)|1^3D_1\rangle + \sin(\phi)|2^3S_1\rangle \ . \tag{4.134}$$

Using the measured leptonic width of the $\psi(3770)$ and resolving a two-fold ambiguity in favor of the value of the mixing angle favored by Cornell coupled channel calculations [191], Rosner finds [106] $\phi = (12 \pm 2)^\circ$. Employing the NR results of Table 4.15, the ratios of E1 transitions to various χ_c states are:

$$\begin{aligned} \frac{\Gamma(\psi(3770) \to \gamma\chi_{c1})}{\Gamma(\psi(3770) \to \gamma\chi_{c0})} &= 1.32 \left(\frac{-\frac{\sqrt{3}}{2} + \tan(\phi)}{\sqrt{3} + \tan(\phi)} \right)^2 , \\ \frac{\Gamma(\psi(3770) \to \gamma\chi_{c2})}{\Gamma(\psi(3770) \to \gamma\chi_{c0})} &= 1.30 \left(\frac{\frac{\sqrt{3}}{10} + \tan(\phi)}{\sqrt{3} + \tan(\phi)} \right)^2 . \end{aligned} \tag{4.135}$$

Measuring these branching ratios is experimentally challenging. [The only existing data is contained in an unpublished Ph. D. thesis based on MARK III data [216].] CLEO-c may be able to determine some of these branching ratios in the near future.

In the $\bar{b}b$ system CLEO III [171] has presented evidence for the production of $\Upsilon(1D)$ states in the four-photon cascade (see Fig. 4.10), $\Upsilon(3S)\to\gamma\chi_b(2P)$, $\chi_b(2P)\to\gamma\Upsilon(1D)$, $\Upsilon(1D)\to\gamma\chi_b(1P)$, $\chi_b(1P)\to\gamma\Upsilon(1S)$, followed by the $\Upsilon(1S)$ annihilation into e^+e^- or $\mu^+\mu^-$.

In addition to the four-photon cascade via the $\Upsilon(1D)$ states, they observe events with the four-photon cascade via the $\Upsilon(2S)$ state: $\Upsilon(3S) \to \gamma\chi_b(2P)$, $\chi_b(2P) \to \gamma\Upsilon(2S)$, $\Upsilon(2S) \to \gamma\chi_b(1P)$, $\chi_b(1P) \to \gamma\Upsilon(1S)$, $\Upsilon(1S)\to l^+l^-$ The product branching ratio for this entire decay sequence (including $\Upsilon(1S)\to l^+l^-$) is predicted to be $3.84 \cdot 10^{-5}$ [217], thus comparable to the predicted $\Upsilon(1D)$ production rate. In the four-photon cascade via the $\Upsilon(1D)$ the second highest energy photon is due to the third transition, while in these cascades the second highest energy photon is due to the second photon transition (see Fig. 4.10). This allows the discrimination of the $\Upsilon(1D)$ signal from the $\Upsilon(2S)$ background events.

CLEO III [171] finds their data are dominated by the production of one $\Upsilon(1D)$ state consistent with the $J = 2$ assignment and a mass $(10161.1\pm0.6\pm1.6)$ MeV, which is consistent with the predictions from potential models and lattice QCD calculations.

The signal product branching ratio obtained is $\mathcal{B}(\gamma\gamma\gamma\gamma l^+l^-)_{\Upsilon(1D)} = (2.5 \pm 0.5 \pm 0.5) \cdot 10^{-5}$. The first error is statistical, while the second one is systematic. The significance of the signal is 10.2 standard deviations. This branching ratio is consistent with the theoretically estimated rates. Godfrey and Rosner [217], summing over $\Upsilon(1D_{1,2,3})$ contributions, obtained 3.76×10^{-5}; while the predicted rate [200, 217] for the $\Upsilon(1D_2)$ state alone is 2.6×10^{-5}.

Forming the ratio of $\Upsilon(1D)$ to $\Upsilon(2S)$ four-photon cascades would allow the measurement in a fairly model independent way of the estimate of the total width of the $\Upsilon(1D)$ state, if the individual $\Upsilon(2P_J)$ and $\Upsilon(1P_{J'})$ transitions could be resolved.

6.3 M1 transitions

For M1 transitions, the leading order NRQCD prediction for the overlap $\mathcal{M}_{if}$ is independent of the potential model. The spin independence and orthogonality of states guarantee that the spatial overlap matrix is one for states within the same multiplet and zero for allowed transitions between multiplets, which have different radial quantum numbers.

Including relativistic corrections, e.g., finite size corrections, will spoil these exact results and induce a small overlap between states with different radial quantum numbers. Such $n \neq n'$ transitions are denoted hindered.

6.3.1 Model predictions

Within the (NR) model used for the E1 transitions (i.e., a nonrelativistic treatment except for finite size corrections and $\kappa_Q = 0$) the M1 transition rates and overlap matrix elements $\mathcal{M}$ for $\bar{c}c$ and $\bar{b}b$ S states are shown in Table 4.24.

Numerous papers have considered these M1 transitions including full relativistic corrections [182, 184–186, 201, 217, 218]. There are several sources of uncertainty that contribute making M1 transitions particularly complicated to calculate. In addition to the usual issues associated with the form of the long range potential there is the unknown value for the anomalous magnetic moment for the quark (κ_Q). Furthermore, the results depend explicitly on the quark masses and on other details of the potential (see Eqs. 4.128). For the models (RA) and (RB) used for the E1 transitions, $\kappa_Q = -1$. The theoretical uncertainty in the value of κ_Q will eventually be reduced by lattice calculations in quarkonium systems.

6.3.2 Comparison with experiment

M1 transitions have only been observed in the $\bar{c}c$ system. The allowed transitions in the $\bar{c}c$ system below threshold are shown in Fig. 4.12. The transitions within the $1P$ system are tiny ($\approx$ 1 eV). Only the $J/\psi \to \eta_c$ and $\psi' \to \eta_c$ are observed experimentally [10]. For the $\bar{b}b$ system CLEO [219] sees no evidence for the hindered M1 transition $\Upsilon(3\mathrm{S}) \to \eta_b(1\mathrm{S})$. The 90% cl upper bound on the branching ratio varies from $4 - 6 \times 10^{-4}$ depending on the mass splitting. For the expected splitting ≈ 910 MeV the bound is 5.3×10^{-4} [219]. This rules out a number of older models [182, 201]. A comparison of the experimental results with a variety of more modern models is shown in Table 4.25. For each model the assumptions for the mixture of scalar and vector confinement and the value of κ_Q is exhibited explicitly. For the model of Lahde [185] the results are also shown without including the exchange term (NEX). This (NEX) piece neglects the time ordering of photon emission and potential interaction, which vanishes in the NR limit. Generally models with a scalar confining interaction and/or a sizable negative anomalous quark magnetic moment are favored.

6.4 Higher order corrections

6.4.1 Higher multipole contributions

In lowest order, only the E1 amplitude contributes to χ_c states radiative transitions. In higher order in v^2/c^2 a M2 amplitude contributes for $J = 1, 2$ and an E3 amplitudes is also possible for the $J = 2$ state. To order v^2/c^2 these M2 and E3 corrections to the dominant E1 term can contribute to angular distributions but cannot contribute to total decay rates. This comes from the orthogonality of terms in the multipole expansion.

Table 4.24: M1 transition rates for S-wave quarkonium states using the NR model described in text. Finite size corrections are included in the calculation of $\mathcal{M}$ (see Eq. (4.121)) and $\kappa_Q = 0$.

Transition $i \xrightarrow{\text{M1}} f$		k (MeV)	$\Gamma(i \to f)$(NR) (eV)	$\mathcal{M}_{if}$(NR)
		$\bar{c}c$		
$1^3S_1(3.097)$	$1^1S_0(2.979)$	115	1,960	0.998
$2^3S_1(3.686)$	$2^1S_0(3.638)$	48	140	0.999
$2^1S_0(3.638)$	$1^3S_1(3.097)$	501	538	0.033
$2^3S_1(3.686)$	$1^1S_0(2.979)$	639	926	0.053
		$\bar{b}b$		
$1^3S_1(9.460)$	$1^1S_0(9.400)$	60	8.953	1.000
$2^1S_0(9.990)$	$1^3S_1(9.460)$	516	2.832	0.013
$2^3S_1(10.023)$	$2^1S_0(9.990)$	33	1.509	1.000
$2^3S_1(10.023)$	$1^1S_0(9.400)$	604	2.809	0.018
$3^1S_0(10.328)$	$2^3S_1(10.023)$	300	0.620	0.014
$3^1S_0(10.328)$	$1^3S_1(9.460)$	831	3.757	0.007
$3^3S_1(10.355)$	$3^1S_0(10.328)$	27	0.826	1.000
$3^3S_1(10.355)$	$2^1S_0(9.990)$	359	0.707	0.019
$3^3S_1(10.355)$	$1^1S_0(9.400)$	911	2.435	0.009

Table 4.25: Comparison of M1 transition overlaps with experiment for various models. The transition overlap $I \equiv \frac{M(1^3S_1)}{2m_Q}\mathcal{M}_{if}$ is from nS spin triplet to the n'S spin singlet S states in the $\bar{c}c$ and $\bar{b}b$ systems. The experimental upper bounds are 90% cl.

Type			Transition $I_{n,n'}$					
Model	parameters		(n,n') $[\bar{c}c]$		(n,n') $[\bar{b}b]$			
	η	κ_Q	$(1,1)$	$(2,1)$	$(1,1)$	$(2,1)$	$(3,1)$	$(3,2)$
Cornell [191]	NR	0	0.84	0.028	0.92	0.017	0.007	0.018
GOS84 [184]	0	0	0.86	0.075	0.88	0.058	–	–
	0	-1	0.58	0.054	0.081	0.007	–	–
	1	0	0.65	0.127	0.91	0.048	–	–
	1	-1	0.39	0.029	0.049	0.021	–	–
EFG02 [186]	0	0	0.84	0.036	0.91	0.018	0.013	0.016
	1	0	1.06	0.027	1.08	0.011	0.009	0.007
	-1	-1	0.62	0.045	0.75	0.025	0.026	0.017
Lahde02 [185]	NEX	0	0.87	0.011	0.92	0.020	0.009	0.016
	1	0	0.67	0.049	0.88	0.032	0.014	0.037
EXP			0.66 ± 0.10	0.042 ± 0.004		< 0.045	< 0.020	< 0.080
Ref			[10]	[10] [210]		[209]	[219]	[209]

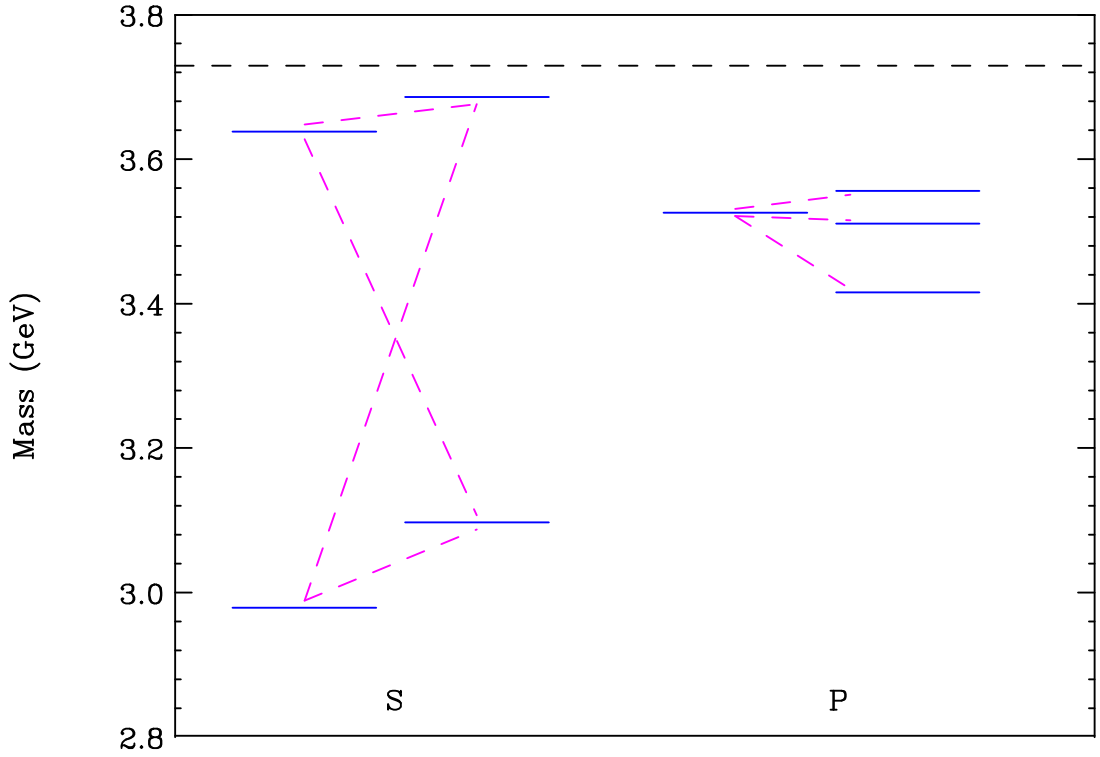

Fig. 4.12: Allowed M1 transitions in the narrow $\bar{c}c$. The $1P$ transition rates are unobservably small ($\approx 1eV$).

It was originally suggested by Karl, Meshkov and Rosner [220] that these corrections can be studied by measuring the angular correlations between the two photons in the transition $\psi' \to \chi_c + \gamma \to J/\psi + 2\gamma$. These effects can also be studied for χ_c states directly produced in hadron collisions, B decays or $\bar{p}p$ annihilation by measuring the combined angular distributions of the photon and the l^+l^- pair produced in the subsequent J/ψ decay. The details of these correlations have been calculated by Sebastian, Grotch and Ridener [221].

For the photon transition from a χ_{cJ} state there are $J+1$ normalized helicity amplitudes, A_ν. Defining $|a| = \sqrt{E1^2 + M2^2 + E3^2}$, $a_1 = E1/|a|$, $a_2 = M2/|a|$ and $a_3 = E3/|a|$ the relation between helicity and multipole amplitudes is:

$$A_\nu = \sum_\ell a_\ell \left(\frac{2\ell+1}{2J+1}\right)^{\frac{1}{2}} \langle \ell, 1; 1, \nu - 1 | J, \nu \rangle \,. \tag{4.136}$$

Allowing for an anomalous magnetic moment κ_c and mixing between the $2S$ and $1D$ states the theoretical predictions for

$$\psi' \to \chi_{cJ} + \gamma \quad \text{and} \quad \chi_{cJ} \to J/\psi + \gamma$$

are shown in Table 4.26 along with a comparison with present experimental results. The S–D mixing parameter is $\mathcal{E}_{2S,1P} X = -\tan\phi\, \mathcal{E}_{1D,1P}$ where ϕ is defined in Eq. (4.134). In the notation of Eq. (4.127) the other model dependent parameter is defined by $\mathcal{E}_{1D,1P} Y = \int dr\, r \left(r \frac{du_{12}^{(0)}}{dr} - u_{12}^{(0)} \right) u_{11}^{(0)}$.

As can be seen from Table 4.26 a nonzero E3 amplitude in the $\psi' \to \chi_{c2} + \gamma$ decay is evidence for S–D mixing in the ψ'. Also note that the M2 term is sensitive to a possible anomalous magnetic moment, κ_c, for the charm quark. The recent BES results [223] for the M2 and E3 contributions do not differ significantly from zero. Additional high statistics studies of these angular distributions will

be necessary to determine the size of S–D mixing and shed light on the magnitude of the charm quark magnetic moment.

6.5 Coupling to virtual decay channels

When light quark loops are included in the description of quarkonium systems, the physical quarkonium states are not pure potential-model eigenstates and the effects of coupling to real and virtual heavy-light meson pairs must be included. Our command of quantum chromodynamics is inadequate to derive a realistic description of the interactions that communicate between the $\bar{Q}Q$ and $\bar{Q}q + \bar{q}Q$ sectors. However, the physical picture is that wave functions corresponding to physical states are now linear combinations of potential-model $\bar{Q}Q$ eigenstates plus admixtures of open heavy-flavour-meson pairs. The open heavy-flavour pieces have the spatial structure of bound states of heavy-flavour mesons: they are virtual contributions for states below threshold (see Section 3.3 in Chapter 3 for more details).

Far below heavy flavour threshold, the nonrelativistic potential model is a good approximation to the dynamics of the $\bar{Q}Q$ system. For excited states above the first few levels, the coupling of $\bar{Q}Q$ to heavy-flavour-meson pairs modifies wave functions, masses, and transition rates. In particular, this modifies electromagnetic transition rates considered in the previous subsections. In addition to these contributions, which involved photon coupling to a heavy (anti)quark, the contributions of light quark currents can no longer be neglected. The mass differences among the $\bar{Q}u$, $\bar{Q}d$ and $\bar{Q}s$ mesons, induce large SU(3) symmetry breaking effects. This destroys the cancellation among the light quark EM current contributions.

To compute the E1 radiative transition rates, we must take into account both the standard $(\bar{Q}Q)$ $\rightarrow (\bar{Q}Q)\gamma$ transitions and the transitions between (virtual) decay channels in the initial and final states. This second set of transitions contains light quark contributions for states near threshold. Recently, the effects of configuration mixing on radiative decay rates in the $\bar{c}c$ system were reexamined [207] within the Cornell coupled-channel formalism. A full outline of the calculational procedure appears in Refs. [177, 191]. (In particular, see Section IV.B of Ref. [191].)

Expectations for E1 transition rates among spin-triplet levels are shown in Table 4.27. Both the rates calculated between single-channel potential-model eigenstates (in italics) and the rates that result from the Cornell coupled-channel model are shown, to indicate the influence of the open-charm channels.

The $1^3\mathrm{D}_1$ transition rates at the mass of $\psi(3770)$ and at the predicted $1^3\mathrm{D}_1$ centroid, 3815 MeV, are shown. For the $\psi(3770)$, with its total width of about 24 MeV, the $1^3\mathrm{D}_1(3770) \rightarrow \chi_{c0}\,\gamma(338)$ transition might someday be observable with a branching fraction of 1%. For the $1^3\mathrm{D}_2$ and $1^3\mathrm{D}_3$ levels, the radiative decay rates were calculated at the predicted $1^3\mathrm{D}_1$ centroid, 3815 MeV, at the mass calculated for the states (3831 MeV and 3868 MeV, respectively), and at the mass of $X(3872)$. The model reproduces the trends of transitions to and from the χ_c states in broad outline. For these low-lying states, the mixing through open-charm channels results in a mild reduction of the rates.

This study was done in the Cornell coupled channel model. It would be useful to do a similarly detailed study of these effects in other models.

6.6 B_c states

Quarkonium systems with unequal quark and antiquark masses, i.e., B_c mesons, are theoretical interesting, but are not easily accessible in e^+e^- collisions. They can be produced in significant numbers in hadron collisions (see Chapter 5, Section 8). CDF has reported the discovery of the ground state B_c meson via its semileptonic weak decay [224]. Theoretical calculations for E1 and M1 radiative transitions have been presented by a number of authors [186, 192, 225, 226] even though the whole excitation spectrum remains to be observed experimentally.

Table 4.26: M2 and E3 multipole amplitudes for radiative transitions involving χ_c states. The values of X and Y are model dependent and are defined in the text. Note $X = 0$ if no S–D mixing.

	$\chi_{cJ} \to J/\psi + \gamma$		
J	theory [221]	E835 [222]	PDG04 [10]
2	$a_2 \approx -\frac{\sqrt{5}}{3}\frac{k}{4m_c}(1+\kappa_c)$	$-0.093^{+0.039}_{-0.041} \pm 0.006$	-0.13 ± 0.05
2	$a_3 \approx 0$	$0.020^{+0.055}_{-0.044} \pm 0.009$	$0.011^{+0.041}_{-0.033}$
1	$a_2 \approx -\frac{k}{4m_c}(1+\kappa_c)$	$0.002 \pm 0.032 \pm 0.004$	$-0.002^{+0.008}_{-0.017}$
	$\psi' \to \chi_{cJ} + \gamma$		
J	theory [221]		BES [223]
2	$a_2 \approx -\frac{\sqrt{3}}{2\sqrt{10}}\frac{k}{m_c}[(1+\kappa_c)(1+\frac{\sqrt{2}}{5}X) - i\frac{1}{5}X]/[1-\frac{1}{5\sqrt{2}}X]$		$-0.051^{+0.054}_{-0.036}$
2	$a_3 \approx -\frac{12\sqrt{2}}{175}\frac{k}{m_c}X[1+\frac{3}{8}Y]/[1-\frac{1}{5\sqrt{2}}X]$		$-0.027^{+0.043}_{-0.029}$
1	$a_2 \approx -\frac{k}{4m_c}[(1+\kappa_c)(1+\frac{2\sqrt{2}}{5}X) + i\frac{3}{10}X]/[1+\frac{1}{\sqrt{2}}X]$		

Table 4.27: Calculated and observed rates for E1 radiative transitions among charmonium levels from Ref. [207]. Values in *italics* result if the influence of open-charm channels is not included. Measured rates are shown for comparison. Experimental values are calculated from world averages [10], except for $\mathcal{B}(\psi' \to \gamma^3 P_J)$ whose values are taken from the recent CLEO-c measurement [210].

Transition	k_γ (MeV)	width (keV)	k_γ (MeV)	width (keV)	k_γ (MeV)	width (keV)
	P state					
S state	χ_{c2}		χ_{c1}		χ_{c0}	
J/ψ	429	*300* $\to$287	390	*228* $\to$216	303	*113* $\to$107
[exp]		430 ± 40		290 ± 50		119 ± 16
ψ'	129	*23* $\to$23	172	*33* $\to$32	261	*36* $\to$38
[exp]		25.9 ± 2.1		25.5 ± 2.2		26.2 ± 2.6
	P state					
D state	χ_{c2}		χ_{c1}		χ_{c0}	
$1^3D_1(3770)$	208	*3.2* $\to$3.9	251	*183* $\to$59	338	*254* $\to$225
$1^3D_1(3815)$	250	*5.5* $\to$6.8	293	*128* $\to$120	379	*344* $\to$371
$1^3D_2(3815)$	251	*50* $\to$40	293	*230* $\to$191		
$1^3D_2(3831)$	266	*59* $\to$45	308	*264* $\to$212		
$1^3D_2(3872)$	303	*85* $\to$45	344	*362* $\to$207		
$1^3D_3(3815)$	251	*199* $\to$179				
$1^3D_3(3868)$	303	*329* $\to$286				
$1^3D_3(3872)$	304	*341* $\to$299				

7 HADRONIC TRANSITIONS[14]

7.1 Theoretical approaches

Hadronic transitions (HTs)

$$\Phi_i \to \Phi_f + h \tag{4.137}$$

are important decay modes of heavy quarkonia [Φ_i, Φ_f and h stand for the initial-, final-state quarkonia and the emitted light hadron(s)]. For instance, the branching ratio of $\psi' \to J/\psi + \pi + \pi$ is approximately 50%. In the $c\bar{c}$ and $b\bar{b}$ systems, the typical mass difference $M_{\Phi_i} - M_{\Phi_f}$ is around a few hundred MeV, so that the typical momentum of h is low. In the single-channel picture, the light hadron(s) h are converted from the gluons emitted by the heavy quark Q or antiquark $\bar{Q}$ in the transition. The typical momentum of the emitted gluons is too low for perturbative QCD to be reliable. Certain nonperturbative approaches are thus needed for studying HTs. In the following, we briefly review two feasible approaches: namely, the *QCD multipole expansion* (QCDME) and the *Chiral Lagrangian for Heavy Mesons*.

A. QCD Multipole expansion

Heavy $Q\bar{Q}$ bound states can be calculated by solving the Schrödinger equation with a given potential model. For $c\bar{c}$ and $b\bar{b}$ quarkonia, the typical radius is $a = \sqrt{\langle r^2 \rangle} \sim \mathcal{O}(10^{-1})$ fm. With such a small radius, the idea of QCDME can be applied to the soft gluon emissions in HTs. QCDME is an expansion in powers of $\boldsymbol{x} \cdot \boldsymbol{\nabla}$ operating on the gluon field, where $\boldsymbol{x}$ is the separation between Q and $\bar{Q}$ in the quarkonium. For a gluon with a typical momentum $k \sim$ few hundred MeV, the expansion parameter is actually $ak \sim \mathcal{O}(10^{-1})$, ensuring convergence[15]. Note that the convergence of QCDME does not depend on the value of the QCD coupling constant.

QCDME has been studied by many authors [227–231]. The gauge invariant formulation is given in Ref. [230]. Let $\psi(x)$ and $A^a_\mu(x)$ be the quark and gluon fields. Following Refs. [230, 231], we introduce

$$\Psi(\boldsymbol{x}, t) \equiv U^{-1}(\boldsymbol{x}, t)\psi(x), \quad \frac{\lambda_a}{2} A^{a\prime}_\mu(\boldsymbol{x}, t) \equiv U^{-1}(\boldsymbol{x}, t)\frac{\lambda_a}{2} A^a_\mu(x) U(\boldsymbol{x}, t) - \frac{i}{g_s} U^{-1}(\boldsymbol{x}, t)\partial_\mu U(\boldsymbol{x}, t), \tag{4.138}$$

with

$$U(\boldsymbol{x}, t) = P \exp\left[ig_s \int_{\boldsymbol{X}}^{\boldsymbol{x}} \frac{\lambda_a}{2} \boldsymbol{A}^a(\boldsymbol{x}', t) \cdot d\boldsymbol{x}'\right], \tag{4.139}$$

in which P is the path-ordering operation, the path is along the straight-line connecting the two ends, and $\boldsymbol{X} \equiv (\boldsymbol{x}_1 + \boldsymbol{x}_2)/2$ is the c.o.m. coordinate of Q and $\bar{Q}$. It is shown in Ref. [230] that, in the Lagrangian, $\Psi(\boldsymbol{x}, t)$ serves as the *dressed* (*constituent*) quark field. Now we make the multipole expansion [230]

$$A^{a\prime}_0(\boldsymbol{x}, t) = A^{a\prime}_0(\boldsymbol{X}, t) - (\boldsymbol{x} - \boldsymbol{X}) \cdot \boldsymbol{E}^a(\boldsymbol{f}X, t) + \cdots, \quad \boldsymbol{A}^{a\prime}(\boldsymbol{X}, t) = -\frac{1}{2}(\boldsymbol{x} - \boldsymbol{X}) \times \boldsymbol{B}^a(\boldsymbol{X}, t) + \cdots, \tag{4.140}$$

where $\boldsymbol{E}^a$ and $\boldsymbol{B}^a$ are colour-electric and colour-magnetic fields, respectively. The Hamiltonian is then [230]

$$H^{\rm eff}_{\rm QCD} = H^{(0)}_{\rm QCD} + H^{(1)}_{\rm QCD}, \tag{4.141}$$

with $H^{(0)}_{\rm QCD}$ the sum of the kinetic and potential energies of the heavy quarks, and

$$H^{(1)}_{\rm QCD} = H_1 + H_2, \quad H_1 \equiv Q_a A^a_0(\boldsymbol{X}, t), \quad H_2 \equiv -\boldsymbol{d}_a \cdot \boldsymbol{E}^a(\mathbf{X}, \mathbf{t}) - \mathbf{m_a} \cdot \mathbf{B^a}(\mathbf{X}, \mathbf{t}) + \cdots, \tag{4.142}$$

in which Q_a, $\boldsymbol{d}_a$, and $\boldsymbol{m}_a$ are the colour charge, colour-electric dipole moment, and colour-magnetic dipole moment of the $Q\bar{Q}$ system, respectively. Equation (4.141) is regarded as an effective Hamiltonian

[14] Authors: D. Z. Besson, A. Deandrea, F. A. Harris, Y.-P. Kuang, S. L. Olsen

[15] We know from classical electrodynamics that the coefficient of the $(ak)^l$ term in the multipole expansion contains a factor $\frac{1}{(2l+1)!!}$. Hence the expansion actually works better than what might be expected by simply estimating the size of $(ak)^l$.

[230]. Considering that the heavy quark may have an anomalous magnetic moment, we take g_E and g_M to denote the effective coupling constants for the electric and magnetic multipole gluon emissions (MGE), respectively.

We shall take $H^{(0)}_{\rm QCD}$ as the zeroth order Hamiltonian, and take $H^{(1)}_{\rm QCD}$ as a perturbation. This is different from the ordinary perturbation theory since $H^{(0)}_{\rm QCD}$ is not a free field Hamiltonian. The general formula for the S matrix element in this expansion has been given in Ref. [231], which is

$$\langle f|S|i\rangle = -i2\pi\delta(E_f+\omega_f-E_i)\left\langle f\left|H_2\frac{1}{E_i-H^{(0)}_{\rm QCD}+i\partial_0-H_1}\cdots\frac{1}{E_i-H^{(0)}_{\rm QCD}+i\partial_0-H_1}H_2\right|i\right\rangle, \tag{4.143}$$

where ω_f is the energy of the emitted gluons. Explicit evaluations of the S matrix elements in various cases will be presented in Section 7.2.

B. Chiral Lagrangian for heavy mesons

In the effective Lagrangian approach one can construct a heavy meson multiplet field analogous to the one introduced for heavy-light mesons. Symmetry-breaking terms can be easily added to the formalism as we shall see in the following. As in the single heavy quark case, an effective Lagrangian describing the low-momentum interactions of heavy quarkonia with light mesons can be written down. The heavy quarkonium multiplets are described by a simple trace formalism [232]. Parity P and charge conjugation C, which determine selection rules for electromagnetic and hadronic transitions are exactly conserved quantum numbers for quarkonium, together with J. If spin-dependent interactions are neglected, it is natural to describe the spin singlet $m\,^1l_J$ and the spin triplet $m\,^3l_J$ by means of a single multiplet $J(m,l)$. For the case $l=0$, when the triplet $s=1$ collapses into a single state with total angular momentum $J=1$, this is readily realized:

$$J=\frac{(1+\not{v})}{2}[H_\mu\gamma^\mu-\eta\gamma_5]\frac{(1-\not{v})}{2}\ . \tag{4.144}$$

Here v^μ denotes the four velocity associated to the multiplet J; H_μ and η are the spin 1 and spin 0 components respectively; the radial quantum number has been omitted. The expressions for the general wave $J^{\mu_1\cdots\mu_l}$ can be found in Appendix C of Ref. [233].

For illustrative purpouses let us start by considering radiative transitions, whose analysis can be easily carried out in terms of the multiplet field introduced above. The Lagrangian for radiative decays is:

$$\mathcal{L}=\sum_{m,n}\delta(m,n)\langle\overline{J}(m)\ J_\mu(n)\rangle v_\nu F^{\mu\nu}+h.c., \tag{4.145}$$

where a sum over velocities is understood, $F^{\mu\nu}$ is the electromagnetic tensor, the indices m and n represent the radial quantum numbers, $J(m)$ stands for the multiplet with radial number m and $\delta(m,n)$ is a dimensional parameter (the inverse of a mass), to be fixed from experimental data and which also depends on the heavy flavour. The Lagrangian (4.145) conserves parity and charge conjugation and is invariant under the spin transformation. It reproduces the electric dipole selection rules $\Delta\ell=\pm1$ and $\Delta s=0$. It is straightforward to obtain the corresponding radiative widths:

$$\Gamma(^3P_J\to\,^3S_1\gamma)=\frac{\delta^2}{3\pi}k^3\frac{M_{S_1}}{M_{P_J}}, \tag{4.146}$$

$$\Gamma(^3S_1\to\,^3P_J\gamma)=\frac{(2J+1)}{9\pi}\delta^2k^3\frac{M_{S_1}}{M_{P_J}}, \tag{4.147}$$

$$\Gamma(^1P_1\to\,^1S_0\gamma)=\frac{\delta^2}{3\pi}k^3\frac{M_S}{M_P}, \tag{4.148}$$

where k is the photon momentum. Once the radial numbers n and m have been fixed, the Lagrangian (4.145) describes four no spin-flip transitions with a single parameter; this allows three independent predictions. The previous decay widths can be compared with those of the electric transitions of Sec. 6.1.3 and in particular with formula (4.118). The ratio of the masses in the previous widths should be put to one in the nonrelativistic limit and the free parameter δ of the effective Lagrangian encodes the information of the overlap integral of equation (4.116).

The effective heavy-meson description of quarkonium does not seem to present special advantages to describe heavy quarkonium annihilation. In the following we shall concentrate on quarkonium hadronic transitions.

The heavy quark spin symmetry leads to general relations for the differential decay rates in hadronic transitions among quarkonium states that essentially reproduce the results of a QCD double multipole expansion for gluonic emission. Further use of chiral symmetry leads to differential pion decay distributions valid in the soft regime [234, 235]. At the lowest order in the chiral expansion for the emitted pseudoscalars we find a selection rule allowing only for even (odd) number of emitted pseudoscalars for transitions between quarkonium states of orbital angular momenta different by even (odd) units. Such a rule can be violated by higher chiral terms, by chiral breaking, and by terms breaking the heavy quark spin symmetry. Specialization to a number of hadronic transitions reproduces (by elementary tensor construction) the known results from the expansion in gluon multipoles, giving a simple explanation for the vanishing of certain coefficients, which would otherwise be allowed in the chiral expansion. In certain cases, such as for instance ${}^3P_0 \to {}^3P_2 \pi\pi$, ${}^3P_1 \to {}^3P_2 \pi\pi$, or D–S transitions via 2π, the final angular and mass distributions are uniquely predicted from heavy quark spin and the lowest-order chiral expansion.

An important class of hadronic transitions between heavy-quarkonium states is provided by the decays with emission of two pions, for example:

$$\psi' \to J/\psi \, \pi\pi \, . \tag{4.149}$$

To describe these processes one can use the chiral symmetry for the pions and the heavy-quark spin symmetry for the heavy states. The first of these is expected to hold when the pions have small energies. We notice that the velocity superselection rule applies at $q^2 = q^2_{\rm max}$, when the energy transfer to the pion is maximal. Therefore, we expect these approximations to be valid in the whole energy range only if $q^2_{\rm max}$ is small.

Nonetheless a number of interesting properties of these transitions can be derived on the basis of the heavy quark symmetry alone. Therefore, before deriving the pion couplings by means of chiral symmetry, we discuss the implications of the heavy quark spin symmetry in hadronic transitions.

As an example, we consider transitions of the type ${}^3S_1 \to {}^3S_1 + h$ and ${}^1S_0 \to {}^1S_0 + h$, where h can be light hadrons, photons, etc. By imposing the heavy quark spin symmetry, one is led to describe these processes by an interaction Lagrangian:

$$\mathcal{L}_{SS'} = \langle J' \bar{J} \rangle \Pi_{SS'} + h.c. \ , \tag{4.150}$$

where the dependence upon the pion field is contained in the as-yet-unspecified operator $\Pi_{SS'}$. It is immediate to derive from $\mathcal{L}_{SS'}$ the averaged modulus square matrix elements for the transitions ${}^3S_1 \to {}^3S_1 + h$ and ${}^1S_0 \to {}^1S_0 + h$ with an arbitrary fixed number of pions in the light final state h. We obtain:

$$|\mathcal{M}({}^3S_1 \to {}^3S_1 + h)|^2_{\rm av.} = |\mathcal{M}({}^1S_0 \to {}^1S_0 + h)|^2_{\rm av.} = 4 M_S M_{S'} |\Pi_{SS',h}|^2, \tag{4.151}$$

where M_S and M'_S are the average masses of the two S-wave multiplets; $\Pi_{SS',h}$ is the appropriate tensor for the emission of the light particles h, to be calculated from the operator $\Pi_{SS'}$. By denoting with $d\Gamma$ the generic differential decay rate, we have:

$$d\Gamma({}^3S_1 \to {}^3S_1 + h) = d\Gamma({}^1S_0 \to {}^1S_0 + h) \ . \tag{4.152}$$

This is the prototype of a series of relations, which can be derived for hadronic transitions as a consequence of the spin independence of the interaction terms. In all the known cases they coincide with those calculated in the context of a QCD double multipole expansion. We note, however, that we do not even need to specify the nature of the operator Π, which may depend on light fields different from the pseudoscalar mesons (e.g., the photon, or a light hadron, etc), provided that the interaction term we are building is invariant under parity, charge conjugation, and the other symmetries relevant to the transition considered.

A useful symmetry that can be used in processes involving light quarks is the chiral symmetry. It is possible to build up an effective Lagrangian, which allows to study transitions among quarkonium states with emissions of soft light pseudoscalars, considered as the Goldstone bosons of the spontaneously broken chiral symmetry.

The light mesons are described as pseudo-Goldstone bosons, included in the matrix $\Sigma = \xi^2$, where we use the standard notation of chiral perturbation theory. Frequently occurring quantities are the functions of ξ and its derivatives $\mathcal{A}_\mu$ and $\mathcal{V}_\mu$ given by:

$$\mathcal{V}_\mu = \frac{1}{2}\left(\xi^\dagger \partial_\mu \xi + \xi \partial_\mu \xi^\dagger\right) \qquad \text{and} \qquad \mathcal{A}_\mu = \frac{1}{2}\left(\xi^\dagger \partial_\mu \xi - \xi \partial_\mu \xi^\dagger\right). \tag{4.153}$$

The octet of vector resonances (ρ, etc.) can be introduced as the gauge multiplet associated with the hidden group SU(3)$_H$ (see Ref. [236]), designated as ρ_μ in the following.

By imposing the heavy quark spin symmetry, parity and charge conjugation invariance, and by assuming that the pseudoscalar meson coupling are described by the lowest order (at most two derivatives) chiral invariant operators, we can establish the following selection rules for hadronic transitions:

$$\begin{aligned} &\text{even number of emitted pseudoscalars} \leftrightarrow \Delta l = 0, 2, 4, ... \\ &\text{odd number of emitted pseudoscalars} \leftrightarrow \Delta l = 1, 3, 5, ... \end{aligned} \tag{4.154}$$

In fact the spin independent operator describing $\Delta l = 0, 2, 4, ...$ transitions has charge conjugation $C = +1$. On the other hand, the lowest order, chiral invariant terms with positive charge conjugation are:

$$\langle \mathcal{A}_\mu \mathcal{A}_\nu \rangle, \qquad \langle (\mathcal{V}_\mu - \rho_\mu)(\mathcal{V}_\nu - \rho_\nu) \rangle, \tag{4.155}$$

whose expansion contains an even number of pseudoscalar mesons. Spin independence of the interaction, on the other hand, requires that the $\Delta l = 1, 3, 5, ...$ transitions are described by $C = -1$ operators. At the lowest order we can form just one chiral invariant term with $C = -1$:

$$\langle \mathcal{A}_\mu (\mathcal{V}_\nu - \rho_\nu) \rangle, \tag{4.156}$$

whose expansion contains an odd number (≥ 3)of pseudoscalar mesons.

This selection rule is violated at higher orders of the chiral expansion or by allowing for terms that explicitly break the heavy quark or the chiral symmetries.

To further characterize the hadronic transitions respecting chiral symmetry, we consider below explicit expressions for the most general operators $\Pi_{ll'}$. For simplicity, we limit ourselves to those contributing to two or three pion emissions:

$$\begin{aligned} \Pi_{SS'} &= A_{SS'} \langle \mathcal{A}_\rho \mathcal{A}^\rho \rangle + B_{SS'} \langle (v \cdot \mathcal{A})^2 \rangle, \\ \Pi^\mu_{PS} &= D_{PS}\, \epsilon^{\mu\nu\rho\sigma} v_\nu \langle \mathcal{A}_\rho (\mathcal{V}_\sigma - \rho_\sigma) \rangle, \\ \Pi^{\mu\nu}_{PP'} &= A_{PP'} \langle \mathcal{A}_\rho \mathcal{A}^\rho \rangle g^{\mu\nu} + B_{PP'} \langle (v \cdot \mathcal{A})^2 \rangle g^{\mu\nu} + C_{PP'} \langle \mathcal{A}^\mu \mathcal{A}^\nu \rangle, \\ \Pi^{\mu\nu}_{DS} &= C_{DS} \langle \mathcal{A}^\mu \mathcal{A}^\nu \rangle. \end{aligned} \tag{4.157}$$

The constants $A_{ll'}$, $B_{ll'}$, $C_{ll'}$ and $D_{ll'}$ are arbitrary parameters of dimension $(\text{mass})^{-1}$, to be fixed from experiment. One can easily derive amplitudes, decay rates and distributions for the corresponding hadronic transitions.

For instance, the amplitude for the decay (4.149) is given by:

$$\mathcal{M}(^3S_1 \to {}^3S_1 + \pi\pi) = \frac{4i\sqrt{M_S M_{S'}}}{f_\pi^2}\epsilon' \cdot \epsilon^* \left(A_{SS'} p_1 \cdot p_2 + B_{SS'} v \cdot p_1 v \cdot p_2\right) \tag{4.158}$$

where ϵ and ϵ' are the polarisation vectors of quarkonium states; p_1, p_2 are the momenta of the two pions. It is well known that the use of chiral symmetry arguments leads to a general amplitude for the process in question, which contains a third independent term given by:

$$C_{SS'} \frac{4i\sqrt{M_S M_{S'}}}{f_\pi^2} \left(\epsilon' \cdot p_1 \epsilon^* \cdot p_2 + \epsilon' \cdot p_2 \epsilon^* \cdot p_1\right) \quad . \tag{4.159}$$

In the nonrelativistic limit in QCDME, Yan [230] finds $C_{SS'} = 0$. It is interesting to note that, within the present formalism, this result is an immediate consequence of the chiral and heavy quark spin symmetries. However, these symmetries are not exact and corrections to the symmetry limit are expected.

In the chiral Lagrangian (CL) approach, the $\pi^0 - \eta - \eta'$ mixings can be derived, which should be taken into account in predicting single pseudoscalar meson transitions of heavy quarkonia (cf. Section 7.2). Let us define

$$\hat{m} \equiv \begin{pmatrix} m_u & 0 & 0 \\ 0 & m_d & 0 \\ 0 & 0 & m_s \end{pmatrix}. \tag{4.160}$$

The Lagrangian that gives mass to the pseudoscalar octet (massless in the chiral limit) and causes $\pi^0 - \eta$ mixing is

$$\mathcal{L}_m = \lambda_0 \langle \hat{m}(\Sigma + \Sigma^\dagger)\rangle, \tag{4.161}$$

and that giving rise to the mixing of η' with π^0 and η is

$$\mathcal{L}_{\eta\eta'} = \frac{if_\pi}{4}\tilde{\lambda}\langle \hat{m}(\Sigma - \Sigma^\dagger)\rangle \eta', \tag{4.162}$$

where $\hat{\lambda}$ is a parameter with the dimension of a mass. At first order in the mixing angles the physical states $\tilde{\pi}^0$, $\tilde{\eta}$, and $\tilde{\eta}'$ determined from the above Lagrangians are:

$$\tilde{\pi}^0 = \pi^0 + \epsilon\eta + \epsilon'\eta', \qquad \tilde{\eta} = \eta - \epsilon\pi^0 + \theta\eta', \qquad \tilde{\eta}' = \eta' - \theta\eta - \epsilon'\pi^0, \tag{4.163}$$

in which the mixing angles are

$$\epsilon = \frac{(m_d - m_u)\sqrt{3}}{4(m_s - \dfrac{m_u + m_d}{2})}, \qquad \epsilon' = \frac{\tilde{\lambda}(m_d - m_u)}{\sqrt{2}(m_{\eta'}^2 - m_{\pi^0}^2)}, \quad \theta = \sqrt{\frac{2}{3}}\ \frac{\tilde{\lambda}\left(m_s - \dfrac{m_u + m_d}{2}\right)}{m_{\eta'}^2 - m_\eta^2}. \tag{4.164}$$

7.2 Predictions for hadronic transitions in the single-channel approach

In this section, we give the predictions for HTs in the single-channel approach. In this approach, the amplitude of HT is diagrammatically shown in Fig. 4.13 in which there are two complicated vertices: namely, the MGE vertex of the heavy quarks and the vertex of hadronization (H) describing the conversion of the emitted gluons into light hadrons. In the following, we shall treat them separately.

Let us first consider the HT processes $n_i^3S_1 \to n_f^3S_1 + \pi + \pi$. To lowest order, these are double electric-dipole transitions (E1E1). The transition amplitude can be obtained from the S matrix element (4.143). After some algebra, we obtain [230, 231, 237]

$$\mathcal{M}_{E1E1} = i\frac{g_E^2}{6} \sum_{KLK'L'} \langle \Phi_f h|\boldsymbol{x}\cdot\boldsymbol{E}|KL\rangle \left\langle KL\left|\frac{1}{E_i - H_{\rm QCD}^{(0)} - iD_0}\right|K'L'\right\rangle \langle K'L'|\boldsymbol{x}\cdot\boldsymbol{E}|\Phi_i\rangle, \tag{4.165}$$

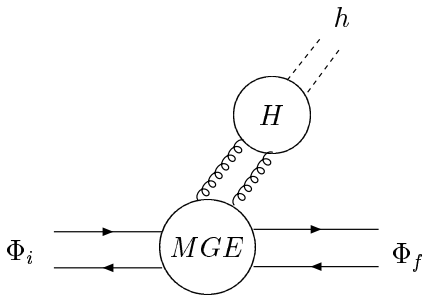

Fig. 4.13: Diagram for a typical hadronic transition in the single-channel QCDME approach.

where $(D_0)_{bc} \equiv \delta_{bc}\partial_0 - g_s f_{abc} A^a_0$, and $|KL\rangle$ is the intermediate state with principal quantum number K and orbital angular momentum L. According to the angular momentum selection rule, $L = L' = 1$. The intermediate states in the HT are the states after the emission of the first gluon and before the emission of the second gluon (cf. Fig. 4.13), i.e., they are states with a gluon and a colour-octet $Q\bar{Q}$. These are the so-called hybrid states. It is difficult to calculate these states from the first principles of QCD. So we shall take a reasonable model for it. The model should *reasonably reflect the main properties of the hybrid states* and should *contain as few free parameters as possible* in order not to affect the predictive power of the theory. The quark confining string (QCS) model [238] satisfies these requirements [16] Explicit calculations with the QCS are given in Ref. [237]; the transition amplitude (4.165) then becomes

$$\mathcal{M}_{E1E1} = i\frac{g_E^2}{6}\sum_{KL}\frac{\langle\Phi_f|x_k|KL\rangle\langle KL|x_l|\Phi_i\rangle}{E_i - E_{KL}}\langle\pi\pi|E^a_k E^a_l|0\rangle, \tag{4.166}$$

We see that, in this approach, the transition amplitude contains two factors: namely, the heavy quark MGE factor (the summation) and the H factor $\langle\pi\pi|E^a_k E^a_l|0\rangle$. The first factor can be calculated for a given potential model. Let us now consider the second factor. Its scale is the light hadron mass scale, which is very low (highly nonperturbative), and there is, therefore, no currently reliable way of calculating it from the first principles of QCD. Thus we take a phenomenological approach based on PCAC and the soft pion technique in Ref. [240]. From the standard tensor reduction, this H factor can be written as [237]

$$\frac{g_E^2}{6}\langle\pi_\alpha(q_1)\pi_\beta(q_2)|E^a_k E^a_l|0\rangle = \frac{\delta_{\alpha\beta}}{\sqrt{(2\omega_1)(2\omega_2)}}\left[C_1\delta_{kl}q_1^\mu q_{2\mu} + C_2\left(q_{1k}q_{2l} + q_{1l}q_{2k} - \frac{2}{3}\delta_{kl}\boldsymbol{q}_1\cdot\boldsymbol{q}_2\right)\right], \tag{4.167}$$

where C_1 and C_2 are two unknown constants. For a given $\pi\pi$ invariant mass $M_{\pi\pi}$, the C_1 term is isotropic (S-wave), while the C_2 term is angular dependent (D-wave). In the nonrelativistic single-channel (NRSC) approach, orbital angular momentum conservation leads to the conclusion that the MGE factor is proportional to δ_{kl}. Thus only the C_1 term contributes to the S-state to S-state transitions[17]. In this case, the $n_i^3S_1 \to n_f^3S_1 + \pi + \pi$ transition rate can be expressed as [237]

$$\Gamma(n_i^3S_1 \to n_f^3S_1\ \pi\ \pi) = |C_1|^2 G |f^{111}_{2010}|^2, \tag{4.168}$$

where G is a phase-space factor given in Ref. [237] and

$$f^{LP_iP_f}_{n_il_in_fl_f} \equiv \sum_K \frac{\int R_f(r)r^{P_f}R^*_{KL}(r)r^2dr \int R^*_{KL}(r')r'^{P_i}R_i(r')r'^2dr'}{M_i - E_{KL}}, \tag{4.169}$$

[16] Another possible model satisfying the requirements is the MIT bag model for the hybrid states, which can also lead to reasonable predictions [239].

[17] This is consistent with the CL approach in the nonrelativistic limit ($v = 0$) [cf. (4.158)].

Table 4.28: The values of $|C_1|^2$ and the predicted $\pi\pi$ transition rates (in keV) determined for the Υ system using the Cornell model and the BGT model. The corresponding updated experimental values of the transition rates [10] are also listed for comparison. $\pi\pi$ stands for the sum over all the $\pi^+\pi^-$ and $\pi^0\pi^0$ channels.

	Cornell	BGT	Expt.
$\|C_1\|^2$	83.4×10^{-6}	67.8×10^{-6}	
$\Gamma(\Upsilon'\to\Upsilon\pi\pi)$ (keV)	8.6	7.8	12.0 ± 1.8
$\Gamma(\Upsilon''\to\Upsilon\pi\pi)$ (keV)	0.44	1.2	1.72 ± 0.35
$\Gamma(\Upsilon''\to\Upsilon'\pi\pi)$ (keV)	0.78	0.53	1.26 ± 0.40

with R_i, R_f, and R_{KL} the radial wave functions of the initial, final, and intermediate states, respectively.

There is only one overall unknown constant C_1 left in this transition amplitude, which can be determined by taking the well-measured HT rate $\Gamma(\psi'\to J/\psi\pi\pi)$. The updated experimental values are [10]

$$\Gamma_{\rm tot}(\psi') = 281 \pm 17 \text{ keV}, \;\; \mathcal{B}(\psi'\to J/\psi\pi^+\pi^-) = (31.7 \pm 1.1)\%, \;\; \mathcal{B}(\psi'\to J/\psi\pi^0\pi^0) = (18.8 \pm 1.2)\%. \tag{4.170}$$

Given these, we can then predict all the S-state to S-state $\pi\pi$ transitions rates in the Υ system. Let us take the Cornell [177, 191] and the Buchmüller–Grunberg–Tye (BGT) [141, 193] potential models as examples to show the extracted $|C_1|$ values and the predicted rates in the Υ system. The results are listed in Table 4.28[18] in which the experimental errors are dominated by the uncertainty of the total width. We see that the BGT model predicted ratios $\Gamma(\Upsilon''\to\Upsilon\pi\pi)/\Gamma(\Upsilon'\to\Upsilon\pi\pi) \approx 1.2/7.8 = 0.15$ and $\Gamma(\Upsilon''\to\Upsilon'\pi\pi)/\Gamma(\Upsilon'\to\Upsilon\pi\pi) \approx 0.53/7.8 = 0.07$ are close to the corresponding experimental values 1.72/12.0=0.14 and 1.26/12.0=0.11. However, the predicted absolute partial widths are smaller than the experimental values by roughly a factor of 50–75%. Moreover, when the $M_{\pi\pi}$ distributions are considered, the situation will be more complicated. We shall deal with these issues in Section 7.3.

Note that the phase space factor G in $\Upsilon''\to\Upsilon\pi\pi$ is much larger than that in $\Upsilon'\to\Upsilon\pi\pi$, $G(\Upsilon''\to\Upsilon\pi\pi)/\, G(\Upsilon'\to\Upsilon\pi\pi) = 33$ [237]. One may naively expect that $\Gamma(\Upsilon''\to\Upsilon\pi\pi) > \Gamma(\Upsilon'\to\Upsilon\pi\pi)$. However, we see from Table 4.28 that the measured $\Gamma(\Upsilon''\to\Upsilon\pi\pi)/\Gamma(\Upsilon'\to\Upsilon\pi\pi) \approx 0.14$. The reason why the predicted ratio is close to the experimental value is that the contributions from various intermediate states to the overlap integrals in the summation in f^{111}_{3010} [cf. (4.169)] *drastically cancel* each other due to the fact that the Υ'' wave function contains two nodes. This is *characteristic* of such intermediate state models (QCS or bag model).

The decays $n_i^3S_1\to n_f^3S_1 + \eta$ are dominated by E1M2 transitions. We can predict the ratios $R' \equiv \Gamma(\Upsilon'\to\Upsilon\eta)/\Gamma(\psi'\to J/\psi\eta)$ and $R'' \equiv \Gamma(\Upsilon''\to\Upsilon\eta)/\Gamma(\psi'\to J/\psi\eta)$:

$$R' = \frac{\left(\left|\frac{f^{111}_{2010}(b\bar{b})}{m_b}\right|^2 |\mathbf{q}(b\bar{b})|^3\right)}{\left(\left|\frac{f^{111}_{2010}(c\bar{c})}{m_c}\right|^2 |\mathbf{q}(c\bar{c})|^3\right)}, \qquad R'' = \frac{\left(\left|\frac{f^{111}_{3010}(b\bar{b})}{m_b}\right|^2 |\mathbf{q}(b\bar{b})|^3\right)}{\left(\left|\frac{f^{111}_{2010}(c\bar{c})}{m_c}\right|^2 |\mathbf{q}(c\bar{c})|^3\right)}, \tag{4.171}$$

where $\boldsymbol{q}$ is the momentum of η. The BGT model predicts $R' = 0.0025, \;\; R'' = 0.0013$. Recently BES has obtained an accurate measurement of $\Gamma(\psi'\to J/\psi\eta)$ and $\Gamma(\psi'\to J/\psi\ \pi^0)$ [241] (see Section 7.6A). With the new BES data and the bounds on $\Gamma(\Upsilon'\to\Upsilon\eta)$ and $\Gamma(\Upsilon''\to\Upsilon\eta)$ [10], the experimental bounds are $R'|_{\rm exp} < 0.0098, \;\; R''|_{\rm exp} < 0.0065$ [241]. The predictions are consistent with these bounds.

[18] The updated results listed in Table reftab:c1ht are roughly larger than those in Ref. [237] by a factor of 1.3 since the updated input data $\Gamma(\psi'\to J/\psi\pi\pi)$ is larger than the old experimental value used in Ref. [237] by the same factor of 1.3.

An interesting prediction in the CL approach is the prediction for the ratio

$$R = \frac{\Gamma(\psi' \to J/\psi\ \pi^0)}{\Gamma(\psi' \to J/\psi\ \eta)}, \tag{4.172}$$

which provides a measure of the light-quark mass ratio $r = (m_d - m_u)/(m_s - (m_u + m_d)/2)$. This belongs to the class of hadronic transitions, which violate heavy quark spin symmetry (HQSS) [235]. For heavy mesons, there are only two types of operators that break HQSS. In the parent's rest frame, the most general spin symmetry breaking term is of the form $\mathbf{a} \cdot \boldsymbol{\sigma}$, where $\boldsymbol{\sigma}$ are the Pauli matrices. In an arbitrary frame one observes that any Γ-matrix sandwiched between two projectors $(1 + \not{v})/2$, or $(1 - \not{v})/2$ can be expressed in terms of $\sigma_{\mu\nu}$ sandwiched between the same projectors:

$$\frac{1+\not{v}}{2} 1 \frac{1+\not{v}}{2} = \frac{1+\not{v}}{2}, \qquad \frac{1+\not{v}}{2}\gamma_5\frac{1+\not{v}}{2} = 0, \qquad \frac{1+\not{v}}{2}\gamma_\mu\frac{1+\not{v}}{2} = v_\mu\frac{1+\not{v}}{2},$$

$$\frac{1+\not{v}}{2}\gamma_\mu\gamma_5\frac{1+\not{v}}{2} = \frac{1}{2}\epsilon_{\mu\nu\alpha\beta}v^\nu\frac{1+\not{v}}{2}\sigma^{\alpha\beta}\frac{1+\not{v}}{2}, \; \frac{1+\not{v}}{2}\gamma_5\sigma_{\mu\nu}\frac{1+\not{v}}{2} = -\frac{i}{2}\epsilon_{\mu\nu\alpha\beta}\frac{1+\not{v}}{2}\sigma^{\alpha\beta}\frac{1+\not{v}}{2};$$

there are analogous relations with $(1 + \not{v})/2 \to (1 - \not{v})/2$. We use here $\epsilon_{0123} = +1$. Let us define

$$\sigma^{(\pm)}_{\mu\nu} = \frac{1 \pm \not{v}}{2}\sigma_{\mu\nu}\frac{1 \pm \not{v}}{2}\ . \tag{4.173}$$

In the parent's rest frame, $\sigma^{(\pm)}_{\mu\nu}$ reduce to Pauli matrices. From the previous identities it follows that the most general spin symmetry breaking terms are of the form $G_1^{\mu\nu}\sigma^{(+)}_{\mu\nu}$, or $G_2^{\mu\nu}\sigma^{(-)}_{\mu\nu}$, with $G_i^{\mu\nu}$ two arbitrary antisymmetric tensors. One expects that any insertion of the operator $\sigma^{(\pm)}_{\mu\nu}$ gives a suppression factor $1/m_Q$.

Using partial conservation of axial-vector current, Ioffe and Shifman [242] give the prediction

$$R = \frac{27}{16}\left[\frac{\mathbf{p}_\pi}{\mathbf{p}_\eta}\right]^3\left[\frac{m_d - m_u}{m_s - (m_u + m_d)/2}\right]^2. \tag{4.174}$$

The new BES experiment (see Section 7.6A) [241] provides a new precision value of R. With the conventional values of the current quark masses, the prediction of (4.174) is smaller than the BES value by about a factor of 3 [241]. So (4.174) should be regarded as an order of magnitude estimate.

The calculation of R in the CL approach is straightforward. The most general spin breaking Lagrangian for the processes $\psi' \to J/\psi\pi^0, \eta$ is

$$\mathcal{L} = i\epsilon_{\mu\nu\rho\lambda}\left[\langle J'\sigma^{\mu\nu}\bar{J}\rangle - \langle\bar{J}\sigma^{\mu\nu}J'\rangle\right]v^\rho\,\partial^\lambda\left[\frac{iA}{4}\langle\hat{m}(\Sigma - \Sigma^\dagger)\rangle + B\eta'\right] + h.c.\,. \tag{4.175}$$

The couplings A and B have dimension $(\text{mass})^{-1}$; the B term contributes to the ratio (4.172) via the mixing $\pi^0 - \eta'$ and $\eta - \eta'$. There are no terms with the insertion of two σ terms; the two P and C conserving candidates $\epsilon_{\mu\nu\rho\lambda}\left[\langle J'\sigma^{\mu\tau}\bar{J}\sigma_\tau{}^\nu\rangle + \langle\bar{J}\sigma^{\mu\tau}J'\sigma_\tau{}^\nu\rangle\right]v^\rho\partial^\lambda\langle\hat{m}(\Sigma - \Sigma^\dagger)\rangle$ and $\epsilon_{\mu\nu\rho\lambda}\left[\langle J'\sigma^{\mu\nu}\bar{J}\sigma^{\rho\lambda}\rangle + \langle\bar{J}\sigma^{\mu\nu}J'\sigma^{\rho\lambda}\rangle\right]\langle\hat{m}(\Sigma - \Sigma^\dagger)\rangle$ both vanish.

Using the Lagrangian (4.175) and taking into account the mixings (4.163) and (4.164), we can calculate the ratio (4.172)

$$R = \frac{27}{16}\left[\frac{\mathbf{p}_\pi}{\mathbf{p}_\eta}\right]^3\left[\frac{m_d - m_u}{m_s - (m_u + m_d)/2}\right]^2\left[\frac{1 + \dfrac{2B}{3A}\dfrac{\hat{\lambda}f_\pi}{m^2_{\eta'} - m^2_{\pi^0}}}{1 + \dfrac{B}{A}\dfrac{\hat{\lambda}f_\pi}{m^2_{\eta'} - m^2_\eta}}\right]^2\ . \tag{4.176}$$

If we neglect the $\pi^0-\eta'$ and $\eta-\eta'$ mixings, (4.176) reduces to the simple result (4.174). So far B/A in (4.176) is not determined yet. Taking the $\eta-\eta'$ mixing angle $\theta_P\approx -20^\circ$ [10] and using the new BES data on R [241], one can determine B/A from (4.176): $B/A=-1.42\pm 0.12$ or -3.11 ± 0.15 [241].

The $\pi\pi$ transitions between P-wave quarkonia, $2^3P_{J_i}\to 1^3P_{J_f}+\pi+\pi$, have been studied in Ref. [237]. The obtained transition rates $\Gamma(2^3P_{J_i}\to 1^3P_{J_f}\pi\pi)$ are of the order of 10^{-1}–10^{-2} keV [237]. The relations between different $\Gamma(2^3P_{J_i}\to 1^3P_{J_f}\pi\pi)$ reflect the symmetry in the E1E1 multipole expansion [230], so that experimental tests of these relations are of special interest.

In the CL approach, the single pseudoscalar meson transitions between heavy quarkonia states such as

$$^3P_{J'}\to\ ^3P_J\pi^0\ \text{ and }\ ^3P_J\eta \tag{4.177}$$

are chiral-breaking but spin conserving [235], which are important for transitions forbidden in the SU(3) $\times$ SU(3) symmetry limit.

To first order in the chiral breaking mass matrix we consider the quantities:

$$\langle\hat{m}(\Sigma+\Sigma^\dagger)\rangle\ \text{ and }\ \langle\hat{m}(\Sigma-\Sigma^\dagger)\rangle. \tag{4.178}$$

The first quantity is parity even, while the second is parity odd; both have $C=+1$.

The only term spin-conserving and of leading order in the current quark masses contributing to the transition (4.177) is

$$\langle J_\mu\bar{J}_\nu\rangle v_\rho\epsilon^{\mu\nu\rho\sigma}\partial_\sigma\left[\alpha\frac{if_\pi}{4}\langle\hat{m}(\Sigma-\Sigma^\dagger)\rangle+\beta f_\pi\eta'\right], \tag{4.179}$$

where α and β are coupling constants of dimensions $(\text{mass})^{-2}$. The direct coupling to η' contributes through the mixing (4.163). The spin symmetry of the heavy sector gives relations among the modulus square matrix elements of the transitions between the two P-wave states. In particular we find that

$$|\mathcal{M}|^2(^3P_0\to^3P_0\pi)=|\mathcal{M}|^2(^3P_2\to^3P_0\pi)=0, \tag{4.180}$$

and that all non-vanishing matrix elements can be expressed in terms of $^3P_0\to^3P_1\pi$:

$$\begin{aligned}
&|\mathcal{M}|^2(^3P_1\to^3P_1\pi)=\frac{1}{4}|\mathcal{M}|^2(^3P_0\to^3P_1\pi), \qquad |\mathcal{M}|^2(^3P_1\to^3P_2\pi)=\frac{5}{12}|\mathcal{M}|^2(^3P_0\to^3P_1\pi),\\
&|\mathcal{M}|^2(^3P_2\to^3P_2\pi)=\frac{3}{4}|\mathcal{M}|^2(^3P_0\to^3P_1\pi), \qquad |\mathcal{M}|^2(^1P_1\to^1P_1\pi)=|\mathcal{M}|^2(^3P_0\to^3P_1\pi),
\end{aligned} \tag{4.181}$$

where π stays for π^0 or η. The relations (4.181) can be generalized for any spin-conserving transition between $l=1$ multiplets, leading to the same results as the QCD double multipole expansion [230]. Predictions for widths can be easily obtained from (4.179).

Now we consider the $\pi\pi$ transitions of D-wave quarkonia. Theoretical studies of HTs of D-wave quarkonia have been carried out by several authors in different approaches leading to quite different predictions [237,243–248]. We briefly review the approach in Refs. [247,248], and compare the predictions with recent experimental results.

Since the $\psi(3770)$ (or ψ'') lies above the $D\bar{D}$ threshold, it is believed that it decays mainly into $D\bar{D}$ [10]. Experimental observations show that the directly measured $e^+e^-\to\psi(3770)$ cross-section and the $e^+e^-\to\psi(3770)\to D\bar{D}$ cross-section are different [249], suggesting considerable non-$D\bar{D}$ decay modes of $\psi(3770)$. $\psi(3770)\to J/\psi\ \pi\pi$ is one possibility.

If $\psi(3770)$ is regarded as a pure $1D$ state, the predicted leptonic width will be smaller than the experimental value by an order of magnitude. The $\psi(3770)$ is often regarded as a mixture of the $1D$ and $2S$ states [247,248,250]: $\psi'=|2S\rangle\cos\theta+|1D\rangle\sin\theta$, $\psi(3770)=-|2S\rangle\sin\theta+|1D\rangle\cos\theta$. θ can be determined by fitting the ratio of the leptonic widths of ψ' and $\psi(3770)$. The determination of θ in

the Cornell potential model [177, 191] and the improved QCD motivated potential model by Chen and Kuang (CK) [251] (which leads to more successful phenomenological results) are: $\theta = -10^\circ$ (Cornell) and $\theta = -12^\circ$ (CK).

The rate of this E1E1 transition is [247]

$$\Gamma(\psi(3770)\to J/\psi\pi\pi) = |C_1|^2\left[\sin^2\theta\, G(\psi')\,|f^{111}_{2010}(\psi')|^2 + \frac{4}{15}\left|\frac{C_2}{C_1}\right|^2\cos^2\theta\, H(\psi'')\,|f^{111}_{1210}(\psi'')|^2\right]. \tag{4.182}$$

Since there is no available data to determine C_2, we take an approximation to estimate C_2. In Ref. [237], it is assumed that $\langle\pi\pi|E^a_k E^a_l|0\rangle \propto \langle gg|E^a_k E^a_l|0\rangle$, i.e., that the factor describing the conversion of the two gluons into $\pi\pi$ is approximately independent of the pion momenta in the HTs under consideration. In this approximation, we obtain [237]

$$C_2 \approx 3C_1. \tag{4.183}$$

So it is possible that $C_2/C_1 \sim \mathcal{O}(1)$.

Table 4.29: The predicted transition rate $\Gamma(\psi(3770)\to J/\psi\ \pi^+\pi^-)$ (in keV) in the Cornell model and the CK model with the updated input data (4.170). The corresponding branching ratios are listed in the brackets using the total width of $\psi(3770)$ given in Ref. [10].

	$\Gamma(\psi(3770)\to J/\psi\pi^+\pi^-)$ (keV)	
	Cornell	CK
$C_2 \approx 3C_1$	139 $[(0.59 \pm 0.07)\%]$	147 $[(0.62 \pm 0.07)\%]$
$C_2 \approx C_1$	26 $[(0.11 \pm 0.01)\%]$	32 $[(0.14 \pm 0.02)\%]$

For comparison, we list the predicted rate $\Gamma(\psi(3770)\to J/\psi\ \pi^+\pi^-)$ with $C_2/C_1 = 3$ and $C_2/C_1 = 1$ in Table 4.29.[19] Note that S–D mixing only affects a few percent of the rate, so that the rate is essentially $\Gamma(\psi(2D)\to J/\psi\ \pi^+\pi^-)$.

Recently, BES has measured the rate $\Gamma(\psi(3770)\to J/\psi + \pi^+ + \pi^-)$ based on 27.7 pb^{-1} data of $\psi(3770)$. The result is $\Gamma(\psi(3770)\to J/\psi + \pi^+ + \pi^-) = 80 \pm 32 \pm 21$ keV [252] (see Eq. (4.191) in Section 7.6C). Equation (4.182) is in agreement with the central value of the BES result with $C_2/C_1 \approx 2$. Considering the large error in the BES experiment, C_2/C_1 can still be in the range $0.8 \le C_2/C_1 \le 2.8$. We expect more precise future measurements to give a better determination of C_2/C_1.

For the Υ system, the state mixings are much smaller [253]. Neglecting such mixings, the predicted rate of $\Upsilon(1^3D_1)\to\Upsilon\pi\pi$ in the Cornell model with $C_2/C_1 = 3$ was $\Gamma(\Upsilon(1^3D_1)\to\Upsilon\pi\pi) \approx 24$ keV [237]. Taking the central value $C_2/C_1 \approx 2$ determined from BES data, the prediction is $\Gamma(\Upsilon(1^3D_1)\to\Upsilon\pi\pi) \approx 11$ keV. Considering the above range of C_2/C_1, we predict 1.8 keV $\le \Gamma(\Upsilon(1^3D_1) \to \Upsilon\pi\pi) \le 21$ keV.

HTs are useful processes to investigate the h_c [or $\psi(1^1P_1)$] and h_b [or $\Upsilon(1^1P_1)$] states. h_c and h_b are of special interest since the difference between the mass of the 1^1P_1 state and the centre-of-gravity of the 1^3P_J states gives useful information about the spin-dependent interactions between Q and $\bar{Q}$. The possibilities to detect h_c and h_b at e^+e^- colliders, in $^3S_1\to\pi^0\,^1P_1$, $^1P_1\to\pi\pi\,^3S_1$, and $^1P_1\to\pi^0\,^3S_1$ transitions have been studied in Refs. [229, 237, 248, 255, 256]; h_c could also be detected at the B factories [257], depending on the value for the $B\to h_c\,K$ branching ratio. So far, the h_b has not been experimentally found, while the h_c has probably been observed, based on recent preliminary results presented by CLEO [258] and E835 [259]. CLEO has observed significant excess of events in $\psi(2S)\to\pi^0 h_c\to\pi^0\gamma\eta_c$, in both exclusive and inclusive η_c decays. E835 has a significant excess of events

[19] The values listed in Table 4.29 are larger than those given in Refs. [247, 248] since the updated input data values are larger.

in $\bar{p}p \to h_c \to \eta_c\gamma \to 3\gamma$. The mass of the CLEO and E835 candidates are compatible, and very close to the centre-of-gravity. For more details we refer to Chapter 3.

7.3 Nonrelativistic coupled-channel approach to hadronic transitions

Since a heavy quarkonium Φ lying above the threshold can decay into a pair of heavy flavour mesons $\mathcal{D}\bar{\mathcal{D}}$ [$\mathcal{D}$ stands for D mesons (for $c\bar{c}$) and B mesons (for $b\bar{b}$)], there must exist Φ–$\mathcal{D}$–$\bar{\mathcal{D}}$ couplings as shown in Fig. 4.14.

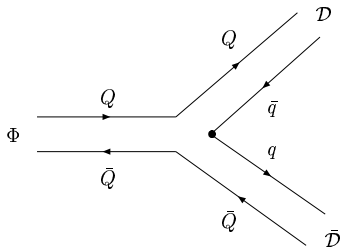

Fig. 4.14: Coupling of the heavy quarkonium Φ to its decay channel $\mathcal{D}\bar{\mathcal{D}}$.

A complete theory should include not only the part describing Φ, but also the part corresponding to the $\mathcal{D}\bar{\mathcal{D}}$ sector as well. Such a theory is the so-called coupled-channel (CC) theory.

It is hard to study the Φ–$\mathcal{D}$–$\bar{\mathcal{D}}$ vertex from the first principles of QCD, since it is the vertex of three bound states. There are various models describing CC effects; the two well-accepted models are the Cornell CC model (CCCM) [177, 191, 260] and the unitary quark model (UQM) [253]. The Φ–$\mathcal{D}$–$\bar{\mathcal{D}}$ vertex in the UQM is taken to be the $^3P_0$ quark-pair-creation (QPC) mechanism [261]. The parameters in the UQM are carefully adjusted so that the model gives a better fit to the $c\bar{c}$ and $b\bar{b}$ spectra, leptonic widths, etc. It is shown that the QPC model gives acceptable results even for OZI-allowed productions of light mesons [261, 262], which is relevant in the calculation of the HT amplitudes in the CC theory.

The formulation of the theory of HTs in the framework of the UQM was given in Ref. [263]. The Feynman diagrams for $n_i^3S_1 \to n_f^3S_1\pi\pi$ are shown in Fig. 4.15. We see that there are more channels of $\pi\pi$ transitions in this theory than in the single-channel theory. Figures 4.15(a)–4.15(d) are based on the QCDME mechanism; we designate this the MGE part. Figures 4.15(e) and 4.15(f) are based on a new $\pi\pi$ transition mechanism via QPC; we designate this the QPC part. Figure 4.15(a) is similar to Fig. 4.13 but with state mixings, so the single-channel amplitude mentioned in Section 7.2 is only a part of Fig. 4.15(a).

Table 4.30: $\Gamma(\Upsilon' \to \Upsilon\pi\pi)$, $\Gamma(\Upsilon'' \to \Upsilon\pi\pi)$, and $\Gamma(\Upsilon'' \to \Upsilon'\pi\pi)$ predicted in CC theory, with $\cos\vartheta = -1$ and -0.676, together with the updated experimental values [10]. $\pi\pi$ stands for the sum over all the $\pi^+\pi^-$ and $\pi^0\pi^0$ channels.

	Theory		Expt.
	$\cos\vartheta = -1$	$\cos\vartheta = -0.676$	
$\Gamma(\Upsilon' \to \Upsilon\pi\pi)$ (keV)	14	13	12.0 ± 1.8
$\Gamma(\Upsilon'' \to \Upsilon\pi\pi)$ (keV)	1.1	1.0	1.72 ± 0.35
$\Gamma(\Upsilon'' \to \Upsilon'\pi\pi)$ (keV)	0.1	0.3	1.26 ± 0.40

Since state mixings and the QPC vertices are all different in the $c\bar{c}$ and the $b\bar{b}$ systems, the predictions for theΥ HT rates by taking the input (4.170) will be different from those in the single-channel

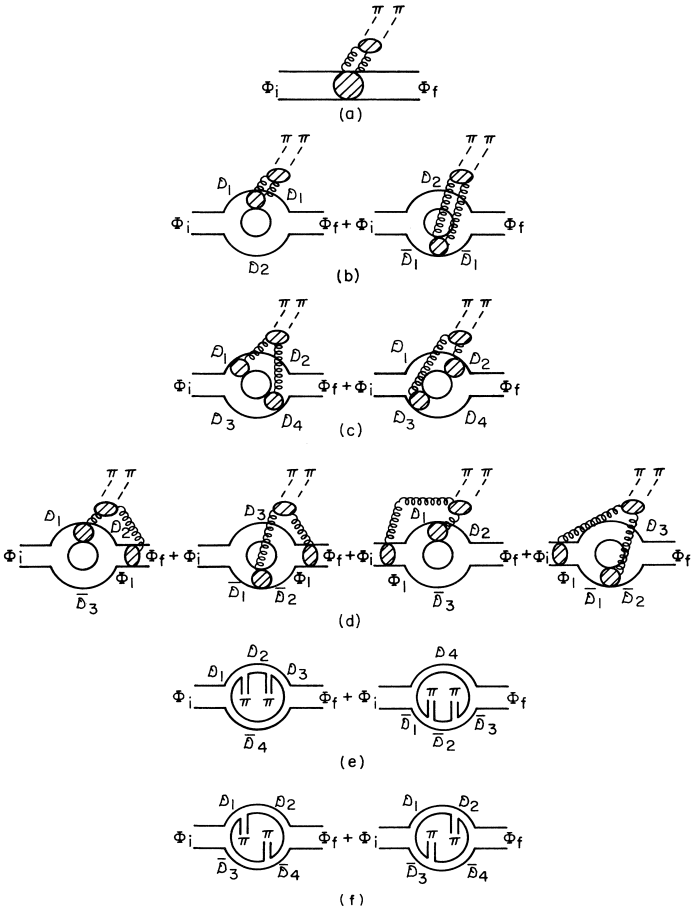

Fig. 4.15: Diagrams for hadronic transitions in the CC approach. Quoted from Ref. [263].

theory. Such predictions were studied in Ref. [263]. Note that for a given QPC model, the QPC part is fixed, while the MGE part still contains an unknown parameter C_1 after taking the approximation $C_2 \approx 3C_1$. Since there is interference between the MGE and the QPC parts, the phase of C_1 is important; explicitly, $C_1 = |C_1|\, e^{i\vartheta}$. The data of the HT rate and $M_{\pi\pi}$ distribution in $\psi' \to J/\psi\, \pi\pi$ can be taken as inputs to determine C_1 and ϑ [263]. Considering the error bars in the $M_{\pi\pi}$ distribution, ϑ is restricted in the range $-1 \leq \cos\vartheta \leq -0.676$ [263]. The predicted transition rates in the Υ system are listed in Table 4.30 together with the experimental results for comparison. We see that the obtained $\Gamma(\Upsilon' \to \Upsilon\pi\pi)$ is in good agreement with the experiment, and the results of $\Gamma(\Upsilon'' \to \Upsilon\pi\pi)$ and $\Gamma(\Upsilon'' \to \Upsilon'\pi\pi)$ are in agreement with the experiment at the level of 2σ and 2.4σ, respectively.

Next we look at the predicted $M_{\pi\pi}$ distributions. It is pointed out in Ref. [265] that there is a tiny difference between the measured $M_{\pi\pi}$ distributions in $\psi' \to J/\psi\pi\pi$ and $\Upsilon' \to \Upsilon\pi\pi$. In the single-channel theory, the formulas for these two $M_{\pi\pi}$ distributions are the same. In the CC theory, once C_1 and ϑ are determined, the $M_{\pi\pi}$ distribution of $\Upsilon' \to \Upsilon\pi\pi$ is uniquely determined. It is shown in Ref. [263] that the prediction fits the experiment [265] very well

However, the situation of the $M_{\pi\pi}$ distributions of $\Upsilon'' \to \Upsilon\pi^+\pi^-$ and $\Upsilon'' \to \Upsilon'\pi^+\pi^-$ are more complicated. Comparison of the CC predictions with the CLEO experiment will be shown in Section 7.5E.

7.4 Application of the QCD multipole expansion to radiative decays of the J/ψ

In the above sections, QCDME is applied to various HTs in which Φ_i and Φ_f are composed of the same heavy quarks. In this case, the dressed (constituent) quark field $\Psi(\mathbf{x},t)$ needs not actually to be quantized. Now we generalize QCDME theory to processes including changes of heavy quark flavour and heavy quark pair annihilation or creation, for which the quantization of $\Psi(\mathbf{x},t)$ is needed. This has been studied in Ref. [231] with the electroweak interactions included as well.

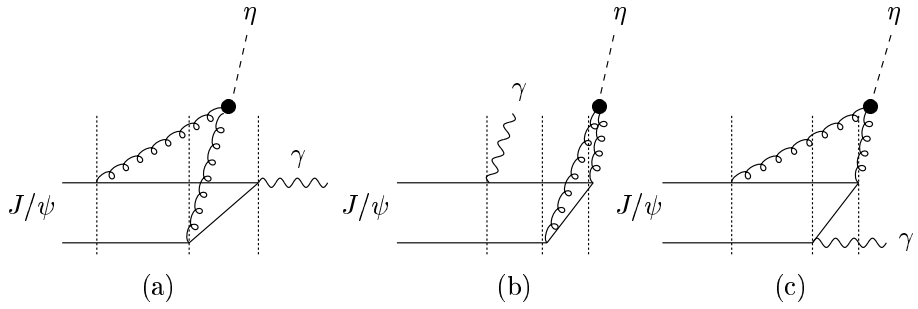

Fig. 4.16: Feynman diagrams for the radiative decay process $J/\psi\to\gamma+\eta$.

An example of application of such a theory is $J/\psi\to\gamma\eta$ (see Section 5.5 for a discussion in the framework of Ref. [154]). This process has been studied in the framework of perturbative QCD and the nonrelativistic quark model in Ref. [264], but the predicted rate is significantly smaller than the experimental value. The η momentum in this process is $q_\eta = 1.5$ Gev. If η is converted from two emitted gluons from the heavy quark, the typical gluon momentum is then $k \sim q_\eta/2 \sim 750$ MeV. At this momentum scale perturbative QCD does not work well but QCDME works [231]. The Feynman diagrams for this process in the QCDME approach are shown in Fig. 4.16, in which the intermediate states marked between two vertical dotted lines are all treated as bound states. In this sense this approach is nonperturbative.

Since this process is dominated by E1M2 transition; the transition rate depends on the pseudoscalar nonet mixing angle θ_P. Taking the value $\theta_P \approx -20^\circ$ determined from the $\eta\to\gamma\gamma$ and $\eta'\to\gamma\gamma$ rates [10], we obtain [231]

$$\Gamma(J/\psi\to\gamma\eta) = 0.041\left(\frac{\alpha_M}{\alpha_E}\right)\text{ keV}, \qquad \mathcal{B}(J/\psi\to\gamma\eta) = (4.7\pm0.2)\times10^{-4}\left(\frac{\alpha_M}{\alpha_E}\right). \tag{4.184}$$

With the reasonable value $\alpha_M/\alpha_E = 1.8$, the predicted branching ratio can agree with the experimental value $B_{\rm exp}(J/\psi\to\gamma\eta) = (8.6\pm0.8)\times10^{-4}$ [10]. To avoid the uncertainties from α_M/α_E and θ_P, we take the ratio of $\Gamma(J/\psi\to\gamma\eta)$ to another E1M2 transition rate $\Gamma(\psi'\to J/\psi\eta)$. The theoretical prediction is [231]

$$R_\eta \equiv \frac{\Gamma(J/\psi\to\gamma\eta)}{\Gamma(\psi'\to J/\psi\eta)} = 0.012. \tag{4.185}$$

In R_η, uncertainties in the H factors cancel, so R_η offers a direct test of the MGE mechanism. (4.185) is in agreement with the experimental value $R_\eta|_{\rm exp} = 0.009\pm0.003$ [10] at the 1σ level.

This approach can also be applied to $J/\psi\to\gamma\eta'$. With $\theta_P \approx -20^\circ$, we obtain

$$R_{\eta'} \equiv \frac{\Gamma(J/\psi\to\gamma\eta')}{\Gamma(\psi'\to J/\psi\eta)} = \left|\frac{\mathbf{q}(J/\psi\to\gamma\eta')}{\mathbf{q}(J/\psi\to\gamma\eta))}\right|^3\left|\frac{m_{\eta'}^2(\sqrt{2}\cos\theta_P+\sin\theta_P)}{m_\eta^2(\cos\theta_P-\sqrt{2}\sin\theta_P)}\right|^2 R_\eta = 0.044. \tag{4.186}$$

This is also in agreement with the experimental value $R_{\eta'}|_{\rm exp} = 0.044\pm0.010$ [10].

We would like to mention that this approach is not suitable for $\Upsilon\to\gamma\eta$ since the typical gluon momentum in this process is $k \sim q_\eta/2 \sim 2.4$ Gev, appropriate for perturbative QCD, but not for QCDME.

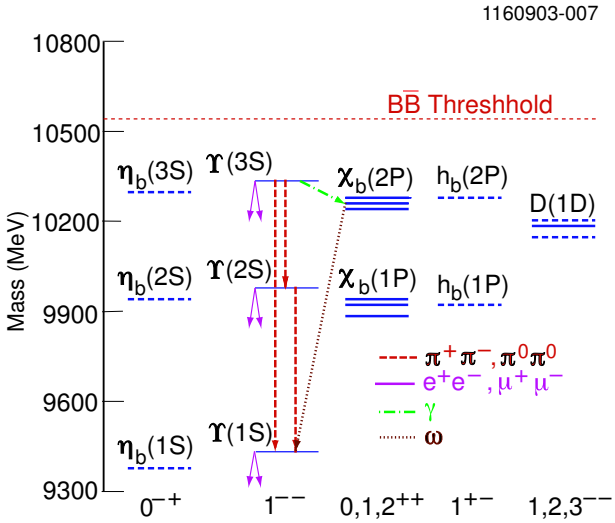

Fig. 4.17: Allowed photon, dipion, and omega transitions allowed within the $b\bar{b}$ system.

7.5 Hadronic transition experiments in the $b\bar{b}$ system

A. Experimental analysis of hadronic transitions — bottomonium

We see from Eq. (4.166) that, in the framework of QCDME, the transition amplitude contains an MGE factor and a H factor. Selection rules, as well as the limited phase space, restrict the possible transitions. A summary of the rich spectroscopy afforded by bottomonia is shown in Fig. 4.17

The principal experimental observables here are the partial widths for the transitions between bottomonia and the Dalitz plot variables: the $\pi\pi$ and $\Upsilon\pi$ invariant mass spectra, and the angular distributions between final-state particles. To measure the transition $\Upsilon''\to\Upsilon\pi\pi$, for example, in electron–positron annihilation data (where Υ'' is produced at rest, and polarized along the beam axis), one can use the constraint that the Υ energy can be inferred directly from the measurement of the pion four-momenta to calculate the mass recoiling against the dipion system. As with the $\gamma\gamma$ cascades, one differentiates the "exclusive" case in which the Υ decays to a clean, background-free topology, such as $\mu^+\mu^-$ or e^+e^-, from the "inclusive" case in which all events are accepted, and one calculates the mass recoiling against all oppositely-signed dipion pairs. In the former case, one, therefore, selects events consistent with the cascade: $\Upsilon''\to\Upsilon\pi\pi$, $\Upsilon\to l^+l^-$, allowing one to isolate a very clean sample, but at the expense of lower overall efficiency owing to the small ($\sim 2\%$) dileptonic BR's of the final state Υ's.

B. Branching ratios and partial widths

The CLEO II mass spectra recoiling against charged dipions, for data taken at the Υ' [266], are shown in Figs. 4.18 and 4.19, and illustrate the trade-off between the higher statistical power of the inclusive data sample vs. the better signal-to-noise of the exclusive data sample.[20]

Branching ratios are calculated based directly on the number of events found in each peak. Predictions for the partial widths in the nonrelativistic single-channel and coupled-channel theories are shown in Tables 4.28 and 4.30. In addition to CLEO, the tabulated branching ratios for $\Upsilon'\to\Upsilon\pi\pi$ also include measurements made by the ARGUS [265], CLEO I [267], CUSB-I [268], and Crystal Ball [269] collaborations. The CLEO II collaboration are also able to derive estimates for the transition rates for $\Upsilon''\to\Upsilon' + X$ by performing a hand scan of the events it reconstructs in $\Upsilon''\to\Upsilon' + X$, $\Upsilon'\to\Upsilon\pi^+\pi^-$, $\Upsilon\to l^+l^-$, and using the unitarity constraint that the sum of the dipion transitions plus the radiative tran-

[20] Because of the poor signal-to-noise ratio, the $\Upsilon''\to\Upsilon\pi^0\pi^0$ transitions cannot be studied inclusively.

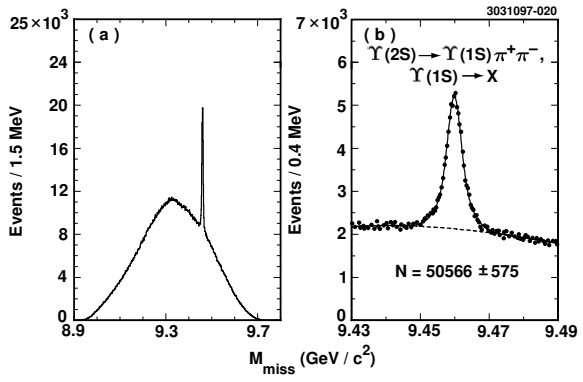

Fig. 4.18: Mass recoiling against two oppositely charged tracks, assumed to be pions, for data taken at the Υ' resonance.

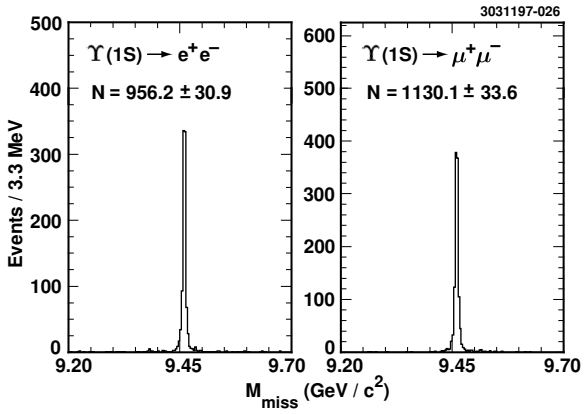

Fig. 4.19: Mass recoiling against two oppositely charged tracks, assumed to be pions, for data taken at the Υ' resonance, with the additional restriction that there be exactly four charged tracks in the event, and that the two most energetic charged tracks be consistent with e^+e^- or $\mu^+\mu^-$.

sitions must saturate the overall $\Upsilon''\to\Upsilon' + X$ decay rate to determine X. These values have been compiled along with the direct observation of the $\Upsilon''\to\Upsilon'\pi^0\pi^0$ and $\Upsilon''\to\Upsilon'\pi^+\pi^-$ transitions. According to isospin symmetry, the $\pi^+\pi^-$ transition rate is expected to be twice that of the $\pi^0\pi^0$ transition, modulo the ratios of available phase space ($\pi^0\pi^0/\pi^+\pi^-$) (1.36 for $\Upsilon''\to\Upsilon'\pi^0\pi^0$ and 1.02 for $\Upsilon''\to\Upsilon\pi^0\pi^0$). The measurements to date are generally consistent with this expectation, with the exception of $\Upsilon''\to\Upsilon'\pi^+\pi^-$. Curiously, despite an inability to match the dipion mass distributions for the $\Upsilon''\to\Upsilon\pi\pi$ transitions (Secs. 7.2 and 7.3), the QCDME approach gives a better match for this partial width than for $\Upsilon''\to\Upsilon'\pi\pi$.

C. Angular distributions

In the nonrelativistic limit, orbital angular momentum and spin are separately conserved. The spin of a bottomonium resonance produced at e^+e^- colliders lies along the beam axis. In $\Upsilon(nS)\to\Upsilon\pi^+\pi^-$, the orbital angular momentum between the pions, or the orbital angular momentum between the dipion system and Υ is a useful observable in addition to the polarization of Υ. Predictions for the populations of the allowed angular momentum states have been made for both the ψ system as well as the Υ system [240,270]. All measurements to date (e.g., by verifying in exclusive events that the angular distribution of the leptons relative to the beam axis follows $dN/d(cos\theta) \sim 1+cos^2\theta$) from ARGUS, CLEO, and CUSB give strong evidence that the daughter Υ is indeed polarized along the beam axis in the dipion transitions, and are consistent with an S-wave decay. The other allowed amplitude is a possible D-wave contribution in the dipion system [cf. Eq. (4.167)]. Convincing evidence for a large D-wave component of the

dipion system has not yet been presented, although it has received some theoretical attention [271–273], and suggestions for non-S-wave anisotropy are found in both the $\Upsilon''\to\Upsilon\pi^+\pi^-$ [266] and $\Upsilon'\to\Upsilon\pi^+\pi^-$ data [265, 274], both of which show $\sim 2\sigma$ indications of a D-wave contribution at the few percent level [266]. Mapping out the ratio of D-wave to S-wave amplitudes as a function of dipion mass in the Υ'' system is a project requiring substantially more statistics than have been accumulated to date; expectations are that a D-wave amplitude would be more observable at low values of invariant mass, corresponding to higher energy release in the Υ'' decay. Such an analysis is currently underway at CLEO and should mature within the next year.

D. Single pion transitions

For dipion transitions Yan [230], collaborating with Kuang [237], and their work later extended by Zhou and Kuang [263], estimated the magnitude of the second piece of the product matrix element, the hadronization term of the transition amplitude. An immediate consequence of the multipole approach is the expected suppression of the case $X = \eta$ relative to $X = \pi\pi$. The former system has the wrong quantum numbers for two $E1$ gluons, and proceeds in lowest order as either $E1 \cdot M2$ or $M1 \cdot M1$ in QCDME. Since the mass dependence of the chromomagnetic transitions goes as m^{-4} (m = quark mass), QCDME, therefore predicts that the ratio for $\mathcal{B}(\Upsilon'\to\Upsilon\eta)/\mathcal{B}(\Upsilon'\to\Upsilon\pi\pi)$ should be substantially smaller than the ratio $\mathcal{B}(\psi'\to\psi\eta)/\mathcal{B}(\psi'\to\psi\pi\pi)$. By contrast, if the ratio of $\pi^+\pi^-$ to η transitions were governed by phase space alone, the η transition would be about 15% of the $\pi^+\pi^-$ transition for $\Upsilon'\to\Upsilon$. The most recent CLEO analysis yielded an upper limit: $\mathcal{B}(\Upsilon'\to\Upsilon\eta) < 0.0028$, in qualitative agreement with the rule given above.

The isospin-violating decay $\psi(2S)\to\pi^0\psi(1S)$ and the M1 transition $\psi(2S)\to\eta\psi(1S)$ have been observed in the charmonium sector; searches for the corresponding transitions in the bottomonium sector have resulted only in the upper limit: $\Upsilon'\to\Upsilon\pi^0$ <0.11%. The typically poorer energy resolution in neutral particle measurements, coupled with small predicted branching fractions, makes observation of such decays difficult.

E. Dipion mass spectra

The dipion mass spectra are calculated directly from the pion four-momenta. As stated before, the invariant mass spectra are expected to peak at high mass values. This is, in fact, what is observed for the transition $\Upsilon'\to\Upsilon\pi^+\pi^-$, as shown in Fig. 4.20, and entirely consistent with an exhaustive study of this process by the ARGUS collaboration [265]. Also shown in Fig. 4.20 are the $\pi^0\pi^0$ mass spectra for $\Upsilon''\to\Upsilon\pi^0\pi^0$ and $\Upsilon''\to\Upsilon'\pi^0\pi^0$.

The current data show peaking at high mass for the $\Upsilon''\to\Upsilon'\pi^+\pi^-$ and $\Upsilon'\to\Upsilon\pi\pi$ transitions, consistent with the expectation for S→S transitions (and also consistent with charmonium results). This is the process for which the multipole expansion model, owing to the smallness of the expansion parameter, claims to have the greatest predictive power. However, the $\pi^0\pi^0$ and $\pi^+\pi^-$ invariant mass distributions in the $\Upsilon''\to\Upsilon\pi^+\pi^-$ transition show a "double bump" structure that disagrees with the gluon field multipole expansion model as well as with the expectation that the matrix element for a transition with these quantum numbers should approach zero at threshold. This is perhaps an indication that the average value of Q^2 is too large to make predictions reliably using the multipole model. It may also be an indication that a low-mass 0++ scalar (e.g., the σ) may be contributing to the intermediate state.

There have been various attempts to explain the double-peaked shape. Ref. [272,275,276] assumed the existence of a four-quark state Υ_1, which enhances the low-$M_{\pi\pi}$ region. So far such a resonance is not found experimentally. Ref. [277] assumed a large QPC part in the $\Upsilon''\to\Upsilon\pi\pi$ amplitude whose interference with the MGE part may form a double-peaked shape. However, the systematic calculation shown in Section 7.3 does not support this assumption. Recently, another attempt considering certain models for a σ meson resonance around 500 MeV in the final state $\pi\pi$ interactions [278, 279] have been

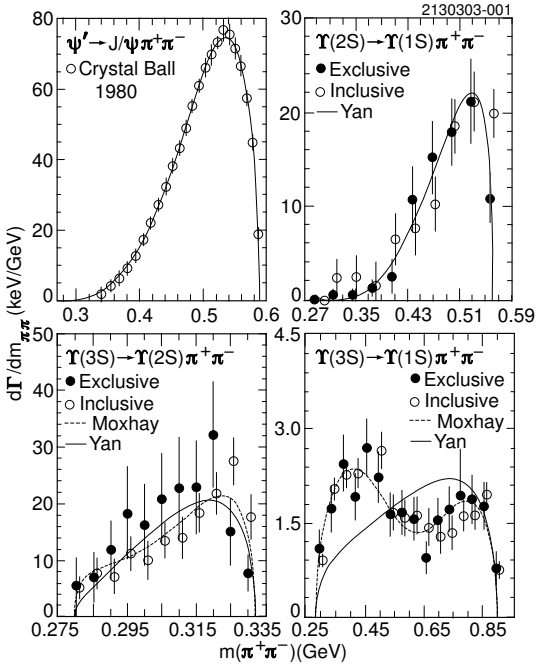

Fig. 4.20: Left: $\pi^+\pi^-$ recoil mass spectra from CLEO II using data taken at the peak of the Υ'' for a) exclusive transitions, and b) inclusive transitions, as indicated [266]. Right: $\pi^0\pi^0$ recoil mass spectrum for exclusives with the indicated cuts on dilepton mass [266].

proposed. By adjusting the free parameters in the models, the CLEO data on the $M_{\pi\pi}$ distributions can be fitted. However, the model need to be tested in other processes. Therefore, the HT $\Upsilon''\to\Upsilon\pi\pi$ is still an interesting process needing further investigation.

F. Three-pion transitions

With their large Υ'' data sample in hand, the CLEO collaboration is able to probe beyond the now-familiar dipion transitions. Of particular interest are ω-mediated transitions, which have been long-suggested as a possible path to the η_b, via: $\Upsilon''\to\eta_b\omega$. In QCDME, by colour conservation, this must correspond to three E1 gluon emissions. Although direct decays $\Upsilon''\to\eta_b\omega$ were not found, CLEO has observed significant production of Υ via $\Upsilon''\to\chi_b'(2P)\gamma$, $\chi_b'(2P)\to\Upsilon\omega$, as shown in Figs. 4.21 and 4.22.

What is actually observed are two recoil mass peaks, corresponding to decays from the χ_b'(2P) (J=2) and (J=1) states. In fact, large partial widths for such decays had been predicted (albeit indirectly) in the original QCDME formulation of Gottfried. As pointed out by Voloshin, since the ω is spin 1, the matrix element should be largely independent of the spin of the parent 2P, consistent with observation. The measured branching fractions ($\mathcal{B}(\chi_b'(J=2)\to\Upsilon\omega) = (1.0\pm0.3\pm0.1)\%$ and $\mathcal{B}(\chi_b'(J=1)\to\Upsilon\omega) = (1.6\pm0.3\pm0.24)\%$ are unexpectedly large, given the limited phase space for these decays.

G. Hadronic transitions from the $\Upsilon(4S)$

Observation of hadronic transitions from the $\Upsilon(4S)$, interesting on its own merits, would provide essential information on the $\Upsilon(4S)$ wave function. Since the $\Upsilon(4S)$ resonance is above the threshold for $B\bar{B}$ production, measurement of the dipion transitions, with partial widths a factor 10^{-4} smaller than the dominant strong decays to open bottom, require data samples of order 10^8 $\Upsilon(4S)$ events. The BaBar and Belle experiments now have accumulated samples of 100M $\Upsilon(4S)$ events and may produce the first signals for such dipion transitions soon. CLEO have produced the most recent results on these transitions, resulting only in upper limits: $\Upsilon(4S)\to\Upsilon'\pi\pi < 0.039\%$; $\Upsilon(4S)\to\Upsilon\pi\pi < 0.012\%$. Interest in such

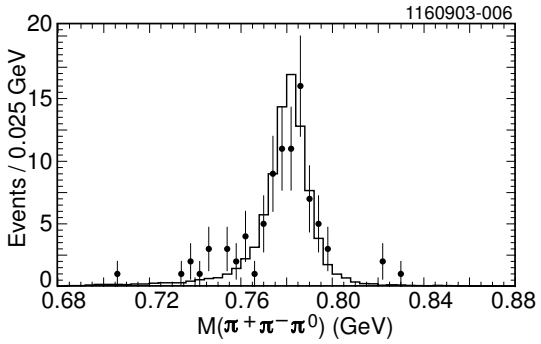

Fig. 4.21: Invariant mass of three pions in events consistent with $\Upsilon'' \to \chi_b' \gamma$; $\chi_b' \to \Upsilon \pi^+ \pi^- \pi^0$.

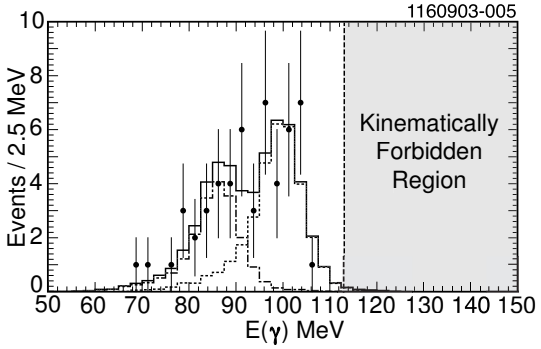

Fig. 4.22: Photon energy distribution for the previous figure's data sample, showing fits to the J=2 and J=1 states. Transitions from the J=0 state are kinematically forbidden (as indicated).

decays has recently been promoted by the BES claim of the corresponding decay in the charmonium sector: $\psi(3770) \to J\psi\pi^+\pi^-$.

H. Unanswered questions

Aside from a first-principles explanation of the dipion mass spectrum in the $\Upsilon'' \to \Upsilon\pi^+\pi^-$ spectrum (such a three-body decay does not, unfortunately, easily lend itself to lattice gauge techniques), much experimental work remains. Among the dipion transitions one would like to observe are the η transitions between the S states, or one of the two dipion transitions involving the singlet $1\,^1P_1$ state: the isospin-violating decay $\Upsilon'' \to h_b(1^1P_1)\pi^0$, or $\Upsilon'' \to h_b\pi^+\pi^-$ [21], as well as the dipion transitions between the χ_b states: $\chi_b' \to \chi_b\pi\pi$. Owing to the larger total widths of the χ_b' (J=2 and J=0) states relative to the J=1 state, the first observation of this decay might be expected in the transition between the J=1 states. Transitions at higher order in QCDME, e.g., $\Upsilon'' \to \eta_b\omega$ (E1E1M1 transition), and also HT to the η_b, which is accessible through two routes, each of which involves a radiative and a hadronic transition: either $\Upsilon'' \to h_b(1^1P_1)\pi\pi$; followed by $h_b(1^1P_1) \to \eta_b\gamma$, or $\Upsilon'' \to \chi_b'\gamma$; $\chi_b' \to \eta_b\pi^+\pi^-$, would both help complete our picture of heavy quark spectroscopy (see Chapter 3). Also extremely interesting would be the observation of HTs from the recently discovered triplet D-bottomonia states ($\Upsilon(1^3D_J)$), e.g., $\Upsilon(1^3D_2) \to \Upsilon\pi^+\pi^-$, or $\Upsilon(1^3D_2) \to \Upsilon(1S)\eta$. Currently, only an upper limit exists for the product branching fraction: $\Upsilon'' \to \chi_{b,J=2}'\gamma$, $\chi_{b,J=2}' \to 1^3D$, $1^3D \to \Upsilon\pi\pi$ of 1.1×10^{-4} for the J=2 D-state, and

[21] For this $S \to P$ transition, Kuang & Yan predict a dipion mass distribution that peaks at *low* values of invariant mass. This is understood by the following argument: such a transition $1^- \to 0^+1^+$ can only proceed in P wave, which suppresses the high mass region.

2.7×10^{-4}, including all the D-states. A 90% c.l. upper limit is also set for the same decay chain, but with an η rather than dipion transition, of 2.3×10^{-4}.

7.6 Hadronic transition experiments in the $c\bar{c}$ system

Hadron transitions in the charmonium system where there is experimental information include $\pi^+\pi^- \to J/\psi\ \pi^0$, $\pi^+\pi^- \to J/\psi\ \eta$, and $\pi^+\pi^- \to J/\psi\ \pi\pi$. Recently evidence has been presented on $\psi(3770) \to J/\psi\ \pi^+\pi^-$ decays, and very recently, Belle announced the discovery of the $X(3872)$ [280], which is detected via $X(3872) \to J/\psi\ \pi^+\pi^-$, making it another means to study hadronic transitions. Here recent experimental results on $\pi^+\pi^- \to J/\psi\ \pi^0$, $\pi^+\pi^- \to J/\psi\ \eta$, $\pi^+\pi^- \to J/\psi\ \pi\pi$ and $\psi(3770) \to J/\psi\ \pi^+\pi^-$ will be summarized. We will shortly mention the $X(3872) \to J/\psi\ \pi^+\pi^-$ transition, which has been discussed in detail in Chapter 3, Section 8.2.

A. $\pi^+\pi^- \to J/\psi\ \pi^0$, $\pi^+\pi^- \to J/\psi\ \pi^0\ \pi^0$ *and* $\pi^+\pi^- \to J/\psi\ \eta$

Experimental results for the processes $\psi\,' \to J/\psi\ \pi^0$ and $J/\psi\ \eta$ are few and were mainly taken in the 1970s and 80s [281–285]. Recently, however, BES, using a sample of $(14.0 \pm 0.6) \times 10^6\ \psi\,'$ events collected with the BES II detector [286], studied $\psi\,'$ decaying into $J/\psi(\pi^0, \eta)$, with π^0 and η decaying to two photons, and J/ψ to lepton pairs [241]. Events with two charged tracks identified as an electron pair or muon pair and two or three photon candidates are selected. A five constraint (5C) kinematic fit to the hypothesis $\psi\,' \to \gamma\gamma l^+l^-$ with the invariant mass of the lepton pair constrained to J/ψ mass is performed, and the fit probability is required to be greater than 0.01.

To remove the huge background from $\psi\,' \to \gamma\chi_{c1,c2}$ under the $\psi\,' \to J/\psi\ \pi^0$ signal, the invariant mass of the highest energy gamma and the J/ψ, $M_{\gamma_h,J/\psi}$ is required to be less than 3.49 or greater than 3.58 Gev/c^2. Figure 4.23 shows, after this requirement, the distribution of invariant mass, $M_{\gamma\gamma}$, where the smooth background is due to $\psi(2S) \to \gamma\chi_{c1,2}$ and $J/\psi\ \pi^0\pi^0$. A Breit Wigner with a double Gaussian mass resolution function to describe the π^0 resonance plus a third-order background polynomial is fitted to the data.

In the $\psi\,' \to J/\psi\ \eta$ channel, the main backgrounds are from $\psi\,' \to J/\psi\ \pi^0\pi^0$ and $\gamma\chi_{c1,c2}$. By requiring $M_{\gamma_h,J/\psi} < 3.49$ Gev/c^2, most background from $\psi\,' \to \gamma\chi_{c1,c2}$ is removed. The resultant plot shown in Fig. 4.24 shows a clear η signal superimposed on background, mainly from $\psi\,' \to \pi^0\pi^0 J/\psi$. A fit is made using a Breit–Wigner resonance convoluted with a mass resolution function for the η signal plus a polynomial background, where the width of the η is fixed to its Particle Data Group (PDG) value [10] and the background function is determined from $\psi\,' \to J/\psi\ \pi^0\pi^0$ Monte Carlo simulated events that satisfy the same criteria as the data.

Table 4.31: Recent BES results on $\psi\,' \to J/\psi\ \pi^0$ and $\psi\,' \to J/\psi\ \eta$.

Channel	$J/\psi\ \pi^0$		$J/\psi\ \eta$	
Final state	$\gamma\gamma e^+e^-$	$\gamma\gamma\mu^+\mu^-$	$\gamma\gamma e^+e^-$	$\gamma\gamma\mu^+\mu^-$
Number of events	123 ± 18	155 ± 20	2465 ± 101	3290 ± 148
Efficiency (%)	11.21	13.34	26.94	34.07
Sys. error (%)	9.68	8.77	8.54	8.40
Correction factor	0.962	0.974	0.962	0.974
BR (%)	$0.139 \pm 0.020 \pm 0.013$	$0.147 \pm 0.019 \pm 0.013$	$2.91 \pm 0.12 \pm 0.21$	$3.06 \pm 0.14 \pm 0.25$
Combine BR (%)	$0.143 \pm 0.014 \pm 0.013$		$2.98 \pm 0.09 \pm 0.23$	
PDG (%) [10]	0.096 ± 0.021		3.16 ± 0.22	

Using the fitting results and the efficiencies and correction factors for each channel, the branching fractions listed in Table 4.31 are determined. The BES $\mathcal{B}(\psi\,' \to J/\psi\ \pi^0)$ measurement has improved precision by more than a factor of two compared with other experiments, and the $\psi\,' \to J/\psi\ \eta$ branching

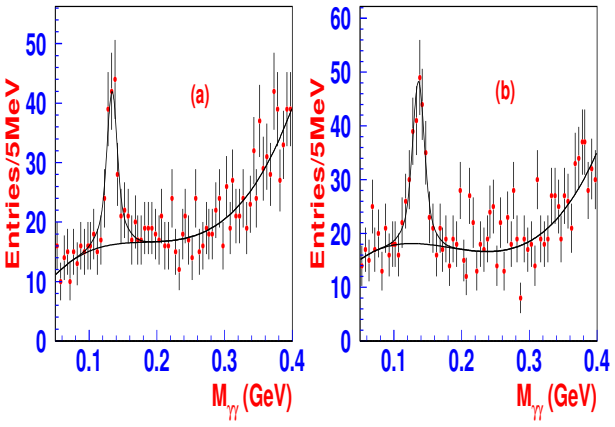

Fig. 4.23: Two-photon invariant mass distribution for candidate $\psi\,' \to \pi^0 J/\psi$ events for (a) $\gamma\gamma e^+e^-$ and (b) $\gamma\gamma\mu^+\mu^-$.

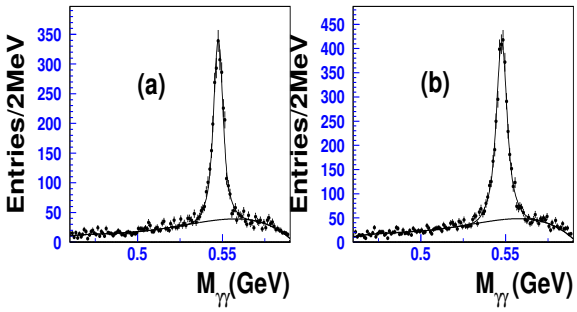

Fig. 4.24: Two-photon invariant mass distribution for candidate $\psi\,' \to \eta J/\psi$ events for (a) $\gamma\gamma e^+e^-$ and (b) $\gamma\gamma\mu^+\mu^-$.

fraction is the most accurate single measurement. The BES $\mathcal{B}(\psi\,' \to J/\psi\ \pi^0)$ agrees better with the Mark II result [284] than with the Crystal Ball result [285]. For the comparison of the BES result with related theoretical predictions, see Section 7.2.

In another recent BES analysis [287], based on a sample of approximately 4×10^6 $\pi^+\pi^-$ events obtained with the BES I detector [288], a different technique is used for measuring branching fractions for the inclusive decay $\pi^+\pi^- \to J/\psi$ anything, and the exclusive processes for the cases where $X = \eta$ and $X = \pi\pi$. Inclusive $\mu^+\mu^-$ pairs are reconstructed, and the number of $\pi^+\pi^- \to J/\psi X$ events is determined from the $J/\psi \to \mu^+\mu^-$ peak in the $\mu^+\mu^-$ invariant mass distribution. The exclusive branching fractions are determined from fits to the distribution of masses recoiling from the J/ψ with Monte Carlo determined distributions for each individual channel.

Selected events are required to have more than one and less than six charged tracks and must have two identified muon tracks with zero net charge. The two muon tracks must satisfy a one constraint kinematic fit to the J/ψ mass. Shown in Fig. 4.25 is the dimuon invariant mass distribution, $m_{\mu\mu}$, for these events. A clear peak at the J/ψ mass is evident above background.

The mass recoiling against the J/ψ candidates, m_X is determined from energy and momentum conservation. In order to distinguish $\psi(2S) \to J/\psi\pi^+\pi^-$ and $\psi(2S) \to J/\psi\pi^0\pi^0$ events, separate m_X histograms are made for events with no additional charged tracks and those with additional charged tracks. To reduce background and improve the quality of the track momentum measurements, events used for this part of the analysis are required to have a kinematic fit $\chi^2 < 7$. The m_X histograms for

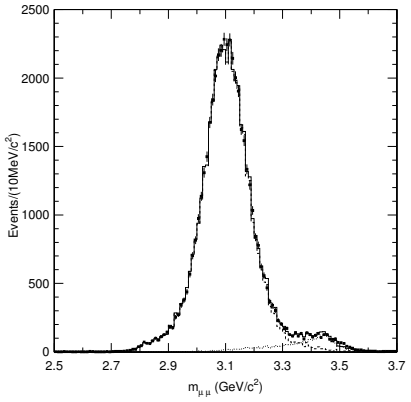

Fig. 4.25: Distribution of dimuon invariant mass, $m_{\mu\mu}$, for events that pass the $J/\psi \to \mu^+\mu^-$ kinematic fit. Dots with error bars are data. Also shown is the fit (solid histogram) to the distribution with signal (long dashed histogram) and background (short dashed histogram) shapes.

events with and without additional charged tracks, selected according to the above requirements, are shown in Figs. 4.26 and 4.27.

To determine the number of exclusive decays and separate $\psi(2S) \to J/\psi\pi^0\pi^0$ and $\psi(2S) \to J/\psi\pi^+\pi^-$ events, m_X histograms for events with and without additional charged tracks, shown in Figs. 4.26 and 4.27, are fit simultaneously. Contributions from the $\psi(2S) \to \gamma\chi_{c0}, \chi_{c0} \to \gamma J/\psi$ are expected to be very small [10] and are not included in the fit. The influence of $\pi^+\pi^- \to J/\psi\pi^0$ is also small, indeed there is no indication of such a component in Fig. 4.26, and this channel is also not included. The m_X distributions for $\psi(2S) \to \gamma\chi_{c1}, \chi_{c1} \to \gamma J/\psi$, $\psi(2S) \to \gamma\chi_{c2}, \chi_{c2} \to \gamma J/\psi$, and the background are broad and rather similar in shape, as can be seen in Fig. 4.26. Since these are difficult to distinguish, the χ_{c2} to χ_{c1} ratio is constrained using calculated efficiencies and the PDG world average branching fractions for the two processes.

To avoid a number of systematic errors, the channels of interest are normalized to the observed number of $J/\psi\pi^+\pi^-$ events; ratios of the studied branching fractions to that for $\mathcal{B}(\pi^+\pi^- \to J/\psi\pi^+\pi^-)$ are reported. The advantage of normalizing in this way is that many of the muon selection systematic errors largely cancel, as well as the systematic error due to the χ^2 requirement.

Table 4.32: Final branching ratios and branching fractions. PDG04-exp results are single measurements or averages of measurements, while PDG04-fit are results of their global fit to many experimental measurements. For the value marked with an asterisk, the PDG gives the reciprocal. The BES results in the second half of the table are calculated using the PDG value of $\mathcal{B}_{\pi\pi} = \mathcal{B}(\pi^+\pi^- \to J/\psi\pi^+\pi^-) = (31.7 \pm 1.1)\%$.

Case	This result	PDG04-exp	PDG04-fit
$\mathcal{B}(J/\psi \text{ anything})/\mathcal{B}_{\pi\pi}$	$1.867 \pm 0.026 \pm 0.055$	2.016 ± 0.150 [289]	$1.821 \pm 0.036^*$
$\mathcal{B}(J/\psi\pi^0\pi^0)/\mathcal{B}_{\pi\pi}$	$0.570 \pm 0.009 \pm 0.026$	–	0.59 ± 0.05
$\mathcal{B}(J/\psi\eta)/\mathcal{B}_{\pi\pi}$	$0.098 \pm 0.005 \pm 0.010$	0.091 ± 0.021 [284]	0.100 ± 0.008
$\mathcal{B}(J/\psi \text{ anything})$ (%)	$59.2 \pm 0.8 \pm 2.7$	55 ± 7	57.6 ± 2.0
$\mathcal{B}(J/\psi\pi^0\pi^0)$ (%)	$18.1 \pm 0.3 \pm 1.0$	–	18.8 ± 1.2
$\mathcal{B}(J/\psi\eta)$ (%)	$3.11 \pm 0.17 \pm 0.31$	2.9 ± 0.5	3.16 ± 0.22

The final branching fraction ratios and branching fractions are shown in Table 4.32, along with the PDG results, including their experimental averages and global fit results. For the ratio of $\mathcal{B}(\psi(2S)$

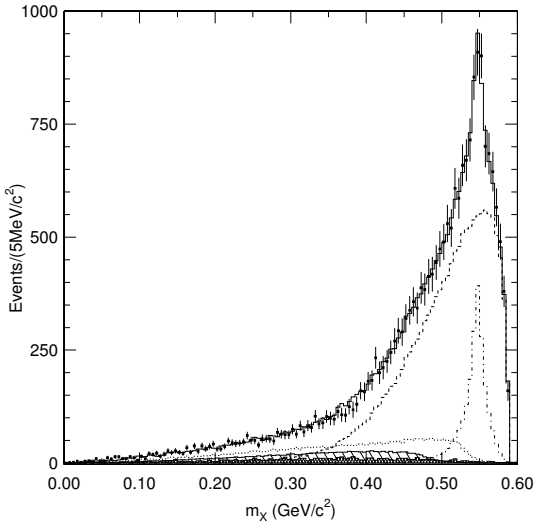

Fig. 4.26: Fit of the m_X distribution events with no additional charged tracks. Shown are the data (points with error bars), the component histograms, and the final fit. For the components, the large, long-dash histogram is $\psi(2S) \to J/\psi\pi\pi$, the narrow, dash–dot histogram is $\psi(2S) \to J/\psi\eta$, the broad, short-dashed histogram is $\pi^+\pi^- \to \gamma\chi_{c1}, \chi_{c1} \to \gamma J/\psi$, the broad, hatched histogram is $\pi^+\pi^- \to \gamma\chi_{c2}, \chi_{c2} \to \gamma J/\psi$, and the lowest cross-hatched histogram is the combined $e^+e^- \to \gamma\mu^+\mu^-$ and $e^+e^- \to \psi(2S), \psi(2S) \to (\gamma)\mu^+\mu^-$ background. The final fit is the solid histogram.

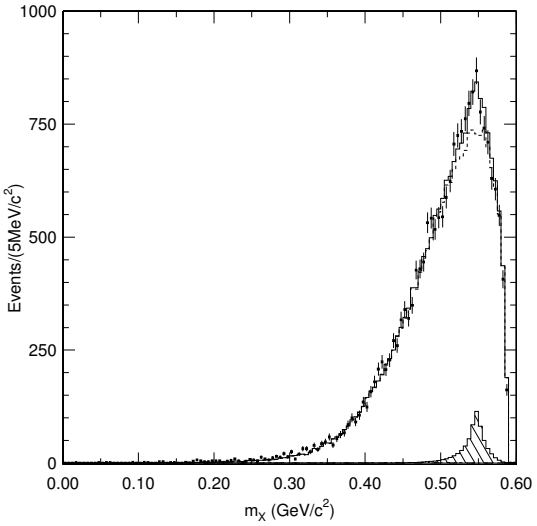

Fig. 4.27: Fit of the m_X distribution for events with any number of additional charged tracks. Shown are the data (points with error bars), the component histograms, and the final fit (solid histogram). The dashed histogram is $\psi(2S) \to J/\psi\pi^+\pi^-$, and the hatched histogram is $\psi(2S) \to J/\psi\eta$. There is very little evidence for $\psi(2S) \to \gamma\chi_{c1/2}, \chi_{c1/2} \to \gamma J/\psi$. This distribution is composed predominantly of $\psi(2S) \to J/\psi\pi^+\pi^-$.

$\to J/\psi\pi^0\pi^0$) to $\mathcal{B}(\psi(2S) \to J/\psi\pi^+\pi^-)$, the PDG does not use the previous experimental results and gives no average value. For the other branching fraction ratios, only one measurement exists for each, and Table 4.32 lists the single measurements quoted by the PDG. The results for $\mathcal{B}(J/\psi \text{ anything})/\mathcal{B}(\psi(2S) \to J/\psi\pi^+\pi^-)$ and $\mathcal{B}(J/\psi\eta)/\mathcal{B}(\psi(2S) \to J/\psi\pi^+\pi^-)$ have smaller errors than the previous results.

To determine the branching fractions, the ratios are multiplied by the PDG value for $\mathcal{B}(\psi(2S) \to J/\psi\pi^+\pi^-) = (31.7 \pm 1.1)\%$. The agreement for both the ratios of branching fractions and the calculated branching fractions using the PDG result for $\mathcal{B}(\pi^+\pi^- \to J/\psi\pi^+\pi^-)$ with the PDG fit results is good, and the determination of $\mathcal{B}(J/\psi\eta)$ agrees well with the determination from $\psi(2S) \to \gamma\gamma J/\psi$ decays above.

B. $\pi^+\pi^- \to J/\psi\ \pi^+\pi^-$

The process $\pi^+\pi^- \to J/\psi\ \pi^+\pi^-$, is the largest decay mode of the $\psi(2S)$ [10]. Early investigation of this decay by Mark I [290] found that the $\pi^+\pi^-$ mass distribution was strongly peaked towards higher mass values, in contrast to what was expected from phase space. Further, angular distributions strongly favored S-wave production of $J/\psi\ \pi\pi$, as well as an S-wave decay of the dipion system. The challenge of describing the mass spectrum attracted considerable theoretical interest [227,229,230,237,240,256,291].

The $\pi^+\pi^- \to J/\psi\ \pi\pi$ decay was studied by BES [292], using 22,800 almost background free exclusive $\psi(2S) \to \pi^+\pi^- J/\psi$, $J/\psi \to l^+l^-$ events, where l signifies either e or μ, from a data sample of 3.8×10^6 $\psi(2S)$ decays.

The angular distributions were fit using the general decay amplitude analysis of Cahn [270]. The decay can be described in terms of partial wave amplitudes, $M_{l,L,S}$, where $\mathbf{l}$ is the $\pi\pi$ angular momentum, $\mathbf{L}$ is J/ψ X ($X \to \pi^+\pi^-$) angular momentum, $\mathbf{S}$ is the channel spin ($\mathbf{S} = \mathbf{s} + \mathbf{l}$), and $\mathbf{s}$ is the spin of the J/ψ. Parity conservation and charge conjugation invariance require both L and l to be even. The partial waves can be truncated after a few terms. Considering only M_{001}, M_{201}, and M_{021} [293]:

$$\frac{d\Gamma}{d\Omega_{J/\psi}} \propto [|M_{001}|^2 + |M_{201}|^2 + \frac{1}{4}|M_{021}|^2(5 - 3\cos^2\theta^*_{J/\psi}) + \frac{1}{\sqrt{2}}\Re\{M_{021}M^*_{001}\}(3\cos^2\theta^*_{J/\psi} - 1)], \tag{4.187}$$

$$\frac{d\Gamma}{d\Omega_{\pi}} \propto [|M_{001}|^2 + \frac{1}{4}|M_{201}|^2(5 - 3\cos^2\theta^*_{\pi}) + |M_{021}|^2 + \frac{1}{\sqrt{2}}\Re\{M_{201}M^*_{001}\}(3\cos^2\theta^*_{\pi} - 1)], \tag{4.188}$$

$$\frac{d\Gamma}{d\Omega_{\mu}} \propto [|M_{001}|^2(1 + \cos^2\theta^*_{\mu}) + \frac{1}{10}(|M_{201}|^2 + |M_{021}|^2)(13 + \cos^2\theta^*_{\mu})], \tag{4.189}$$

where $\theta^*_{J/\psi}$ is the polar angle of the J/ψ relative to the beam direction in the lab, θ^*_{π} is the angle between the momenta of J/ψ and π^+ in the rest frame of the $\pi\pi$ system, and θ^*_{μ} is the angle between the beam direction and μ^+ in the rest frame of the J/ψ. The $d\Omega$'s are measured in their respective rest frames, and the $M_{l,L,S}$ are functions of $m_{\pi\pi}$.

There are three complex numbers to be obtained. According to Cahn, if the $\psi(2S)$ and J/ψ are regarded as inert, then $M_{l,L,S} = e^{i\delta^0_l(m_{\pi\pi})}|M_{l,L,S}|$, where $\delta^0_l(m_{\pi\pi})$ is the isoscalar phase shift for quantum number l. The phase angles are functions of $m_{\pi\pi}$. Interpolating the S-wave, isoscalar phase shift data found in Ref. [272,294], BES took δ^0_0 to be $\approx 45^\circ$ and $\delta^0_2 \approx 0$. Using these values as input, BES obtained the combined fit to Eqs. (4.187)–(4.189), shown in Fig. 4.28. The fit yields a nonzero result for $|M_{201}|$, indicating that the dipion system contains some D-wave, which is shown by the non-flat angular distribution for $\cos\theta^*_{\pi}$ seen in Fig. 4.28. On the other hand $|M_{021}|/|M_{001}|$, which measures the amount of D-wave of the J/ψ–X system relative to the S-wave, is consistent with zero, which is indicated by the flat angular distribution for $\cos\theta^*_X$ shown in Fig. 4.28

Observation of a small D-wave contribution is interesting theoretically since, as we have seen in Eqs. (4.180) and (4.168), there is only S-wave contribution in the NRSC approach, i.e.,*the existence of a small D-wave contribution implies that the present NRSC theory should be improved to contain systematic relativistic and coupled-channel contributions*.

The $m_{\pi\pi}$ invariant mass spectrum has been fit with the Novikov–Shifman model and other models, as shown in Fig. 4.29. As can be seen, they give nearly identical fits.

Mannel and Urech have constructed an effective Lagrangian using chiral symmetry arguments to describe the decay of heavy excited S-wave spin-1 quarkonium into a lower S-wave spin-1 state [295]. Using total rates, as well as the invariant mass spectrum from Mark II via ARGUS [265], the parameters of this theory have been obtained. More recently, M. L. Yan *et al.* [296] have pointed out that this model allows D-wave contributions. BES fit the joint $\cos\theta^*_{\pi}$–$m_{\pi\pi}$ distribution using the amplitude of Mannel and Urech. The results are given in Ref. [292], along with the results from Ref. [295] which are based on ARGUS–Mark II [265].

C. $\psi(3770) \to J/\psi\ \pi^+\pi^-$

BES has reported evidence for $\psi(3770) \to J/\psi\ \pi^+\pi^-$ based on 27.7 pb^{-1} of data taken in the centre-of-mass (c.m.) energy region around 3.773 Gev using the BES II detector [252].

To search for the decay of $\psi(3770) \to J/\psi\ \pi^+\pi^-$, $J/\psi \to e^+e^-$ or $\mu^+\mu^-$, $\mu^+\mu^-\pi^+\pi^-$ and $e^+e^-\pi^+\pi^-$ candidate events are selected. They are required to have four charged tracks with zero total charge. Each track is required to have a good helix fit, to be consistent with originating from the primary

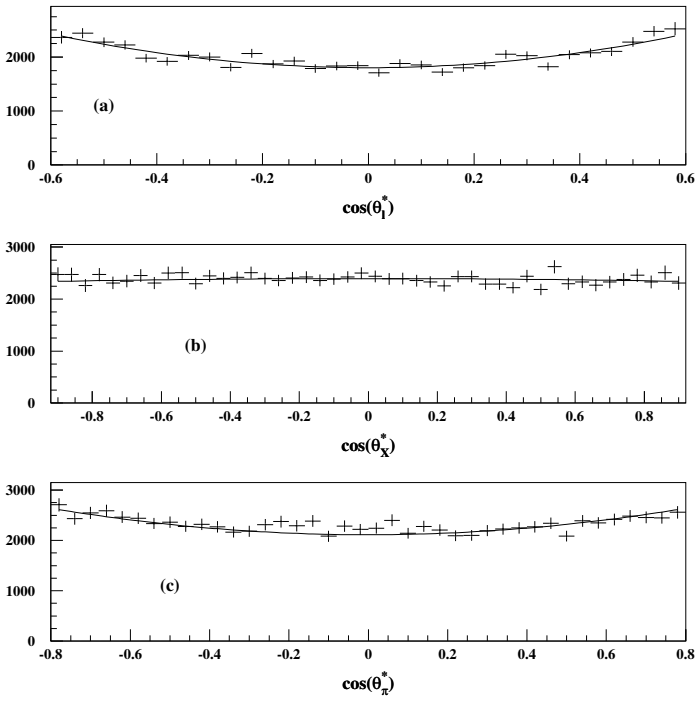

Fig. 4.28: Angular distributions of **(a)** $\cos\theta^*_\mu$, **(b)** $\cos\theta^*_X$, and **(c)** $\cos\theta^*_\pi$. The fit shown uses the partial wave analysis description of Cahn [293].

event vertex, and to satisfy $|\cos\theta| < 0.85$, where θ is the polar angle. Pions and leptons must satisfy particle identification requirements.

In order to reduce background and improve momentum resolution, events are subjected to four-constraint kinematic fits to either the $e^+e^- \to \mu^+\mu^-\pi^+\pi^-$ or the $e^+e^- \to e^+e^-\pi^+\pi^-$ hypothesis. Events with a confidence level greater than 1% are accepted. Figure 4.30(a) shows the dilepton masses determined from the fitted lepton momenta of the accepted events. There are clearly two peaks. The lower mass peak is mostly due to $\psi(3770) \to J/\psi\ \pi^+\pi^-$, while the higher one is produced via radiative return to the peak of the $\psi(2S)$.

A maximum likelihood fit to the mass distribution in Fig. 4.30(a), using a Gaussian function to describe the peak near the J/ψ mass, two Gaussian functions to represent the second peak from radiative return to the $\psi(2S)$ peak, and a polynomial to represent the broad background, yields a signal of 17.8 ± 4.8 events with a significance of $6.2\ \sigma$.

Backgrounds from QED radiative processes with γ conversion, two-photon backgrounds, such as $e^+e^- \to e^+e^-\mu^+\mu^-$ (where the slow muons are misidentified as pions) and $e^+e^- \to e^+e^-\pi^+\pi^-$, and $e^+e^- \to \tau^+\tau^-$, are negligibly small, as are $J/\psi\ \pi^+\pi^-$ events produced in the continuum process, $e^+e^- \to l^+l^-\pi^+\pi^-$. However, there is a contribution from $\psi(2S) \to J/\psi\ \pi^+\pi^-$ that can pass the event selection criteria and yield fitted dilepton masses around 3.097 Gev. This is the main background to $\psi(3770) \to J/\psi\ \pi^+\pi^-$, as shown in Fig. 4.30(b). Here the histogram shows the dilepton mass distribution for $\psi(2S) \to J/\psi\ \pi^+\pi^-$ from a Monte Carlo simulation. The higher peak is due to the radiative return to the $\psi(2S)$ peak, and the lower peak is from the tail of the $\psi(2S)$. The points with error bars show the total contribution from $\psi(2S)$ and $\psi(3770)$ production and decay. From the simulation, it is estimated that $6.0 \pm 0.5 \pm 0.6$ out of 17.8 ± 4.8 events in the peak near 3.1 Gev in Fig. 4.30(a) are due to $\psi(2S) \to J/\psi\ \pi^+\pi^-$, where the first error is statistical and the second one is the systematic error arising from the uncertainty in the $\psi(2S)$ resonance parameters.

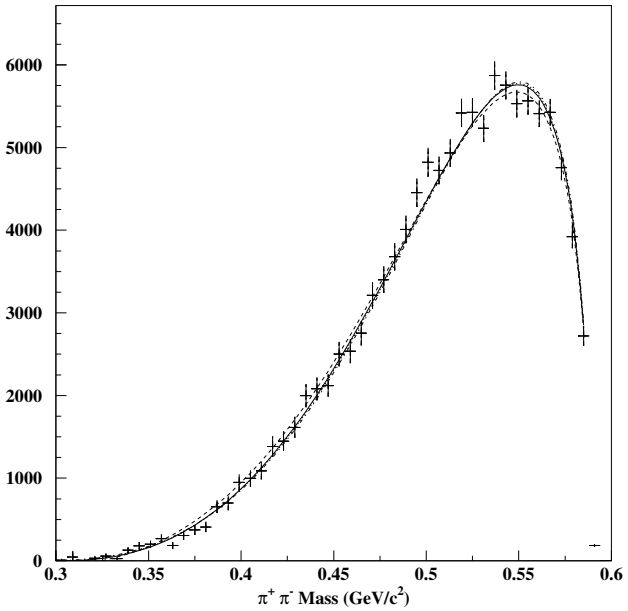

Fig. 4.29: Fits to the $m_{\pi\pi}$ distribution from $\pi^+\pi^- \to \pi^+\pi^- \; J/\psi$. The points are the data corrected for efficiency, and the curves are the fit results. The smooth curve is the Novikov–Shifman model. The other models, which are described in Ref. [292], give similar results.

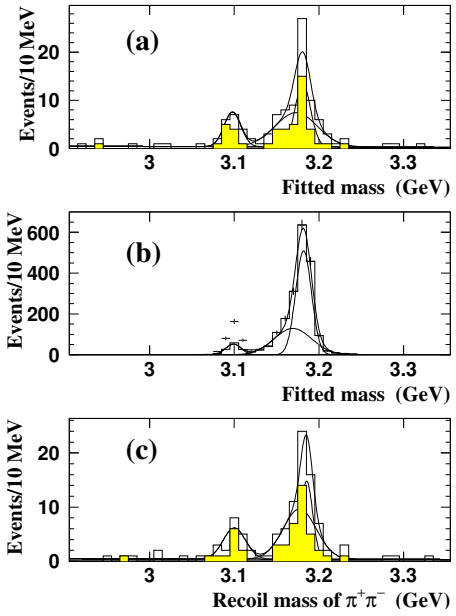

Fig. 4.30: Distributions of dilepton masses for (a) data and (b) Monte Carlo sample for events passing the selection for $\psi(3770) \to \pi^+\pi^- J/\psi$. The hatched histogram in (a) is for $J/\psi \to \mu^+\mu^-$, while the open one is for $J/\psi \to e^+e^-$. The histogram in (b) is for $\psi(2S) \to J/\psi\pi^+\pi^-$, while the points with error bars are the sum of $\psi(3770) \to J/\psi\pi^+\pi^-$ and $\psi(2S) \to J/\psi\pi^+\pi^-$. (c) Distribution of mass recoiling against the $\pi^+\pi^-$ system calculated using measured momenta for events that pass the kinematic fit requirement, where the hatched histogram is for $J/\psi \to \mu^+\mu^-$ and the open one is for $J/\psi \to e^+e^-$.

With the calculated cross-sections for $\psi(3770)$ production at each energy point around 3.773 Gev and the corresponding luminosities, the total number of $\psi(3770)$ events in the data sample is determined to be $N^{\rm prod}_{\psi(3770)} = (1.85 \pm 0.37) \times 10^5$, where the error is mainly due to the uncertainty in the observed cross-section for $\psi(3770)$ production. The detection efficiency for the decay channel is determined to be $\epsilon_{\psi(3770)\to J/\psi\ \pi^+\pi^-, J/\psi\to l^+l^-} = 0.160 \pm 0.002$, where the error is statistical. Using these numbers and the known branching fractions for $J/\psi \to e^+e^-$ and $\mu^+\mu^-$ [10], the branching fraction for the non-$D\bar{D}$ decay $\psi(3770) \to J/\psi\ \pi^+\pi^-$ is measured to be

$$\mathcal{B}(\psi(3770) \to J/\psi\ \pi^+\pi^-) = (0.34 \pm 0.14 \pm 0.08)\%, \tag{4.190}$$

where the first error is statistical and the second systematic. Using $\Gamma_{\rm tot}$ from the PDG [10], this branching fraction corresponds to a partial width of

$$\Gamma(\psi(3770) \to J/\psi\ \pi^+\pi^-) = (80 \pm 32 \pm 21)\ \ {\rm keV}. \tag{4.191}$$

The dominant systematic uncertainty is due to the uncertainty in the total number of $\psi(3770)$ produced ($\pm 24\%$). Other systematic uncertainties are due to the efficiency ($\pm 10\%$), the background shape ($\pm 6\%$), and $\psi(2S) \to J/\psi\ \pi^+\pi^-$ background subtraction ($\pm 7\%$).

CLEOc has analyzed a sample of $\psi(3770)$ decays (4.5×10^4) [209]. Although the sample is smaller, they have a larger detection efficiency (37%). They find two events in the signal region, consistent with the estimated background, and set a preliminary upper limit $\mathcal{B}(\psi(3770) \to J/\psi\ \pi^+\pi^-) < 0.26\%$ (90% CL). The result does not confirm the BES result, but is not inconsistent with it either. CLEOc is now analyzing a sample of about 50 pb^{-1}, and the situation should be better understood when this is completed. See Section 7.2 for the comparison of the BES result with the related theoretical prediction.

D. $X(3872) \to J/\psi\ \pi^+\pi^-$

The Belle group has recently reported the observation of the $X(3872)$, a charmonium-like particle with mass 3872.0 ± 0.8 MeV that decays to $J/\psi\ \pi^+\pi^-$ [280]. For a review on the charmonium assignments (and their problems) for the $X(3872)$ we refer to Chapter 3, Section 8.2, and [297].

The $\pi^+\pi^-$ invariant mass distribution for this process, shown in Fig. 3.33(a) in Chapter 3, has a stronger concentration at high mass values than QCDME [230] expectations for D-wave to S-wave transitions, and is also more pronounced than that seen in the S-wave to S-wave $\psi' \to J/\psi\ \pi^+\pi^-$ process, which is shown in Fig. 3.33(b). This concentration at high $\pi^+\pi^-$ masses in $X(3872) \to J/\psi\ \pi^+\pi^-$ has been experimentally confirmed by the CDF experiment [298].

8 DECAYS OF THE B_c[22]

Besides new spectroscopy, production and decay observables, the investigation of the long-lived heavy quarkonium B_c, the pseudoscalar ground state of the $\bar{b}c$ system, provides the possibility to get model-independent information on some electroweak parameters, like the CKM matrix elements, in the heavy quark sector [299, 300]. The first experimental observation of the B_c meson by the CDF collaboration [224, 301] confirmed the theoretical predictions (and postdictions) on its mass, production rate and lifetime [186, 192, 225, 226, 302–309]. Tevatron [310] and LHC [311] will provide in the near future new data with increased statistics, opening the field to full experimental investigation and systematic test of the theory.

Decays of the B_c meson were considered in the pioneering paper by Bjorken of 1986 [312]. A lot of work has been done after that in order to understand long-lived doubly heavy hadrons.[23] Surprisingly, the Bjorken's estimates of total widths and various branching fractions are close to what is evaluated now in a more rigorous way. The B_c properties determined by the strong interactions can be investigated in the framework of effective field theories for heavy quarkonia, i.e., NRQCD [14, 314], potential NRQCD [41, 42] or vNRQCD [315] (see also Chapters 1, 3 and 6). In contrast to the Wilson coefficients, the hadronic matrix elements of operators composed by the effective fields of the nonrelativistic heavy quarks cannot be evaluated in a perturbative manner. So, one has to use nonperturbative methods such as QCD sum rules (SR) [316], operator product expansion (OPE) for inclusive estimates and potential models (PM).

The measured B_c lifetime is equal to

$$\tau[B_c] = 0.46^{+0.18}_{-0.16} \pm 0.03 \text{ ps}, \tag{4.192}$$

which is close to the value expected by Bjorken. The B_c decays were, at first, calculated in PM [317–326]. We do not distinguish here among relativistic and nonrelativistic PM, light-front, Bethe–Salpeter or quasi-potential approaches, calculations with or without confined quark-propagators and so on, because (1) relativistic corrections to the initial and final state heavy quarkonium form factors are suppressed by powers of the heavy quark velocity (at least, by a factor 10); (2) light mesons in the final states are usually factorized, and corrections to the factorization are small; (3) heavy-light mesons in the final states are

[22] Author: V. V. Kiselev

[23] Reviews on the physics of B_c meson and doubly heavy baryons can be found in Refs. [186, 192, 225, 226, 302] and [313], respectively. For the doubly heavy baryons see also Chapter 3.

quite accurately described by potential models adjusted to the decays of such mesons. As a consequence the different models agree on most of the decay channels.

The results of PM for the B_c lifetime agree with each others after having been adjusted on the semileptonic decays of the B mesons. The OPE evaluations of inclusive decays give lifetime and widths [305] in agreement with PM, if one sums up the dominant exclusive modes. On the other hand, SR of QCD gave at first semileptonic B_c widths, which were one order of magnitude smaller than those of PM and OPE [327]. The reason was identified in the missing Coulomb resummation [306–308, 319]. At present, all mentioned approaches give close results for the lifetime and decay modes of the B_c if similar sets of parameters are used. Nevertheless, various questions remain open:

- What is the appropriate normalization point of the non-leptonic weak Lagrangian in the B_c decays?
- What are the values of the masses for the c and b quarks that have to be used (see in this respect Chapter 6)?
- What are the implications of the NRQCD symmetries for the B_c form factors?
- How consistent is our understanding of hadronic matrix elements characterizing the B_c decays with the data from other heavy hadrons?

In the following of this section we shortly review the B_c decays by summarizing the theoretical predictions in the different frameworks and discussing how direct experimental measurements can help to answer the above questions.

8.1 B_c lifetime and inclusive decay rates

The B_c decay processes can be divided into three classes [305]:

1) the $\bar{b}$-quark decay with the spectator c quark,

2) the c-quark decay with the spectator $\bar{b}$ quark and

3) the annihilation channel $B_c^+ \to l^+\nu_l(c\bar{s}, u\bar{s})$, where $l = e,\ \mu,\ \tau$.

In the $\bar{b}\to\bar{c}c\bar{s}$ decays one separates also the Pauli interference with the c quark from the initial state. In accordance with the given classification, the total width is the sum over the partial widths

$$\Gamma(B_c \to X) = \Gamma(b \to X) + \Gamma(c \to X) + \Gamma(\text{ann.}) + \Gamma(\text{PI}). \tag{4.193}$$

We will see that the dominant contribution to the B_c lifetime is expected to be given by the charmed quark decays ($\approx 70\%$), the b-quark decays and the weak annihilation are expected to add about 20% and 10%, respectively, while the Pauli interference term gives a valuable contribution in the $\bar{b}\to c\bar{c}s$ decays at the level of -1.5%, which we have included in the b-quark decay fraction. The above percentages were obtained in [309]. Somewhat different figures may be obtained in different approaches, e.g., C. H. Chang *et al.* obtain in [305] about 70% for the fraction of c-quark decays, about 22% for the fraction of b-quark decays without Pauli interference, about 17% for the fraction of weak annihilation and about -9% for the fraction of the Pauli interference.

The annihilation width, Γ(ann.), can be reliably estimated in the framework of inclusive approaches. Let us consider, for instance, the effective weak interaction Hamiltonian in the quark transition $b\to c\bar{u}d$:

$$H_{\text{eff}} = \frac{G_F}{2\sqrt{2}} V_{cb}V_{ud}^*\{C_+(\mu)O_+ + C_-(\mu)O_-\}, \tag{4.194}$$

with

$$O_\pm = \bar{u}_i\gamma_\nu(1-\gamma_5)d_i\ \bar{b}_j\gamma^\nu(1-\gamma_5)c_j \pm \bar{u}_i\gamma_\nu(1-\gamma_5)d_j\ \bar{b}_i\gamma^\nu(1-\gamma_5)c_j, \tag{4.195}$$

where i, j are colour indices. The factors $C_\pm(\mu)$ account for the corrections induced by hard gluons to the corresponding four-fermion operators. A review on the evaluation of $C_\pm(\mu)$ can be found in [328]. The normalization condition is given by $C_\pm(m_b) = 1$. A natural choice for μ in decays with given

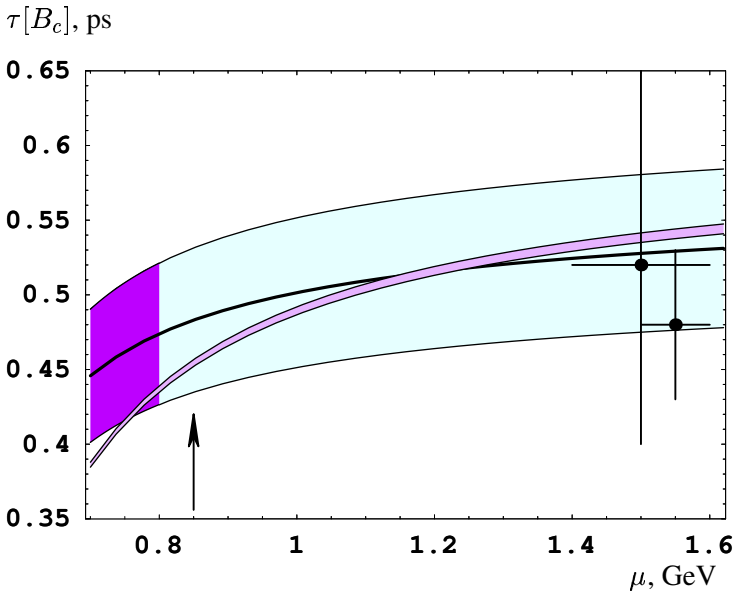

Fig. 4.31: The B_c lifetime calculated in QCD sum rules versus the scale of the hadronic weak Lagrangian in the decay of the charm quark. The wide shaded region, taken from Ref. [308], shows the uncertainty of the semi-inclusive estimates, the dark shaded region is the preferable choice as given by the lifetimes of charmed mesons. The dots represent the values in the OPE approach by M. Beneke and G. Buchalla (left point) and A. Onishchenko (right point) taken from Refs. [305]. The narrow shaded region represents the result of [309] obtained by summing up the exclusive channels with a variation of the hadronic scale in the decays of the $\bar{b}$ in the range of $1 < \mu_b < 5$ Gev. The arrow points to the preferable prescription of $\mu = 0.85$ Gev as discussed in [308].

initial and final hadronic states should correspond to the scale at which the hadronic matrix elements are evaluated. We also define

$$\begin{aligned} a_1(\mu) &= \frac{1}{2N_c}\big[C_+(\mu)(N_c+1) + C_-(\mu)(N_c-1)\big], \\ a_2(\mu) &= \frac{1}{2N_c}\big[C_+(\mu)(N_c+1) - C_-(\mu)(N_c-1)\big]. \end{aligned} \tag{4.196}$$

Then, we obtain

$$\Gamma(\text{ann.}) = \sum_{i=\tau,c} \frac{G_F^2}{8\pi} |V_{bc}|^2 f_{B_c}^2 M m_i^2 (1 - m_i^2/m_{Bc}^2)^2 \cdot C_i \,, \tag{4.197}$$

where $f_{B_c} \approx 400$ MeV (see below), $C_\tau = 1$ for the $\tau^+\nu_\tau$-channel, $C_c = 3|V_{cs}|^2 a_1^2$ for the $c\bar{s}$-channel, and the gluon corrections for the annihilation into hadrons go in the factor $a_1 = 1.22 \pm 0.04$ (see [328]). This estimate of the quark contribution does not depend on a hadronization model, since a large energy release, of the order of the meson mass, takes place. Moreover, one can see that the contributions from light leptons and quarks can be neglected.

As for the non-annihilation decays, in the approach of the OPE for the quark currents of weak decays [305], one takes into account α_s corrections to the free quark decays and uses the quark–hadron duality for the final states. Then one considers the matrix element for the transition operator over the meson state. The latter allows one also to take into account the effects caused by the motion and virtuality of the decaying quark inside the meson because of the interaction with the spectator. In this way the $\bar{b} \to \bar{c}c\bar{s}$ decay mode turns out to be suppressed almost completely due to the Pauli interference with the charm quark from the initial state. Besides, the c-quark decays with the spectator $\bar{b}$ quark are essentially suppressed in comparison with the free quark decays because of the large binding energy in the initial state.

Table 4.33: Summary of theoretical predictions in various approaches for the branching ratios of the B_c decay modes calculated in the framework of the inclusive OPE approach (see M. Beneke and G. Buchalla in [305]), by summing up the exclusive modes in potential models (for instance, in the model of [318, 319] used in [308]) and according to the semi-inclusive estimates in the sum rules of QCD and NRQCD [307–309].

B_c decay mode	OPE, %	PM, %	SR, %
$\bar{b}\to\bar{c}l^+\nu_l$	3.9 ± 1.0	3.7 ± 0.9	2.9 ± 0.3
$\bar{b}\to\bar{c}u\bar{d}$	16.2 ± 4.1	16.7 ± 4.2	13.1 ± 1.3
$\sum \bar{b}\to\bar{c}$	25.0 ± 6.2	25.0 ± 6.2	19.6 ± 1.9
$c\to sl^+\nu_l$	8.5 ± 2.1	10.1 ± 2.5	9.0 ± 0.9
$c\to su\bar{d}$	47.3 ± 11.8	45.4 ± 11.4	54.0 ± 5.4
$\sum c\to s$	64.3 ± 16.1	65.6 ± 16.4	72.0 ± 7.2
$B_c^+\to\tau^+\nu_\tau$	2.9 ± 0.7	2.0 ± 0.5	1.8 ± 0.2
$B_c^+\to c\bar{s}$	7.2 ± 1.8	7.2 ± 1.8	6.6 ± 0.7

In an exclusive approach it is necessary to sum up widths of different decay modes calculated in potential models. Considering the semileptonic decays due to the $\bar{b}\to\bar{c}l^+\nu_l$ and $c\to sl^+\nu_l$ transitions, one finds that the hadronic final states are practically saturated by the lightest $1S$ state in the $(\bar{c}c)$ system, i.e., η_c and J/ψ and the $1S$ states in the $(\bar{b}s)$ system, i.e., B_s and B_s^*. Further, the $\bar{b}\to\bar{c}u\bar{d}$ channel, for example, can be calculated through the decay width of $\bar{b}\to\bar{c}l^+\nu_l$, taking into account colour factors and hard gluon corrections to the four-quark interaction. It can be also obtained as a sum over the widths of decays to $(u\bar{d})$ bound states.

The results of the calculation of the B_c total width in the inclusive OPE and exclusive PM approaches give values that are consistent with each other, if one takes into account the most significant uncertainty, which is related to the choice of the quark masses (especially of the charm quark):

$$\tau[B_c^+]_{\text{OPE, PM}} = 0.55 \pm 0.15 \text{ ps}. \tag{4.198}$$

So, for instance, M. Beneke and G. Buchalla using OPE [305] give the estimate 0.4–0.7 ps (see Fig. 4.31), which slightly corrects a result by I. Bigi [305]: 0.4 ps. As for the potential approach, despite huge differences in details of exclusive estimates, models usually give a lifetime close to 0.4–0.6 ps, although the estimates strongly depend on the choice of the charm quark mass. We refer to the pioneering paper by M. Lusignoli and M. Masetti [317]. The obtained value agrees with the measured one (4.192). In Table 4.33 the reader may find summarized several theoretical results for inclusive decay channels.

The OPE estimates of inclusive decay rates agree with recent semi-inclusive calculations in the sum rules of QCD and NRQCD [307, 308], where one assumes the saturation of hadronic final states by the ground levels in the $c\bar{c}$ and $\bar{b}s$ systems as well as the factorization that allows to relate the semileptonic and hadronic decay modes. The Coulomb resummation plays an essential role in the B_c decays and removes the disagreement between the estimates in sum rules and OPE. In contrast to OPE, where the basic uncertainty is given by the heavy quark masses, these parameters are fixed by the two-point sum rules for bottomonia and charmonia, so that the accuracy of SR calculations for the total width of the B_c is determined by the choice of the scale μ for the hadronic weak Lagrangian in decays of charmed quarks. We show this dependence in Fig. 4.31, where $m_c/2 < \mu < m_c$. The dark shaded region corresponds to the scales preferred by the data on the charmed meson lifetimes. Choosing the scale in the $c\to s$ decays of B_c to be equal to $\mu_{B_c}^2 \approx (0.85 \text{ GeV})^2$, putting $a_1(\mu_{B_c}) = 1.20$ and neglecting the contributions of a nonzero a_2 in the charmed quark decays, in the framework of semi-inclusive sum rule calculations one obtains [308]

$$\tau[B_c]_{\text{SR}} = 0.48 \pm 0.05 \text{ ps}, \tag{4.199}$$

which agrees with the direct sum of exclusive channels presented in the next sections. In Fig. 4.31 we also show the exclusive estimate of the lifetime from Ref. [309].

8.2 Exclusive decays

Typical values for the exclusive decay branching ratios of the B_c, as obtained in QCD SR [308,309], are shown in Table 4.34 at given values of the factors $a_{1,2}$ and lifetime. The uncertainty of such predictions is about 15%, and the numbers essentially agree with most of the potential models within the theoretical uncertainties of the QCD SR estimates. In square bracket we show the marginal deviations from the central values obtained in some potential models.

In addition to the decay channels with a J/ψ well detectable through its leptonic mode, one could expect significant information on the dynamics of B_c decays coming from channels with a single heavy mesons, if the experimental efficiency is good enough to extract a signal from the cascade decays. Since decays to excited charmonia in the final state (like P waves) [331, 332], radiative leptonic modes [333] and some rare decays [334] are out of reach for the experimental facilities of the nearest future, we do not display them in Table 4.34.

In [309] the $\bar{b}$ decay to the doubly charmed states is predicted to give

$$\mathcal{B}(B_c^+ \to \bar{c}c\, c\bar{s}) \approx 1.39\%. \tag{4.200}$$

Comparing the width with the estimate from the spectator decay [305],

$$\Gamma(B_c^+ \to \bar{c}c\, c\bar{s})\big|_{\rm SR} \approx 20 \cdot 10^{-15}\,{\rm GeV}, \tag{4.201}$$

$$\Gamma(B_c^+ \to \bar{c}c\, c\bar{s})\big|_{\rm spect.} \approx 90 \times 10^{-15}\,{\rm GeV}, \tag{4.202}$$

we see that they differ by a factor of about $1/4.5$. The SR result is in agreement with an estimate in OPE by M. Beneke and G. Buchalla of [305], though the uncertainty is quite large ($\approx 60\%$) due to the mentioned uncertainty in the renormalization point as well as in the charm quark mass.

At present we can say that an accurate direct measurement of the B_c lifetime can provide information on the masses of the c and b quarks and the normalization point of the non-leptonic weak Lagrangian in the B_c decays (the a_1 and a_2 factors). The experimental study of semileptonic decays and the extraction of ratios of form factors can test the spin symmetry of NRQCD and HQET and decrease the uncertainties in the corresponding theoretical evaluation of the quark parameters as well as the hadronic matrix elements. The measurement of branching fractions for semileptonic and non-leptonic modes and their ratios can give information on the values of the factorization parameters, which depend again on the normalization of the non-leptonic weak Lagrangian. The charm quark counting in the B_c decays is related to the overall contribution of b quark decays as well as to the suppression of $\bar{b}\to c\bar{c}\bar{s}$ transitions because of the destructive interference, whose value depends on the nonperturbative parameters (roughly said, the leptonic constant) and on the non-leptonic weak Lagrangian.

8.2.1 Semileptonic decays

The semileptonic decay rates estimated in the QCD sum rules for 3-point correlators [335] are underestimated in [327], because large Coulomb-like corrections were not taken into account. The recent analysis of SR in [306–308] decreased the uncertainty, so that the estimates agree with the calculations in the potential models.

(A) Coulomb resummation

For the heavy quarkonium $\bar{b}c$, where the relative quark velocity is small, Coulomb-like $\alpha_{\rm s}/v$ corrections are important and have to be resummed. It is well known that taking into account these corrections in two-point sum rules numerically enhances the Born value of the spectral density by a factor two or three [316].

Table 4.34: QCD SR predictions [308, 309] for the branching ratios of exclusive B_c^+ decays with the choice of factors: $a_1^c = 1.20$ and $a_2^c = -0.317$ in the non-leptonic decays of the c quark, and $a_1^b = 1.14$ and $a_2^b = -0.20$ in the non-leptonic decays of the $\bar{b}$ quark. The lifetime of the B_c is taken $\tau[B_c] \approx 0.45$ ps. The uncertainty of the widths is estimated to be about 15%. The numbers in square brackets show the marginal values obtained in some potential models [325, 326, 329, 330]. The maximal difference is of one order of magnitude.

Mode	BR, %		Mode	BR, %	
$B_c^+ \to \eta_c e^+ \nu$	0.75	[0.5]	$B_c^+ \to \eta_c D_s^{*+}$	0.27	[0.07]
$B_c^+ \to \eta_c \tau^+ \nu$	0.23	[0.2]	$B_c^+ \to J/\psi D_s^+$	0.17	[0.05]
$B_c^+ \to \eta_c' e^+ \nu$	0.020	[0.05]	$B_c^+ \to J/\psi D_s^{*+}$	0.67	[0.5]
$B_c^+ \to \eta_c' \tau^+ \nu$	0.0016	[–]	$B_c^+ \to \eta_c D^+$	0.015	[0.04]
$B_c^+ \to J/\psi e^+ \nu$	1.9	[1]	$B_c^+ \to \eta_c D^{*+}$	0.010	[0.002]
$B_c^+ \to J/\psi \tau^+ \nu$	0.48	[0.35]	$B_c^+ \to J/\psi D^+$	0.009	[0.002]
$B_c^+ \to \psi' e^+ \nu$	0.094	[0.2]	$B_c^+ \to J/\psi D^{*+}$	0.028	[0.014]
$B_c^+ \to \psi' \tau^+ \nu$	0.008	[–]	$B_c^+ \to B_s^0 \pi^+$	16.4	[1.6]
$B_c^+ \to D^0 e^+ \nu$	0.004	[0.02]	$B_c^+ \to B_s^0 \rho^+$	7.2	[2.4]
$B_c^+ \to D^0 \tau^+ \nu$	0.002	[0.08]	$B_c^+ \to B_s^{*0} \pi^+$	6.5	[1.3]
$B_c^+ \to D^{*0} e^+ \nu$	0.018	[0.004]	$B_c^+ \to B_s^{*0} \rho^+$	20.2	[11]
$B_c^+ \to D^{*0} \tau^+ \nu$	0.008	[0.016]	$B_c^+ \to B_s^0 K^+$	1.06	[0.2]
$B_c^+ \to B_s^0 e^+ \nu$	4.03	[1]	$B_c^+ \to B_s^{*0} K^+$	0.37	[0.13]
$B_c^+ \to B_s^{*0} e^+ \nu$	5.06	[1.2]	$B_c^+ \to B_s^0 K^{*+}$	–	
$B_c^+ \to B^0 e^+ \nu$	0.34	[0.08]	$B_c^+ \to B_s^{*0} K^{*+}$	–	
$B_c^+ \to B^{*0} e^+ \nu$	0.58	[0.15]	$B_c^+ \to B^0 \pi^+$	1.06	[0.1]
$B_c^+ \to \eta_c \pi^+$	0.20	[0.12]	$B_c^+ \to B^0 \rho^+$	0.96	[0.2]
$B_c^+ \to \eta_c \rho^+$	0.42	[0.3]	$B_c^+ \to B^{*0} \pi^+$	0.95	[0.08]
$B_c^+ \to J/\psi \pi^+$	0.13	[0.08]	$B_c^+ \to B^{*0} \rho^+$	2.57	[0.6]
$B_c^+ \to J/\psi \rho^+$	0.40	[0.2]	$B_c^+ \to B^0 K^+$	0.07	[0.01]
$B_c^+ \to \eta_c K^+$	0.013	[0.008]	$B_c^+ \to B^0 K^{*+}$	0.015	[0.012]]
$B_c^+ \to \eta_c K^{*+}$	0.020	[0.018]	$B_c^+ \to B^{*0} K^+$	0.055	[0.006]
$B_c^+ \to J/\psi K^+$	0.011	[0.007]	$B_c^+ \to B^{*0} K^{*+}$	0.058	[0.04]
$B_c \to J/\psi K^{*+}$	0.022	[0.016]	$B_c^+ \to B^+ \overline{K^0}$	1.98	[0.18]
$B_c^+ \to D^+ \overline{D}^0$	0.0053	[0.0018]	$B_c^+ \to B^+ \overline{K^{*0}}$	0.43	[0.09]
$B_c^+ \to D^+ \overline{D}^{*0}$	0.0075	[0.002]	$B_c^+ \to B^{*+} \overline{K^0}$	1.60	[0.06]
$B_c^+ \to D^{*+} \overline{D}^0$	0.0049	[0.0009]	$B_c^+ \to B^{*+} \overline{K^{*0}}$	1.67	[0.6]
$B_c^+ \to D^{*+} \overline{D}^{*0}$	0.033	[0.003]	$B_c^+ \to B^+ \pi^0$	0.037	[0.004]
$B_c^+ \to D_s^+ \overline{D}^0$	0.00048	[0.0001]	$B_c^+ \to B^+ \rho^0$	0.034	[0.01]
$B_c^+ \to D_s^+ \overline{D}^{*0}$	0.00071	[0.00012]	$B_c^+ \to B^{*+} \pi^0$	0.033	[0.003]
$B_c^+ \to D_s^{*+} \overline{D}^0$	0.00045	[0.00005]	$B_c^+ \to B^{*+} \rho^0$	0.09	[0.03]
$B_c^+ \to D_s^{*+} \overline{D}^{*0}$	0.0026	[0.0002]	$B_c^+ \to \tau^+ \nu_\tau$	1.6	
$B_c^+ \to \eta_c D_s^+$	0.28	[0.07]	$B_c^+ \to c\bar{s}$	4.9	

(B) Primary modes

In practice, the most important information comes from the ψ mode, since this charmonium is clearly detected in experiments [224, 301]. In addition to the investigation of various form factors and their dependence on the momentum transfer squared, the measurement of the decay to ψ', could answer the question of the reliability of QCD predictions for the decays to excited states. At present, finite energy sum rules predict the width of the $B_c^+ \to \psi' l^+ \nu$ decay in reasonable agreement with potential models if one takes into account an uncertainty of about 50%.

(C) Relations between the form factors

In the limit of infinitely heavy quark masses, the NRQCD and HQET Lagrangians possess spin symmetry. The most familiar implication of such symmetry is the common Isgur–Wise function determining the form factors in the semileptonic decays of single heavy hadrons. In contrast to weak decays with a light spectator quark, the B_c decays to ψ, η_c and $B_s^{(*)}$ involve the heavy spectator, so that the spin symmetry works only at recoil momenta close to zero, where the spectator enters the heavy hadron in the final state with no hard gluon rescattering. Hence, we expect relations between the form factors in the vicinity of zero recoil. The normalization of the form factor is not fixed, as it is in decays of hadrons with a single heavy quark, since the heavy quarkonia wave functions are flavour dependent. In practice, the ratios of form factors, which are fixed at zero recoil, are expected to exhibit a dependence on the momentum transfer squared, which is not significant in actual numerical estimates in the restricted region of the physical phase space. The SR estimates of the form factors show a good agreement with the expectations, whereas the deviations can be traced back to the difference in the q^2 evolution of the form factors from the zero recoil point. This can be neglected within the accuracy of the SR method for the transitions of $B_c \to \bar{c}c$, as shown in [307]. The $1/m_Q$ deviations from the symmetry relations in the decays of $B_c^+ \to B_s^{(*)} e^+ \nu$ are about 10–15%, as found in the QCD sum rules considered in [308]. Form factors for specific decay channels have been considered also in [322, 331].

The combinations of relations derived in [307, 308] reproduce the only equality in [336], which was found for each mode in the strict limit of $v_1 = v_2$ also considered by Sanchis–Lozano in [337].

8.2.2 Leptonic decays

The dominant leptonic decay of the B_c is given by the $\tau \nu_\tau$ mode (see Table 4.33). However, it has a low experimental efficiency of detection because of the hadronic background in the τ decays. Recently, in Refs. [333] the enhancement of muon and electron channels in the radiative modes has been studied. The additional photon removes the helicity suppression for the leptonic decay of pseudoscalar particles, leading to an increase of the muonic mode by about a factor two.

(A) Leptonic constant of B_c

In NRQCD the calculation of the leptonic constant for the heavy quarkonium with two-loop accuracy requires the two-loop matching of the NRQCD currents with the currents in full QCD,

$$J_\nu^{\rm QCD} = \bar{Q}_1 \gamma_5 \gamma_\nu Q_2, \quad \mathcal{J}_\nu^{\rm NRQCD} = -\chi^\dagger \psi \, v_\nu, \qquad J_\nu^{\rm QCD} = \mathcal{K}(\mu_{\rm hard}; \mu_{\rm fact}) \, \mathcal{J}_\nu^{\rm NRQCD}(\mu_{\rm fact}),$$

where the scale $\mu_{\rm hard}$ gives the normalization point for the matching of NRQCD with full QCD, while $\mu_{\rm fact}$ denotes the normalization point for the calculations in perturbation theory in NRQCD.

For the pseudoscalar heavy quarkonium composed of heavy quarks with different flavours, the Wilson coefficient $\mathcal{K}$ has been calculated with two-loop accuracy in Refs. [338] and [339]. In NRQCD the current $\mathcal{J}_\nu^{\rm NRQCD}$ has nonzero anomalous dimension, so that we find

$$\langle 0 | \mathcal{J}_\nu^{\rm NRQCD}(\mu) | \bar{Q} Q \rangle = \mathcal{A}(\mu) \, v_\nu f_{\bar{Q}Q}^{\rm NRQCD} M_{\bar{Q}Q}, \tag{4.203}$$

where, in terms of nonrelativistic quarks, the leptonic constant for the heavy quarkonium is given by the well-known relation with the wave function at the origin.

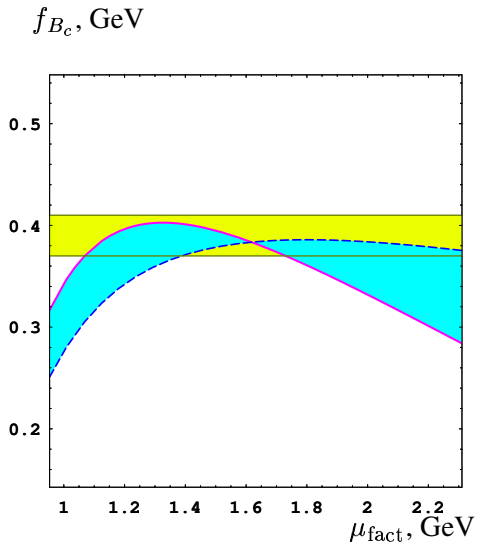

Fig. 4.32: The leptonic constant of the B_c is presented versus the soft scale of normalization. The shaded region restricted by curves corresponds to the change of the hard scale from $\mu_{\rm hard} = 3$ Gev (the dashed curve) to $\mu_{\rm hard} = 2$ Gev (the solid curve) with the initial condition for the evolution of the normalization factor $\mathcal{A}(\mu_{\rm fact})$, $\mathcal{A}(1.2\ {\rm GeV}) = 1$ and $\mathcal{A}(1\ {\rm GeV}) = 1$ respectively, in the nonrelativistic current matrix element. The horizontal band is the region expected from the QCD sum rules [306,327,340] and scaling relations for the leptonic constants of heavy quarkonia [341]. In the overlap region, the leptonic constant of B_c depends weakly on the parameters.

Following the method described in [342,343], one can estimate the wave function of the $\bar{b}c$ quarkonium using the static potential given in [342]. Details of the calculations can be found in [344]. The result of the calculation of the B_c leptonic constant is shown in Fig. 4.32. The final result of the two-loop calculation is

$$f_{B_c} = 395 \pm 15\ {\rm MeV}, \tag{4.204}$$

which is close to an early estimate by S. Capstick and S. Godfrey in [304].

The result on f_{B_c} is in agreement with the scaling relation derived from the quasi-local QCD sum rules [341], which use the regularity in the heavy quarkonium mass spectra, i.e., the fact that the splitting between the quarkonium levels after averaging over the spins of the heavy quarks depends weakly on the quark flavours. So, the scaling law for S-wave quarkonia has the form

$$\frac{f_n^2}{M_n}\left(\frac{M_n}{M_1}\right)^2\left(\frac{m_1+m_2}{4\mu_{12}}\right)^2 = \frac{c}{n}, \tag{4.205}$$

where n is the radial quantum number, $m_{1,2}$ the masses of the heavy quarks composing the quarkonium, μ_{12} the reduced mass and c a dimensional constant independent on both the quark flavours and n. The accuracy depends on the heavy quark masses, and is discussed in detail in [341]. The parameter c can be extracted from the known leptonic constants of ψ and Υ.

8.2.3 Non-leptonic modes

With respect to the inclusive non-leptonic widths, which can be estimated in the framework of quark–hadron duality (see Table 4.33), the calculation of exclusive modes usually involves factorization [86, 345], which, as expected, can be quite accurate for the B_c, since the quark–gluon sea is suppressed in the heavy quarkonium. Thus, the important parameters are the factors a_1 and a_2 in the non-leptonic weak Lagrangian, which depend on the normalization point.

The agreement of QCD SR estimates for the non-leptonic decays of the charm quark in the B_c with the values predicted by potential models is rather good for the direct transitions with no permutation of

colour lines, i.e., processes involving the factor a_1 in the non-leptonic amplitude. In contrast, the sum rule predictions are significantly enhanced in comparison with the values calculated in potential models for transitions with colour permutation, i.e., for processes involving the factor a_2 (see Table 4.34). Further, for transitions $\bar{b}\to c\bar{c}s$ where the interference is significantly involved the size of the interference is about 35–50% of the width evaluated by neglecting interference terms. These estimates are in agreement with the potential models of Refs. [322, 325].

At large recoils as in $B_c^+\to\psi\pi^+(\rho^+)$, the spectator picture of transition can be broken by hard gluon exchanges [346]. The spin effects in such decays were studied in [332]. Typically recoil effects are taken into account to some extent in any relativistic approach like [322].

For the widths of non-leptonic c-quark decays the sum rule estimates are typically greater than those of potential models[24]. In this respect we note that the QCD SR calculations are consistent with the inclusive ones. Summing up the calculated exclusive widths, the total width of the B_c meson is shown in Fig. 4.31, which points to a good agreement of the exclusive calculations with those of OPE and semi-inclusive estimates.

Another interesting point is the possibility to extract the factorization parameters a_1 and a_2 in the c-quark decays by measuring the ratios of widths

$$\frac{\Gamma(B_c^+\to B^{(*)+}\bar{K}^{(*)0})}{\Gamma(B_c^+\to B^{(*)0}K^{(*)+})}=\left|\frac{V_{cs}}{V_{cd}^2}\right|^2\frac{a_2^2}{a_1^2}, \tag{4.206}$$

where one should take identical sets of pseudoscalar and vector states in both decays. This procedure can give a test for the factorization approach itself.

The suppressed decays caused by the flavour changing neutral currents were studied in [334].

(A) CP violation in B_c decays

CP violation in B_c decays can be investigated in the same way as in B decays. The expected CP asymmetry of $\mathcal{A}(B_c^\pm\to J/\psi D^\pm)$ is about 4×10^{-3}, when the corresponding branching ratio is suppressed as 10^{-4} [299]. Therefore, the direct study of CP violation in B_c decays is practically difficult because of the low relative yield of B_c with respect to ordinary B mesons: $\sigma(B_c)/\sigma(B)\sim10^{-3}$.

As mentioned at the beginning, the B_c meson is expected to be copiously produced in future colliders. In such circumstances a possible challenge is whether one could get an opportunity to extract some information about the CKM unitarity triangle from the B_c in a model independent way. Indeed, there is such an opportunity for the angle γ using the strategy of the reference triangles [352] in the decays of doubly heavy hadrons. This strategy for the study of CP violation in B_c decays was originally proposed by M. Masetti [299], independently investigated by R. Fleischer and D. Wyler [299] and extended to the case of doubly heavy baryons in [353]. Other possibilities include the lepton tagging of B_s in the $B_c^\pm\to B_s^{(*)}l^\pm\nu$ decays for the study of mixing and CP violation in the B_s sector [354], and a possible transverse polarization of the τ lepton in $B_c\to\tau\bar{\nu}_\tau\gamma$ [347].

The triangle strategy is based on the direct determination of absolute values for the set of four decays, at least: the decays of the hadron into the tagged D^0 meson, the tagged $\bar{D}^0$ meson, the tagged CP-even state of D^0, and the decay of the anti-hadron into the tagged CP-even state of D^0. To illustrate the point, let us consider the decays

$$B_c^+\to D^0D_s^+\quad\text{and}\quad B_c^+\to\bar{D}^0D_s^+.$$

The corresponding diagrams with the decay of $\bar{b}$-quark are shown in Figs. 4.33 and 4.34.

The exclusive modes do not have penguin terms at the leading order in the Fermi constant G_F that we consider here. However, the diagram with the weak annihilation of two constituents, i.e., the

[24] See also the recent discussions on the B_c decays in [329, 330, 347–351].

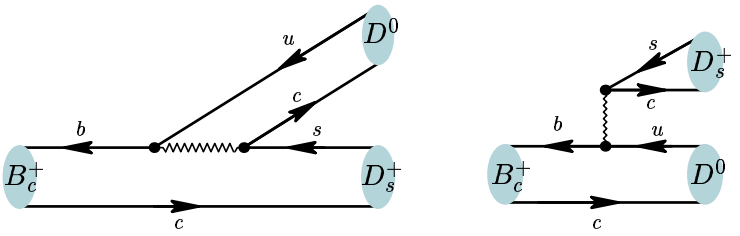

Fig. 4.33: The diagrams of $\bar{b}$-quark decay contributing to the weak transition $B_c^+ \to D^0 D_s^+$.

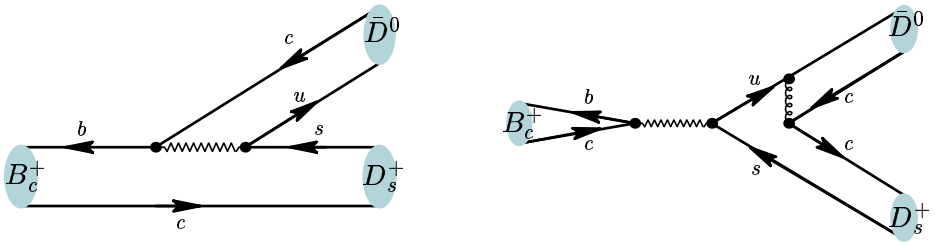

Fig. 4.34: The diagrams of $\bar{b}$-quark decay contributing to the weak transition $B_c^+ \to \bar{D}^0 D_s^+$.

charmed quark and beauty antiquark in the B_c^+ meson, can contribute at the next order in α_s as shown in Fig. 4.34 for the given final state. Nevertheless, we see that such diagrams have the same weak-interaction structure as at tree level. The magnitude of the α_s corrections to the absolute values of the corresponding decay widths is discussed in [300]. We expect the sides of the reference-triangles to be of the same order of magnitude, which makes the method an attractive way to extract the angle γ.

The predictions of QCD sum rules for the exclusive decays of B_c are summarized in Table 4.35 at fixed values of $a_{1,2}$ and lifetime. For the sake of completeness and comparison we show the estimates for the channels with the neutral D meson and charged D^+ as well as for the vector states in addition to the pseudoscalar ones.

First, we see that the similar decay modes without the strange quark in the final state can also be used, in principle, for the extraction of γ, however, these channels are more problematic since the sides of the reference-triangles significantly differ from each other[25], so that the measurements have to be extremely accurate to get useful information on the angle, which means that one has to accumulate a huge statistics for the dominant mode.

Second, the decay modes with the vector neutral D meson in the final state are useless for the purpose of the CKM measurement under the discussed approach. However, the modes with the vector charged D^* and D_s^* mesons can be important for the extraction of γ. For instance, one could consider the modes $D^{*+} \to D^0 \pi^+$ and $D^0 \to K^- \pi^+$. The neutral charmed meson should be carefully treated in order to avoid misidentification with the primary one. Otherwise, one could use the mode with the neutral pion, $D^{*+} \to D^+ \pi^0$, whose detection in an experimental facility could be problematic. The same considerations apply to the vector meson D_s^{*+}, whose radiative electromagnetic decay is also problematic for the detection, since the photon could be easily lost. On the other hand, the loss of the photon does not disturb the analysis in the case of fully reconstructed D_s^+ and B_c^+.

In the BTeV [310] and LHCb [311] experiments one expects the B_c production at the level of several billion events. Therefore, one expects 10^4–10^5 decays of B_c in the gold-plated modes under interest.

[25] The ratio of widths is basically determined by $|V_{cb} V_{ud} a_2|^2 / |V_{ub} V_{cd} a_1|^2 \sim 110$, if we ignore the interference effects.

Table 4.35: QCD SR predictions [300] for the branching ratios of exclusive B_c^+ decays with the choice of factors: $a_1^b = 1.14$ and $a_2^b = -0.20$ in the non-leptonic decays of $\bar{b}$ quark. The lifetime of the B_c is taken $\tau[B_c] \approx 0.45$ ps. For comparison we show in square brackets minimal values estimated in the potential models of [299].

Mode	BR, 10^{-6}		Mode	BR, 10^{-6}	
$B_c^+ \to D^+ \overline{D}^0$	53	[18]	$B_c^+ \to D^+ D^0$	0.32	[0.1]
$B_c^+ \to D^+ \overline{D}^{*0}$	75	[20]	$B_c^+ \to D^+ D^{*0}$	0.28	[0.07]
$B_c^+ \to D^{*+} \overline{D}^0$	49	[9]	$B_c^+ \to D^{*+} D^0$	0.40	[0.4]
$B_c^+ \to D^{*+} \overline{D}^{*0}$	330	[30]	$B_c^+ \to D^{*+} D^{*0}$	1.59	[0.4]
$B_c^+ \to D_s^+ \overline{D}^0$	4.8	[1]	$B_c^+ \to D_s^+ D^0$	6.6	[1.7]
$B_c^+ \to D_s^+ \overline{D}^{*0}$	7.1	[1.2]	$B_c^+ \to D_s^+ D^{*0}$	6.3	[1.3]
$B_c^+ \to D_s^{*+} \overline{D}^0$	4.5	[0.5]	$B_c^+ \to D_s^{*+} D^0$	8.5	[8.1]
$B_c^+ \to D_s^{*+} \overline{D}^{*0}$	26	[2]	$B_c^+ \to D_s^{*+} D^{*0}$	40.4	[6.2]

The experimental challenge is the efficiency of detection. One usually gets a 10% efficiency for the observation of distinct secondary vertices outstanding from the primary vertex of beam interaction. Next, one has to take into account the branching ratios of D_s and D^0 mesons. This efficiency crucially depends on whether one can detect the neutral kaons and pions or not. So, for the D_s meson the corresponding branching ratios grow from 4% (no neutral K and π) to 25%. The same interval for the neutral D^0 is from 11% to 31%. The detection of neutral kaon is necessary for the measurement of decay modes into the CP-odd state D_2 of the neutral D^0 meson, however, one can omit this cross-check channel from the analysis in dealing with the CP-even state D_1. The corresponding intervals of branching ratios reachable by the experiments are from 0.5% to 1.3% for the CP-even state and from 1.5% to 3.8% for the CP-odd state of D^0. A pessimistic estimate for the product of branching ratios is about 2×10^{-4}, which results in 2–20 reconstructed events.

REFERENCES

[1] C. Patrignani, Phys. Rev. D **64**, 034017 (2001) [arXiv:hep-ex/0104003].

[2] T. Sjostrand, "PYTHIA 5.7 and JETSET 7.4: Physics and manual," arXiv:hep-ph/95 08391.

[3] H. m. Hu and A. Tai, in *Proc. of the e^+e^- Physics at Intermediate Energies Conference* ed. Diego Bettoni, eConf **C010430**, T24 (2001) [arXiv:hep-ex/0106017].

[4] J. C. Chen, G. S. Huang, X. R. Qi, D. H. Zhang and Y. S. Zhu, Phys. Rev. D **62**, 034003 (2000).

[5] G. Garzoglio *et al.*, Nucl. Instrum. Meth. A **519**, 558 (2004).

[6] M. Andreotti *et al.* [Fermilab E835 Collaboration], Phys. Rev. Lett. **91**, 091801 (2003) [arXiv:hep-ex/0308055].

[7] M. Benayoun, S. I. Eidelman, V. N. Ivanchenko and Z. K. Silagadze, Mod. Phys. Lett. A **14**, 2605 (1999) [arXiv:hep-ph/9910523].

[8] J. Z. Bai *et al.* [BES Collaboration], Phys. Rev. D **57**, 3854 (1998).

[9] B. Aubert *et al.* [BaBar Collaboration], Phys. Rev. D **69**, 011103 (2004) [arXiv:hep-ex/0310027].

[10] S. Eidelman *et al.* [Particle Data Group Collaboration], Phys. Lett. B **592**, 1 (2004).

[11] T. Appelquist and H. D. Politzer, Phys. Rev. Lett. **34**, 43 (1975).

[12] R. Barbieri, R. Gatto and E. Remiddi, Phys. Lett. B **61**, 465 (1976).

[13] W. E. Caswell and G. P. Lepage, Phys. Lett. B **167**, 437 (1986).

[14] G. T. Bodwin, E. Braaten and G. P. Lepage, Phys. Rev. D **51**, 1125 (1995) [Erratum-ibid. D **55**, 5853 (1997)] [arXiv:hep-ph/9407339].

[15] G. T. Bodwin, E. Braaten and G. P. Lepage, Phys. Rev. D **46**, 1914 (1992) [arXiv:hep-lat/9205006].

[16] N. Brambilla, D. Eiras, A. Pineda, J. Soto and A. Vairo, Phys. Rev. D **67**, 034018 (2003) [arXiv:hep-ph/0208019].

[17] M. Beneke, arXiv:hep-ph/9703429; S. Fleming, I. Z. Rothstein and A. K. Leibovich, Phys. Rev. D **64**, 036002 (2001) [arXiv:hep-ph/0012062].

[18] A. Pineda and A. Vairo, Phys. Rev. D **63**, 054007 (2001) [Erratum-ibid. D **64**, 039902 (2001)] [arXiv:hep-ph/0009145].

[19] A. Petrelli, M. Cacciari, M. Greco, F. Maltoni and M. L. Mangano, Nucl. Phys. B **514**, 245 (1998) [arXiv:hep-ph/9707223].

[20] F. Maltoni, *Quarkonium phenomenology*, PhD thesis (Univ. of Pisa, 1999) [http://www.fis.uniroma3.it/∼maltoni/thesis.ps].

[21] H. W. Huang and K. T. Chao, Phys. Rev. D **54**, 3065 (1996) [Erratum-ibid. D **56**, 7472 (1997 ERRAT,D60,079901.1999)] [arXiv:hep-ph/9601283].

[22] R. Barbieri, M. Caffo, R. Gatto and E. Remiddi, Phys. Lett. B **95**, 93 (1980); Nucl. Phys. B **192**, 61 (1981).

[23] P. B. Mackenzie and G. P. Lepage, Phys. Rev. Lett. **47**, 1244 (1981).

[24] M. Gremm and A. Kapustin, Phys. Lett. B **407**, 323 (1997) [arXiv:hep-ph/9701353].

[25] A. Czarnecki and K. Melnikov, Phys. Rev. Lett. **80**, 2531 (1998) [arXiv:hep-ph/9712222].

[26] M. Beneke, A. Signer and V. A. Smirnov, Phys. Rev. Lett. **80**, 2535 (1998) [arXiv:hep-ph/9712302].

[27] R. Barbieri, G. Curci, E. d'Emilio and E. Remiddi, Nucl. Phys. B **154**, 535 (1979); K. Hagiwara, C. B. Kim and T. Yoshino, Nucl. Phys. B **177**, 461 (1981).

[28] A. Vairo, Mod. Phys. Lett. A **19**, 253 (2004) [arXiv:hep-ph/0311303].

[29] G. T. Bodwin and A. Petrelli, Phys. Rev. D **66**, 094011 (2002) [arXiv:hep-ph/0205210].

[30] J. P. Ma and Q. Wang, Phys. Lett. B **537**, 233 (2002) [arXiv:hep-ph/0203082].

[31] A. A. Penin, A. Pineda, V. A. Smirnov and M. Steinhauser, Nucl. Phys. B **699**, 183 (2004) [arXiv:hep-ph/0406175].

[32] G. T. Bodwin and Y. Q. Chen, Phys. Rev. D **64**, 114008 (2001) [arXiv:hep-ph/0106095]; ibid. D **60**, 054008 (1999) [arXiv:hep-ph/9807492]; E. Braaten and Y. Q. Chen, Phys. Rev. D **57**, 4236 (1998) [Erratum-ibid. D **59**, 079901 (1999)] [arXiv:hep-ph/9710357].

[33] M. L. Mangano and A. Petrelli, Phys. Lett. B **352**, 445 (1995) [arXiv:hep-ph/9503465].

[34] F. Maltoni, arXiv:hep-ph/0007003.

[35] R. Mussa, *talk at the 2^{nd} QWG Workshop, Fermilab, 2003*, http://www.qwg.to.infn.it/WS-sep03/index.html.

[36] G. T. Bodwin, D. K. Sinclair and S. Kim, Phys. Rev. D **65**, 054504 (2002) [arXiv:hep-lat/0107011].

[37] G. T. Bodwin, D. K. Sinclair and S. Kim, Phys. Rev. Lett. **77**, 2376 (1996) [arXiv:hep-lat/9605023].

[38] E. J. Eichten and C. Quigg, Phys. Rev. D **52**, 1726 (1995) [arXiv:hep-ph/9503356].

[39] G. S. Bali, Phys. Rept. **343**, 1 (2001) [arXiv:hep-ph/0001312].

[40] A. Vairo, arXiv:hep-ph/0212271.

[41] A. Pineda and J. Soto, Nucl. Phys. Proc. Suppl. **64**, 428 (1998) [arXiv:hep-ph/9707481].

[42] N. Brambilla, A. Pineda, J. Soto and A. Vairo, Nucl. Phys. B **566**, 275 (2000) [arXiv:hep-ph/9907240].

[43] N. Brambilla, A. Pineda, J. Soto and A. Vairo, Phys. Lett. B **470**, 215 (1999) [arXiv:hep-ph/9910238].

[44] N. Brambilla and A. Vairo, arXiv:hep-ph/0004192.

[45] S. Titard and F. J. Yndurain, Phys. Rev. D **49**, 6007 (1994) [arXiv:hep-ph/9310236]; F. J. Yndurain,

arXiv:hep-ph/0007333.

[46] A. Pineda, Nucl. Phys. B **494**, 213 (1997) [arXiv:hep-ph/9611388].

[47] A. Pineda, Phys. Rev. D **66**, 054022 (2002) [arXiv:hep-ph/0110216].

[48] A. Pineda, Acta Phys. Polon. B **34**, 5295 (2003) [arXiv:hep-ph/0404225].

[49] K. Melnikov and A. Yelkhovsky, Phys. Rev. D **59**, 114009 (1999) [arXiv:hep-ph/9805270]; A. A. Penin and A. A. Pivovarov, "Bottom quark pole mass and |V(cb)| matrix element from R(e+ e- → b Nucl. Phys. B **549**, 217 (1999) [arXiv:hep-ph/9807421].

[50] A. Gray *et al.* [HPQCD collaboration], Nucl. Phys. Proc. Suppl. **119**, 592 (2003) [arXiv:hep-lat/0209022].

[51] N. Brambilla, D. Eiras, A. Pineda, J. Soto and A. Vairo, Phys. Rev. Lett. **88**, 012003 (2002) [arXiv:hep-ph/0109130].

[52] N. Brambilla, A. Pineda, J. Soto and A. Vairo, Phys. Lett. B **580**, 60 (2004) [arXiv:hep-ph/0307159].

[53] N. Brambilla, A. Pineda, J. Soto and A. Vairo, Phys. Rev. D **63**, 014023 (2001) [arXiv:hep-ph/0002250].

[54] G. Amoros, M. Beneke and M. Neubert, Phys. Lett. B **401**, 81 (1997) [arXiv:hep-ph/9701375].

[55] G. S. Bali and A. Pineda, Phys. Rev. D **69**, 094001 (2004) [arXiv:hep-ph/0310130]; M. Foster and C. Michael [UKQCD Collaboration], Phys. Rev. D **59**, 094509 (1999) [arXiv:hep-lat/9811010]; G. S. Bali, N. Brambilla and A. Vairo, Phys. Lett. B **421**, 265 (1998) [arXiv:hep-lat/9709079]; M. D'Elia, A. Di Giacomo and E. Meggiolaro, Phys. Lett. B **408**, 315 (1997) [arXiv:hep-lat/9705032].

[56] A. Di Giacomo, H. G. Dosch, V. I. Shevchenko and Y. A. Simonov, Phys. Rept. **372**, 319 (2002) [arXiv:hep-ph/0007223]; N. Brambilla, arXiv:hep-ph/0012211; M. Baker, N. Brambilla, H. G. Dosch and A. Vairo, Phys. Rev. D **58**, 034010 (1998) [arXiv:hep-ph/9802273].

[57] A. Vairo, Nucl. Phys. Proc. Suppl. **115**, 166 (2003) [arXiv:hep-ph/0205128].

[58] G. S. Adams *et al.* [CLEO Collaboration], submitted to Phys. Rev. Lett. [arXiv:hep-ex/0409027].

[59] J. Z. Bai *et al.* [BES Collaboration], Phys. Lett. B **550**, 24 (2002) [arXiv:hep-ph/0209354].

[60] J. Z. Bai *et al.* [BES Collaboration], Phys. Rev. D **65**, 052004 (2002) [arXiv:hep-ex/0010072].

[61] T. A. Armstrong *et al.* [E760 Collaboration], Nucl. Phys. B **373**, 35 (1992).

[62] T. A. Armstrong *et al.* [E760 Collaboration], Phys. Rev. Lett. **70**, 2988 (1993).

[63] B. I. Eisenstein *et al.* [CLEO Collaboration], Phys. Rev. Lett. **87**, 061801 (2001) [arXiv:hep-ex/0104042].

[64] M. Andreotti *et al.* [Fermilab E835 Collaboration], Phys. Lett. B **584**, 16 (2004).

[65] J. Z. Bai *et al.* [BES Collaboration], Phys. Rev. Lett. **81**, 3091 (1998) [arXiv:hep-ex/9807001].

[66] J. Z. Bai *et al.* [BES Collaboration], Phys. Rev. D **60**, 072001 (1999) [arXiv:hep-ex/9812016].

[67] J. Z. Bai *et al.* [BES Collaboration], Phys. Rev. D **67**, 032004 (2003) [arXiv:hep-ex/0109040].

[68] D. M. Asner *et al.* [CLEO Collaboration], Phys. Rev. Lett. **92**, 142001 (2004) [arXiv:hep-ex/0312058].

[69] S. Bagnasco *et al.* [E835 Collaboration], Phys. Lett. B **553**, 237 (2002); N. Pastrone [E835 Collaboration], arXiv:hep-ex/0306032; R. Mussa, *talk at the 2nd QWG Workshop, Fermilab, 2003*, http://www.qwg.to.infn.it/WS-sep03/index.html.

[70] D. E. Groom *et al.* [Particle Data Group Collaboration], Eur. Phys. J. C **15**, 1 (2000).

[71] S. Fleming and A. K. Leibovich, Phys. Rev. Lett. **90**, 032001 (2003) [arXiv:hep-ph/0211303]; Phys. Rev. D **67**, 074035 (2003) [arXiv:hep-ph/0212094].

[72] B. Nemati *et al.* [CLEO Collaboration], Phys. Rev. D **55**, 5273 (1997) [arXiv:hep-ex/9611020].

[73] S. Behrends *et al.* [CLEO Collaboration], Phys. Rev. D **31**, 2161 (1985).

[74] M. Artuso *et al.* [CLEO Collaboration], Phys. Rev. D **67**, 052003 (2003) [arXiv:hep-ex/0211029].

[75] S. J. Brodsky *et al.*, Phys. Lett. B **73**, 203 (1978); K. Koller and T. Walsh, Nucl. Phys. B **140**, 449 (1978).

[76] F. Maltoni and A. Petrelli, Phys. Rev. D **59**, 074006 (1999) [arXiv:hep-ph/9806455].

[77] S. Catani and F. Hautmann, Nucl. Phys. Proc. Suppl. **39BC**, 359 (1995) [arXiv:hep-ph/9410394].

[78] I. Z. Rothstein and M. B. Wise, Phys. Lett. B **402**, 346 (1997) [arXiv:hep-ph/9701404].

[79] D. Buskulic *et al.* [ALEPH Collaboration], Z. Phys. C **69**, 365 (1996).

[80] M. Kramer, Phys. Rev. D **60**, 111503 (1999) [arXiv:hep-ph/9904416].

[81] C. W. Bauer *et al.*, Phys. Rev. D **63**, 014006 (2001); C. W. Bauer *et al.*, Phys. Rev. D **63**, 114020 (2001).

[82] C. W. Bauer and I. W. Stewart, Phys. Lett. B **516**, 134 (2001) [arXiv:hep-ph/0107001]; C. W. Bauer, D. Pirjol and I. W. Stewart, Phys. Rev. D **65**, 054022 (2002) [arXiv:hep-ph/0109045].

[83] F. Hautmann, Nucl. Phys. B **604**, 391 (2001) [arXiv:hep-ph/0102336].

[84] D. M. Photiadis, Phys. Lett. B **164**, 160 (1985).

[85] C. W. Bauer, C. W. Chiang, S. Fleming, A. K. Leibovich and I. Low, Phys. Rev. D **64**, 114014 (2001) [arXiv:hep-ph/0106316].

[86] M. J. Dugan and B. Grinstein, Phys. Lett. B **255**, 583 (1991).

[87] K. Hagiwara *et al.* [Particle Data Group Collaboration], Phys. Rev. D **66**, 010001 (2002).

[88] X. Garcia i Tormo and J. Soto, Phys. Rev. D **69**, 114006 (2004) [arXiv:hep-ph/0401233]; X. G. i. Tormo, arXiv:hep-ph/0410052.

[89] S. Fleming and A. K. Leibovich, Phys. Rev. D **70**, 094016 (2004) [arXiv:hep-ph/0407259].

[90] A. Duncan and A. H. Mueller, Phys. Lett. B **93**, 119 (1980).

[91] S. J. Brodsky and G. P. Lepage, Phys. Rev. D **24**, 2848 (1981).

[92] V. L. Chernyak and A. R. Zhitnitsky, Nucl. Phys. B **201**, 492 (1982) [Erratum-ibid. B **214**, 547 (1983)].

[93] V. N. Baier and A. G. Grozin, Z. Phys. C **29**, 161 (1985).

[94] J. Bolz, P. Kroll and G. A. Schuler, Phys. Lett. B **392**, 198 (1997) [arXiv:hep-ph/9610265] and Eur. Phys. J. C **2**, 705 (1998) [arXiv:hep-ph/9704378].

[95] V. L. Chernyak and A. R. Zhitnitsky, Phys. Rept. **112**, 173 (1984).

[96] V. M. Braun and I. E. Filyanov, Z. Phys. C **48**, 239 (1990) [Sov. J. Nucl. Phys. **52**, 126 (1990 YAFIA,52,199-213.1990)]; P. Ball, V. M. Braun, Y. Koike and K. Tanaka, Nucl. Phys. B **529**, 323 (1998) [arXiv:hep-ph/9802299]; M. Beneke and T. Feldmann, Nucl. Phys. B **592**, 3 (2001) [arXiv:hep-ph/0008255].

[97] V. Braun, R. J. Fries, N. Mahnke and E. Stein, Nucl. Phys. B **589**, 381 (2000) [Erratum-ibid. B **607**, 433 (2001)] [arXiv:hep-ph/0007279].

[98] M. E. B. Franklin *et al.*, Phys. Rev. Lett. **51**, 963 (1983).

[99] N. E. Adam *et al.* [CLEO Collaboration], Phys. Rev. Lett. **94**, 012005 (2005) [arXiv:hep-ex/0407028].

[100] M. Ablikim *et al.* [BES Collaboration], arXiv:hep-ex/0408047.

[101] W. S. Hou and A. Soni, Phys. Rev. Lett. **50**, 569 (1983).

[102] S. J. Brodsky, G. P. Lepage and S. F. Tuan, Phys. Rev. Lett. **59**, 621 (1987).

[103] Y. Q. Chen and E. Braaten, Phys. Rev. Lett. **80**, 5060 (1998) [arXiv:hep-ph/9801226].

[104] T. Feldmann and P. Kroll, Phys. Rev. D **62**, 074006 (2000) [arXiv:hep-ph/0003096].

[105] M. Suzuki, Phys. Rev. D **63**, 054021 (2001).

[106] J. L. Rosner, Phys. Rev. D **64**, 094002 (2001) [arXiv:hep-ph/0105327].

[107] M. Ablikim *et al.* [BES Collaboration], Phys. Lett. B **614**, 37 (2005) [arXiv:hep-ex/0407037].

[108] M. Ablikim *et al.* [BES Collaboration], Phys. Rev. D **70**, 112003 (2004) [arXiv:hep-ex/0408118].

[109] M. Ablikim *et al.* [the BES Collaboration], Phys. Rev. D **70**, 112007 (2004) [Erratum-ibid. D **71**, 019901 (2005)] [arXiv:hep-ex/0410031].

[110] J. Z. Bai *et al.* [BES Collaboration], Phys. Rev. Lett. **92**, 052001 (2004) [arXiv:hep-ex/0310024]; J. Z. Bai *et al.* [BES Collaboration], Phys. Rev. D **69**, 012003 (2004) [arXiv:hep-ex/0310023].

[111] J. Z. Bai *et al.* [BES Collaboration], Phys. Rev. D **69**, 072001 (2004) [arXiv:hep-ex/0312016].

[112] A. Seiden, H. F. W. Sadrozinski and H. E. Haber, Phys. Rev. D **38**, 824 (1988).

[113] A. Bramon, R. Escribano and M. D. Scadron, Phys. Lett. B **403**, 339 (1997) [arXiv:hep-ph/9703313].

[114] S. A. Dytman [CLEO Collaboration], arXiv:hep-ex/0307035.

[115] Z. Dziembowski, Phys. Rev. D **37**, 768 (1988).

[116] G. P. Lepage and S. J. Brodsky, Phys. Rev. D **22**, 2157 (1980).

[117] J. Bolz and P. Kroll, Z. Phys. A **356**, 327 (1996) [arXiv:hep-ph/9603289].

[118] N. G. Stefanis and M. Bergmann, Phys. Rev. D **47**, 3685 (1993) [arXiv:hep-ph/9211250]; V. L. Chernyak, A. A. Ogloblin and I. R. Zhitnitsky, Z. Phys. C **42**, 583 (1989) [Yad. Fiz. **48**, 1398 (1988 SJNCA,48,889-895.1988)];

[119] N. Isgur and C. H. Llewellyn Smith, Nucl. Phys. B **317**, 526 (1989); A. V. Radyushkin, Nucl. Phys. A **527**, 153C (1991).

[120] V. Y. Petrov and M. V. Polyakov, arXiv:hep-ph/0307077.

[121] J. Bolz and P. Kroll, Eur. Phys. J. C **2**, 545 (1998) [arXiv:hep-ph/9703252].

[122] J. Botts and G. Sterman, Nucl. Phys. B **325**, 62 (1989); H. n. Li and G. Sterman, Nucl. Phys. B **381**, 129 (1992).

[123] J. Bolz, R. Jakob, P. Kroll, M. Bergmann and N. G. Stefanis, Z. Phys. C **66**, 267 (1995) [arXiv:hep-ph/9405340].

[124] J. Z. Bai *et al.* [BES Collaboration], Phys. Lett. B **591**, 42 (2004) [arXiv:hep-ex/0402034].

[125] D. Pallin *et al.* [DM2 Collaboration], Nucl. Phys. B **292**, 653 (1987).

[126] M. W. Eaton *et al.*, Phys. Rev. D **29**, 804 (1984).

[127] T. A. Armstrong *et al.* [E760 Collaboration], Phys. Rev. D **47**, 772 (1993).

[128] Seon-Hee Seo, proceedings of CIPANP 03, New York May, 19-24 2003.

[129] C. Carimalo, Int. J. Mod. Phys. A **2**, 249 (1987).

[130] F. Murgia and M. Melis, Phys. Rev. D **51**, 3487 (1995) [arXiv:hep-ph/9412205]; R. G. Ping, H. C. Chiang and B. S. Zou, Phys. Rev. D **66**, 054020 (2002).

[131] M. Claudson, S. L. Glashow and M. B. Wise, Phys. Rev. D **25**, 1345 (1982).

[132] H. Fritzsch and J. D. Jackson, Phys. Lett. B **66**, 365 (1977).

[133] K. T. Chao, Nucl. Phys. B **317**, 597 (1989).

[134] T. Feldmann, P. Kroll and B. Stech, Phys. Rev. D **58**, 114006 (1998) [arXiv:hep-ph/9802409]; Phys. Lett. B **449**, 339 (1999) [arXiv:hep-ph/9812269].

[135] T. Feldmann and P. Kroll, Eur. Phys. J. C **5**, 327 (1998) [arXiv:hep-ph/9711231].

[136] F. Yuan and K. T. Chao, Phys. Rev. D **56**, 2495 (1997) [arXiv:hep-ph/9706294].

[137] R. M. Baltrusaitis *et al.* [Mark-III Collaboration], Phys. Rev. D **33**, 629 (1986).

[138] D. Bisello *et al.* [DM2 collaboration], Nucl. Phys. B **350**, 1 (1991).

[139] J. Z. Bai *et al.* [BES Collaboration], Phys. Lett. B **578**, 16 (2004) [arXiv:hep-ex/0308073].

[140] H. C. Huang, arXiv:hep-ex/0305068.

[141] W. Buchmüller and S. H. H. Tye, Phys. Rev. D **24**, 132 (1981).

[142] P. Kroll and M. Raulfs, Phys. Lett. B **387**, 848 (1996) [arXiv:hep-ph/9605264]; I. V. Musatov and A. V. Radyushkin, Phys. Rev. D **56**, 2713 (1997) [arXiv:hep-ph/9702443].

[143] M. Diehl, P. Kroll and C. Vogt, Eur. Phys. J. C **22**, 439 (2001) [arXiv:hep-ph/0108220]; A. P. Bakulev, S. V. Mikhailov and N. G. Stefanis, arXiv:hep-ph/0312141.

[144] C. Quigg and J. L. Rosner, Phys. Rept. **56**, 167 (1979).

[145] P. Kroll and K. Passek-Kumericki, Phys. Rev. D **67**, 054017 (2003) [arXiv:hep-ph/0210045].

[146] A. Ali and A. Y. Parkhomenko, Eur. Phys. J. C **30**, 183 (2003) [arXiv:hep-ph/0304278].

[147] S. M. Wong, Nucl. Phys. A **674**, 185 (2000) [arXiv:hep-ph/9903221]; Eur. Phys. J. C **14**, 643 (2000) [arXiv:hep-ph/9903236].

[148] J. Z. Bai *et al.* [BES Collaboration], Phys. Rev. D **67**, 112001 (2003) [arXiv:hep-ex/0304012].

[149] J. Z. Bai *et al.* [BES Collaboration], Phys. Rev. D **69**, 092001 (2004) [arXiv:hep-ex/0401011].

[150] A. Andrikopoulou, Z. Phys. C **22**, 63 (1984); P. H. Damgaard, K. Tsokos and E. L. Berger, Nucl. Phys. B **259**, 285 (1985).

[151] E. Braaten and J. Lee, Phys. Rev. D **67**, 054007 (2003) [arXiv:hep-ph/0211085].

[152] H. W. Huang, C. F. Qiao and K. T. Chao, Phys. Rev. D **54**, 2123 (1996) [arXiv:hep-ph/9601380].

[153] M. Anselmino, R. Cancelliere and F. Murgia, Phys. Rev. D **46**, 5049 (1992).

[154] V. A. Novikov, M. A. Shifman, A. I. Vainshtein and V. I. Zakharov, Nucl. Phys. B **165**, 55 (1980).

[155] T. Feldmann and P. Kroll, Phys. Scripta **T99**, 13 (2002) [arXiv:hep-ph/0201044].

[156] J. P. Ma, Phys. Rev. D **65**, 097506 (2002) [arXiv:hep-ph/0202256].

[157] M. K. Chase, Nucl. Phys. B **174**, 109 (1980); V. N. Baier and A. G. Grozin, Nucl. Phys. B **192**, 476 (1981).

[158] P. Minkowski and W. Ochs, arXiv:hep-ph/0401167.

[159] F. E. Close, G. R. Farrar and Z. p. Li, Phys. Rev. D **55**, 5749 (1997) [arXiv:hep-ph/9610280].

[160] X. G. He, H. Y. Jin and J. P. Ma, Phys. Rev. D **66**, 074015 (2002) [arXiv:hep-ph/0203191].

[161] J. Z. Bai *et al.* [BES Collaboration], Phys. Rev. Lett. **91**, 022001 (2003) [arXiv:hep-ex/0303006].

[162] K. Abe *et al.* [Belle Collaboration], Phys. Rev. Lett. **88**, 181803 (2002) [arXiv:hep-ex/0202017]; Phys. Rev. Lett. **89**, 151802 (2002) [arXiv:hep-ex/0205083].

[163] A. Antonelli *et al.*, Nucl. Phys. B **517**, 3 (1998).

[164] D. Bridges *et al.*, Phys. Lett. B **180**, 313 (1986).

[165] L. Linssen *et al.*, Nucl. Phys. A **469**, 726 (1987); P. Schiavon *et al.*, Nucl. Phys. A **505**, 595 (1989).

[166] O. D. Dalkarov, V. M. Kolybasov, I. S. Shapiro and D. V. Voronov, Phys. Lett. B **392**, 229 (1997).

[167] P. Kroll and W. Schweiger, Nucl. Phys. A **503**, 865 (1989).

[168] A. Ferrer, A. A. Grigorian, V. F. Perepelitsa and P. Sonderegger, Eur. Phys. J. C **10**, 249 (1999).

[169] B. S. Zou and H. C. Chiang, Phys. Rev. D **69**, 034004 (2004) [arXiv:hep-ph/0309273]; B. Kerbikov, A. Stavinsky and V. Fedotov, Phys. Rev. C **69**, 055205 (2004) [arXiv:hep-ph/0402054].

[170] J. L. Rosner, Phys. Rev. D **68**, 014004 (2003) [arXiv:hep-ph/0303079].

[171] G. Bonvicini *et al.* [CLEO Collaboration], Phys. Rev. D **70**, 032001 (2004) [arXiv:hep-ex/0404021].

[172] B. A. Thacker and G. P. Lepage, Phys. Rev. D **43**, 196 (1991).

[173] P. Lepage and C. Davies, Int. J. Mod. Phys. A **19**, 877 (2004); S. A. Gottlieb, Nucl. Phys. Proc. Suppl. **128**, 72 (2004) [Nucl. Phys. Proc. Suppl. **129**, 17 (2004)] [arXiv:hep-lat/0310041] and references therein.

[174] A. Duncan, E. Eichten and H. Thacker, Phys. Rev. Lett. **76**, 3894 (1996) [arXiv:hep-lat/9602005].

[175] P. Colangelo and A. Khodjamirian, arXiv:hep-ph/0010175. See also: A. Y. Khodjamirian, Phys. Lett. B **90**, 460 (1980), Sov. J. Nucl. Phys. **39**, 614 (1984); V. A. Beilin and A. V. Radyushkin,

Nucl. Phys. B **260**, 61 (1985).

[176] J. Baacke, Y. Igarashi and G. Kasperidus, Z. Phys. C **13**, 131 (1982).

[177] E. Eichten, K. Gottfried, T. Kinoshita, K. D. Lane and T. M. Yan, Phys. Rev. D **17**, 3090 (1978) [Erratum-ibid. D **21**, 313 (1980)].

[178] G. Feinberg and J. Sucher, Phys. Rev. Lett. **35**, 1740 (1975).

[179] J. Sucher, Rept. Prog. Phys. **41**, 1781 (1978).

[180] J. S. Kang and J. Sucher, Phys. Rev. D **18**, 2698 (1978).

[181] R. McClary and N. Byers, Phys. Rev. D **28**, 1692 (1983).

[182] V. Zambetakis and N. Byers, Phys. Rev. D **28**, 2908 (1983).

[183] H. Grotch and K. J. Sebastian, Phys. Rev. D **25**, 2944 (1982).

[184] H. Grotch, D. A. Owen and K. J. Sebastian, Phys. Rev. D **30**, 1924 (1984).

[185] T. A. Lahde, Nucl. Phys. **A 714**, 183 (2003) [arXiv:hep-ph/0208110].

[186] D. Ebert, R. N. Faustov and V. O. Galkin, Phys. Rev. D **67**, 014027 (2003) [arXiv:hep-ph/0210381].

[187] E. Eichten, K. Gottfried, T. Kinoshita, J. B. Kogut, K. D. Lane and T. M. Yan, Phys. Rev. Lett. **34**, 369 (1975) [Erratum-ibid. **36**, 1276 (1976)].

[188] T. Appelquist, A. De Rujula, H. D. Politzer and S. L. Glashow, Phys. Rev. Lett. **34**, 365 (1975).

[189] K. Gottfried, CLNS-97-1511 *Talk given at 20th Anniversary Symposium: Twenty Beautiful Years of Bottom Physics, Chicago, IL, 29 Jun - 2 Jul 1997*.

[190] E. Eichten and K. Gottfried, Phys. Lett. B **66**, 286 (1977).

[191] E. Eichten, K. Gottfried, T. Kinoshita, K. D. Lane and T. M. Yan, Phys. Rev. D **21**, 203 (1980).

[192] E. J. Eichten and C. Quigg, Phys. Rev. D **49**, 5845 (1994) [arXiv:hep-ph/9402210].

[193] W. Buchmüller, G. Grunberg and S. H. H. Tye, Phys. Rev. Lett. **45**, 103 (1980) [Erratum-ibid. **45**, 587 (1980)].

[194] C. Quigg and J. L. Rosner, Phys. Rev. D **23**, 2625 (1981).

[195] A. Martin, Phys. Lett. B **93**, 338 (1980).

[196] A. K. Grant, J. L. Rosner and E. Rynes, Phys. Rev. D **47**, 1981 (1993).

[197] W. Buchmüller, Phys. Lett. B **112**, 479 (1982).

[198] D. Pignon and C. A. Piketty, Phys. Lett. **B74**, 108 (1978).

[199] P. Moxhay and J. L. Rosner, Phys. Rev. D **28**, 1132 (1983).

[200] W. Kwong and J. L. Rosner, Phys. Rev. D **38**, 279 (1988).

[201] S. Godfrey and N. Isgur, Phys. Rev. D **32**, 189 (1985).

[202] S. N. Gupta, S. F. Radford and W. W. Repko, Phys. Rev. D **26**, 3305 (1982).

[203] S. N. Gupta, S. F. Radford and W. W. Repko, Phys. Rev. D **30**, 2424 (1984).

[204] S. N. Gupta, S. F. Radford and W. W. Repko, Phys. Rev. D **34**, 201 (1986).

[205] M. Bander, D. Silverman, B. Klima and U. Maor, Phys. Rev. D **29**, 2038 (1984).

[206] F. Daghighian and D. Silverman, Phys. Rev. D **36**, 3401 (1987).

[207] E. J. Eichten, K. Lane and C. Quigg, Phys. Rev. D **69**, 094019 (2004) [arXiv:hep-ph/0401210].

[208] E. J. Eichten, K. Lane and C. Quigg, Phys. Rev. Lett. **89**, 162002 (2002) [arXiv:hep-ph/0206018].

[209] T. Skwarnicki, Int. J. Mod. Phys. A **19**, 1030 (2004) [arXiv:hep-ph/0311243].

[210] S. B. Athar *et al.* [CLEO Collaboration], Phys. Rev. D **70**, 112002 (2004) [arXiv:hep-ex/0408133].

[211] D. Cinabro *et al.* [CLEO Collaboration], arXiv:hep-ex/0207062.

[212] G. D. Crawford *et al.* [CLEO Collaboration], Phys. Lett. B **294**, 139 (1992).

[213] U. Heintz *et al.*, Phys. Rev. D **46**, 1928 (1992).

[214] L. P. Fulcher, Phys. Rev. D **42**, 2337 (1990).

[215] L. P. Fulcher, Phys. Rev. D **39**, 295 (1989).

[216] Y. o. Zhu, Ph. D. Thesis, California Institute of Technology, 1988, Caltech report CALT-68-1513 (unpublished).

[217] S. Godfrey and J. L. Rosner, Phys. Rev. D **65**, 074011 (2001) [Erratum-ibid. D **65**, 039901 (2002)] [arXiv:hep-ph/0104253].

[218] X. Zhang, K. J. Sebastian and H. Grotch, Phys. Rev. D **44**, 1606 (1991).

[219] A. H. Mahmood *et al.* [CLEO Collaboration], arXiv:hep-ex/0207057.

[220] G. Karl, S. Meshkov and J. L. Rosner, Phys. Rev. Lett. **45**, 215 (1980).

[221] K. J. Sebastian, H. Grotch and F. L. Ridener, Phys. Rev. D **45**, 3163 (1992).

[222] M. Ambrogiani *et al.* [E835 Collaboration], Phys. Rev. D **65**, 052002 (2002).

[223] M. Ablikim *et al.* [BES Collaboration], Phys. Rev. D **70**, 092004 (2004) [arXiv:hep-ex/0409034].

[224] F. Abe *et al.* [CDF Collaboration], Phys. Rev. Lett. **81**, 2432 (1998) [arXiv:hep-ex/9805034].

[225] S. S. Gershtein, V. V. Kiselev, A. K. Likhoded and A. V. Tkabladze, Phys. Usp. **38**, 1 (1995) [Usp. Fiz. Nauk **165**, 3 (1995)] [arXiv:hep-ph/9504319].

[226] L. P. Fulcher, Phys. Rev. D **60**, 074006 (1999) [arXiv:hep-ph/9806444].

[227] K. Gottfried, CLNS-376 *Invited paper presented at Int. Symp. on Lepton and Photon Interactions at High Energies, Hamburg, Germany, Aug 25-31, 1977*; Phys. Rev. Lett. **40**, 598 (1978).

[228] G. Bhanot, W. Fischler and S. Rudas, Nucl. Phys. B **155**, 208 (1979); M. E. Peskin, ibid. B **156**, 365 (1979); G. Bhanot and M. E. Peskin, ibid. B **156**, 391 (1979).

[229] M. B. Voloshin, Nucl. Phys. B **154**, 365 (1979); M. B. Voloshin and V. I. Zakharov, Phys. Rev. Lett. **45**, 688 (1980); V. A. Novikov and M. A. Shifman, Z. Phys. C **8**, 43 (1981); M. Shifman, Phys. Rept. **209**, 341 (1991) [Sov. Phys. Usp. **32**, 289 (1989 UFNAA,157,561-598.1989)].

[230] T. M. Yan, Phys. Rev. D **22**, 1652 (1980).

[231] Y.-P. Kuang, Y.-P. Yi and B. Fu, Phys. Rev. D **42**, 2300 (1990).

[232] A. Falk, H. Georgi, B. Grinstein and M.B. Wise, Nucl. Phys. B **343**, 1 (1990).

[233] R. Casalbuoni, A. Deandrea, N. Di Bartolomeo, R. Gatto, F. Feruglio and G. Nardulli, Phys. Rep. **281**, 145 (1997) [arXiv:hep-ph/9605342].

[234] R. Casalbuoni, A. Deandrea, N. Di Bartolomeo, F. Feruglio, R. Gatto and G. Nardulli, Phys. Lett. B **302**, 95 (1993).

[235] R. Casalbuoni, A. Deandrea, N. Di Bartolomeo, R. Gatto, F. Feruglio and G. Nardulli, Phys. Lett. B **309**, 163 (1993) [arXiv:hep-ph/9304280].

[236] M. Bando, T. Kugo and K. Yamawaki, Nucl. Phys. B **259**, 493 (1985); Phys. Rep. **164**, 217 (1988).

[237] Y.-P. Kuang and T.-M. Yan, Phys. Rev. D **24**, 2874 (1981).

[238] S.-H. H. Tye, Phys. Rev. D **13**, 3416 (1976); R.C. Giles and S.-H. H. Tye, Phys. Rev. Lett. **37**, 1175 (1976); Phys. Rev. D **16**, 1079 (77); W. Buchmüller and S.-H. H. Tye, Phys. Rev. Lett. **44**, 850 (1980).

[239] D.-S. Liu and Y.-P. Kuang, Z. Phys. C **37**, 119 (1987); P.-Z. Bi and Y.-M. Shi, Mod. Phys. Lett. A **7**, 3161 (1992).

[240] L. S. Brown and R. N. Cahn, Phys. Rev. Lett. **35**, 1 (1975).

[241] J. Z. Bai *et al.* [BES Collaboration], Phys. Rev. D **70**, 012006 (2004) [arXiv:hep-ex/0403023].

[242] B. L. Ioffe and M. A. Shifman, Phys. Lett. B **95**, 99 (1980).

[243] A. Billoire, R. Lacaze, A. Morel, and H. Navelet, Nucl. Phys. B **155**, 493 (1979).

[244] P. Moxhay, Phys. Rev. D **37**, 2557 (1988).

[245] P. Ko, Phys. Rev. D **47**, 208 (1993).

[246] J. L. Rosner, Phys. Rev. D **67**, 097504 (2003) [arXiv:hep-ph/0302122].

[247] Y.-P. Kuang and T.-M. Yan, Phys. Rev. D **41**, 155 (1990).

[248] Y.-P. Kuang, Phys. Rev. D **65**, 094024 (2002).

[249] R. A. Partridge, CALT-68-1150; R. H. Schindler, SLAC-R-0219; J. Adler, *et al.*, Phys. Rev. Lett. **60**, 89 (1988).

[250] S. Godfrey, Z. Phys. C **31**, 77 (1986).

[251] Y. Q. Chen and Y. P. Kuang, Phys. Rev. D **46**, 1165 (1992) [Erratum-ibid. D **47**, 350 (1993)].

[252] J. Z. Bai *et al.* [BES Collaboration], Phys. Lett. B **605**, 63 (2005) [arXiv:hep-ex/0307028].

[253] K. Heikkilä, S. Ono, and N. A. Törnqvist, Phys. Rev. D **29**, 110 (1984); K. Heikkila, S. Ono and N. A. Tornqvist, Phys. Rev. D **29**, 110 (1984) [Erratum-ibid. D **29**, 2136 (1984)]; S. Ono and N. A. Törnqvist, Z. Phys. C **23**, 59 (1984); N. A. Törnqvist, Phys. Rev. Lett. **53**, 878 (1984); Acta Phys. Polon. B **16**, 503 (1985) [Erratum-ibid. B **16**, 683 (1985)].

[254] A. Tomaradze, *talk at the Hadron 2001 Conference, Protvino, Russia, 2001*.

[255] Crystal Ball Group, Annu. Rev. Nucl. Part. Sci. **33**, 143 (1983).

[256] Y. P. Kuang, S. F. Tuan and T. M. Yan, Phys. Rev. D **37**, 1210 (1988); Y.-P. Kuang, in Proc. Intern. Symp. on Extended Objects and Bound States, March 19-21 (1992), Karuizawa, Japan, eds. O. Hara, S. Ishida, and S. Naka (World Scientific, Singapore,1992).

[257] M. Suzuki, Phys. Rev. D **66**, 037503 (2002) [arXiv:hep-ph/0204043].

[258] A. Tomaradze, *talk at the 3^{nd} QWG Workshop, Beijing, 2004*, http://www.qwg.to.infn.it/WS-oct04/index.html; arXiv:hep-ex/0410090.

[259] C. Patrignani, *talk at the 3^{nd} QWG Workshop, Beijing, 2004*, http://www.qwg.to.infn.it/WS-oct04/index.html; arXiv:hep-ex/0410085.

[260] For example, Ref. [177, 191] and V. E. Zambetakis, "Coupled Channel Mixing Effects And Magnetic Dipole Transitions In Quarkonia. UCLA-86-TEP-2.

[261] A. Le Yaouanc, L. Oliver, O. Pene, and J.-C. Raynal, Phys. Rev. D **8**, 2223 (1973).

[262] M. Chaichian and R. Kogerler, Annals Phys. **124**, 61 (1980).

[263] H.-Y. Zhou and Y.-P. Kuang, Phys. Rev. D **44**, 756 (1991).

[264] J. G. Körner, J. H. Kühn, M. Krammer and H. Schneider, Nucl. Phys. B **229**, 115 (1983).

[265] H. Albrecht *et al.* [ARGUS Collaboration], Z. Phys. C **35**, 283 (1987).

[266] F. Butler *et al.* [CLEO Collaboration], Phys. Rev. D **49**, 40 (1994); I. C. Brock *et al.*, Phys. Rev. D **43**, 1448 (1991).

[267] D. Besson *et al.* [CLEO Collaboration], Phys. Rev. D **30**, 1433 (1984).

[268] V. Fonseca *et al.* [CUSB Collaboration], Nucl. Phys. B **242**, 31 (1984).

[269] D. Gelphman *et al.* [Crystal Ball Collaboration], Phys. Rev. D **32**, 2893 (1985).

[270] R. N. Cahn, Phys. Rev. D **12**, 3559 (1975).

[271] S. Chakravarty and P. Ko, Phys. Rev. D **48**, 1205 (1993).

[272] G. Belanger, T. Degrand and P. Moxhay, Phys. Rev. D **39**, 257 (1989).

[273] D. Morgan and M. R. Pennington, Phys. Rev. D **12**, 1283 (1975).

[274] J. P. Alexander *et al.* [CLEO Collaboration], Phys. Rev. D **58**, 052004 (1998) [arXiv:hep-ex/9802024].

[275] M. B. Voloshin, JETP Lett. **37**, 69 (1983) [Pisma Zh. Eksp. Teor. Fiz. **37**, 58 (1983)]; T. N. Truong, Univeristy of Virginia report (unpublished).

[276] V. V. Anisovich, D. V. Bugg, A. V. Sarantsev and B. S. Zou, Phys. Rev. D **51**, 4619 (1995).

[277] H. J. Lipkin and S. F. Tuan, Phys. Lett. B **206**, 349 (1988); P. Moxhay, Phys. Rev. D **39**, 3497 (1989).

[278] T. Komada, S. Ishida and M. Ishida, Phys. Lett. B **508**, 31 (2001); M. Ishida, S. Ishida, T. Komada and S. I. Matsumoto, Phys. Lett. B **518**, 47 (2001).

[279] M. Uehara, Prog. Theor. Phys. **109**, 265 (2003) [arXiv:hep-ph/0211029].

[280] S. K. Choi *et al.* [Belle Collaboration], Phys. Rev. Lett. **91**, 262001 (2003) [arXiv:hep-ex/0309032].

[281] W. M. Tanenbaum *et al.*, Phys. Rev. Lett. **36**, 402 (1976).

[282] W. Bartel *et al.*, Phys. Lett. B **79**, 492 (1978).

[283] R. Brandelik *et al.* [DASP Collaboration], "Experimental Results On The Decay Sequences Psi-Prime (3685) $\to$ Gamma P(C) Nucl. Phys. B **160**, 426 (1979).

[284] T. Himel *et al.*, Phys. Rev. Lett. **44**, 920 (1980).

[285] M. Oreglia *et al.*, Phys. Rev. Lett. **45**, 959 (1980).

[286] J. Z. Bai *et al.* [BES Collaboration], Nucl. Instrum. Meth. A **458**, 627 (2001).

[287] M. Ablikim *et al.* [BES Collaboration], Phys. Rev. D **70**, 012003 (2004) [arXiv:hep-ex/0404020].

[288] J. Z. Bai *et al.* [BES Collaboration], Nucl. Instrum. Meth. A **344**, 319 (1994).

[289] T. A. Armstrong *et al.* [Fermilab E760 Collaboration], Phys. Rev. D **55**, 1153 (1997).

[290] G. Abrams, Proceedings of the 1975 International Symposium on Lepton and Photon Interactions at High Energies, published by the Stanford Linear Accelerator Center, 36 (1975).

[291] M. B. Voloshin, JETP Lett. **21**, 347 (1975) [Pisma Zh. Eksp. Teor. Fiz. **21**, 733 (1975)].

[292] J. Z. Bai *et al.* [BES Collaboration], Phys. Rev. D **62**, 032002 (2000) [arXiv:hep-ex/9909038].

[293] Two of equations in Ref. [270] omitted interference terms. See [292].

[294] T. Ishida, M. Ishida, S. Ishida, K. Takamatsu and T. Tsuru, arXiv:hep-ph/9712230.

[295] T. Mannel and R. Urech, Z. Phys. C **73**, 541 (1997) [arXiv:hep-ph/9510406].

[296] M. L. Yan, Y. Wei and T. L. Zhuang, Eur. Phys. J. C **7**, 61 (1999) [arXiv:hep-ph/9805354].

[297] S. L. Olsen [Belle Collaboration], Int. J. Mod. Phys. A **20**, 240 (2005) [arXiv:hep-ex/0407033].

[298] D. Acosta *et al.* [CDF II Collaboration], Phys. Rev. Lett. **93**, 072001 (2004) [arXiv:hep-ex/0312021].

[299] M. Masetti, Phys. Lett. B **286**, 160 (1992); R. Fleischer and D. Wyler, Phys. Rev. D **62**, 057503 (2000) [arXiv:hep-ph/0004010]; M. A. Ivanov, J. G. Körner and O. N. Pakhomova, Phys. Lett. B **555**, 189 (2003) [arXiv:hep-ph/0212291]; Y. S. Dai and D. S. Du, Eur. Phys. J. C **9**, 557 (1999) [arXiv:hep-ph/9809386]; J. F. Liu and K. T. Chao, Phys. Rev. D **56**, 4133 (1997).

[300] V. V. Kiselev, J. Phys. G **30**, 1445 (2004) [arXiv:hep-ph/0302241].

[301] F. Abe *et al.*, CDF Collaboration, Phys. Rev. **D58**, 112004 (1998).

[302] S. S. Gershtein *et al.*, Sov. J. Nucl. Phys. **48**, 327 (1988), [Yad. Fiz. **48**, 515 (1988)]; V. V. Kiselev, A. K. Likhoded and A. V. Tkabladze, Sov. J. Nucl. Phys. **46**, 535 (1987) [Yad. Fiz. **46**, 934 (1987)]; S. S. Gershtein, A. K. Likhoded and S. R. Slabospitsky, Int. J. Mod. Phys. A **6**, 2309 (1991); S. S. Gershtein *et al.*, Phys. Rev. D **51**, 3613 (1995); A. V. Berezhnoi, V. V. Kiselev, A. K. Likhoded and A. I. Onishchenko, Phys. Atom. Nucl. **60**, 1729 (1997) [Yad. Fiz. **60N10**, (1997)] [arXiv:hep-ph/9703341].

[303] N. Brambilla and A. Vairo, Phys. Rev. D **62**, 094019 (2000) [arXiv:hep-ph/0002075].

[304] S. Capstick and S. Godfrey, Phys. Rev. D **41**, 2856 (1990).

[305] I. I. Y. Bigi, Phys. Lett. B **371**, 105 (1996) [arXiv:hep-ph/9510325]; M. Beneke and G. Buchalla, Phys. Rev. D **53**, 4991 (1996) [arXiv:hep-ph/9601249]; A. I. Onishchenko, arXiv:hep-ph/9912424; C. H. Chang, S. L. Chen, T. F. Feng and X. Q. Li, Commun. Theor. Phys. **35**, 51 (2001); Phys. Rev. D **64**, 014003 (2001) [arXiv:hep-ph/0007162].

[306] V. V. Kiselev and A. V. Tkabladze, Phys. Rev. D **48**, 5208 (1993).

[307] V. V. Kiselev, A. K. Likhoded and A. I. Onishchenko, Nucl. Phys. B **569**, 473 (2000) [arXiv:hep-

ph/9905359].

[308] V. V. Kiselev, A. E. Kovalsky and A. K. Likhoded, Nucl. Phys. B **585**, 353 (2000) [arXiv:hep-ph/0002127]; arXiv:hep-ph/0006104.

[309] V. V. Kiselev, arXiv:hep-ph/0211021.

[310] K. Anikeev *et al.*, arXiv:hep-ph/0201071.

[311] I. P. Gouz, V. V. Kiselev, A. K. Likhoded, V. I. Romanovsky and O. P. Yushchenko, Phys. Atom. Nucl. **67**, 1559 (2004) [Yad. Fiz. **67**, 1581 (2004)] [arXiv:hep-ph/0211432].

[312] J. D. Bjorken, draft report 07/22/86 (1986) [unpublished].

[313] V. V. Kiselev and A. K. Likhoded, Phys. Usp. **45**, 455 (2002) [Usp. Fiz. Nauk **172**, 497 (2002)] [arXiv:hep-ph/0103169]; A. V. Berezhnoi, V. V. Kiselev and A. K. Likhoded, Phys. Atom. Nucl. **59**, 870 (1996) [Yad. Fiz. **59**, 909 (1996)] [arXiv:hep-ph/9507242]; S. P. Baranov, Phys. Rev. D **54**, 3228 (1996); M. A. Doncheski, J. Steegborn and M. L. Stong, Phys. Rev. D **53**, 1247 (1996) [arXiv:hep-ph/9507220]; A. V. Berezhnoi, V. V. Kiselev, A. K. Likhoded and A. I. Onishchenko, Phys. Rev. D **57**, 4385 (1998) [arXiv:hep-ph/9710339]; V. V. Kiselev and A. E. Kovalsky, Phys. Atom. Nucl. **63**, 1640 (2000) [Yad. Fiz. **63**, 1728 (2000)] [arXiv:hep-ph/9908321]; V. V. Braguta, V. V. Kiselev and A. E. Chalov, Phys. Atom. Nucl. **65**, 1537 (2002) [Yad. Fiz. **65**, 1575 (2002)].

[314] T. Mannel and G. A. Schuler, Z. Phys. C **67**, 159 (1995) [arXiv:hep-ph/9410333].

[315] M. E. Luke, A. V. Manohar and I. Z. Rothstein, Phys. Rev. D **61**, 074025 (2000) [arXiv:hep-ph/9910209]; A. V. Manohar and I. W. Stewart, Phys. Rev. D **63**, 054004 (2001) [arXiv:hep-ph/0003107]; A. H. Hoang, A. V. Manohar and I. W. Stewart, Phys. Rev. D **64**, 014033 (2001) [arXiv:hep-ph/0102257].

[316] M. A. Shifman, A. I. Vainshtein and V. I. Zakharov, Nucl. Phys. B **147**, 448 (1979); ibid. 385 (1979); ibid. 519 (1979); V. A. Novikov, L. B. Okun, M. A. Shifman, A. I. Vainshtein, M. B. Voloshin and V. I. Zakharov, Phys. Rept. **41**, 1 (1978); L. J. Reinders, H. Rubinstein and S. Yazaki, Phys. Rept. **127**, 1 (1985).

[317] M. Lusignoli and M. Masetti, Z. Phys. C **51**, 549 (1991).

[318] V. V. Kiselev, Mod. Phys. Lett. A **10**, 1049 (1995) [arXiv:hep-ph/9409348]; V. V. Kiselev, Int. J. Mod. Phys. A **9**, 4987 (1994).

[319] V. V. Kiselev, A. K. Likhoded and A. V. Tkabladze, Phys. Atom. Nucl. **56**, 643 (1993), Yad. Fiz. **56**, 128 (1993).

[320] V. V. Kiselev and A. V. Tkabladze, Yad. Fiz. **48**, 536 (1988); G. R. Jibuti and Sh. M. Esakia, Yad. Fiz. **50**, 1065 (1989), ibid. **51**, 1681 (1990).

[321] A. Abd El-Hady, J. H. Munoz and J. P. Vary, Phys. Rev. D **62**, 014019 (2000) [arXiv:hep-ph/9909406].

[322] C. H. Chang and Y. Q. Chen, Phys. Rev. D **49**, 3399 (1994).

[323] M. A. Ivanov, J. G. Körner and P. Santorelli, Phys. Rev. D **63**, 074010 (2001) [arXiv:hep-ph/0007169].

[324] D. Scora and N. Isgur, Phys. Rev. D **52**, 2783 (1995) [arXiv:hep-ph/9503486].

[325] A. Y. Anisimov, I. M. Narodetsky, C. Semay and B. Silvestre-Brac, Phys. Lett. B **452**, 129 (1999) [arXiv:hep-ph/9812514]; A. Y. Anisimov, P. Y. Kulikov, I. M. Narodetsky and K. A. Ter-Martirosian, Phys. Atom. Nucl. **62**, 1739 (1999) [Yad. Fiz. **62**, 1868 (1999)] [arXiv:hep-ph/9809249].

[326] P. Colangelo and F. De Fazio, Phys. Rev. D **61**, 034012 (2000) [arXiv:hep-ph/9909423].

[327] P. Colangelo, G. Nardulli and N. Paver, Z. Phys. C **57**, 43 (1993); E. Bagan, H. G. Dosch, P. Gosdzinsky, S. Narison and J. M. Richard, Z. Phys. C **64**, 57 (1994) [arXiv:hep-ph/9403208].

[328] G. Buchalla, A. J. Buras and M. E. Lautenbacher, Rev. Mod. Phys. **68** (1996) 1125 [arXiv:hep-ph/9512380].

[329] R. C. Verma and A. Sharma, Phys. Rev. D **65**, 114007 (2002).

[330] D. Ebert, R. N. Faustov and V. O. Galkin, Mod. Phys. Lett. A **17**, 803 (2002) [arXiv:hep-ph/0204167]; Eur. Phys. J. C **32**, 29 (2003) [arXiv:hep-ph/0308149]; Phys. Rev. D **68**, 094020 (2003) [arXiv:hep-ph/0306306].

[331] C. H. Chang, Y. Q. Chen, G. L. Wang and H. S. Zong, Phys. Rev. D **65**, 014017 (2002) [arXiv:hep-ph/0103036]; Commun. Theor. Phys. **35**, 395 (2001) [arXiv:hep-ph/0102150].

[332] O. N. Pakhomova and V. A. Saleev, Phys. Atom. Nucl. **63**, 1999 (2000); Yad. Fiz. **63**, 2091 (2000) [arXiv:hep-ph/9911313]; V. A. Saleev, arXiv:hep-ph/0007352; V. V. Kiselev, O. N. Pakhomova and V. A. Saleev, J. Phys. G **28**, 595 (2002) [arXiv:hep-ph/0110180]; G. Lopez Castro, H. B. Mayorga and J. H. Munoz, J. Phys. G **28**, 2241 (2002) [arXiv:hep-ph/0205273].

[333] G. Chiladze, A. F. Falk and A. A. Petrov, Phys. Rev. D **60**, 034011 (1999) [arXiv:hep-ph/9811405]; C. H. Chang, J. P. Cheng and C. D. Lu, Phys. Lett. B **425**, 166 (1998) [arXiv:hep-ph/9712325]; T. M. Aliev and M. Savci, Phys. Lett. B **434**, 358 (1998) [arXiv:hep-ph/9804407]; J. Phys. G **24**, 2223 (1998) [arXiv:hep-ph/9805239]; P. Colangelo and F. De Fazio, Mod. Phys. Lett. A **14**, 2303 (1999) [arXiv:hep-ph/9904363].

[334] D. S. Du, X. l. Li and Y. d. Yang, Phys. Lett. B **380**, 193 (1996) [arXiv:hep-ph/9603291]; S. Fajfer, S. Prelovsek and P. Singer, Phys. Rev. D **59**, 114003 (1999) [Erratum-ibid. D **64**, 099903 (2001)] [arXiv:hep-ph/9901252]; T. M. Aliev and M. Savci, Phys. Lett. B **480**, 97 (2000) [arXiv:hep-ph/9908203].

[335] P. Ball, M. Beneke and V. M. Braun, Nucl. Phys. B **452**, 563 (1995) [arXiv:hep-ph/9502300]; Phys. Rev. D **52**, 3929 (1995) [arXiv:hep-ph/9503492]; P. Ball, V. M. Braun and H. G. Dosch, Phys. Rev. D **48**, 2110 (1993) [arXiv:hep-ph/9211244]; A. A. Ovchinnikov and V. A. Slobodenyuk, Sov. J. Nucl. Phys. **50**, 891 (1989) [Yad. Fiz. **50**, 1433 (1989)]; Z. Phys. C **44**, 433 (1989).

[336] E. Jenkins, M. E. Luke, A. V. Manohar and M. J. Savage, Nucl. Phys. B **390**, 463 (1993) [arXiv:hep-ph/9204238].

[337] M. A. Sanchis-Lozano, Nucl. Phys. B **440**, 251 (1995) [arXiv:hep-ph/9502359].

[338] E. Braaten and S. Fleming, Phys. Rev. D **52**, 181 (1995) [arXiv:hep-ph/9501296].

[339] A. I. Onishchenko and O. L. Veretin, arXiv:hep-ph/0302132.

[340] S. Narison, Phys. Lett. B **210**, 238 (1988); V. V. Kiselev and A. V. Tkabladze, Sov. J. Nucl. Phys. **50**, 1063 (1989) [Yad. Fiz. **50**, 1714 (1989)]; T. M. Aliev and O. Yilmaz, Nuovo Cim. A **105**, 827 (1992); S. Reinshagen and R. Rückl, CERN-TH-6879-93 *Invited talk at 28th Rencontres de Moriond: QCD and High Energy Hadronic Interactions, Les Arcs, France, 20-27 Mar 1993*; MPI-PH-93-88 *Invited talk at Workshop on Quantum Field Theoretical Aspects of High Energy Physics, Kyffhauser, Germany, Sep 20-24, 1993*; M. Chabab, Phys. Lett. B **325**, 205 (1994); A. I. Onishchenko, arXiv:hep-ph/0005127.

[341] V. V. Kiselev, Phys. Part. Nucl. **31**, 538 (2000) [Fiz. Elem. Chast. Atom. Yadra **31**, 1080 (2000)]; S. S. Gershtein, V. V. Kiselev, A. K. Likhoded, A. V. Tkabladze, A. V. Berezhnoi and A. I. Onishchenko, arXiv:hep-ph/9803433; V. V. Kiselev, Int. J. Mod. Phys. A **11**, 3689 (1996) [arXiv:hep-ph/9504313]; V. V. Kiselev, Nucl. Phys. B **406**, 340 (1993).

[342] V. V. Kiselev, A. E. Kovalsky and A. I. Onishchenko, Phys. Rev. D **64**, 054009 (2001) [arXiv:hep-ph/0005020].

[343] V. V. Kiselev, A. K. Likhoded, O. N. Pakhomova and V. A. Saleev, Phys. Rev. D **65**, 034013 (2002) [arXiv:hep-ph/0105190].

[344] V. V. Kiselev, arXiv:hep-ph/0304017.

[345] M. A. Shifman, Nucl. Phys. B **388**, 346 (1992); B. Blok, M. Shifman, Nucl. Phys. B **389**, 534 (1993).

[346] S. S. Gershtein *et al.*, arXiv:hep-ph/9803433; V. V. Kiselev, Phys. Lett. B **372**, 326 (1996)

[arXiv:hep-ph/9507228]; arXiv:hep-ph/9605451.

[347] C. H. Chang, A. K. Giri, R. Mohanta and G. L. Wang, J. Phys. G **28**, 1403 (2002) [arXiv:hep-ph/0204279].

[348] M. A. Nobes and R. M. Woloshyn, J. Phys. G **26**, 1079 (2000) [arXiv:hep-ph/0005056].

[349] T. Mannel and S. Wolf, Phys. Rev. D **65**, 074012 (2002) [arXiv:hep-ph/0109250].

[350] J. P. Ma and J. S. Xu, Eur. Phys. J. C **24**, 261 (2002); X. G. Wu, C. H. Chang, Y. Q. Chen and Z. Y. Fang, Phys. Rev. D **67**, 094001 (2003) [arXiv:hep-ph/0209125]; C. H. Chang, arXiv:hep-ph/0205112.

[351] A. Faessler, T. Gutsche, M. A. Ivanov, J. G. Korner and V. E. Lyubovitskij, Eur. Phys. J. directC **4**, 18 (2002) [arXiv:hep-ph/0205287]; C. Q. Geng, C. W. Hwang and C. C. Liu, Phys. Rev. D **65**, 094037 (2002) [arXiv:hep-ph/0110376].

[352] M. Gronau and D. Wyler, Phys. Lett. B **265**, 172 (1991).

[353] V. V. Kiselev and O. P. Yushchenko, Phys. Lett. B **568**, 219 (2003) [arXiv:hep-ph/0211382].

[354] C. Quigg, FERMILAB-CONF-93-265-T *Presented at Summer Workshop on B Physics at Hadron Accelerators, Snowmass, Colorado, 21 Jun - 2 Jul 1993*.